



EUMETSAT

ROM SAF

RADIO OCCULTATION METEOROLOGY

**Validation Report:
Reprocessed Level 1B bending angle,
Level 2A refractivity, Level 2A dry
temperature CDR v1.0 products**

Version 1.2

20 December 2018

ROM SAF Consortium

Danish Meteorological Institute (DMI)
European Centre for Medium-Range Weather Forecasts (ECMWF)
Institut d'Estudis Espacials de Catalunya (IEEC)
Met Office (UKMO)

DOCUMENT AUTHOR TABLE

	Author(s)	Function	Date
Prepared by:	Stig Syndergaard	ROM SAF Project Team	20/12/18
Reviewed by (Internal):	Sean Healy	ROM SAF Science Coordinator	13/06/18
Approved by:	Kent B. Lauritsen	ROM SAF Project Manager	20/12/18

DOCUMENT CHANGE RECORD

Version	Date	By	Description
Version 0.7	04 June 2018	SSY	Unfinished draft for internal review
Version 0.8	12 June 2018	SSY	Still unfinished draft. Added discussions to figures in sections 3.6–3.8. Revised other sections after review of version 0.7 by Sean Healy. Some format updates as well.
Version 0.9	15 June 2018	SSY	First complete draft with all sections included, except for the executive summary. Revised other sections after review of version 0.8 by Sean Healy.
Version 1.0	15 June 2018	SSY	Version for DRR-RE1 review. Updated from version 0.9 with minor changes. Executive summary and references now included.
Version 1.1	31 August 2018	SSY	Updated version implementing the following RIDs from the DRR-RE1 & ORR review: <ul style="list-style-type: none"> – RID 218: Section 3 opening: Added a footnote clarifying the use of the word 'reference'. – RID 240: Section 6.1: Added a paragraph near the end of the section giving an idea of the size of the average impact of the higher order correction, and mentioning that it will be implemented in the future. – RID 224: Section 6.1: Added a comprehensive list of issues that could warrant further investigation in the future. – RID 227: Section 3 opening: Added clarifying text about correlation peaks, and replaced 'at 15 km' with 'with 15 km' in all plots. – RID 245: Section 5: Added a paragraph with a caveat regarding the reliance of the Service Specifications upon the ERA-Interim forecasts. – RID 375: Section 3 opening: Forecast periods now mentioned in parentheses. – RID 375: Section 3.2: Added a paragraph clarifying that there can only be changes to ERA-I data, not to the ERA-I model or the ERA-I system, and made sure to use the words 'data' and 'system' when appropriate. – RID 375: Section 3.2.1: Clarified the use of the terms ERA-I and ECMWF in plots, and clarified sentences containing both ERA-I forecasts and ECMWF operational forecasts throughout the report. – RIDs 019, 020, 213, 215, 216, 217, 219,

DOCUMENT CHANGE RECORD

...continued

Version	Date	By	Description
			<p>220, 221, 223, 225, 226, 228, 230, 231, 232, 233, 234, 236, 237, 238, 239, 241, 242, 243, 244, 360, 364, 377, 379, 381, 385, 391, 400, 403, 510, 512, 515, 516, 518, 519, 520, 521, 522, 523, 525, 526, 527, 528, 529, 530, 531, 532, 533, 535, 536, 537, 538, 540, 542, 543, 544, 546, 547: Editorial/minor changes.</p> <p>In addition the following changes were made:</p> <ul style="list-style-type: none"> – Included a few additional editorials provided by Barbara Scherllin-Pirscher. – Section 6.1: Corrected a mistake in the description of the limitation regarding satellite positions and velocities in BUFR. – Added new Fig.3.31 regarding periods of increased noise for COSMIC-FM5 in response to comments from UCAR. – Added additional correlation plots for bending angle in Figs. 3.62, 3.64, 3.66, and 3.68 in response to comments from UCAR. – Included minor clarifications in a few places in response to comments from UCAR.
Version 1.2	20 December 2018	SSY	<p>Updated version based on ICDR concept discussions at ROM SAF SG22:</p> <ul style="list-style-type: none"> – Page 4: Update of the ROM SAF preface. – Section 1.1: Update of remarks about CDR and ICDR. – Section 1.4: New definitions of product types. – Section 6.2: Now concerning only ICDR products – Section 6.3: New section Concerning only offline products – Annex A: Now describing the ICDR and SeSp requirements. – Annex B: New Annex describing offline data and their SeSp requirements.

ROM SAF

The Radio Occultation Meteorology Satellite Application Facility (ROM SAF) is a decentralised processing center under EUMETSAT which is responsible for operational processing of GRAS radio occultation (RO) data from the Metop satellites and radio occultation data from other missions. The ROM SAF delivers bending angle, refractivity, temperature, pressure, humidity, and other geophysical variables in near real-time for NWP users, as well as reprocessed Climate Data Records (CDRs) and Interim Climate Data Records (ICDRs) for users requiring a higher degree of homogeneity of the RO data sets. The CDRs and ICDRs are further processed into globally gridded monthly-mean data for use in climate monitoring and climate science applications.

The ROM SAF also maintains the Radio Occultation Processing Package (ROPP) which contains software modules that aid users wishing to process, quality-control and assimilate radio occultation data from any radio occultation mission into NWP and other models.

The ROM SAF Leading Entity is the Danish Meteorological Institute (DMI), with Cooperating Entities: i) European Centre for Medium-Range Weather Forecasts (ECMWF) in Reading, United Kingdom, ii) Institut D'Estudis Espacials de Catalunya (IEEC) in Barcelona, Spain, and iii) Met Office in Exeter, United Kingdom. To get access to our products or to read more about the ROM SAF please go to: <http://www.romsaf.org>.

Intellectual Property Rights

All intellectual property rights of the ROM SAF products belong to EUMETSAT. The use of these products is granted to every interested user, free of charge. If you wish to use these products, EUMETSAT's copyright credit must be shown by displaying the words "copyright (year) EUMETSAT" on each of the products used.

List of Contents

Document Change Record	2
List of Contents	6
Executive Summary	7
1 Introduction	8
1.1 Purpose of document	8
1.1.1 List of reprocessed products being validated in this report	8
1.2 Applicable and Reference documents	9
1.2.1 Applicable documents	9
1.2.2 Reference documents	9
1.3 Acronyms and abbreviations	10
1.4 Definitions	11
1.5 Overview of this document	12
2 Background	13
2.1 Missions and time coverage	13
2.2 Input data	13
2.3 ROM SAF reprocessing	14
2.4 Quality control	14
3 Profile comparisons	17
3.1 Comparison across missions	20
3.1.1 Bending angle	20
3.1.2 Refractivity	24
3.1.3 Dry temperature	27
3.2 Comparison against different background models	30
3.2.1 Bending angle	30
3.2.2 Refractivity	32
3.2.3 Dry temperature	33
3.3 Impact of instrument software upgrades	35
3.3.1 Metop upgrades in 2013	36
3.3.2 COSMIC upgrades in 2006	39
3.4 Comparison across years	43
3.4.1 Bending angle	43
3.4.2 Refractivity	48
3.4.3 Dry temperature	54
3.5 Comparison across seasons	57
3.5.1 Bending angle	57
3.5.2 Refractivity	61
3.5.3 Dry temperature	64
3.6 Comparison against products from the EUMETSAT Secretariat	69
3.6.1 Bending angle	69
3.7 Comparison against products from UCAR/CDAAC	74
3.7.1 Bending angle	74

3.7.2	Refractivity	85
3.7.3	Dry temperature	94
3.8	Comparison across local time and hemispheres	103
3.8.1	Bending angle	103
3.8.2	Refractivity	125
3.8.3	Dry temperature	132
4	Compliance with Product Requirements	139
5	Service Specifications	140
5.1	Metop	141
5.1.1	Bending angle	141
5.1.2	Refractivity and dry temperature	142
5.2	COSMIC	143
5.2.1	Bending angle	143
5.2.2	Refractivity and dry temperature	144
5.3	CHAMP	145
5.3.1	Bending angle	145
5.3.2	Refractivity and dry temperature	146
5.4	GRACE	147
5.4.1	Bending angle	147
5.4.2	Refractivity and dry temperature	148
6	Conclusions	149
6.1	Limitations	149
6.2	Interim Climate Data Record	152
6.3	Offline products	152
A	Annex	153
A.1	Interim Climate Data Record	153
A.1.1	Description of ICDR products being validated in this Annex	153
A.1.2	Validation	153
A.1.3	Service Specifications	153
B	Annex	154
B.1	Offline products	154
B.1.1	Description of offline products being validated in this Annex	154
B.1.2	Profile comparisons	154
B.1.3	Service Specifications	156

Executive Summary

The ROM SAF Climate Data Record version 1.0 (CDR v1.0) is based on measurements by the CHAMP, GRACE, COSMIC, and Metop Radio Occultation (RO) missions. The Level 1B and 2A data validated in this report consist of individual profiles of bending angle, refractivity, and dry temperature. The profiles have been generated by the ROM SAF from excess phases, amplitudes, and orbit data (Level 1A) provided by UCAR/CDAAC (CHAMP, GRACE, and COSMIC) and the EUMETSAT Secretariat (Metop).

The bending angle, refractivity, and dry temperature products are validated by statistical comparisons to reference data, including ERA-Interim forecasts and ECMWF operational forecasts, and similar data products from the EUMETSAT Secretariat and UCAR/CDAAC. We also verify that the quality is fairly consistent between the different missions, at least above 6 km, and that it is very consistent over long time periods. In the lower troposphere (below 6 km), comparisons reveal biases in all products, which increase to about 3% near the surface at low latitudes. We investigate small changes in the quality related to instrument software upgrades, and look at the retrieval performance during Sudden Stratospheric Warming events. Finally we look for dependencies on local time and hemispheres, and find small biases in the Metop data at high altitudes (up to 1 K at 35 km), presumably related to errors in the precise orbit determination, as well as small biases in the upper troposphere/lower stratosphere (about 0.1%) related to the ionospheric correction when the L2 signal is not available.

Based on the comparisons to ERA-Interim forecasts, we define the Service Specifications of the ROM SAF CDR v1.0 Level 1B and 2A products for each of the four missions.

We conclude that the quality of the ROM SAF CDR v1.0 generally matches the quality of the corresponding products from the EUMETSAT Secretariat and UCAR/CDAAC, which are considered to deliver state-of-the-art products of good quality to users around the world.

1 Introduction

1.1 Purpose of document

This document describes the validation results for the ROM SAF reprocessed Level 1B and Level 2A products, being parts of GRM-29-R1, GRM-30-R1, GRM-32-R1, and GRM-33-R1. Each of these is considered a Climate Data Record (CDR).

Additionally, the document also serves as validation of a subsequent Interim CDR (ICDR), and report on the quality of the ROM SAF offline Metop Level 1B and Level 2A products. The validation of the ICDR product is addressed in Annex A and the validation of the offline products is described in Annex B.

The report is submitted for a joint Delivery Readiness and Operational Readiness Review in order to decide on the validation status of both the reprocessed and the offline products.

1.1.1 List of reprocessed products being validated in this report

Table 1.1: List of reprocessed products covered by this report.

Product ID	Product name	Product acronym	Product type		Operational satellite input	Dissemination means	Dissemination format
GRM-29-L1-B-R1	Reprocessed Bending Angle	RBAMET	Climate Record	Data	Metop Level 1A data from EUM Secretariat	web	BUFR/netCDF
GRM-29-L2-R-R1	Reprocessed Refractivity Profile	RRPMET	Climate Record	Data	Metop Level 1A data from EUM Secretariat	web	BUFR/netCDF
GRM-29-L2-D-R1	Reprocessed Dry Temperature Profile	RDPMET	Climate Record	Data	Metop Level 1A data from EUM Secretariat	web	BUFR/netCDF
GRM-30-L1-B-R1	Reprocessed Bending Angle	RBACO1	Climate Record	Data	COSMIC Level 1A data from CDAAC	web	BUFR/netCDF
GRM-30-L2-R-R1	Reprocessed Refractivity Profile	RRPCO1	Climate Record	Data	COSMIC Level 1A data from CDAAC	web	BUFR/netCDF
GRM-30-L2-D-R1	Reprocessed Dry Temperature Profile	RDPCO1	Climate Record	Data	COSMIC Level 1A data from CDAAC	web	BUFR/netCDF
GRM-32-L1-B-R1	Reprocessed Bending Angle	RBACHA	Climate Record	Data	CHAMP Level 1A data from CDAAC	web	BUFR/netCDF
GRM-32-L2-R-R1	Reprocessed Refractivity Profile	RRPCHA	Climate Record	Data	CHAMP Level 1A data from CDAAC	web	BUFR/netCDF
GRM-32-L2-D-R1	Reprocessed Dry Temperature Profile	RDPCCHA	Climate Record	Data	CHAMP Level 1A data from CDAAC	web	BUFR/netCDF
GRM-33-L1-B-R1	Reprocessed Bending Angle	RBAGRA	Climate Record	Data	GRACE Level 1A data from CDAAC	web	BUFR/netCDF

Product ID	Product name	Product acronym	Product type	Operational satellite input	Dissemination means	Dissemination format
GRM-33-L2-R-R1	Reprocessed Refractivity Profile	RRPGRA	Climate Data Record	GRACE Level 1A data from CDAAC	web	BUFR/netCDF
GRM-33-L2-D-R1	Reprocessed Dry Temperature Profile	RDPGRA	Climate Data Record	GRACE Level 1A data from CDAAC	web	BUFR/netCDF

1.2 Applicable and Reference documents

1.2.1 Applicable documents

The following list contains documents with a direct bearing on the contents of this document.

- [AD.1] CDOP-3 Proposal: Proposal for the Third Continuous Development and Operations Phase (CDOP-3); Ref: SAF/ROM/DMI/MGT/CDOP3/001 Version 1.2 of 31 March 2016, Ref: EUM/C/85/16/DOC/15, approved by the EUMETSAT Council at its 85th meeting on 28-29 June 2016.
- [AD.2] CDOP-3 Cooperation Agreement: Agreement between EUMETSAT and DMI on the Third Continuous Development and Operations Phase (CDOP-3) of the Radio Occultation Meteorology Satellite Applications Facility (ROM SAF), Ref. EUM/C/85/16/DOC/19, approved by the EUMETSAT Council and signed at its 86th meeting on 7 December 2016.
- [AD.3] ROM SAF Product Requirements Document, Ref. SAF/ROM/DMI/MGT/PRD/001.

1.2.2 Reference documents

The following documents provide supplementary or background information, and could be helpful in conjunction with this document:

- [RD.1] Burrows, C., Healy, S., and Culverwell, I., Improvements to the ROPP refractivity and bending angle operators, Ref: SAF/ROM/METO/REP/RSR/015, 2013.
- [RD.2] Culverwell, I. D. and Healy, S. B., Simulation of L1 and L2 bending angles with a model ionosphere, Ref: SAF/ROM/METO/REP/RSR/017, 2015.
- [RD.3] Gorbunov, M. E., Lauritsen, K. B., Rhodin, A., Tomassini, M., and Kornblueh, L., Radio holographic filtering, error estimation, and quality control of radio occultation data, *J. Geophys. Res.*, *111*, D10 105, 2006.
- [RD.4] ROM SAF, WMO FM94 (BUFR) specification for radio occultation data, SAF/ROM/METO/FMT/BUFR/001, Version 2.4, 2016.
- [RD.5] ROM SAF, Algorithm Theoretical Baseline Document: Level 1B Bending angles., Ref. SAF/ROM/DMI/ALG/BA/001, Version 1.5, 2018.

- [RD.6] ROM SAF, Algorithm Theoretical Baseline Document: Level 2A Refractivity profiles., Ref. SAF/ROM/DMI/ALG/REF/001, Version 1.6, 2018.
- [RD.7] ROM SAF, Algorithm Theoretical Baseline Document: Level 2A dry temperature profiles., Ref. SAF/ROM/DMI/ALG/TDRY/001, Version 1.5, 2018.
- [RD.8] Zeng, Z., Sokolovskiy, S., Schreiner, W., Hunt, D., Lin, J., and Kuo, Y.-H., Ionospheric correction of GPS radio occultation data in the troposphere, *Atmos. Meas. Tech.*, 9, 335–346, <https://doi.org/10.5194/amt-9-335-2016>, 2016.

1.3 Acronyms and abbreviations

ATBD	Algorithm Technical Baseline Document
BUFR	Binary Universal Format for data Representation
CDAAC	COSMIC Data Analysis and Archival Center
CDOP	Continuous Development and Operations Phase
CDR	Climate Data Record
CHAMP	Challenging Mini-Satellite Payload
COSMIC	Constellation Observing System for Meteorology, Ionosphere & Climate
DMI	Danish Meteorological Institute
ECF	Earth-Centered, Fixed
ECI	Earth-Centered, Inertial
ECMWF	European Centre for Medium-Range Weather Forecasts
EPS	EUMETSAT Polar satellite System
EPS-SG	EPS Second Generation
ERA	European Reanalysis
ERA-I	ERA-Interim
EUMETSAT	European Organisation for the Exploitation of Meteorological Satellites
GNSS	Global Navigation Satellite System
GPAC	GNSS RO Processing and Archiving Centre
GPS	Global Positioning System (US)
GRACE	Gravity Recovery and Climate Experiment
GRAS	GNSS Receiver for Atmospheric Sounding
ICDR	Interim CDR
IEEC	Institut d'Estudis Especials de Catalunya (Spain)
Metop	Meteorological Operational polar satellites (EUMETSAT)
NCO	Numerically Controlled Oscillator
NRT	Near Real-Time
NWP	Numerical Weather Prediction
QC	Quality Control
RO	Radio Occultation
ROM SAF	The EUMETSAT Satellite Application Facility responsible for operational processing of radio occultation data from the Metop satellites. Members are DMI (leader), UKMO, ECMWF and IEEC.
ROPP	Radio Occultation Processing Package
SAF	Satellite Application Facility (EUMETSAT)
SSW	Sudden Stratospheric Warming
UCAR	University Corporation for Atmospheric Research

UK	United Kingdom
UKMO	UK Meteorological Office (aka: Met Office)
UTC	Universal Time Coordinated
WMO	World Meteorological Organization

1.4 Definitions

RO data products from the GRAS instrument onboard Metop and RO data from other missions are grouped in *data levels* (Level 0, 1, 2, or 3) and *product types* (NRT, offline, CDR, or ICDR). The data levels and product types are defined below¹. The lists of variables should not be considered as the complete contents of a given data level, and not all data may be contained in a given data level.

Data levels:

Level 0: Raw sounding, tracking and ancillary data, and other GNSS data before clock correction and reconstruction;

Level 1A: Reconstructed full resolution excess phases, total phases, pseudo ranges, SNRs, orbit information, I, Q values, NCO (carrier) phases, navigation bits, and quality information;

Level 1B: Bending angles and impact parameters, tangent point location, and quality information;

Level 2: Refractivity, geopotential height, “dry” temperature profiles (Level 2A), pressure, temperature, specific humidity profiles (Level 2B), surface pressure, tropopause height, planetary boundary layer height (Level 2C), ECMWF model level coefficients (Level 2D), quality information;

Level 3: Gridded or resampled data, that are processed from Level 1 or 2 data, and that are provided as, e.g., daily, monthly, or seasonal means on a spatiotemporal grid, including metadata, uncertainties and quality information.

Product types:

NRT product: Data product delivered less than: (i) 3 hours after measurement (SAF Level 2 for EPS); (ii) 80 min after measurement (SAF Level 2 for EPS-SG Global Mission); (iii) 40 min after measurement (SAF Level 2 for EPS-SG Regional Mission);

Offline product: Data product delivered from less than 5 days to up to 6 months after measurement, depending on the requirements. The evolution of this type of product is driven by new scientific developments and subsequent product upgrades;

CDR: Climate Data Record generated from a dedicated reprocessing activity using a fixed set of processing software². The data record covers an extended time period of several years (with a fixed end point) and constitutes a homogeneous data record appropriate for climate usage;

¹Note that the level definitions differ partly from the WMO definitions: http://www.wmo.int/pages/prog/sat/dataandproducts_en.php

²(i) GCOS 2016 Implementation Plan; (ii) <http://climatemonitoring.info/home/terminology>

ICDR: An Interim Climate Data Record (ICDR) regularly extends in time a (Fundamental or Thematic) CDR using a system having optimum consistency with and lower latency than the system used to generate the CDR³.

1.5 Overview of this document

Chapter 2 gives the background for the validation, and Chapter 3 contains the validation results. Compliance with product requirements is discussed in Chapter 4, whereas Service Specifications are determined in Chapter 5. Conclusions are made in Chapter 6.

³<http://climatemonitoring.info/home/terminology> (the ICDR definition was endorsed at the 9th session of the joint CEOS/CGMS Working Group Climate Meeting on 29 March 2018).

2 Background

The ROM SAF reprocessing #1 consists of the reprocessing of four radio occultation (RO) missions, together covering a period of ~15 years until the end of 2016. The product version numbers of the products validated in this report is 1.0, and the Climate Data Record (CDR) as a whole, is referred to as ROM SAF CDR v1.0.

2.1 Missions and time coverage

The missions, their respective satellites, and the covered periods for each mission are given in Table 2.1. It should be noted that for COSMIC not all RO instruments in the constellation have been operating in the full period, especially towards the end of the period, and for GRACE, both RO instruments are never in operation at the same time. Metop-B was only launched in September 2012, and RO operation started in October 2012. The very early data from CHAMP (until September 2001) has not been included.

Table 2.1: Missions, satellites, and time periods in the ROM SAF reprocessing #1.

Mission	Metop	COSMIC	CHAMP	GRACE
Satellites	Metop-A Metop-B	FM1; FM2; FM3 FM4; FM5; FM6	CHAMP	GRACE-A GRACE-B
Periods	Oct'06–Dec'16	Apr'06–Dec'16	Sep'01–Oct'08	Mar'07–Dec'16

2.2 Input data

The input Level 1A data for Metop (GRM-29-R1) are provided by the EUMETSAT Secretariat as part of their reprocessed Level 1A and 1B data, version 1.4. For COSMIC (GRM-30-R1), CHAMP (GRM-32-R1), and GRACE (GRM-33-R1), the input Level 1A data are provided by UCAR/CDAAC, more specifically, CDAAC reprocessed or post-processed atmPhs and (for COSMIC) gpsBit files. For the CDAAC data, not all missions and time periods share the same version number. Table 2.2 gives an overview of the different providers and the version numbers for the data used as input to the ROM SAF reprocessing #1, whereas Table 2.3 gives more detailed information about the different CDAAC versions and the used time periods.

Table 2.2: Input data providers and versions.

Mission	Metop	COSMIC	CHAMP	GRACE
Data provider	EUM. Secr.	UCAR/CDAAC	UCAR/CDAAC	UCAR/CDAAC
Input versions	1.4	2013.3520 2014.2860 2016.1120	2014.0140	2010.2640 2014.2760

Table 2.3: CDAAC versions and time periods used in ROM SAF reprocessing #1.

CDAAC version	CDAAC name	CDAAC processing mode	year.doy time period
2013.3520	cosmic2013	Re-processed	2006.112–2014.120
2014.2860	cosmic	Post-processed	2014.121–2016.365
2016.1120	cosmic	Post-processed	2016.366
2014.0140	champ2014	Re-processed	2001.245–2008.278
2010.2640	grace	Post-processed	2007.059–2014.089
2014.2760	grace	Post-processed	2014.090–2016.366

2.3 ROM SAF reprocessing

The bending angles, refractivities, and dry temperatures for all missions were retrieved at the ROM SAF at DMI using GPAC system version 2.3.0, with ROPP software version 8.1 as a key integral part. A number of modifications to ROPP 8.1 were made by the ROM SAF team during the reprocessing activity. The modifications affecting the data quality are described in the ATBDs [RD.5, RD.6, RD.7] and will appear in future official releases of ROPP. The Quality Control (QC) of the data analysed in this report is done with ROM SAF QC version 0.1.3.

The GPAC system returns the bending angle, refractivity, and dry temperature in both high-resolution (with a vertical spacing of about 100 m in the interval where measurements were made) and in low-resolution (247 pre-defined levels between the surface and 60 km). The high-resolution profiles are written to a netCDF file together with other key parameters. The low-resolution profiles are also stored in a netCDF file, but additionally also in BUFR format. The low-resolution profiles are thinned/interpolated versions of the high-resolution profiles without any smoothing. Each occultation is marked either nominal or non-nominal (same for low- and high-resolution) according to the QC checks described below. The quality flag definitions are given in the WMO FM94 (BUFR) Specification For Radio Occultation Data [RD.4]. For the validation we have used only nominal high-resolution data passing all QC checks.

2.4 Quality control

The QC checks and the limits given below are generally based on many years of experience with the processing of radio occultation data at the ROM SAF. The limits were chosen after careful analyses and consideration in order to flag “bad” profiles while not erroneously flagging too many “good” profiles.

The bending angle products are quality controlled and flagged as non-nominal if one of the following is true:

- Excess phase processing is flagged as non-nominal by the provider
- The L2 quality score is larger than a value of 30 (cf. [RD.5, section 3.2.11])
- Retrieved impact parameter is not monotonically increasing

- There are no valid bending angles below 20 km or above 60 km impact height (valid values are between -0.001 and 0.1 rad)
- Optimized bending angle is different from the background profile used for statistical optimization by more than $5 \mu\text{rad}$ at any point above 60 km impact height
- Bending angle is different from the bending angle extracted from ERA-Interim forecasts by more than 90% at any point between 10 km and 40 km impact height
- Refractivity processing is flagged as non-nominal

The refractivity and dry temperature products are quality controlled and flagged as non-nominal if one of the following is true:

- Bending angle processing is flagged as non-nominal
- The factor used for scaling the climatology to fit the data below 40 km is different from 1.0 by more than 8% (cf. [RD.6, section 3.2.1])
- The factor used for scaling the climatology to fit the data above 60 km is different from 1.0 by more than 40% (cf. [RD.6, section 3.2.1])
- The weight given to the climatology in the statistical optimization exceeds 10% at any point below 40 km
- Retrieved altitude is not monotonically increasing
- There are no valid refractivities below 20 km or above 60 km altitude (valid values are between 0 and 500 N-units)
- Refractivity is not positive at all altitudes
- Refractivity is different from the refractivity extracted from ERA-Interim forecasts by more than 20% at any point below 5 km
- Refractivity is different from the refractivity extracted from ERA-Interim forecasts by more than 10% at any point between 5 km and 35 km
- Dry temperature is different from the dry temperature extracted from ERA-Interim forecasts by more than 20 K at any point between 30 km and 40 km

The refractivity and dry temperature are both Level 2A data, and share the same quality flag. We note that the dry temperature is retrieved from the refractivity by ignoring the presence of water vapour. This means that the dry temperature is close to the physical temperature if the water vapour contribution to the refractivity is small, which is generally the case in the upper troposphere and in the stratosphere. In general, dry temperature should be considered a variable in its own right, with sometimes large departures from the physical temperature in the lower troposphere. When comparing to ERA-Interim forecasts, the ERA-Interim forward modelled dry temperature is derived from the ERA-Interim forward modelled refractivity in the same manner as the dry temperature product is derived from the refractivity product (except that the forward modelled dry temperature is constrained by the physical temperature at the top of the model). The forward modeling to bending angle, refractivity, and dry temper-

ature was done with the ROPP software version 8.1, which include the vertical interpolation approach described in [RD.1].

As seen, all products are essentially subject to the same quality checks since refractivity (and dry temperature) is flagged if bending angle is flagged and vice versa. Thus, the nominal/non-nominal status apply to all of bending angle, refractivity, and dry temperature.

3 Profile comparisons

In this chapter we compare profiles of bending angle, refractivity, and dry temperature from the ROM SAF CDR v1.0 with reference data¹ from various sources. Most of the plots complement the plots that can be found at <http://www.romsaf.org/re1/index.php>, where monthly profile statistics for the whole period, in different latitude bands, and for all missions and individual satellites, using both ERA-Interim forecasts and ECMWF operational forecasts as background, can be found. The time series plots in Section 3.4 are taken from that site, whereas the monthly profile statistics throughout the chapter are made specifically for this report and should be seen as representative examples serving two purposes:

1. To illustrate the general quality of the ROM SAF CDR v1.0
2. To perform a more in-depth analysis in specific cases of unexpected results

The following sections discuss comparisons in a number of ways. In each section, new ways of comparing data are introduced before they may be used again for specific illustrations in the following sections. To assess the consistency of the data, we look at comparisons across missions, latitude bands, instrument upgrades, years, seasons, local times, and hemispheres. In all cases we show comparisons for both setting and rising occultations for those missions where that is relevant (Metop and COSMIC).

In most cases a background is used to give relative differences. This is indicated in the x-label of the plots with (O-B)/B or (O-C)/B. The C symbolizes the reference data that the comparison is against if it is not against a forecast, whereas the B is always either ERA-Interim forecasts or ECMWF operational forecasts. This is done to avoid divisions by very small numbers (or sometimes negative numbers) when the reference data are not necessarily very smoothly declining at high altitudes.

The references that the ROM SAF CDR v1.0 profiles are compared to are:

- ERA-Interim forecasts
- ECMWF operational forecasts
- Optimized bending angle
- Reprocessed and post-processed products from UCAR/CDAAC
- Reprocessed Metop bending angle from the EUMETSAT Secretariat (v1.4)
- Reprocessed Metop data from the ROM SAF, but based on input data from UCAR

ERA-Interim (ERA-I) forecasts are used most extensively, since they are considered to be of a consistent quality over the 15 year period of the reprocessing. They were extracted from $1^\circ \times 1^\circ$ GRIB files at the reference location of the given occultation (not varying with height), and interpolated to the time of the occultation using the two nearest 3-hourly forecasts (forecast periods of 3, 6, 9, or 12 hours). ECMWF operational forecasts were also extracted from

¹ The use of the word 'reference' here and in the following does not imply that these data are necessarily closer to the truth than the occultation data.

1° × 1° GRIB files at the reference location, but not interpolated in time; profiles were extracted only from the nearest 6-hourly forecast (forecast periods of either 6 or 12 hours). In both cases the forecast profiles were forward modelled to bending angle, refractivity, and dry temperature.

In the plots, the reprocessing activity using input Level 1A data from the EUMETSAT Secretariat is referred to as RE1A. This only contains data from Metop. The reprocessing activity using input data from UCAR/CDAAC is referred to as RE1B. This contains data from COSMIC, GRACE, and CHAMP. Together, these reprocessing activities resulted in ROM SAF CDR v1.0. Additionally, Metop was also reprocessed based on data from UCAR/CDAAC. In the plots, this is also referred to as RE1B. Thus, for COSMIC, GRACE, and CHAMP, there is only RE1B reprocessed data, whereas for Metop, there is both RE1A and RE1B. The latter is not part of the ROM SAF CDR v1.0, but is used for additional validation. When not specifically labeled, plots are showing the statistics of the ROM SAF CDR v1.0 product.

Most plots contain three panels showing monthly statistics of the mean difference to the reference, the standard deviation of the difference, and either the vertical correlation of the difference at 15 km with that over the rest of the profile, or the percentage of nominal observations in the lowest 10 km, from which also the reduction at the lowest altitudes can be seen (e.g., Fig. 3.1). In the following we refer to the latter as the penetration statistics.

The correlation is the ordinary Pearson correlation using relative differences, and is mostly shown for the refractivity products because these are the products where the correlations best reveal degradation due to L2-extrapolation in the troposphere, whereas for bending angle and dry temperature, the correlations are only affected to a smaller degree. Although vertical correlations exist at all altitudes, we have chosen to show only the correlation of the difference at 15 km with that over the rest of the profile because the degradation due to the L2-extrapolation appears to be largest between 10 km and 20 km. Consequently, these curves always peak at 15 km, where the correlation by construction equals one. The number of samples included in the correlation plots is generally different at each level, depending on how far down the profiles reach.

The number of observations only count nominal occultations and is mostly (when given in percent) relative to the total number of profiles that were processed for a given period. These panels are only shown for bending angle, since the numbers are the same for refractivity and dry temperature, only shifting the curves a bit at the bottom due the difference between altitude and impact height. Altitude is the mean sea level altitude, i.e, relative to the geoid. Impact height is the impact parameter with the radius of curvature subtracted.

When the reference is other reprocessed data sets, only occultations that are common to the reference, and also marked nominal by the provider of the reference, are included. For consistency, when plotting both ROM SAF CDR v1.0 and reference data against a common background, it is also only the common nominal occultations that are included.

Regarding the penetration, it should be noted that the extracted background profiles from ERA-I forecasts and ECMWF operational forecasts were generated in conjunction with the ROM SAF CDR v1.0, and only contain data to the lowest altitude of the corresponding profiles from the ROM SAF CDR v1.0 product. Thus, the penetration statistics of the reprocessed products from other providers may be substantially wrong in those cases where the

providers profiles actually reached to lower altitudes than the ROM SAF CDR v1.0 product. Such cases can be identified as those where the number of observations with altitude is illustrated as being basically the same as that of the ROM SAF CDR v1.0 product.

To limit the number of possible plots in this report, we show the monthly profile statistics for a few months only, and use October 2007 and 2016 as baseline months². The quality of the data in these months are considered to be representative of the general quality of the rest of the ROM SAF CDR v1.0 for all missions. When assessing seasonal variations and the impact of instrument software upgrades, statistics from other periods are shown as well, and in particular, Section 3.4 shows time series of the monthly statistics.

In the interest of overview when reading this report, and to limit the number of pages, we have chosen to include up to eight plots of monthly profile statistics on each page (and up to four time series plots on each page in Section 3.4). This makes the figures quite small, and in some cases it can be difficult to see all details in a paper print-out. However, the resolution in the electronic version of the document should be high enough to see all details on a computer screen.

²October was chosen for no particular reason, but using the same month in both 2007 and 2016 is deliberate in that possible seasonal variations in the biases of the model data are kept out of the picture.

3.1 Comparison across missions

In this section we show the statistics against ERA-I forecasts for the four different missions of the ROM SAF CDR v1.0 (Metop, COSMIC, GRACE, CHAMP) to point out differences and similarities. We use the two baseline months (October 2007, October 2016) and show global statistics as well as statistics separated into latitude bands. These are:

Low latitudes: 30°S to 30°N

Mid latitudes: 60°S to 30°S and 30°N to 60°N

High latitudes: 90°S to 60°S and 60°N to 90°N

The points to be made from this section are that the four missions show fairly similar statistics in bending angle, refractivity, and dry temperature. Main exceptions are:

- Different biases at low altitudes (below 6 km), especially at low latitudes, which are believed to be fundamentally linked to the different instruments and their tracking; in comparisons to ERA-I forecasts, the biases near the surface at low latitudes are about 3% in bending angle and refractivity, and 8 K in dry temperature
- Different noise levels resulting in different standard deviations at high altitudes (above 25 km); Metop has the lowest standard deviation, followed by COSMIC, GRACE, and CHAMP
- Different penetration depths into the lower troposphere; Metop and COSMIC penetrating to lower altitudes than GRACE and CHAMP, especially at low latitudes
- Differences between setting and rising occultations for Metop and COSMIC, both in terms of bias and standard deviation, believed to be fundamentally linked to the different instruments and their tracking

3.1.1 Bending angle

Figure 3.1 shows four plots (each with three panels) of the monthly global profile statistics of bending angle for all four missions (except for CHAMP in 2016, which no longer operated at that time). The top plots are for October 2007, and the bottom ones for October 2016. The left plots show the total statistics, whereas the right plots show the statistics for Metop and COSMIC separated into setting and rising occultations (GRACE and CHAMP provide only setting occultations). Figures 3.2, 3.3, and 3.4 show the same for low, mid, and high latitudes.

The (O-B)/B means are very similar among the missions down to about 8 km in all plots. From there, the means are increasingly different downward, especially at low latitudes. In other words, the different missions are biased with respect to each other (and to ERA-I) in the lower moist troposphere. These biases are considered to be fundamentally linked to the different instruments. The GRACE and CHAMP instruments do not have open loop capabilities (as opposed to Metop and COSMIC) and the tracking does not reach as low as Metop and COSMIC. This is reflected in the panels showing the number of observations below 10 km. The means of Metop and COSMIC below 8 km are also different, and for both missions we see a notable difference between setting and rising. These differences are not fully understood, but are believed to be due to the COSMIC instruments tracking lower than the

Metop instruments, in general, and rising not being tracked as low as setting in both missions. The onboard tracking strategy for rising occultations was changed for Metop in 2013 (see Section 3.3). This impacted the mean of Metop rising occultations, especially in the moist lower troposphere, and explains the differences in this region between the 2007 and 2016 plots. The rising/setting differences, and their development over time, are discussed further in Section 3.4. In the lowest part of the troposphere (below ~3 km impact height), all missions are considerably negatively biased against ERA-I. The biases near the surface at low latitudes are about 3%. Part of the biases may be related to super refraction in the moist planetary boundary layer, where the signal may be temporarily lost, posing severe challenges for the tracking and the processing. It should be noted, however, that if very sharp negative vertical gradients are detected in the reference model data (here ERA-I), the reference below that impact height is not computed, and the comparisons consequently do not include such points.

The (O-B)/B standard deviations are different above 25 km reflecting different noise levels for the different missions. This is also considered fundamentally linked to the different instruments. Metop data are the least noisy (which is well known), followed by COSMIC, GRACE and CHAMP. We also see that the standard deviations in 2007 are larger for rising occultations than for setting occultations, for both Metop and COSMIC. For Metop, the changed tracking strategy in 2013 reduced the standard deviations for rising occultations at these high altitudes to the same level as the ones for setting occultations. For COSMIC, the larger standard deviation is due to a varying quality for the FM5 satellite over many months in 2007. This is discussed further in Section 3.4. Around 25–30 km, especially at low latitudes, the standard deviation for COSMIC is lower than for Metop (and the other missions). This is seen to be due to a larger standard deviation for rising Metop occultations in 2007, and a smaller standard deviation for setting COSMIC occultations in 2016. These differences are not fully understood, but they may be related to instrument upgrades for Metop and COSMIC over time. This is discussed further in Section 3.3. Below 25 km the standard deviations are very similar for all missions, but this should be seen in the light of relatively fewer observations for GRACE and CHAMP reaching into the moist lower troposphere.

The percentage of profiles passing the quality control is generally highest for Metop and GRACE (in that order), followed by COSMIC and CHAMP. In the 2007 plots, it is seen that the rising Metop occultations did not penetrate into the lower troposphere as well as setting occultations at the time, especially at low latitudes. The Metop instrument upgrades in 2013 improved on that. In the 2016 plots, the percentage of nominal rising COSMIC occultations is only about 50%, indicating a degradation in the quality of rising COSMIC occultations over time. The sudden decrease in the number of observations below 5 km impact height at high latitudes for all missions is related to the Antarctica, where the orography and the ice sheet limit the penetration.

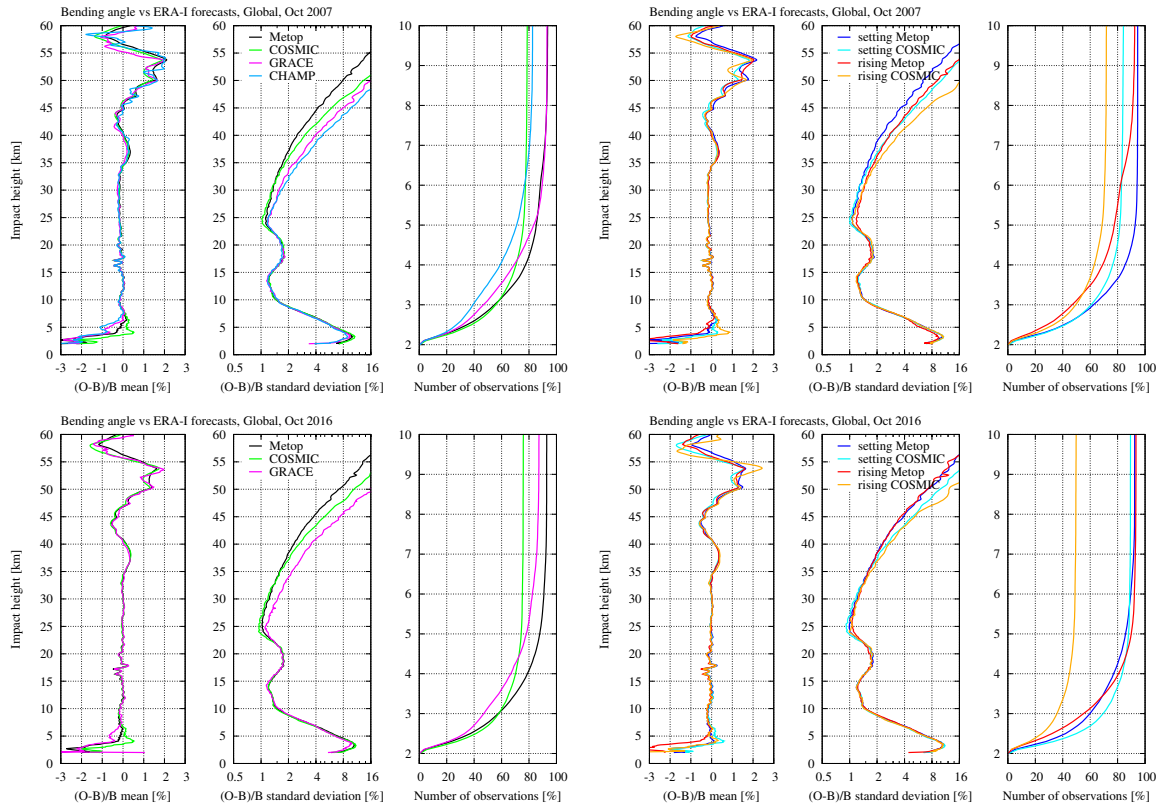


Figure 3.1: Monthly global profile statistics of bending angle for different missions.

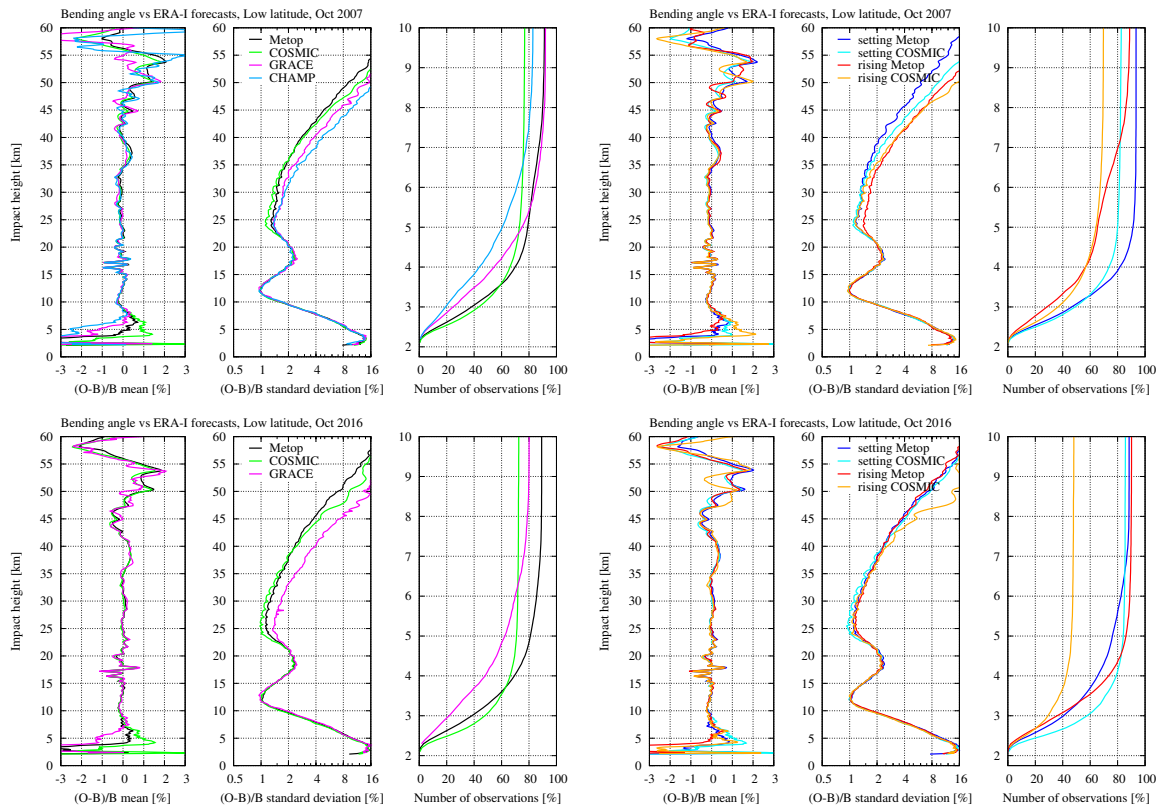


Figure 3.2: Monthly low latitude profile statistics of bending angle for different missions.

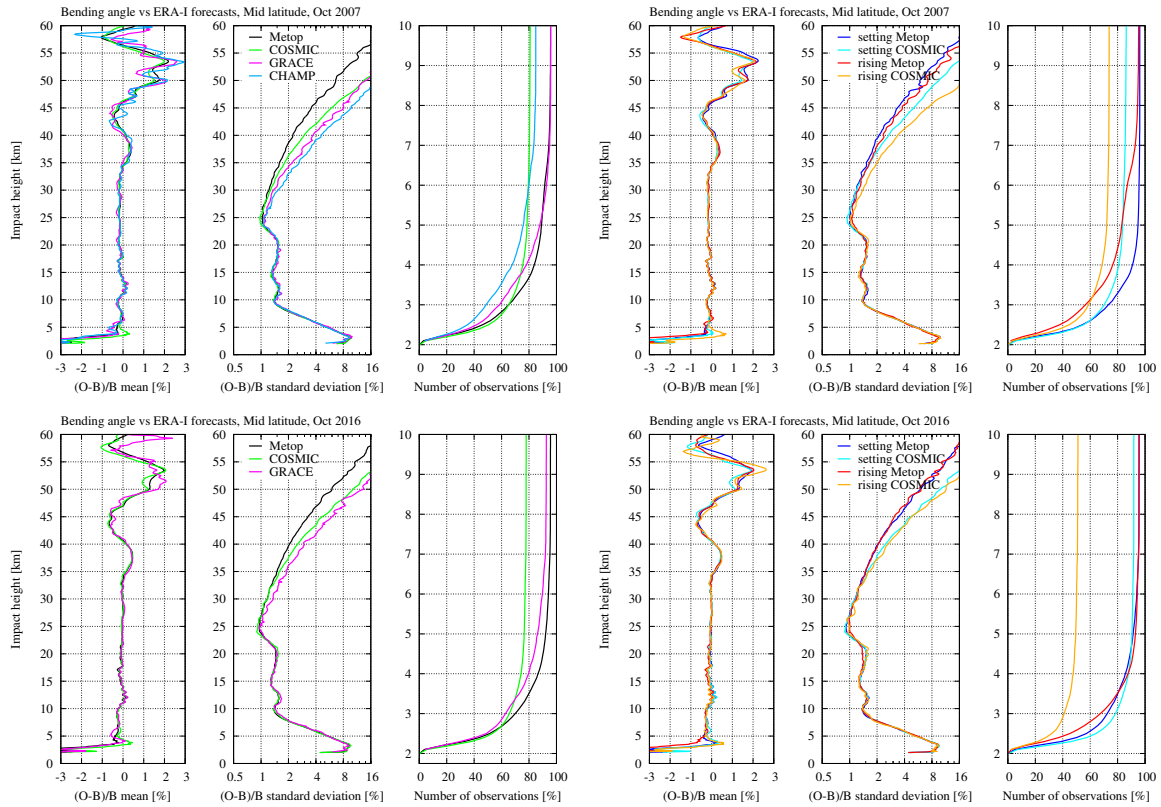


Figure 3.3: Monthly mid latitude profile statistics of bending angle for different missions.

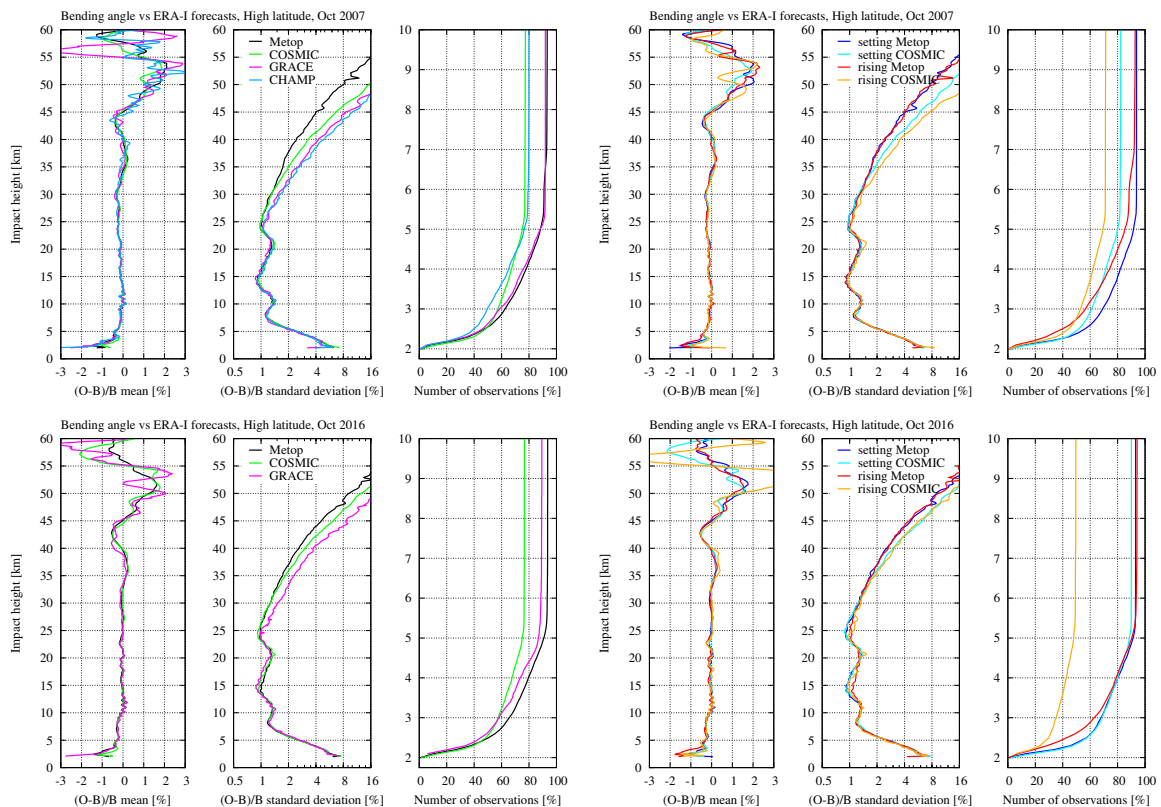


Figure 3.4: Monthly high latitude profile statistics of bending angle for different missions.

3.1.2 Refractivity

In this subsection we show and discuss the plots for refractivity corresponding to the plots for bending angle in the previous subsection. Figure 3.5 shows the global statistics, whereas Figs. 3.6, 3.7, and 3.8 show the statistics for low, mid, and high latitudes. Instead of the number of observations in the third panel of the plots, we here show the vertical correlations of the difference at 15 km with that over the rest of the profile.

The comments made about the $(O-B)/B$ means for bending angle also apply to the refractivity, although the magnitude percentage wise is a little smaller, and the altitude below which the different missions are biased with respect to each other at low latitudes, is about 6 km (as opposed to 8 km impact height).

The $(O-B)/B$ standard deviations above 35 km are notably smaller for Metop than for the other missions. Again, this is considered to be linked to the noise in the data, but it is interesting that the standard deviations for COSMIC, GRACE, and CHAMP are very similar for refractivity, as opposed to in bending angle, where they are more different. This apparent inconsistency is not fully understood, but it is perhaps related to the statistical optimization at higher altitudes (limiting the noise in optimized bending angle) in combination with the error propagation through the Abel transform. The impact of statistical optimization is discussed further in Section 3.2. The comment made for bending angle regarding a lower standard deviation for COSMIC around 25–30 km, can be made for refractivity as well, but the difference is even more subtle here and only visible in the low latitude plots.

In the 2016 plots, between 10 km and 20 km, the standard deviation for Metop is larger than for the other missions. This is understood to be a consequence of the instrument upgrades for Metop in 2013, after which the L2 signal in rising occultations is only tracked above ~ 20 km. This means that the L2-extrapolation into the troposphere is done from a higher altitude for rising Metop occultations than for the other missions. The larger standard deviation is accompanied by a broadening in the vertical correlations as can be seen in the third panels of the 2016 plots. This indicates that differences to ERA-I forecasts are to the same side at adjacent altitudes, and that the error made over a wide vertical range when doing the L2-extrapolation is mostly either positive or negative for a given occultation. The larger standard deviation and vertical correlations are most significant at higher latitudes. This might be interpreted as a larger uncertainty in the extrapolation at higher latitudes. For COSMIC rising occultations, at mid and high latitudes, we can also see a degradation due to the L2-extrapolation in the 2016 plots, but not as much as for Metop. The reason for the difference in this respect between the 2007 and 2016 plots for COSMIC is not fully understood, but could be related to the solar cycle as will be discussed in Section 3.4. Additional analyses on the L2-extrapolation, focusing on the impact on the mean below 20 km (cf. Section 3.3), is provided in Section 3.8.

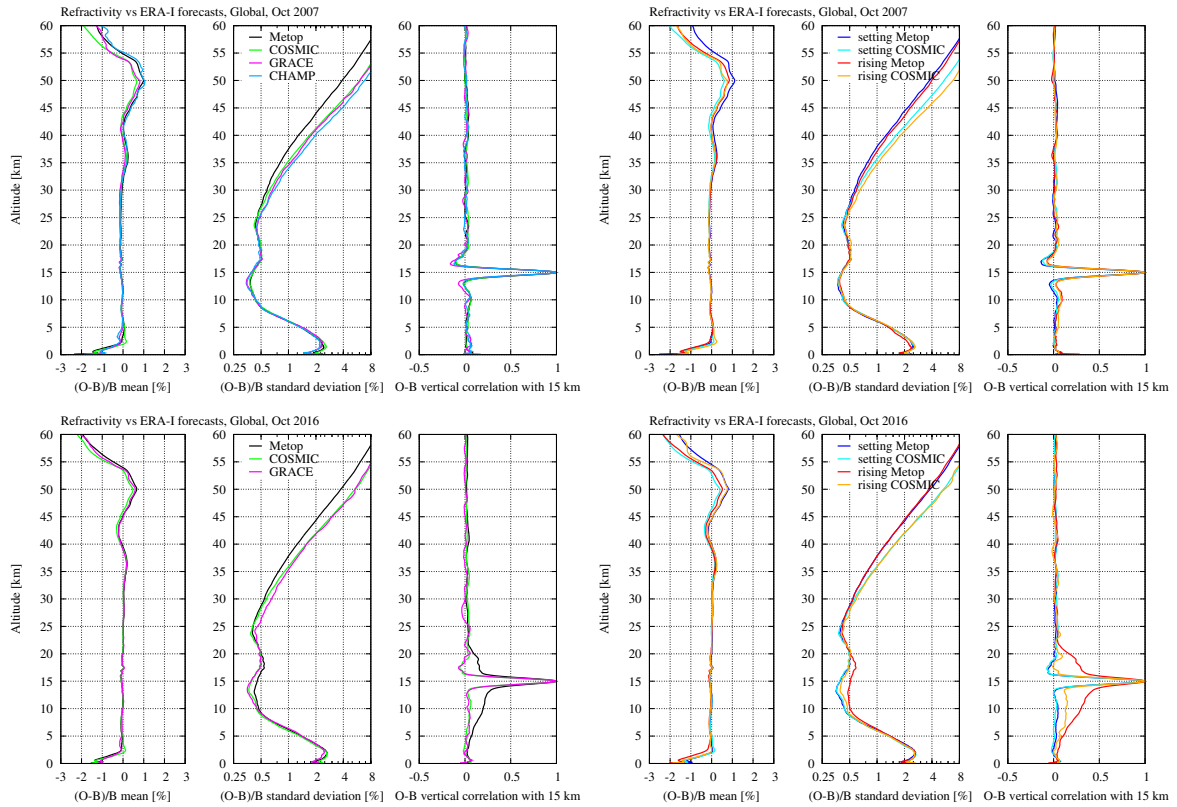


Figure 3.5: Monthly global profile statistics of refractivity for different missions.

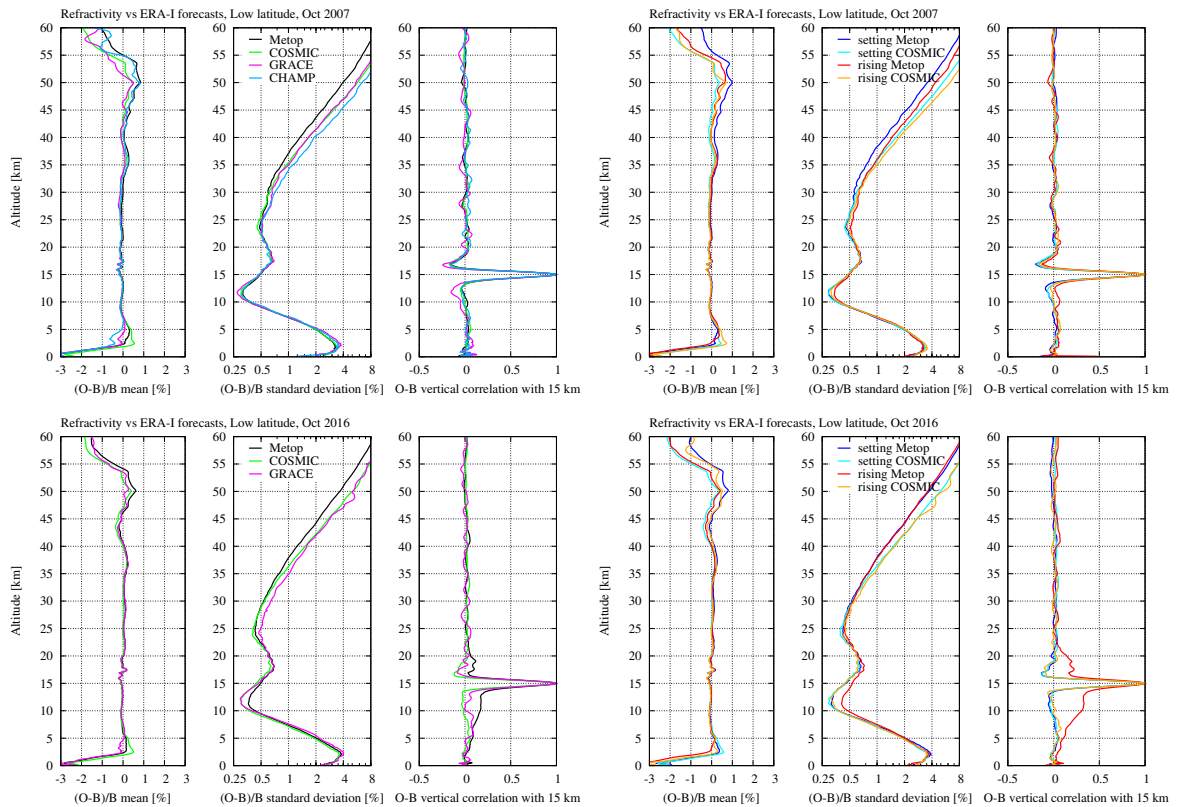


Figure 3.6: Monthly low latitude profile statistics of refractivity for different missions.

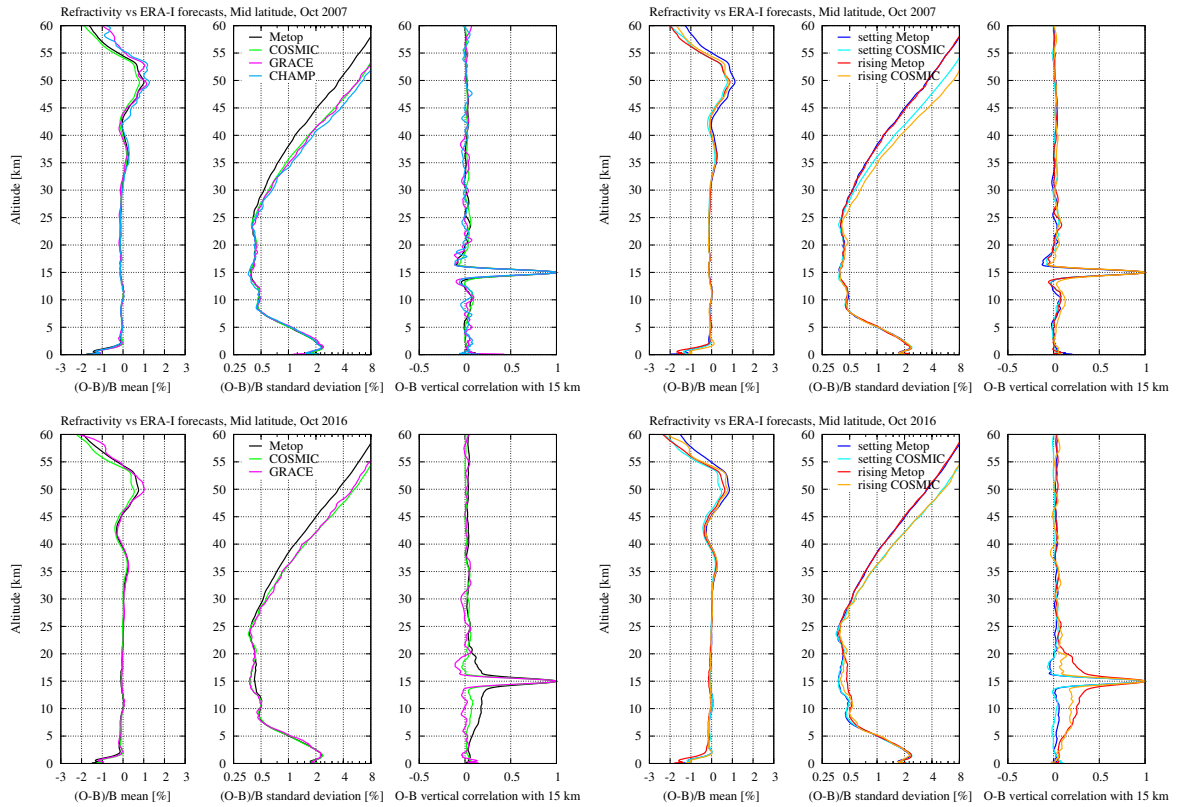


Figure 3.7: Monthly mid latitude profile statistics of refractivity for different missions.

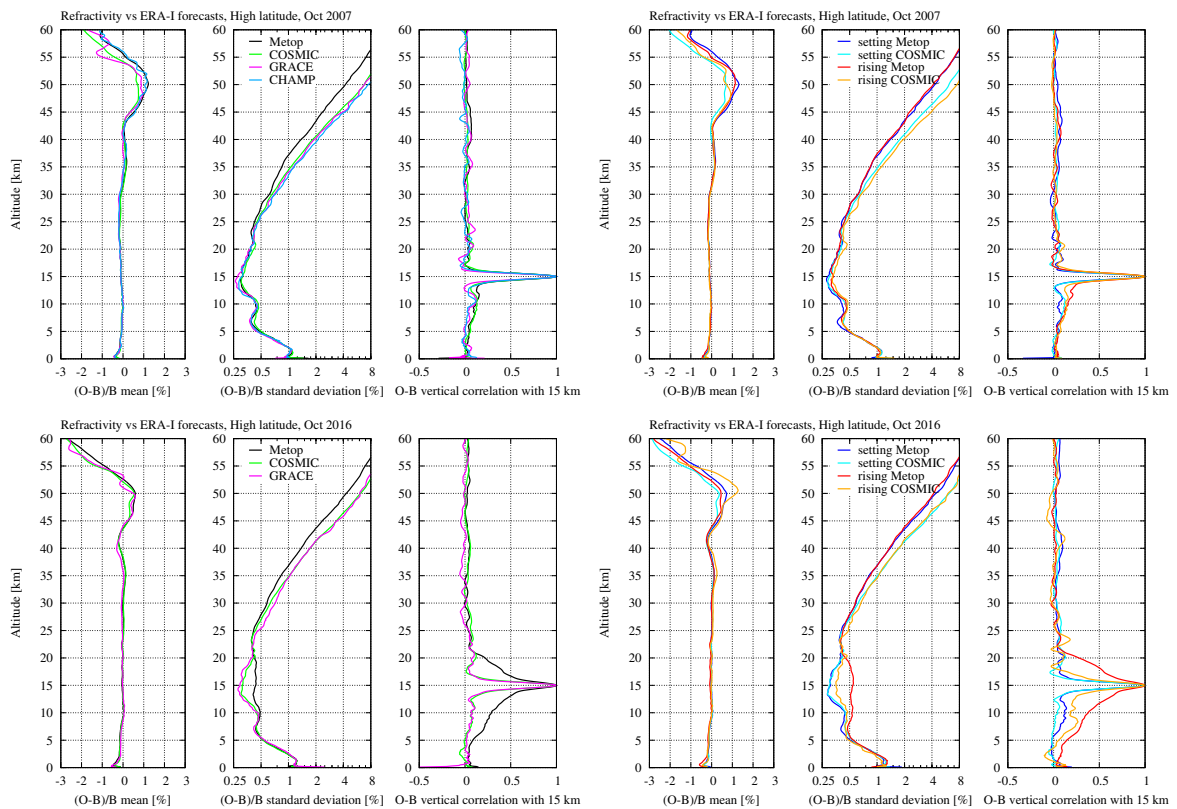


Figure 3.8: Monthly high latitude profile statistics of refractivity for different missions.

3.1.3 Dry temperature

The plots for dry temperature, corresponding to the plots for bending angle and refractivity in the previous subsections, are shown in Figs. 3.9, 3.10, 3.11, and 3.12 .

The (O-B)/B means are basically a mirror of the ones in refractivity up to about 35 km, being a consequence of the equation relating refractivity (N), dry temperature (T), and dry pressure. The relation leads to $\Delta N/N \approx -\Delta T/T$, as long as the pressure difference is small enough to be ignored. When we here plot O-B for dry temperature, the mirroring to (O-B)/B in refractivity is less obvious, but can still be recognized. The mirroring is discussed more in Section 3.2. The means are fairly similar for all missions except for the differences below 6 km already mentioned in the previous subsections. There are also differences at very high altitudes, which were also seen in bending angle and refractivity, but they become more evident in dry temperature because they propagate to slightly lower altitudes than in refractivity (visible in dry temperature down to about 35 km). Although some of these differences are larger than the differences below 6 km, they are not considered as important, and may not be statistically significant given the large standard deviation at high altitudes.

The standard deviations in dry temperature reflect more or less the ones in refractivity, except in the range between 10 km and 20 km in the 2016 plots. Here the effects of the L2-extrapolation are much smaller than for refractivity, although they are still visible in the high latitude plots. The apparent fact that the dry temperature statistics are less sensitive to the effects of the L2-extrapolation is not understood in detail, but we conclude that it is a consequence of the error propagation from refractivity to dry temperature.

The vertical correlations are somewhat similar for the different missions. Interestingly, the statistical differences to ERA-I at altitudes above 20 km correlate slightly with the differences at 15 km, but more so for COSMIC and CHAMP than for Metop and GRACE. Again, the details of this are not understood, but we conclude that it is a consequence of the error propagation from refractivity to dry temperature.

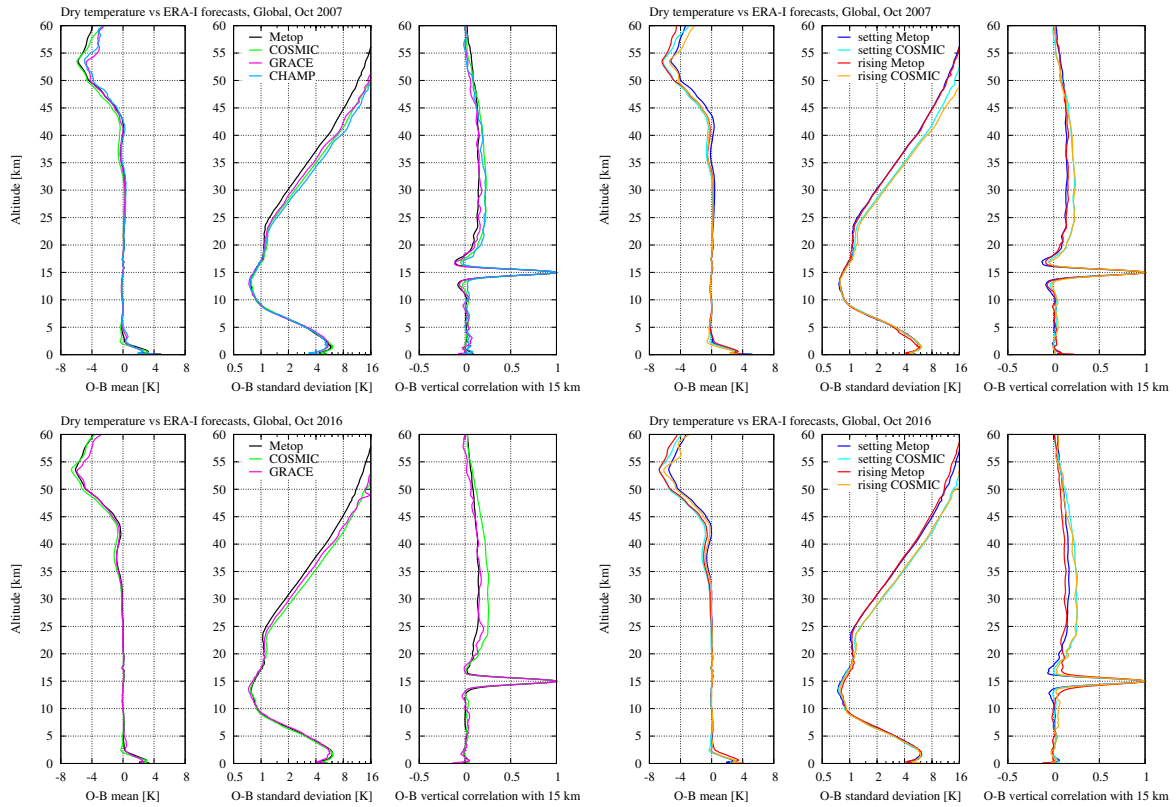


Figure 3.9: Monthly global profile statistics of dry temperature for different missions.

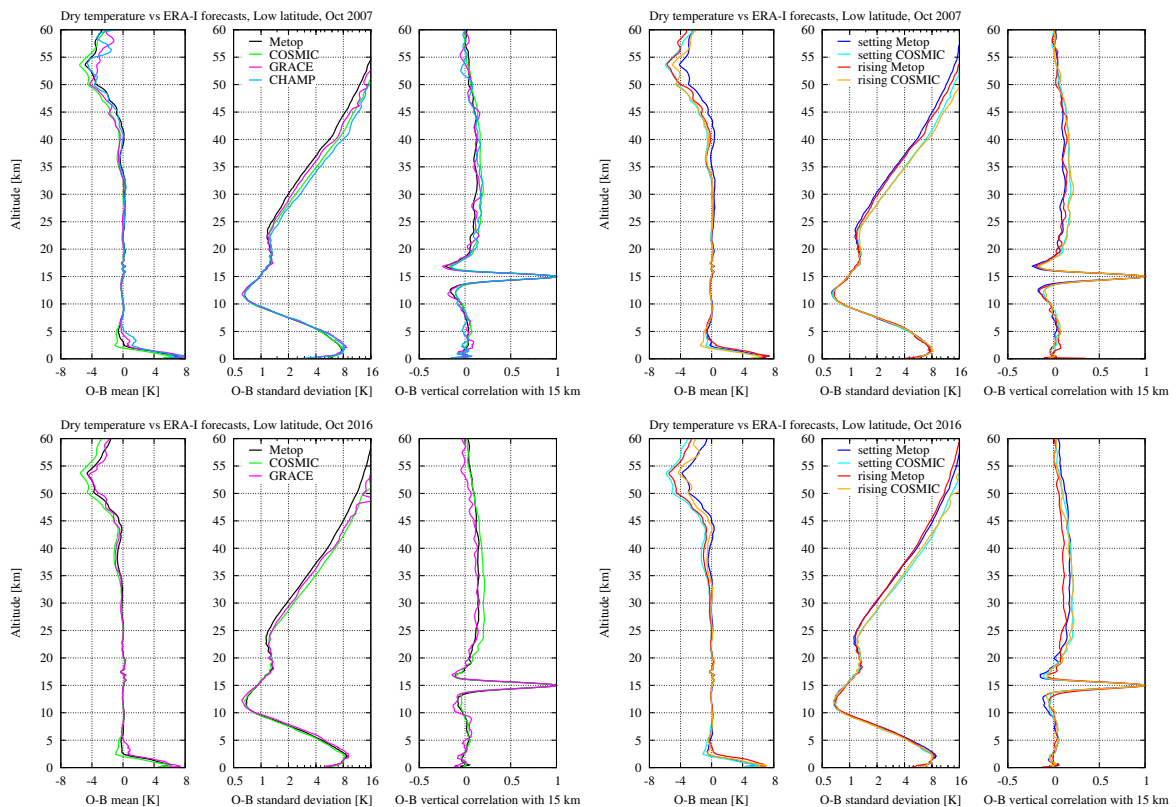


Figure 3.10: Monthly low latitude profile statistics of dry temperature for different missions.

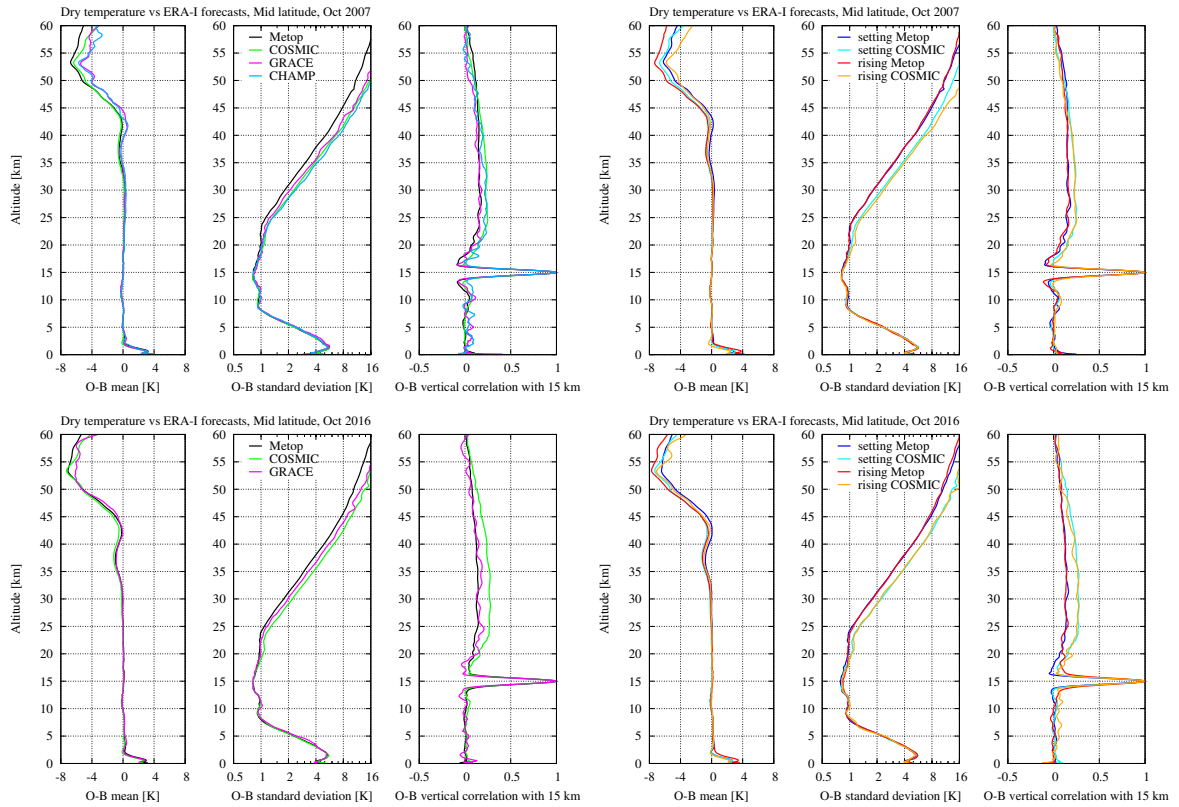


Figure 3.11: Monthly mid latitude profile statistics of dry temperature for different missions.

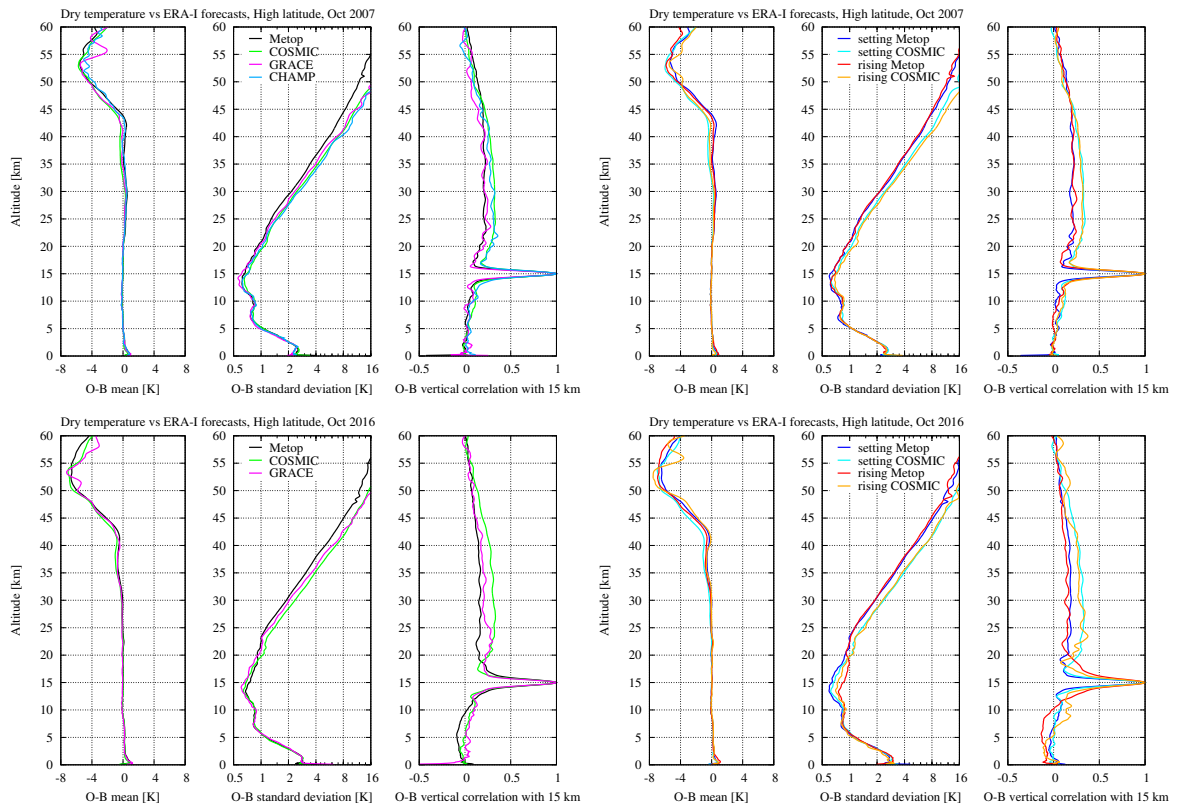


Figure 3.12: Monthly high latitude profile statistics of dry temperature for different missions.

3.2 Comparison against different background models

The purpose of the statistics shown in this section is to demonstrate that the (O-B)/B mean being different from zero at high altitudes (especially above 30 km), seen in most plots throughout this report, is to a large degree due to systematic biases in the model data (ERA-I forecasts and ECMWF operational forecasts) rather than in the occultation data. We show the statistics for Metop and COSMIC against both ERA-I forecasts and ECMWF operational forecasts and discuss the differences, and also discuss the impact of the statistical optimization on the means and standard deviations of all missions. As before, we use the two baseline months (October 2007, October 2016) and show plots that can be compared to the ones in the previous section.

It should be noted that the ERA-I system is based on an ECMWF system as of 2006, and the present operational ECMWF system is a more advanced version (for 2016 including 10 years of development) than the ERA-I system. Thus, as opposed to the ECMWF system, the ERA-I system has not changed over time. Nevertheless, ERA-I data may change over time due to the evolving global observing system, i.e., due to the different types and numbers of observations assimilated in the ERA-I system over time.

The points to be made from this section are that comparisons to different forecast models give very different results at altitudes above 30 km. The similarities between the (O-B)/B means of Metop and COSMIC, setting and rising occultations, as well as the very small differences in the mean between optimized and non-optimized bending angles up to at least 60 km for all missions, suggest that the occultation data in the mean at high altitudes may be more accurate than the models they are compared to. There are no indications that the statistical optimization introduces significant systematic biases below 50 km in the refractivity or dry temperature means, at least not under normal circumstances³.

3.2.1 Bending angle

Figure 3.13 shows the monthly global profile statistics of bending angle when compared to ERA-I forecasts and ECMWF operational forecasts for October 2016 (in the plots labelled ERA-I and ECMWF, respectively). The top plots are for Metop, and the bottom ones for COSMIC. The left plots show the total statistics, whereas the right plots show the statistics separated into setting and rising occultations. The comparisons against ERA-I are identical to the corresponding ones for Metop and COSMIC in Fig. 3.1.

The (O-B)/B means above 30 km are quite different for the two background models, indicating that much of the bias at high altitudes could be due to whichever model we compare against. There are also what appears to be substantial differences below 4 km, between 7 km and 10 km, and around the altitude of the tropopause. It becomes evident that the ragged behaviour between 15 km and 20 km in the ERA-I comparisons is due to its low vertical resolution (the ECMWF operational system having 137 vertical levels in 2016 compared to the 60 levels of the ERA-I system).

The (O-B)/B standard deviations are notably smaller in the comparisons to ERA-I around 25–40 km. However, it should be kept in mind that some of the quality control checks de-

³Normal circumstances here and in the following does not include periods of Sudden Stratospheric Warming events.

scribed in Section 2.4 use the ERA-I forecasts as a reference, and it is therefore likely that this, at least in part, is the reason for the smaller standard deviation when comparing the nominal occultations against ERA-I.

To illustrate that the statistical optimization does not introduce appreciable biases at high altitudes when going from bending angle to refractivity (via the optimized bending angle), Fig. 3.14 shows the statistics of the bending angle for all missions in October 2007 against the optimized bending angle between 40 km and 70 km. The (O-C)/B means (C in the numerator here being the optimized bending angle) up to 60 km are rather small when compared to the means in Fig. 3.13, giving evidence that no systematic bias seems to be introduced in this step, at least not under normal circumstances, and at least not below 60 km impact height. In Section 3.5 we discuss limitations to this conclusion in cases of Sudden Stratospheric Warming (SSW) events. The (O-C)/B standard deviations in Fig. 3.14 reflect the difference in noise levels for the different missions and for setting and rising occultations, corroborating the findings in the previous section. Below 40 km (not shown) the means and standard deviations are virtually zero as a result of the downward decreasing weight given to the background used for statistical optimization.

Figure 3.15 shows the statistics for the optimized bending angle against ERA-I for all missions, confirming the unaltered means and reduced standard deviations at high altitudes. This figure can be compared to the topmost plots of Fig. 3.1.

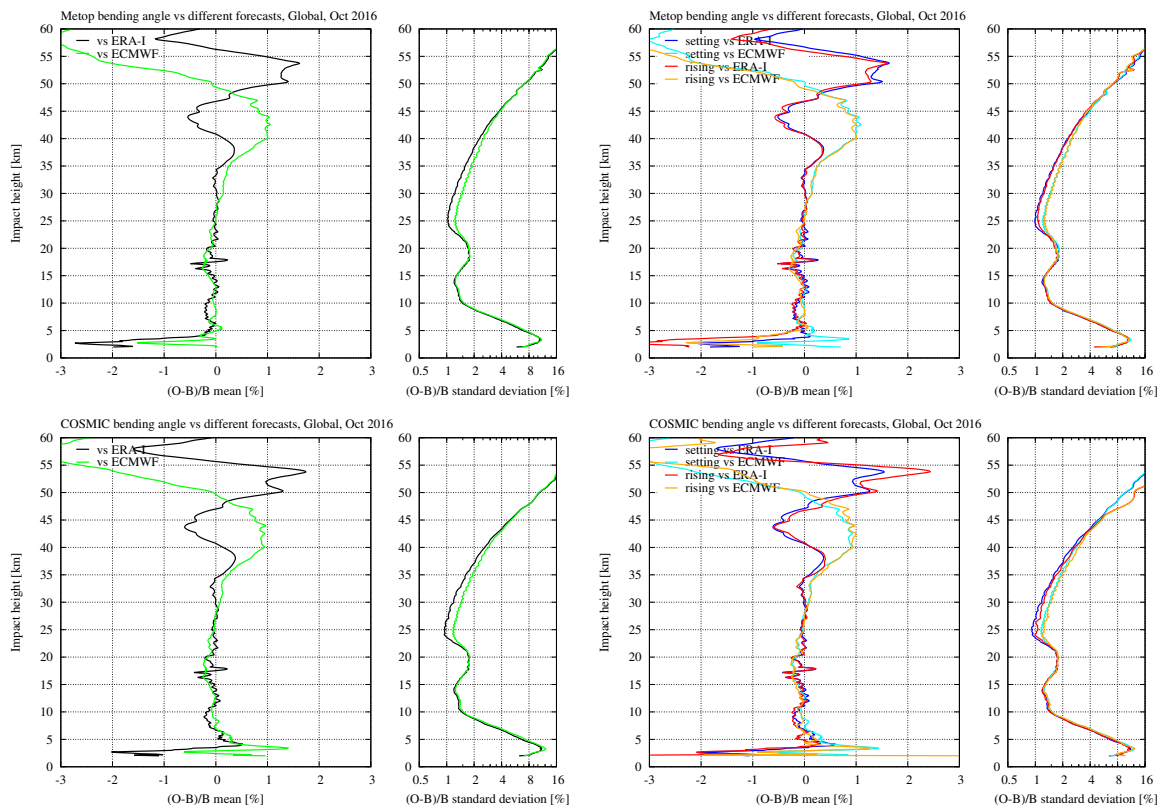


Figure 3.13: Monthly global profile statistics of bending angle against different forecasts.

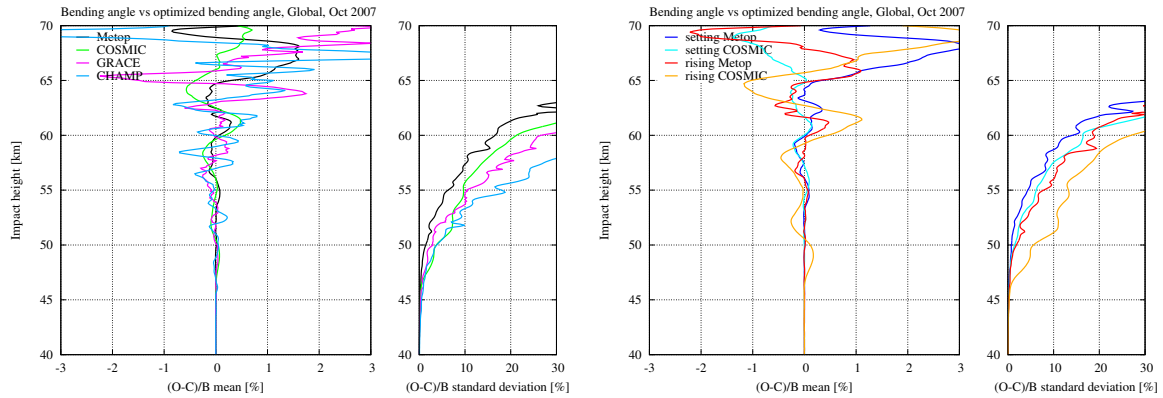


Figure 3.14: Monthly global profile statistics of bending angle against optimized bending angle.

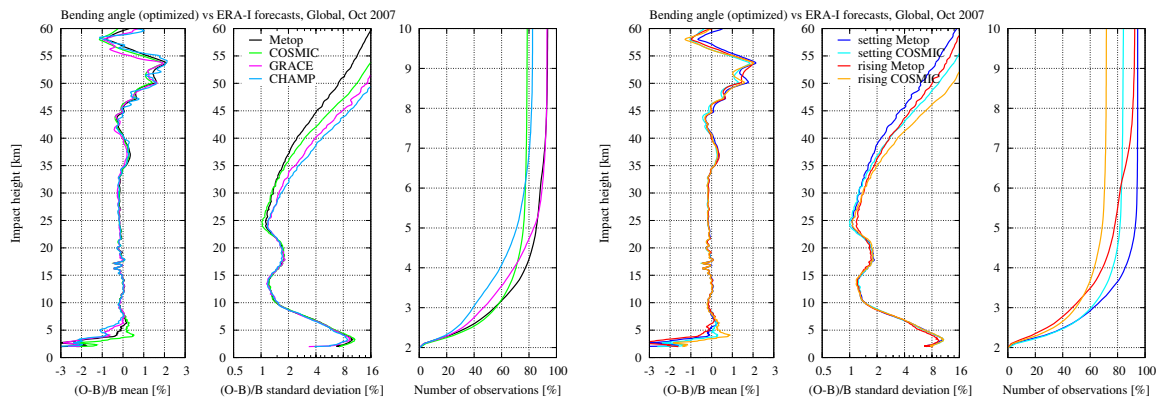


Figure 3.15: Monthly global profile statistics of optimized bending angle against ERA-Interim.

3.2.2 Refractivity

The plots in this subsection (Fig. 3.16) illustrate how the means and standard deviations against both ERA-I forecasts and ECMWF operational forecasts in Fig. 3.13 propagate to refractivity. We note the somewhat similar (O-B)/B means in bending angle and refractivity, and in the light of the smaller differences between Metop and COSMIC, setting and rising occultations, as well as the comparisons in Fig. 3.14, we conclude that the ROM SAF CDR v1.0 refractivity means at high altitudes are likely more accurate than the means given by the forecast models.

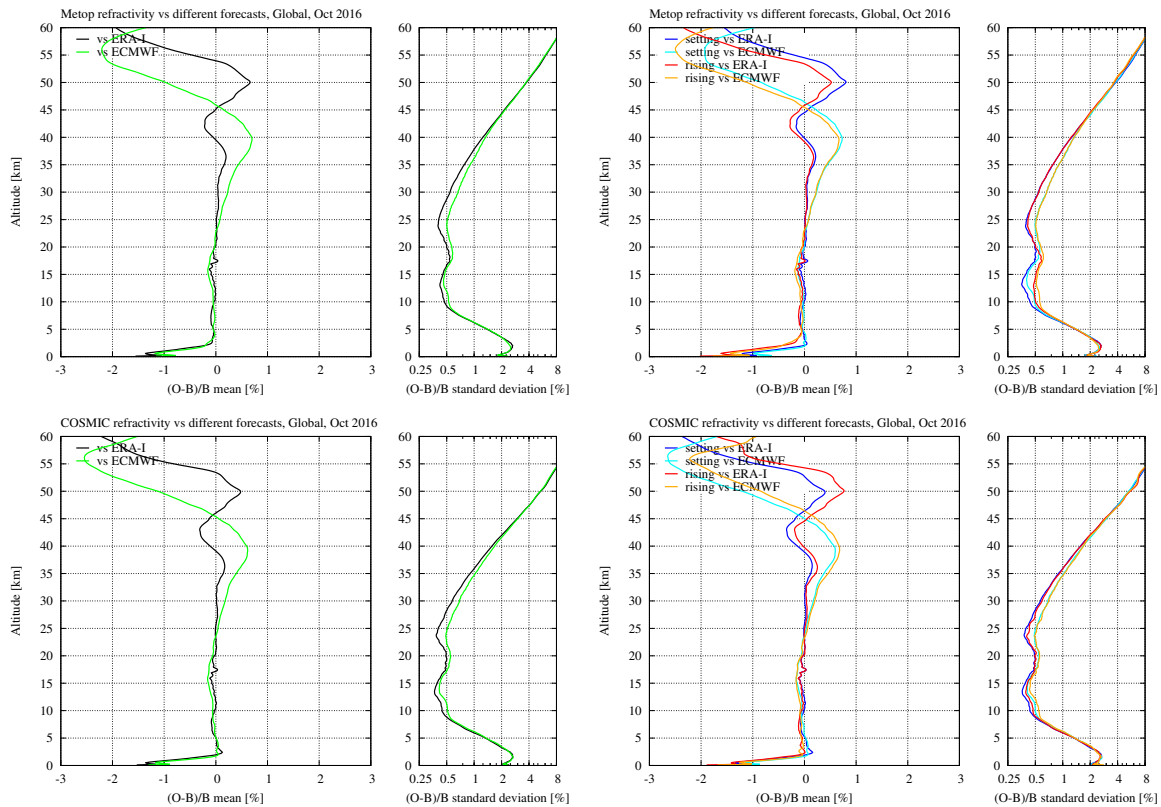


Figure 3.16: Monthly global profile statistics of refractivity against different forecasts.

3.2.3 Dry temperature

The plots for dry temperature, corresponding to the plots for refractivity, are shown in Fig. 3.17. The O-B means are basically mirroring those in Fig. 3.16 up to about 35 km (cf. the discussion in Section 3.1.3). Above 35 km, the mirroring breaks down because the (O-B)/B mean in the dry pressure becomes appreciable. Note that the mirroring would be exact at all altitudes if we were to calculate the dry temperature statistics in percent, and use the derived dry pressure as the vertical coordinate when plotting both refractivity and dry temperature statistics. For reference the corresponding plots for dry pressure are shown in Fig. 3.18.

Although the (O-B)/B mean in dry pressure becomes appreciable above 35 km, and seemingly contribute to a larger O-B mean in dry temperature above this altitude, it should be kept in mind that the temperatures in the background models may be more biased than the occultation data. Analyses in Section 3.8, regarding the effect of an even larger difference between setting and rising occultations for Metop, being hemispheric and local time dependent, show, as a side effect, how a constant bias in bending angle propagates to refractivity and dry temperature.

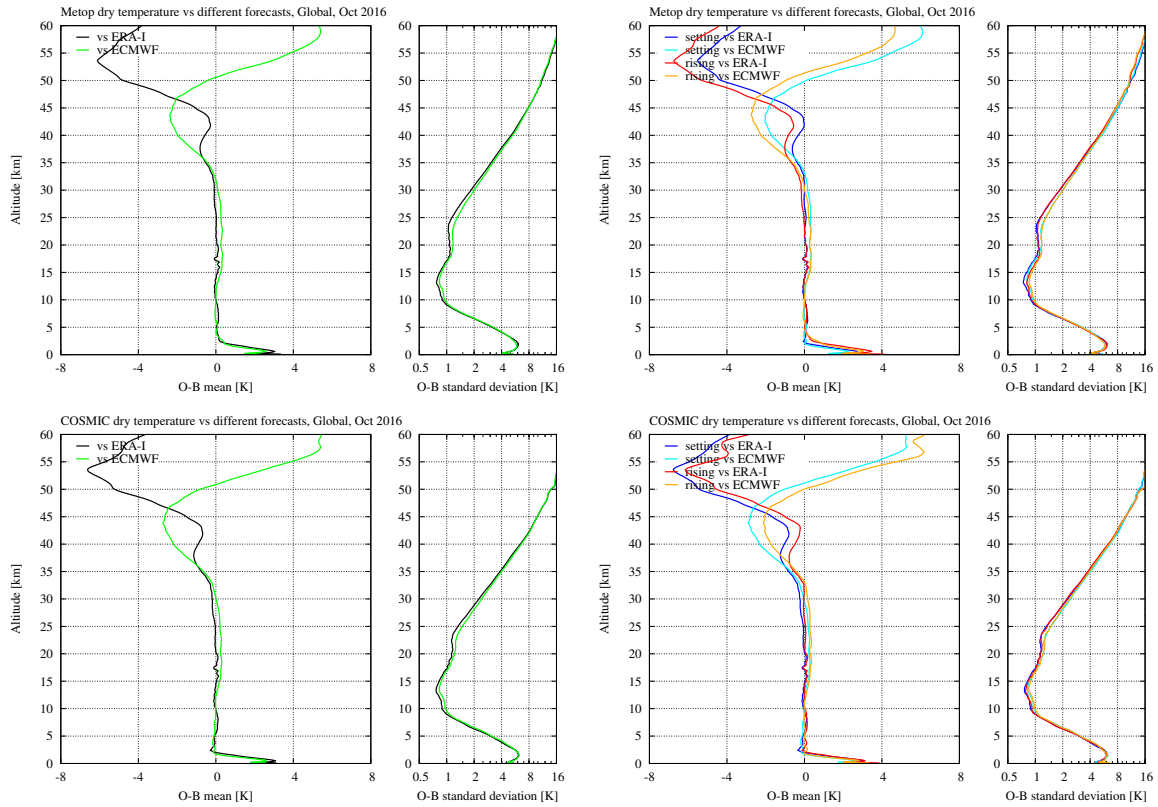


Figure 3.17: Monthly global profile statistics of dry temperature against different forecasts.

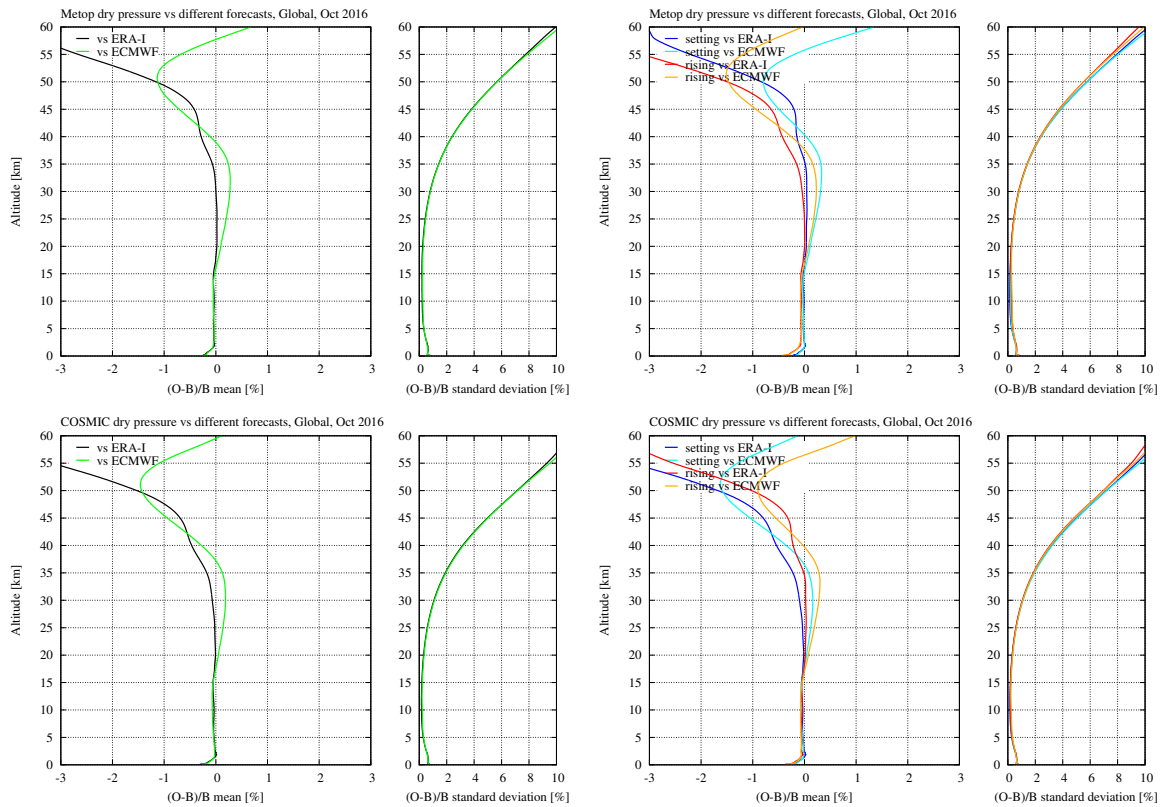


Figure 3.18: Monthly global profile statistics of dry pressure against different forecasts.

3.3 Impact of instrument software upgrades

In this section we show the impact of what we consider to be the most important instrument software upgrades for Metop and COSMIC. These upgrades changed the error characteristics of all products from these missions in different ways (in 2013 for Metop and in 2006 for COSMIC). To limit the number of plots, we show here only the global statistics against ERA-I in the months before and after the upgrades. We will refrain from discussing the reasons and exact dates and times of the upgrades to the different instruments on the various satellites, since there have been many, and not all detailed information is available to us. We therefore limit ourselves to discussing the impact that we can see in the statistics for these two missions of the ROM SAF CDR v1.0.

It should be noted that there have been a number of upgrades to all missions during the course of their lifetime. Section 3.4 discusses notable changes in the statistics for all missions over time in general, including the impact of the instrument upgrades discussed here.

The points to be made from this section are that instrument software upgrades for both Metop and COSMIC changed notably the error characteristics of the ROM SAF CDR v1.0 over a few months in 2013 (Metop) and 2006 (COSMIC). The main impacts on the statistics for Metop are:

- Better penetration below 8 km impact height for rising occultations since April 2013 (Metop-B) and July 2013 (Metop-A)
- Changed biases below 5 km for both setting and rising occultations
- A reduction in the standard deviations at high altitudes, more so for rising than for setting occultations; the standard deviations were slightly larger for rising occultations before
- Introduction of small biases below 20 km for rising occultations, mostly for bending angle and refractivity
- An increase in the standard deviations and vertical correlations between 10 km and 20 km for rising occultations, mostly so for refractivity.

The main impacts on the statistics for COSMIC are:

- A large increase in the number of nominal occultations (especially rising) since July 2006
- A much better penetration below 8 km for setting occultations since July 2006;
- Changed biases below 5 km for both setting and rising occultations since July 2006; additional minor changes since September 2006
- A substantial reduction in the standard deviations since July 2006, more so for rising than for setting occultations; minor improvements since September 2006

Because the changes discussed here for COSMIC happened in the first few months of the mission, these data could be excluded from climate studies without introducing a large gap

in the middle of the time series. We therefore recommend users to consider not using the ROM SAF CDR v1.0 COSMIC data for climate studies before September 2006, or at least not before July 2006.

3.3.1 Metop upgrades in 2013

As already mentioned in Section 3.1, the tracking strategy for rising occultations was changed for Metop in 2013. The change was first made to Metop-B in the spring of 2013 after a series of trials over several months, testing out different tracking strategies. The final change was then made to Metop-A in late June. For a few months before the upgrade to Metop-A, the software and the tracking strategy was stable, but different on the two instruments. Since Metop-A and Metop-B otherwise show very similar statistics, comparisons between the two before and after the upgrade to Metop-A give an opportunity to assess details of the impact of the final change.

Figure 3.19 shows the monthly global profile statistics of bending angle (against ERA-I) for Metop-A and Metop-B separately. The top plots are for May (before the upgrade to Metop-A, but after the final upgrade to Metop-B), and the bottom ones for July (after the upgrade to Metop-A). The left plots show the total statistics, whereas the right plots show the statistics separated into setting and rising occultations.

Differences in the statistics between Metop-A and Metop-B in May are small. Most noticeable is the poorer penetration below 8 km for rising Metop-A occultations, which was rectified with the upgrade to Metop-B as it improved the tracking of the L1 signal in the lower moist troposphere. Also to be noted is the difference in bias for both setting and rising occultations below 5 km, and the difference in standard deviations above 25 km. For July, after the upgrade was also made to Metop-A, the statistics are virtually identical.

Because it can be difficult to see all the details in Fig. 3.19, the differences between Metop-A and Metop-B bending angle statistics for May are shown in Fig. 3.20. Thus, these plots are $(O-B)/B$ for Metop-A minus $(O-B)/B$ for Metop-B, setting and rising occultations. Such differences for the same month excludes monthly variations in the ERA-I data that would otherwise (if plotting differences before and after the upgrades) mix in with the small differences due to the instrument software upgrades. In Fig. 3.20, mean differences are on the left, and standard deviation differences on the right. The differences can be interpreted as the impact of the changed tracking strategy on the bending angle statistics⁴ (plus the improved penetration for rising occultations). Besides the larger differences below 5 km, the plots reveal that the bias changed by about 0.1% for rising occultations below 20 km. This minor bias change is related to the L2-extrapolation (cf. Section 3.1.2), and additional analysis is provided in Section 3.8. The changed tracking strategy also reduced the standard deviation at high altitudes, and more so for rising than for setting occultations. Between 10 km and 20 km, the standard deviation increased a bit for rising occultations, which again is related to the L2-extrapolation, and the corresponding impact in the refractivity statistics was already discussed in Section 3.1.2.

Figures 3.21 and 3.22 show the corresponding plots for refractivity, and Figs. 3.23 and 3.24 the ones for dry temperature. The change in the refractivity bias below 20 km seems consistent with the one in bending angle, and as already mentioned, the impact of the changed

⁴ It was verified that similar plots for July 2013 do not show any large differences.

tracking strategy is much more evident in the refractivity standard deviation, and also associated with a broadening of the vertical correlations in refractivity. Still, the same features are seen in dry temperature, but to a smaller extent.

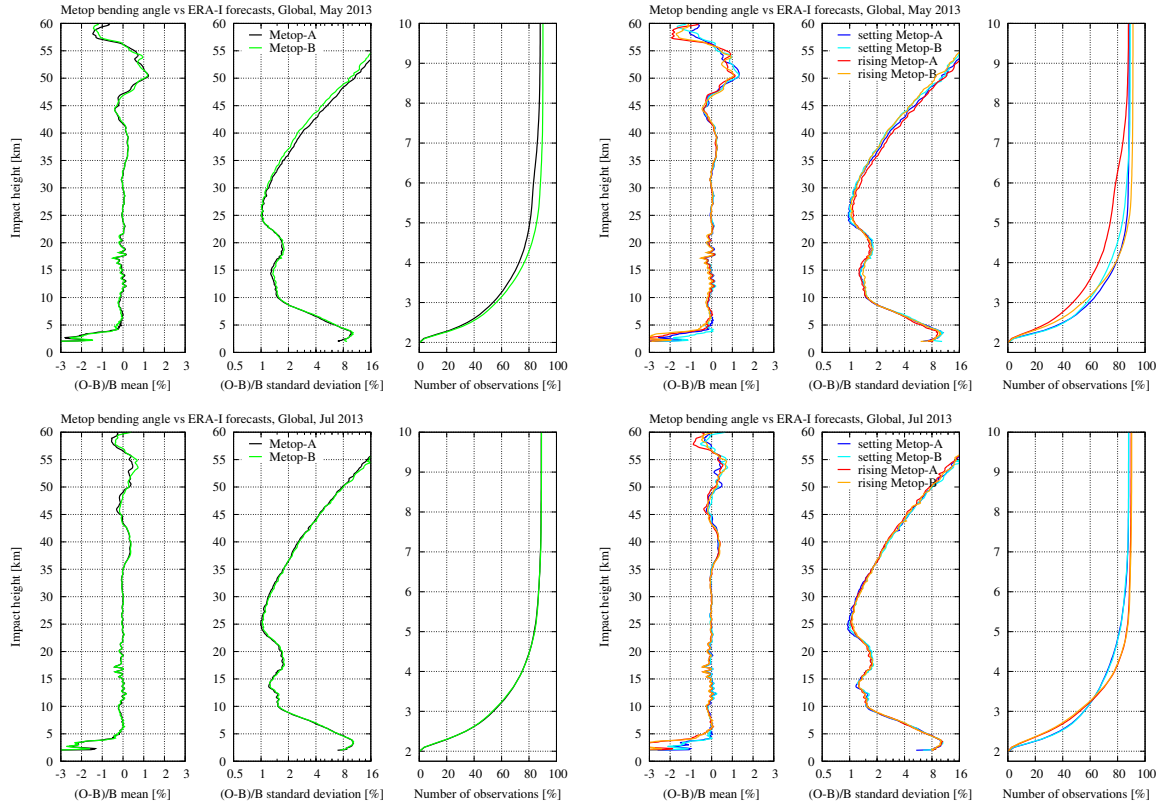


Figure 3.19: Monthly global profile statistics of bending angle from Metop before and after the instrument upgrade to Metop-A in June 2013.

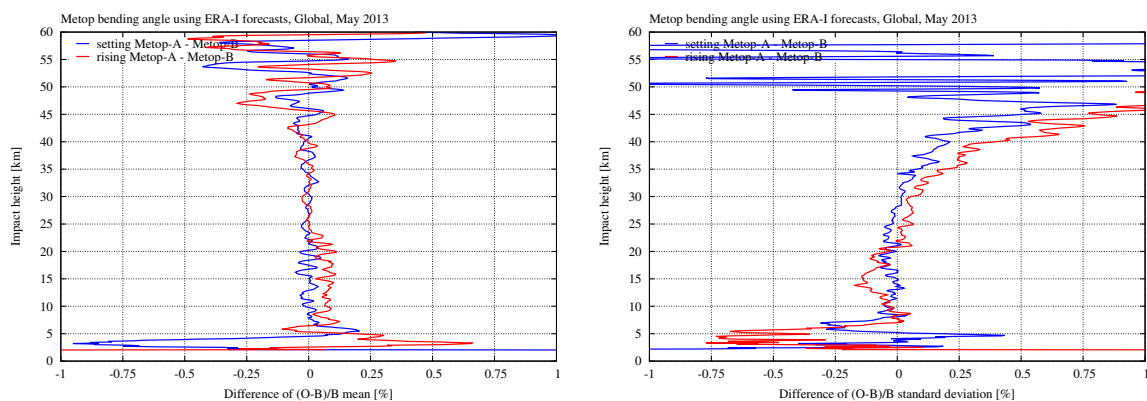


Figure 3.20: Differences between Metop-A and Metop-B bending angle statistics for May 2013.

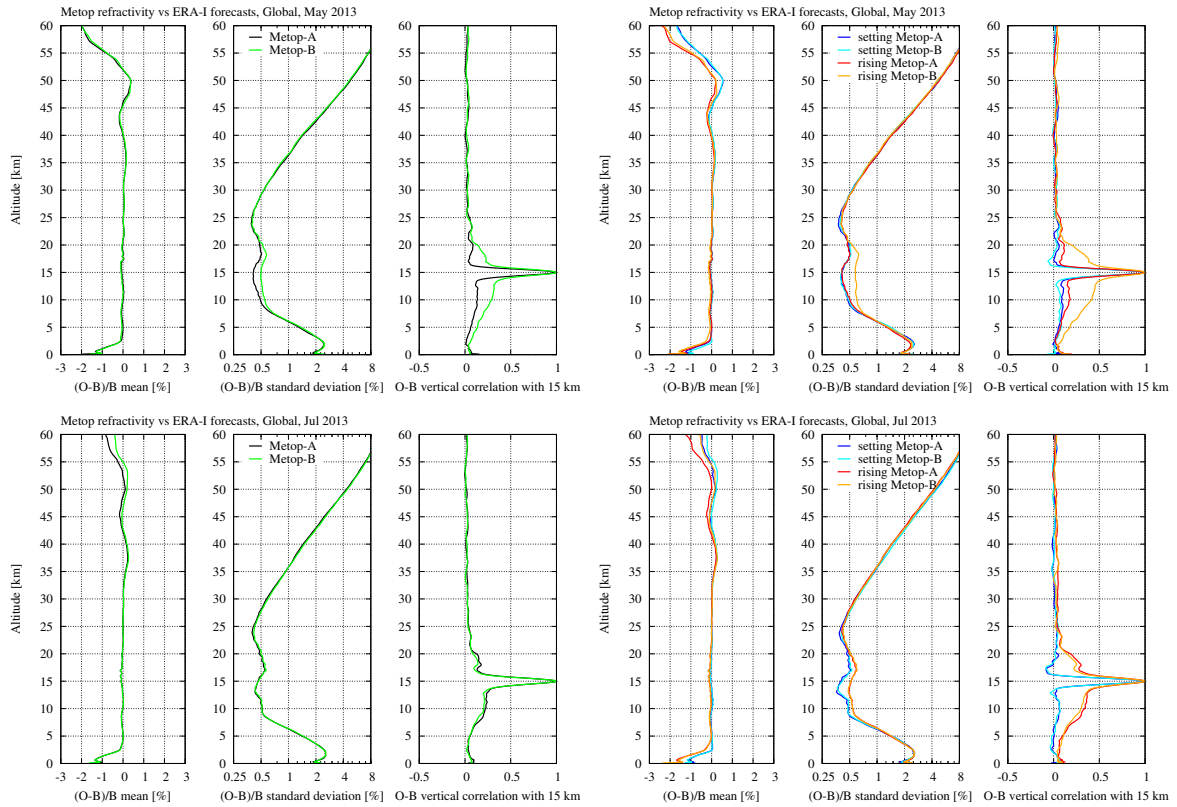


Figure 3.21: Monthly global profile statistics of refractivity from Metop before and after the instrument upgrade to Metop-A in June 2013.

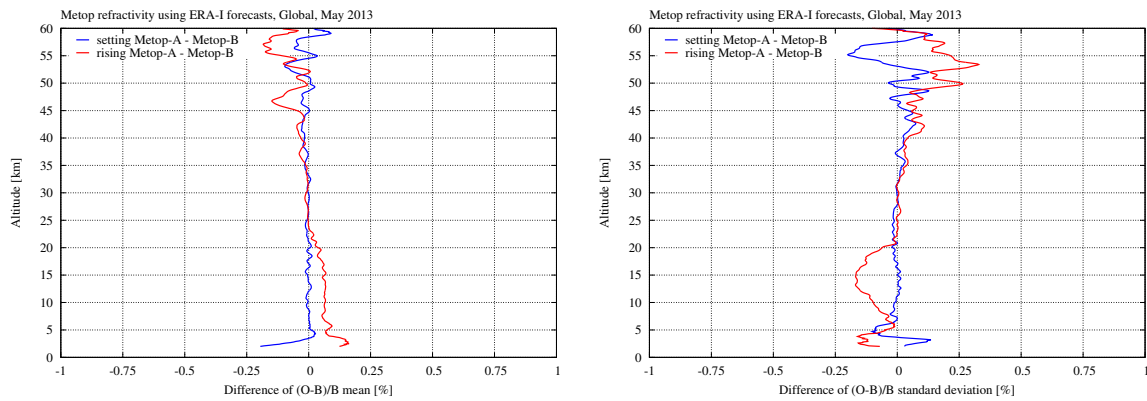


Figure 3.22: Differences between Metop-A and Metop-B refractivity statistics for May 2013.

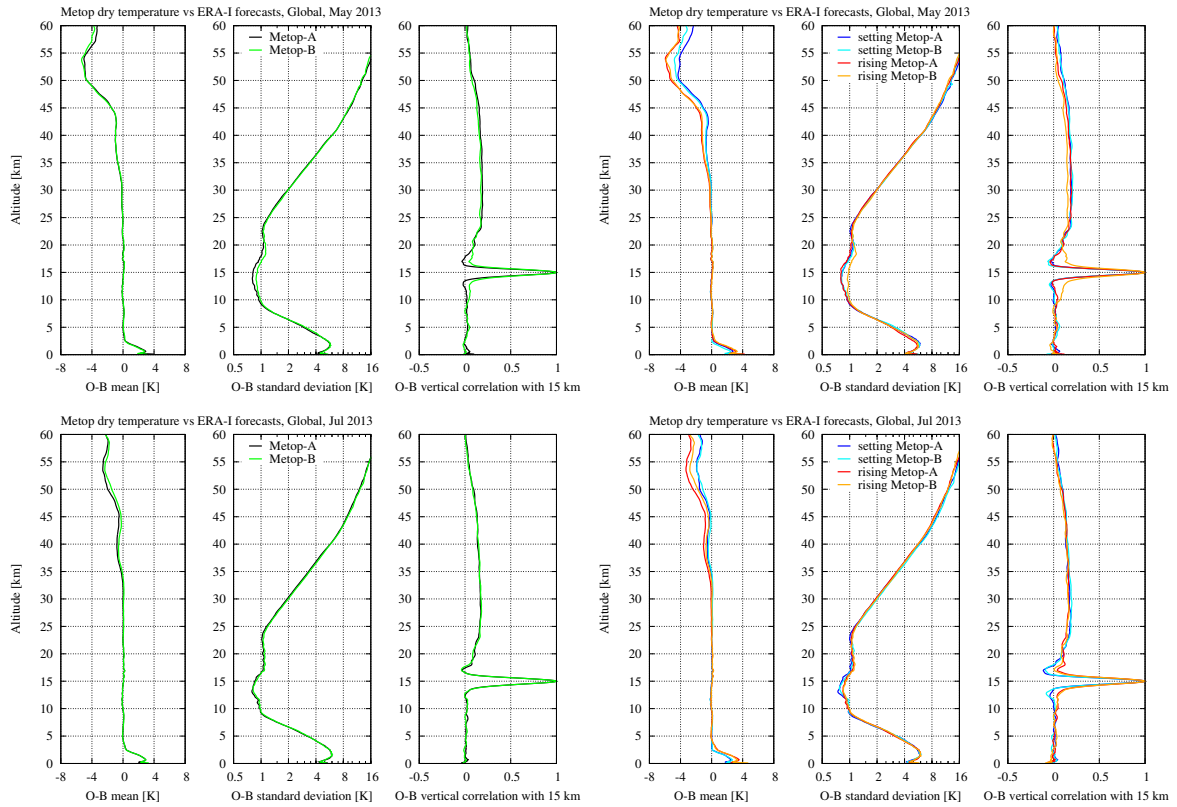


Figure 3.23: Monthly global profile statistics of dry temperature from Metop before and after the instrument upgrade to Metop-A in June 2013.

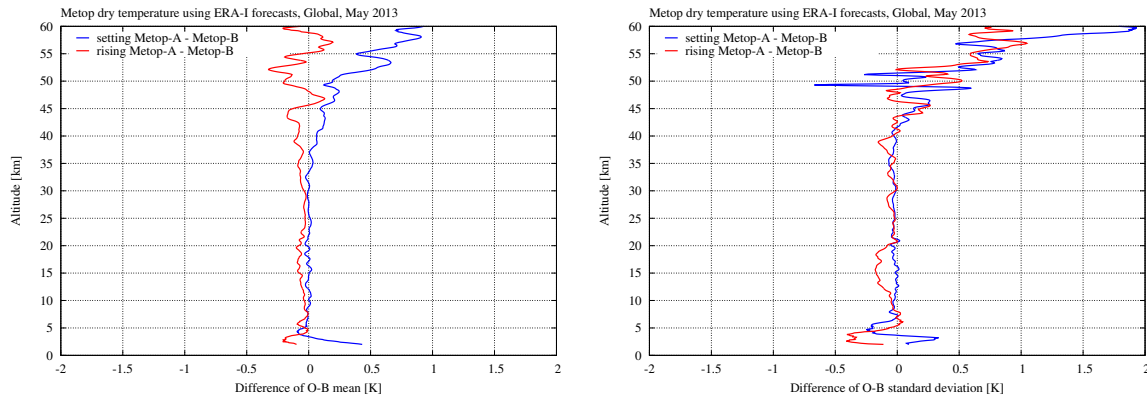


Figure 3.24: Differences between Metop-A and Metop-B dry temperature statistics for May 2013.

3.3.2 COSMIC upgrades in 2006

In the early years of the COSMIC mission there were a number of instrument software upgrades to all six satellites in the constellation. Figures 3.25, 3.26, and 3.27 show the statistics against ERA-I for May, July, and September 2006, revealing the improvements as a result of two important changes to the onboard tracking strategy in June and August. The improvements from May to July are rather large in terms of both the biases, the standard deviations,

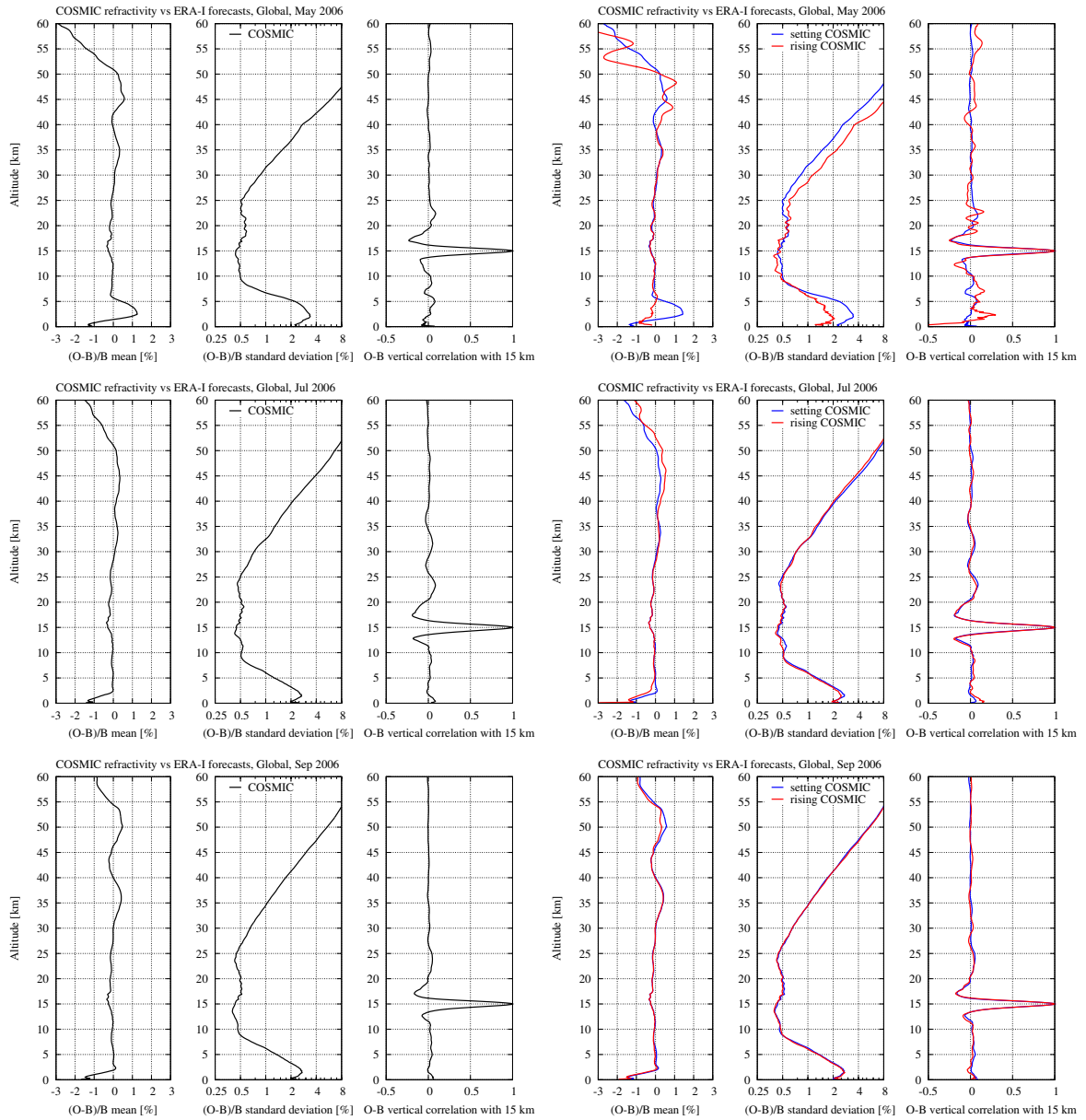


Figure 3.26: Monthly global profile statistics of refractivity from COSMIC before, in between, and after the instrument upgrades to the COSMIC constellation in June and August 2006.

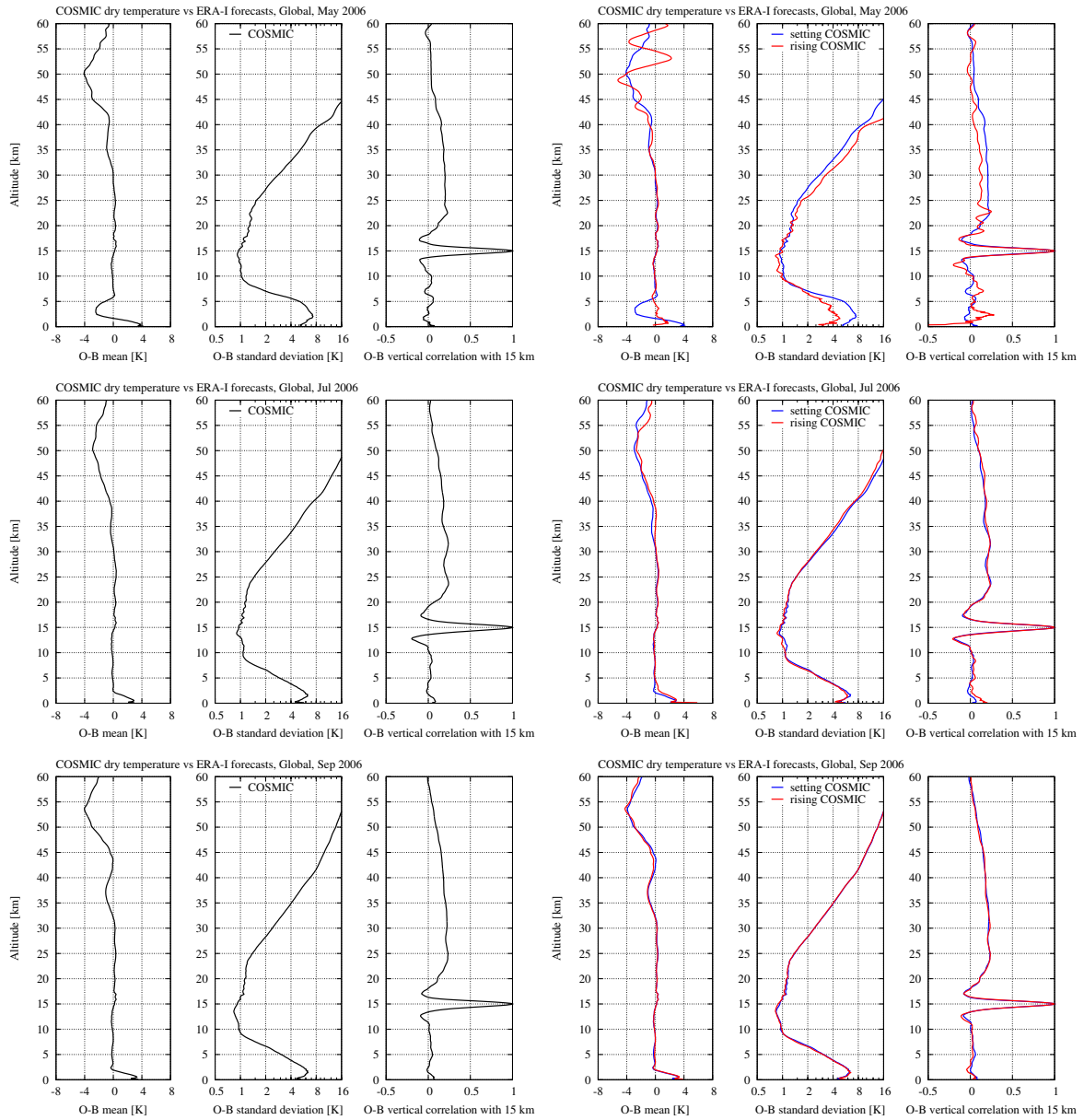


Figure 3.27: Monthly global profile statistics of dry temperature from COSMIC before, in between, and after the instrument upgrades to the COSMIC constellation in June and August 2006.

3.4 Comparison across years

In this section we look at changes in the error characteristics of the data from the four missions over time. We show profile statistics against ERA-I forecasts as in previous sections, and use the same month (October) for different years to avoid the seasonal variations of the model data in the statistics. We only show the statistics for every third year to verify the general constancy of the data quality over many years. Additionally, we also show selected time series from <http://www.romsaf.org/re1/index.php>, and discuss the most important changes and anomalies that can be seen in the statistics over time. The above mentioned site contains a very large number of plots of monthly statistics of the ROM SAF CDR v1.0 against both ERA-I forecasts and ECMWF operational forecasts, supplementing the plots in this report.

The points to be made from this section are that the data quality of the ROM SAF CDR v1.0 is fairly constant over time. Main exceptions are:

- Abrupt changes in biases and standard deviations for rising Metop occultations related to instrument software upgrades in 2013 (see details in Section 3.3)
- Larger biases and standard deviations in the first few months of the COSMIC mission (in 2006), also related to instrument software upgrades
- A period of several months in 2007 with varying noise at high altitudes for rising COSMIC occultations, originating from FM5, and presumably due to instrument anomalies
- A decrease in the otherwise larger refractivity standard deviations and vertical correlations for rising Metop occultations (and a hint of the same for COSMIC, but much smaller) toward the end of the data record, related to the L2-extrapolation in possible combination with changes in the ionosphere following the solar cycle, which peaked in 2014
- Changing biases and standard deviations for CHAMP over the years, but it is unclear how much is related to changes in the occultation data and how much is related to changes in the ERA-I data that are used for comparison

3.4.1 Bending angle

Figure 3.28 shows the monthly global profile statistics of bending angle for the month of October, every third year, in the time periods where the respective missions have provided data (regarding separate setting and rising statistics, we limit ourselves to the two baseline months in 2007 and 2016). The top plots are for Metop, the middle for COSMIC, and the bottom ones for GRACE and CHAMP.

The $(O-B)/B$ means are quite similar for all missions in all years, except for CHAMP, where there are notable differences between the three years (2001, 2004, and 2007) plotted here. A good part of these differences are believed to be related to changes in the ERA-I data, caused by the assimilation of fewer data in those earlier years than in the years after 2007. Some part, e.g., the different biases below 10 km, could be related to instrument software upgrades to the CHAMP instrument over the years (there have been many, especially in the early years). For the other three missions, small differences in the 5–10 km and 20–35 km

ranges, where 2007 stands out more than the other years, are likely also related to changes in the ERA-I data. Differences between the setting and rising biases for Metop below 5 km have already been discussed in the previous sections.

The (O-B)/B standard deviations are also fairly similar over the years for all missions, and more similar than the differences between the missions. The slightly larger standard deviation below 30 km for CHAMP in 2004 is not understood. Possibly it is related to either instrument software upgrades over the years, or to changes in the ERA-I data. The slightly larger standard deviations above 25 km in 2007, most visibly for Metop and COSMIC, could in part be related to changes in the ERA-I data, but is also a result of the larger standard deviations for rising occultations for both missions in 2007 compared to 2016. These were already discussed in Section 3.1.1, and regarding COSMIC, we discuss this further below.

Figures 3.29 and 3.30 show time series of the global monthly (O-B)/B means and standard deviations for all four missions. Most noticeable are the somewhat larger biases in the early years for CHAMP, as well as a change in 2006, likely related to the onset of the assimilation of COSMIC data in the ERA-I system. For COSMIC, we notice the larger biases and standard deviations in the first few months discussed in Section 3.3. From additional plots (see <http://www.romsaf.org/re1/index.php>), there are indications of varying standard deviations for rising COSMIC occultations in 2007 at high altitudes. These can be traced to the FM5 satellite, where it becomes clear that there were three distinct periods from June 2007 to January 2008 with increased noise in rising occultations for that satellite. This is shown in Fig. 3.31⁵, and it explains the larger standard deviation at high altitudes for rising COSMIC in 2007 compared to 2016 in Fig. 3.28. The increased noise is presumably due to instrument anomalies. In Fig. 3.29, an abrupt change in the characteristics of the biases for all missions around the end of 2009 is related to a change in the ERA-I data, which in turn is mainly related to a change in the processing of the COSMIC data that were assimilated. We should note here that setting COSMIC occultations have been assimilated at ECMWF (and thereby in the ERA-I system) since December 2006, whereas the assimilation of rising COSMIC occultations started in November 2007. Metop data were not assimilated until May 2008.

⁵The vertical contours in the middle of the plot are due to about 10 days of no FM5 data in August 2010.

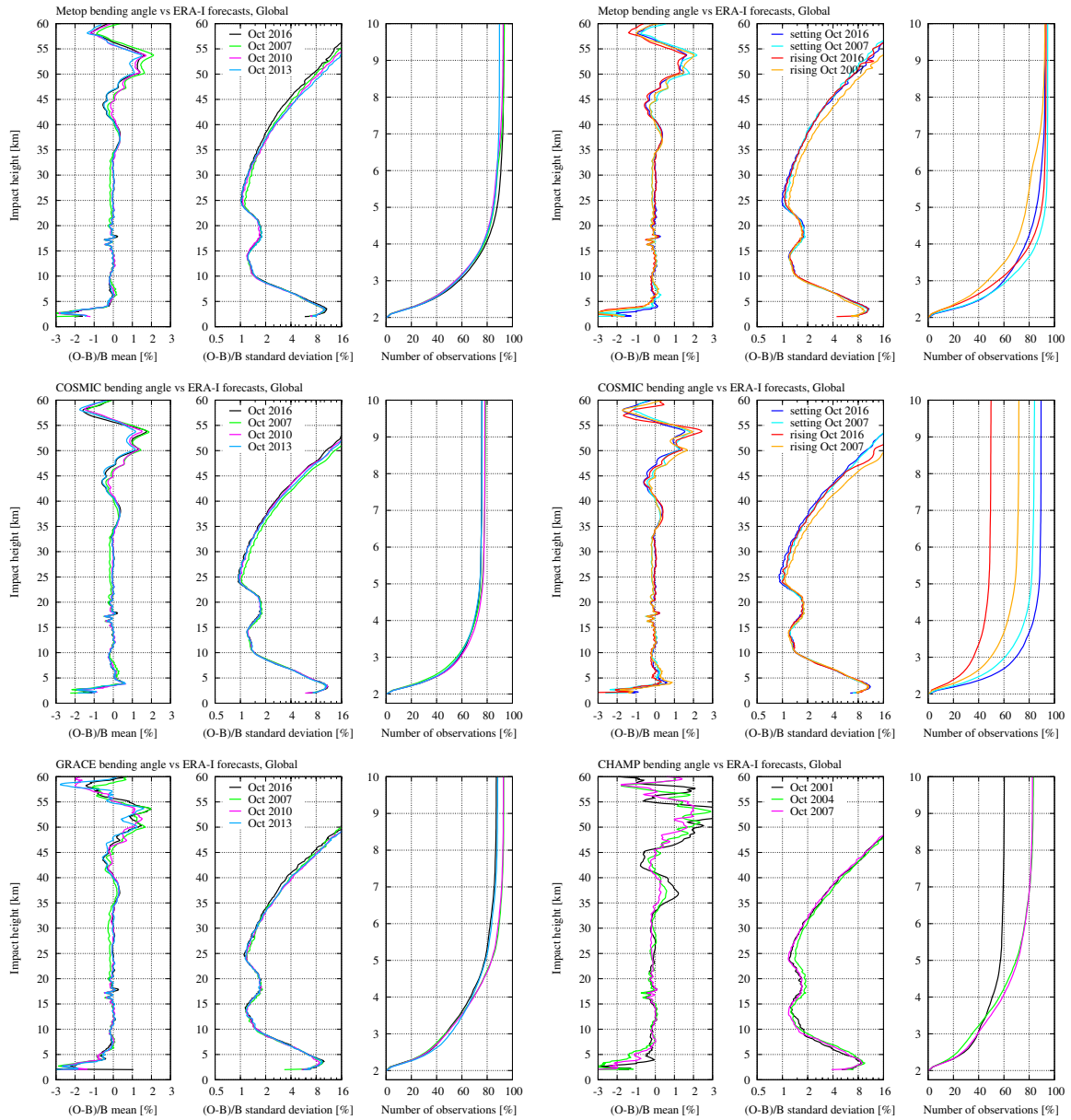


Figure 3.28: Monthly global profile statistics of bending angle for different years.

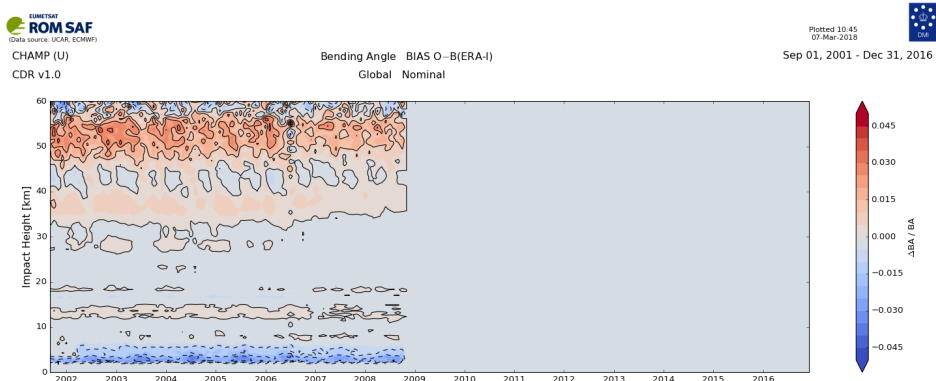
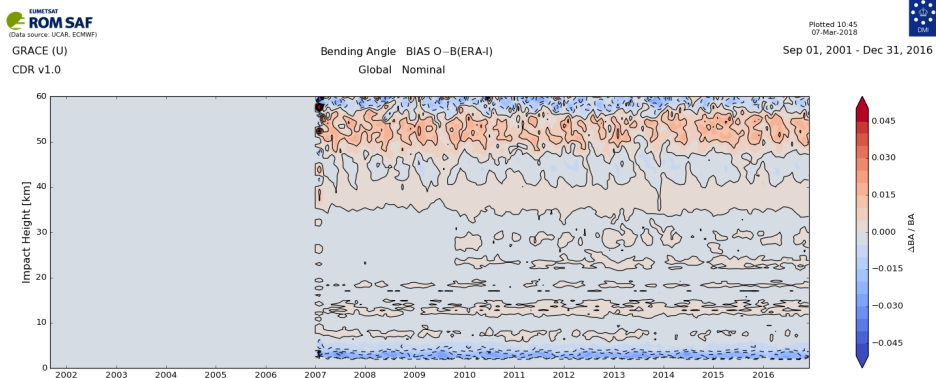
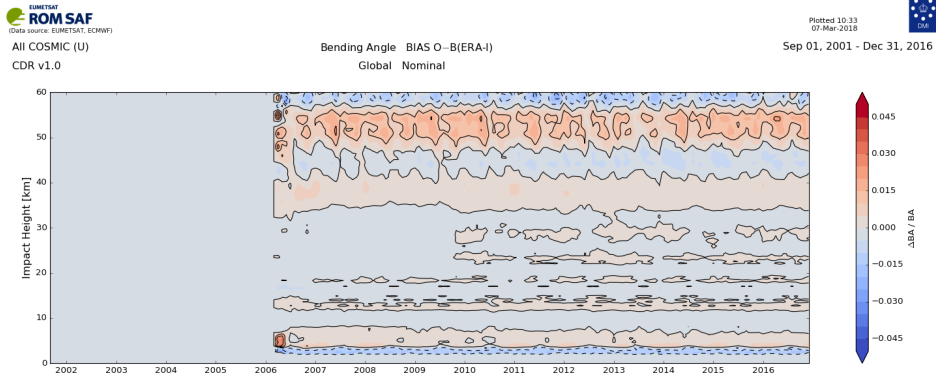
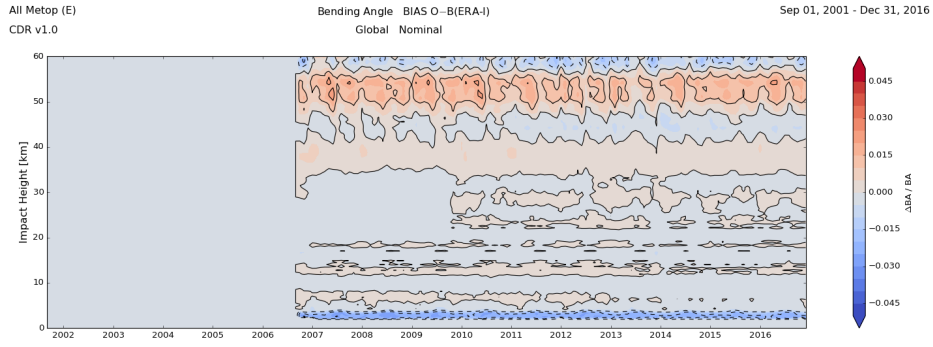


Figure 3.29: Time series of the global monthly bending angle (O-B)/B mean difference to ERA-Interim for the different missions.

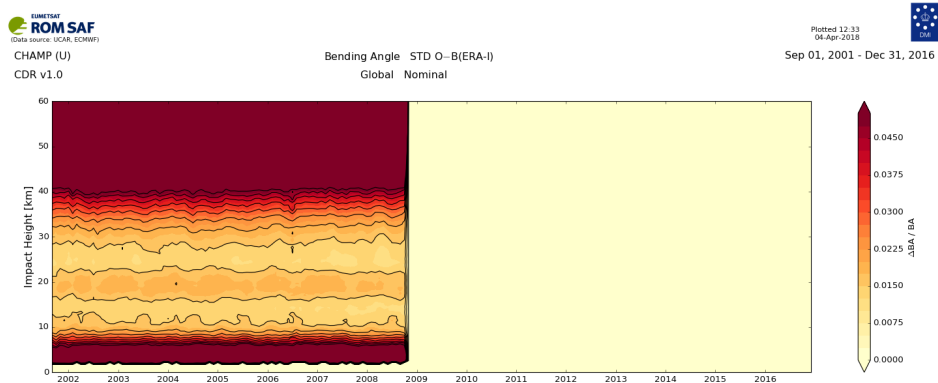
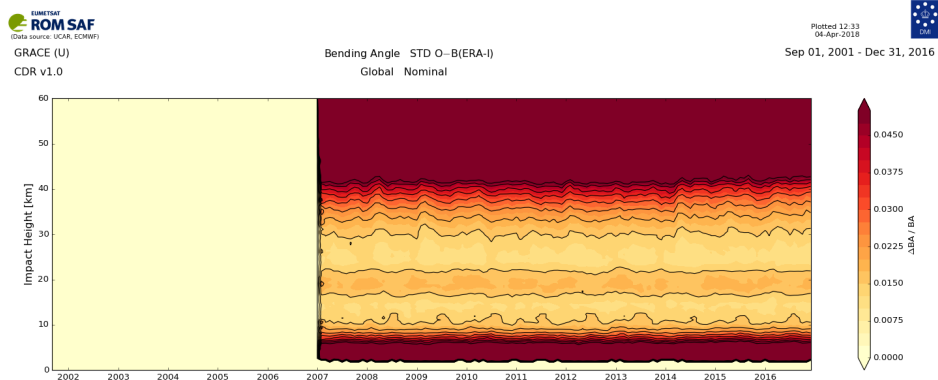
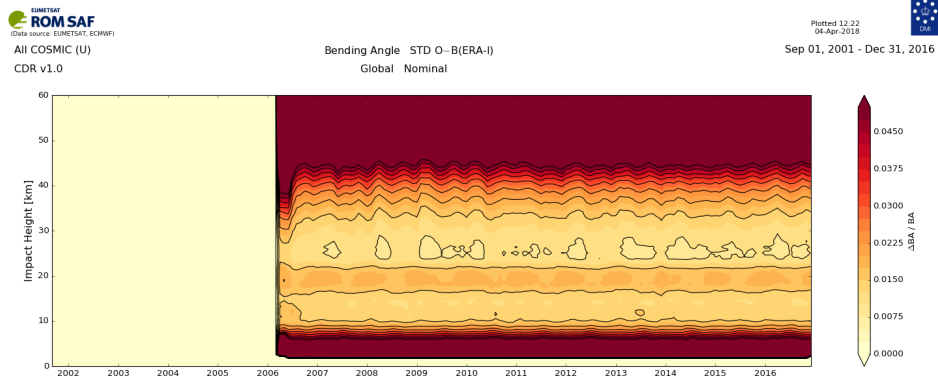
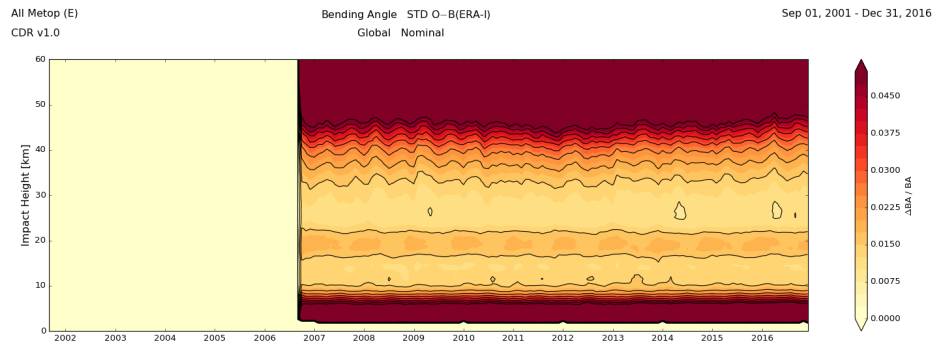


Figure 3.30: Time series of the global monthly bending angle (O-B)/B standard deviation to ERA-Interim for the different missions.

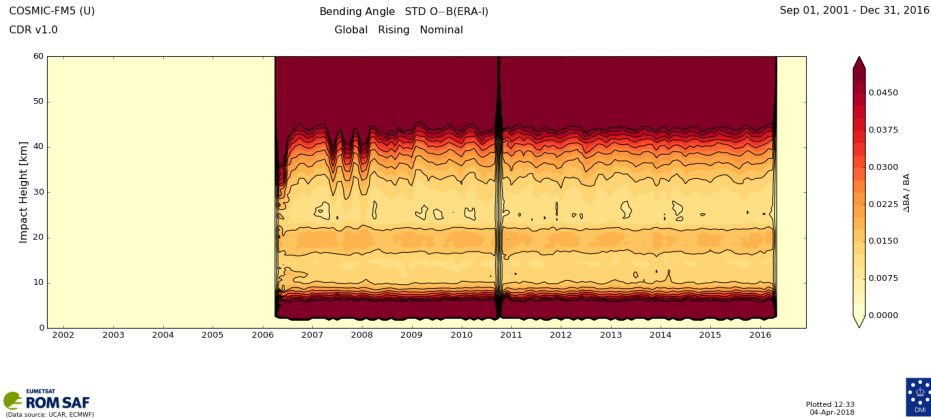


Figure 3.31: Time series of the global monthly bending angle $(O-B)/B$ standard deviation to ERA-Interim for rising COSMIC-FM5.

3.4.2 Refractivity

Figure 3.32 shows the plots for refractivity corresponding to the ones for bending angle in Fig. 3.28. Similar comments can be made, but in addition, we notice the larger $(O-B)/B$ standard deviations and associated broader correlations between 10 km and 20 km for Metop in 2013 and 2016, for rising occultations. The reason was discussed in previous sections (related to instrument software upgrades), but it is interesting that the problem was worse in 2013 than in 2016. This is not fully understood, but since the problem is due to the L2-extrapolation, and the extrapolated L2 bending angle in turn is used for ionospheric correction in the troposphere, it could be a result of a more uncertain L2-extrapolation in the period of generally larger electron density and ionospheric disturbances near the maximum of the ~ 11 year solar cycle, which peaked in 2014. This hypothesis could also explain the slightly larger vertical correlation in the 10–20 km range for rising COSMIC occultations in 2016 compared to 2007.

The time series of the global monthly means and standard deviations for refractivity, corresponding to the ones for bending angle in the previous subsection, are shown in Figs. 3.33 and 3.34. Additionally, Figs. 3.35 and 3.36 show the time series for setting and rising occultations separately, for Metop and COSMIC. We see similar features as in the bending angle plots, but also an anomaly in the $(O-B)/B$ means for all missions in the last couple of months of 2013 (visible in particular as a larger bias between ~ 12 km and 25 km). This is explained by a period of about six weeks where the assimilation of occultation data in the ERA-Interim system were stopped unintentionally (Sean Healy, 2018, personal communication). For Metop, the small negative bias below 20 km in rising occultations after the 2013 instrument upgrades is clearly visible (second plot from the top in Fig. 3.35), and the increased standard deviation in the years thereafter can also be seen (second plot from the top in Fig. 3.36), but it declines near the end of the time series. For COSMIC, it becomes evident that the slight increase in the standard deviation there also peaked in 2014 (raised contours around 2014 and 2015 near 10 km in the bottom plot of Fig. 3.36, but with some seasonal variations included). Other plots for different latitude bands (see <http://www.romsaf.org/re1/index.php>), for both Metop and COSMIC, also indicate a maximum around 2014. These observations together show that the larger bias and standard

deviations that are related to the L2-extrapolation peaked around 2014, and corroborates the hypothesis that the change over time is related to the solar cycle.

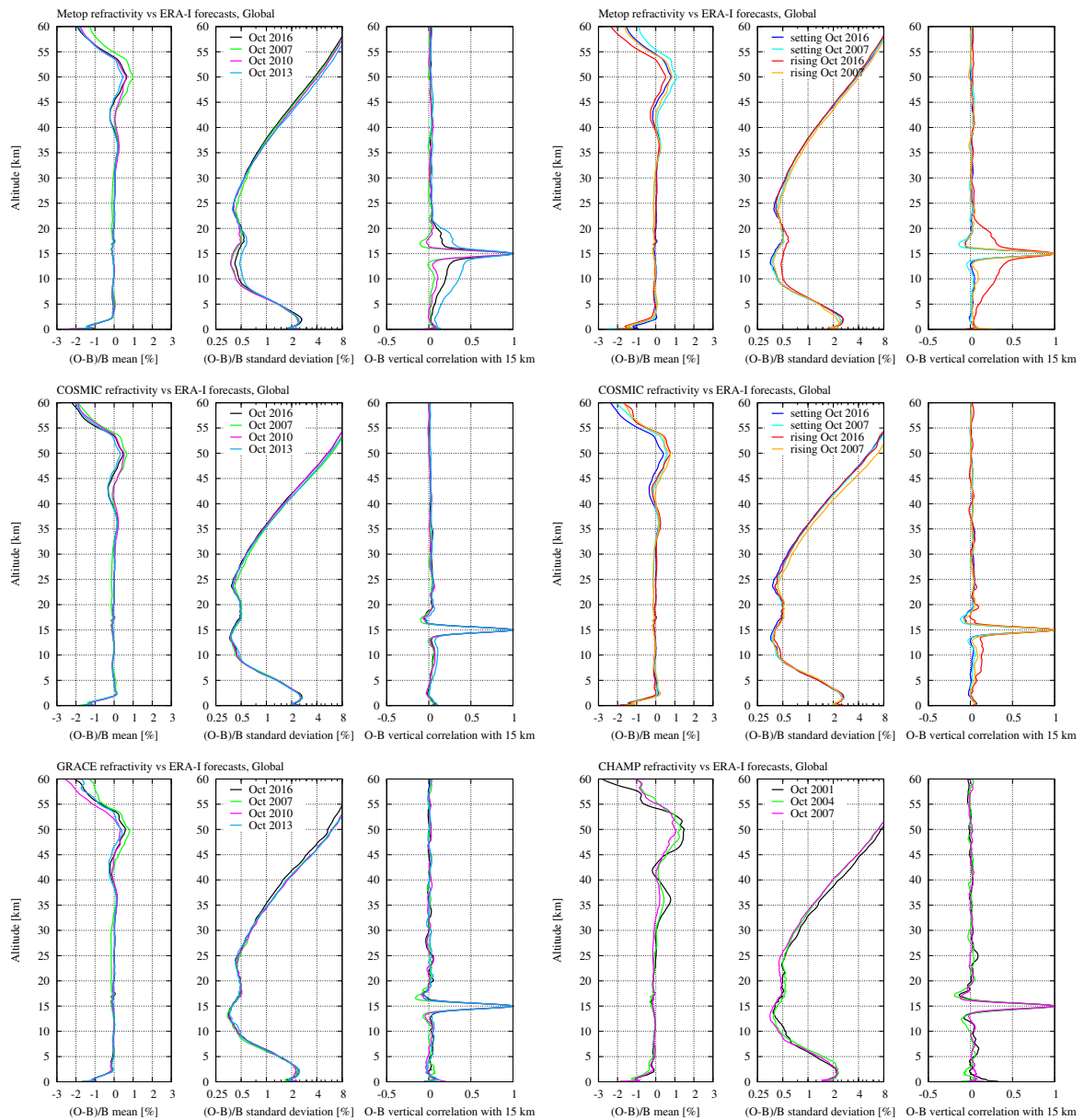


Figure 3.32: Monthly global profile statistics of refractivity for different years.

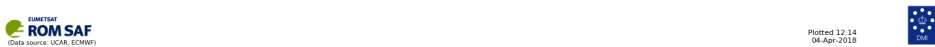
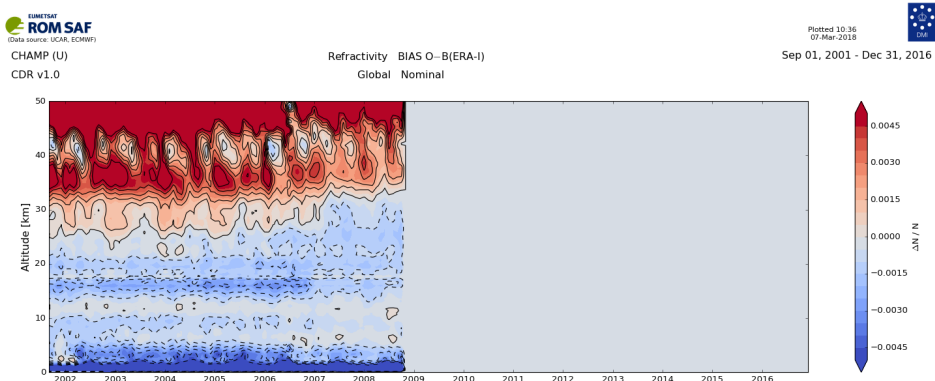
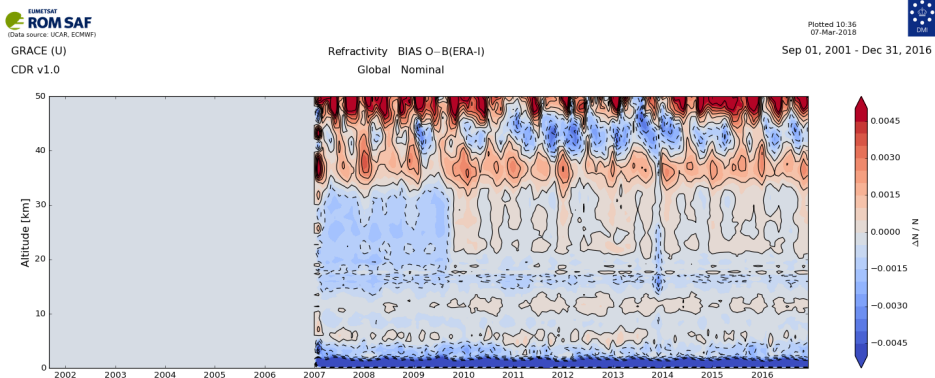
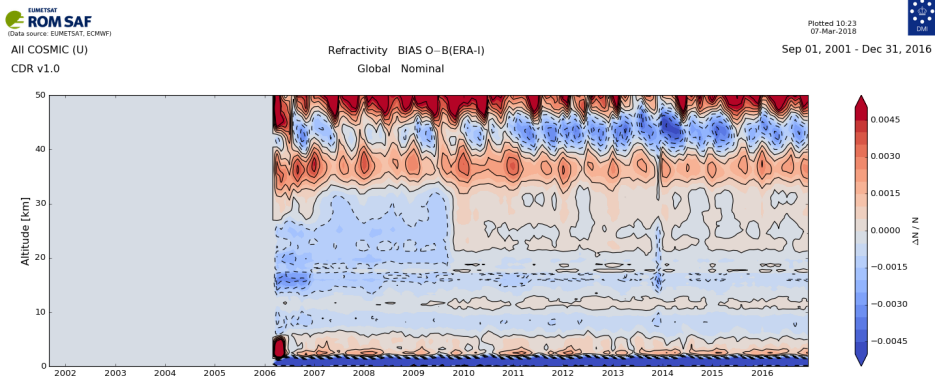
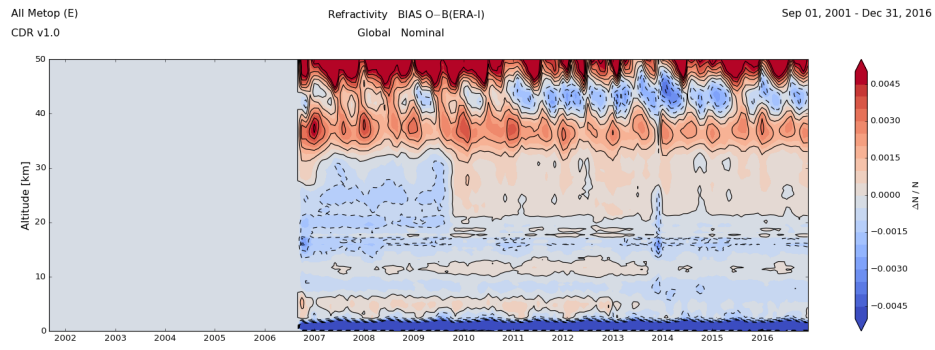


Figure 3.33: Time series of the global monthly refractivity (O-B)/B mean difference to ERA-Interim for the different missions.

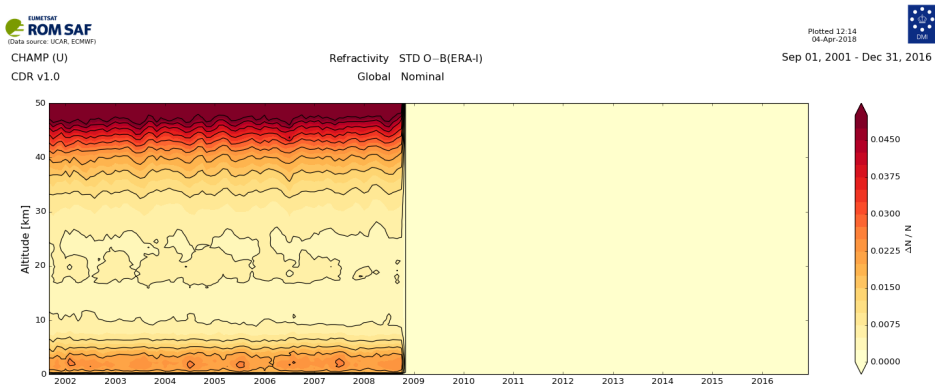
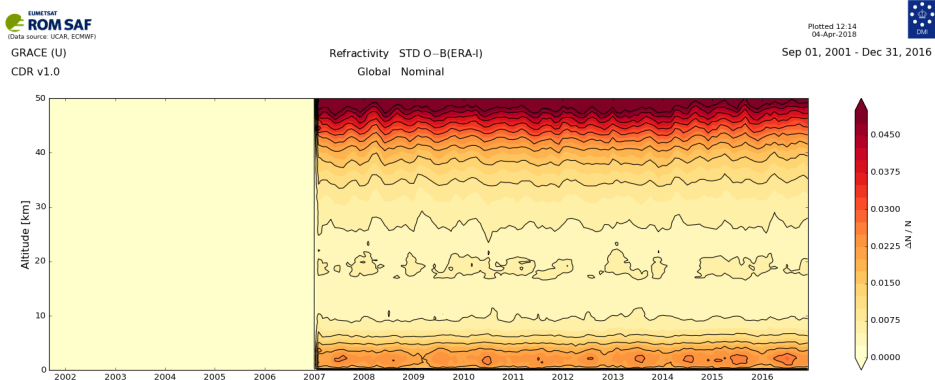
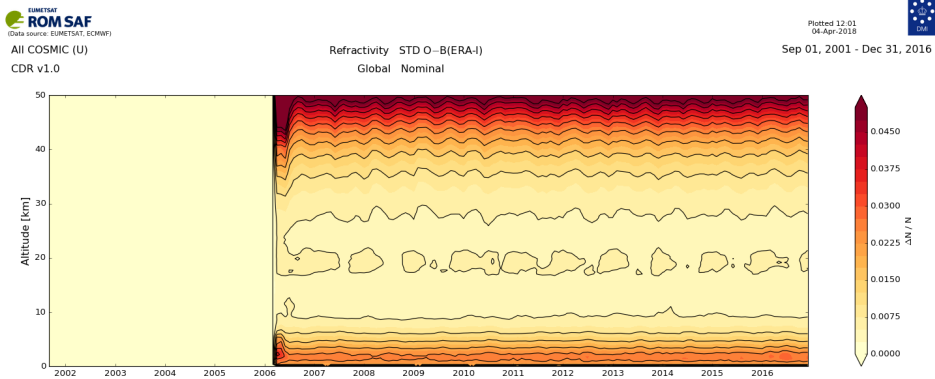
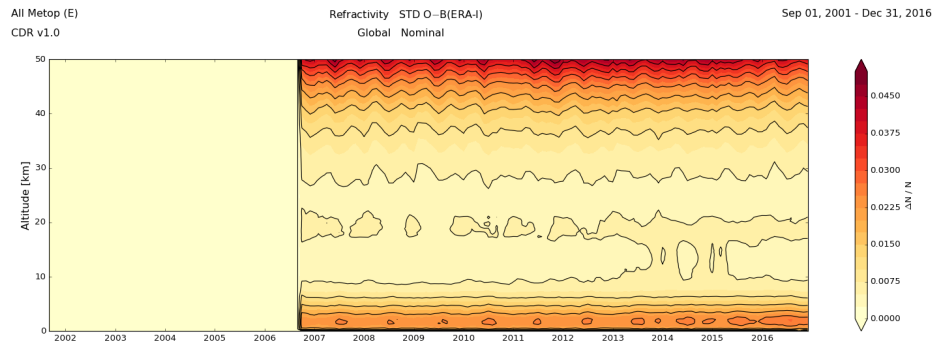


Figure 3.34: Time series of the global monthly refractivity (O-B)/B standard deviation to ERA-Interim for the different missions.

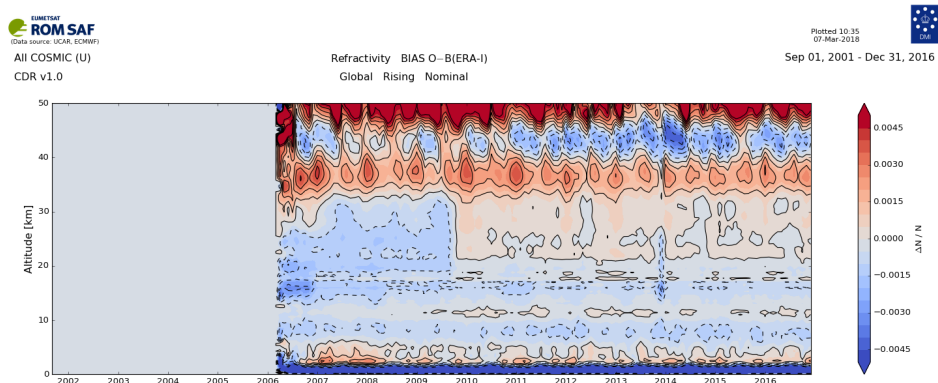
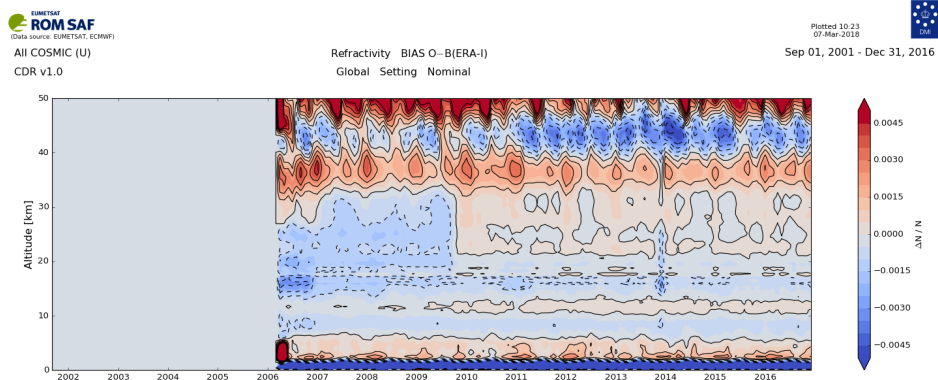
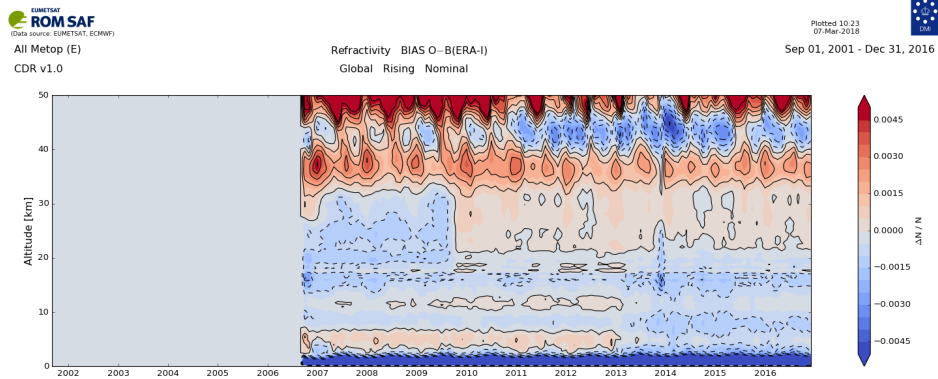
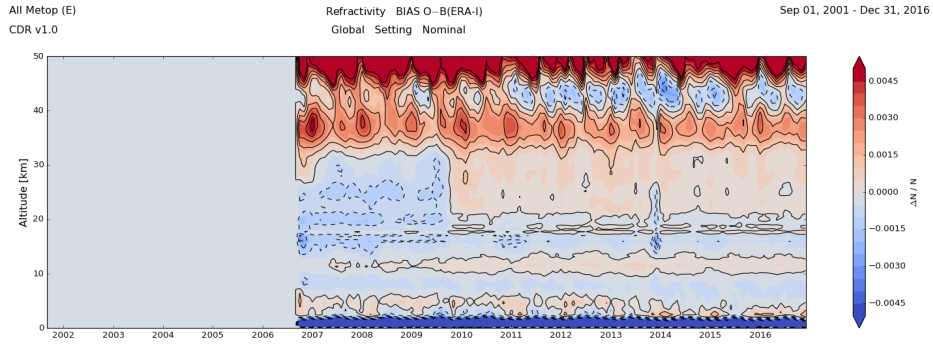


Figure 3.35: Time series of the global monthly refractivity $(O-B)/B$ mean difference to ERA-Interim for setting and rising, Metop and COSMIC.

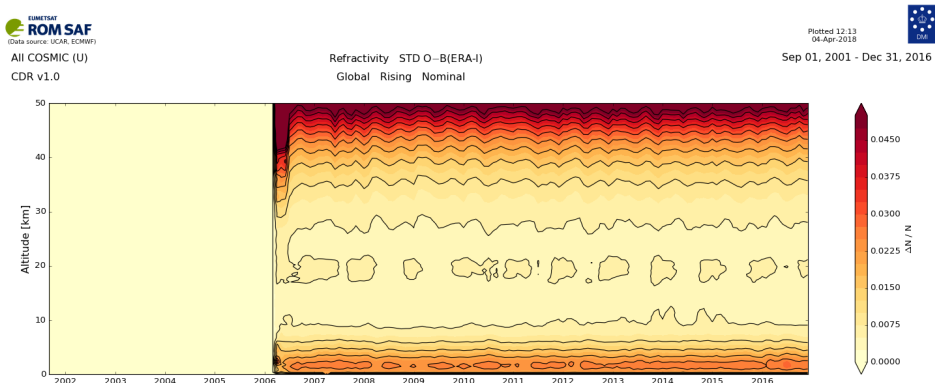
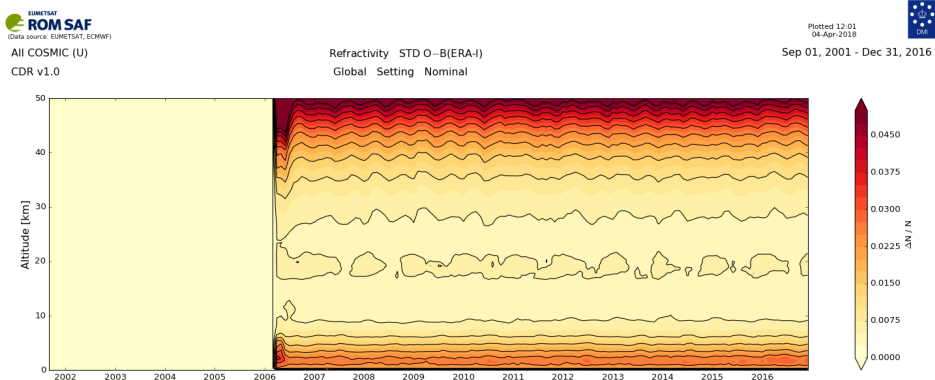
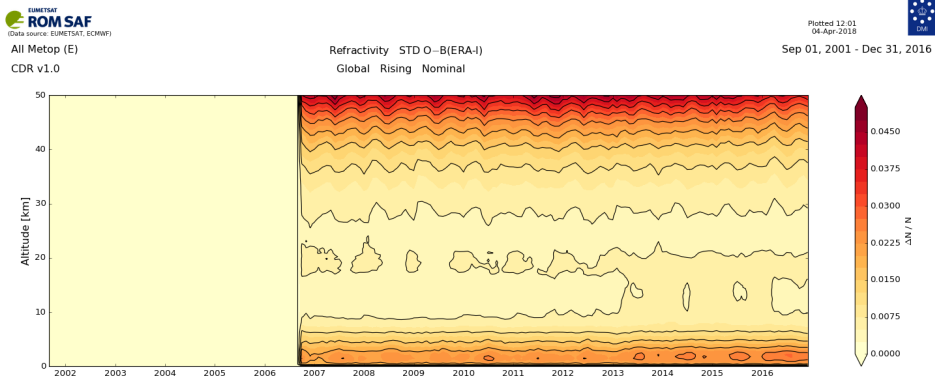
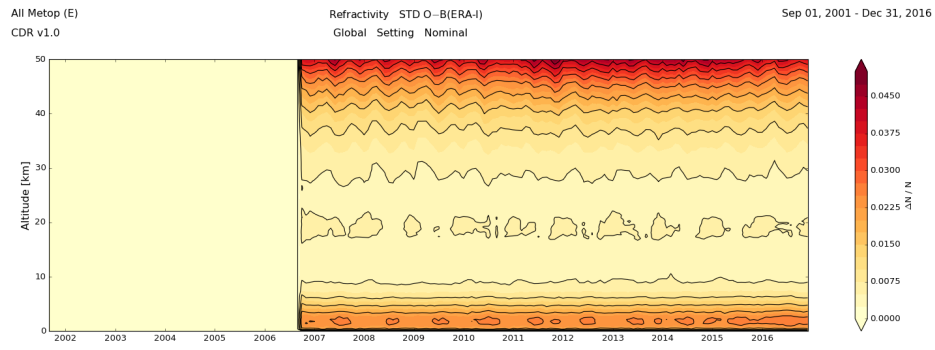


Figure 3.36: Time series of the global monthly refractivity (O-B)/B standard deviation to ERA-Interim for setting and rising, Metop and COSMIC.

3.4.3 Dry temperature

Figures 3.37, 3.38, and 3.39 show plots for dry temperature corresponding to the ones for bending angle and refractivity. Some of the same features can be seen and similar comments can be made, e.g., a small positive bias below 25 km for Metop since 2013 (as opposed to a negative one in refractivity), but generally the features are less obvious in dry temperature. There is nothing to note that was not already discussed in the previous subsections.

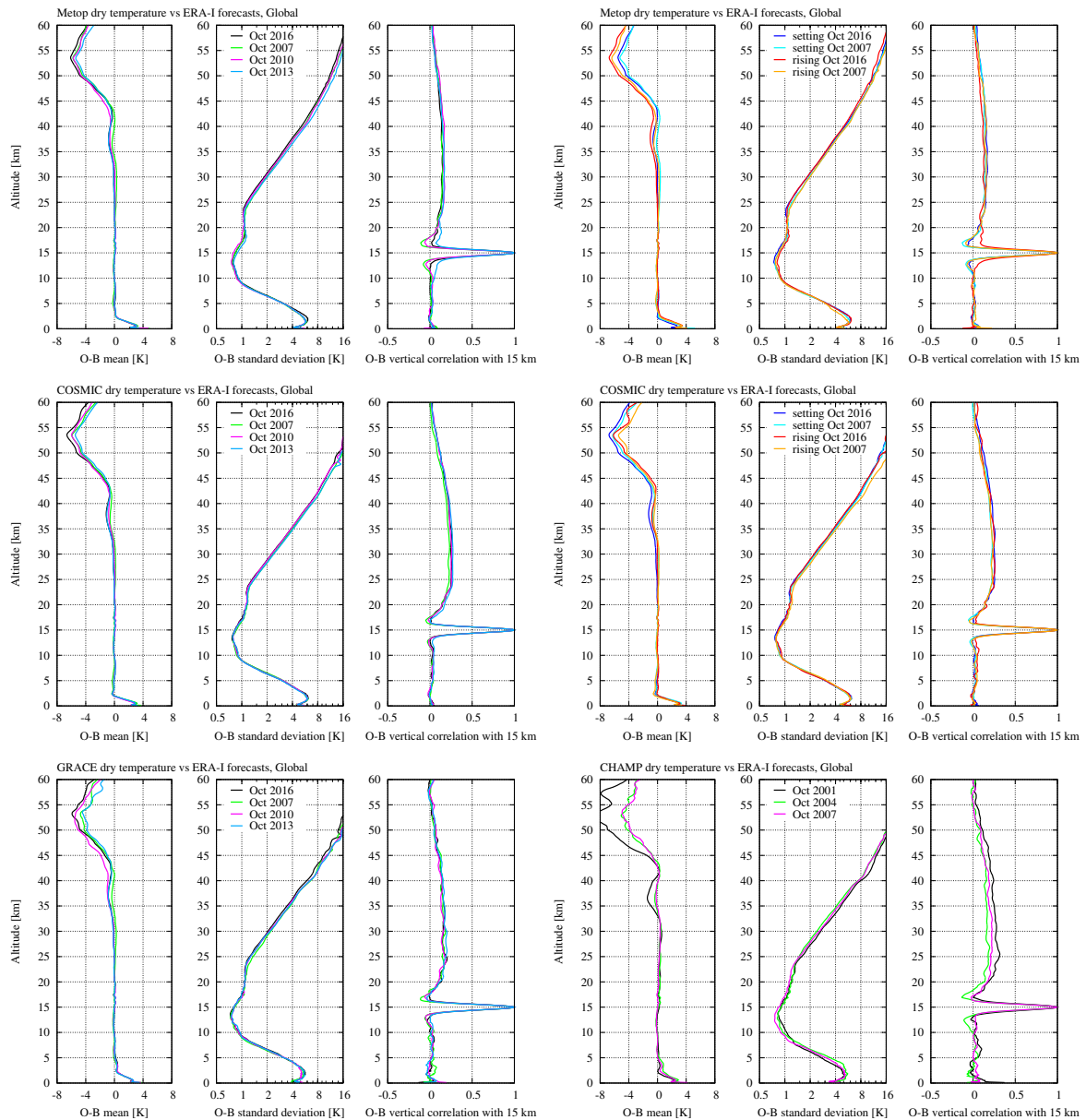


Figure 3.37: Monthly global profile statistics of dry temperature for different years.

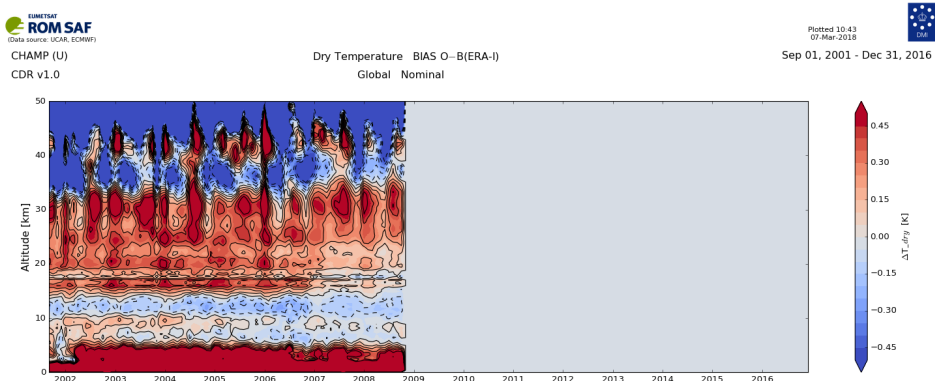
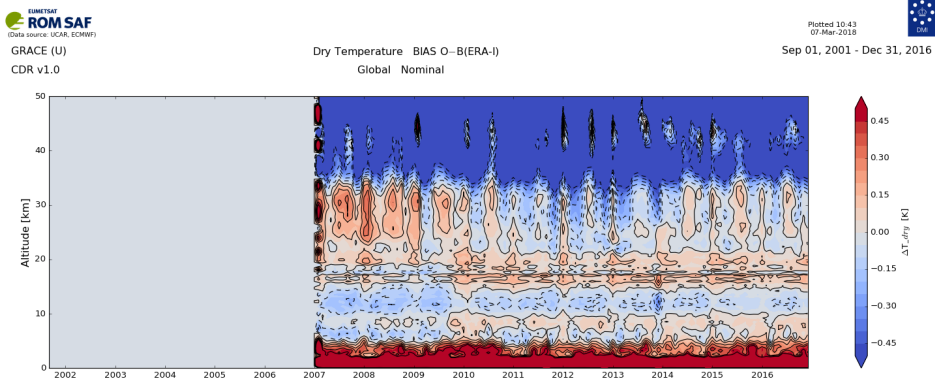
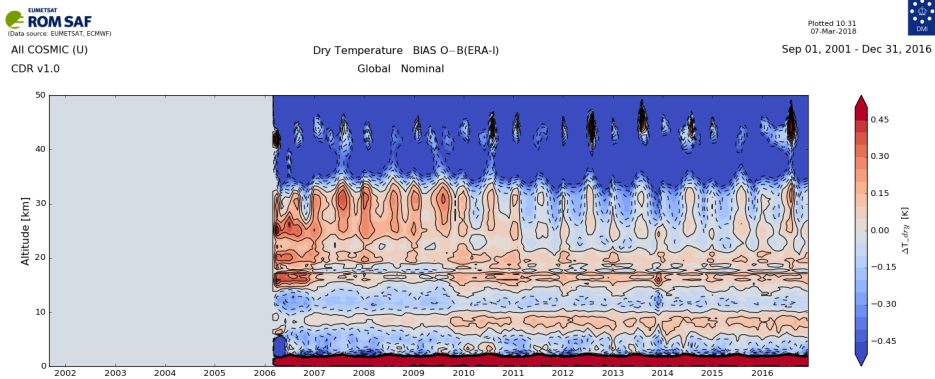
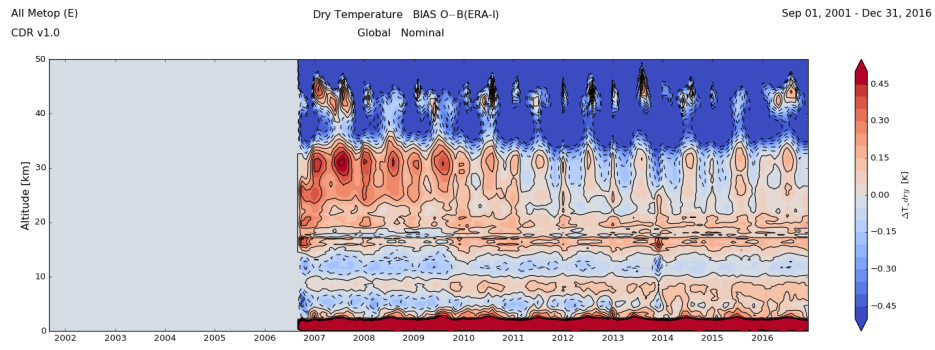


Figure 3.38: Time series of the global monthly dry temperature (O-B)/B mean difference to ERA-Interim for the different missions.

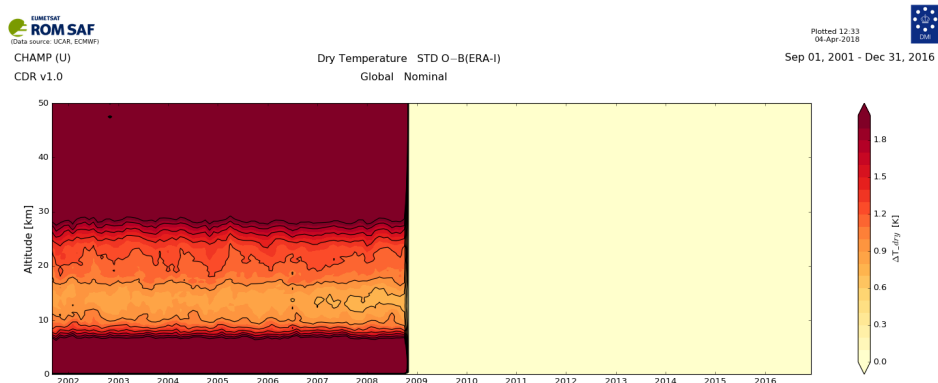
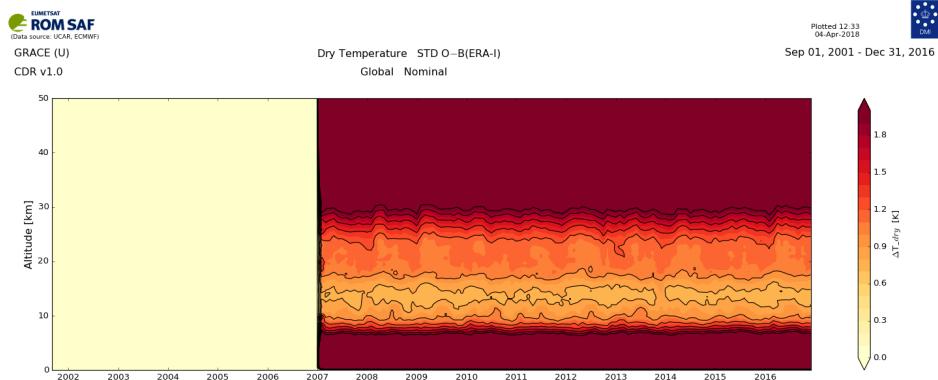
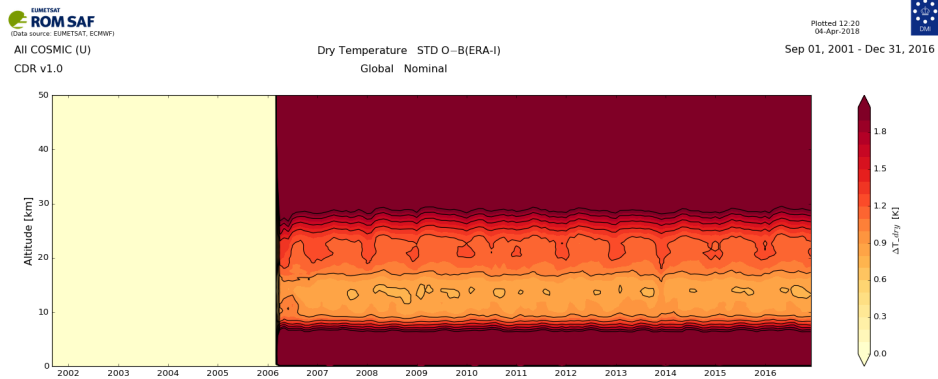
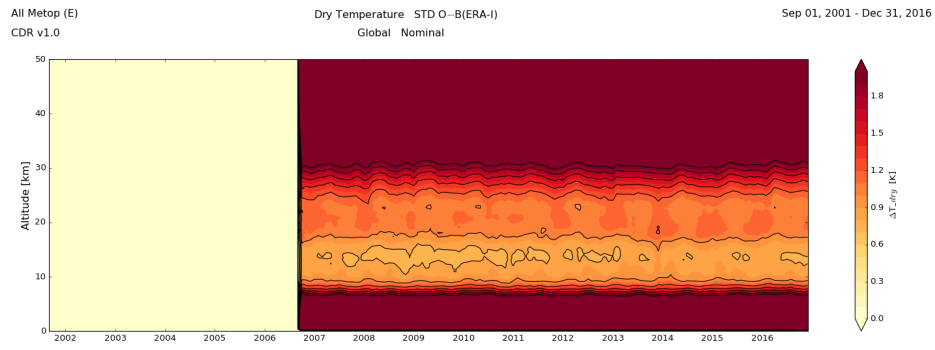


Figure 3.39: Time series of the global monthly dry temperature (O-B)/B standard deviation to ERA-Interim for the different missions.

3.5 Comparison across seasons

In this section we investigate possible seasonal variations in the quality of the ROM SAF CDR v1.0. We show profile statistics against ERA-I forecasts as in previous sections, and use every third month for Metop and COSMIC in 2016 to show the statistics under normal circumstances, as well as two months (January 2013 and February 2016) to show results during periods of Sudden Stratospheric Warming (SSW) events, including the impact of statistical optimization,

The points to be made from this section are that seasonal variations do not seem to have any notable impact on the quality of the data up to 60 km under normal circumstances. However, during SSW events, biases from the statistical optimization may be introduced at high altitudes and result in small overestimations of the mean refractivity and dry temperature in the upper stratosphere and above. Still, the biases in dry temperature are much smaller than the anomalous SSW temperatures, and likely smaller for Metop than for the other missions.

3.5.1 Bending angle

Figure 3.40 shows the monthly global profile statistics of bending angle from Metop and COSMIC for selected months in 2016. The top plots are for January and July, whereas the bottom ones are for April and October.

Focusing on the (O-B)/B means at high altitudes (above 35 km), we see some differences, in particular between the months near the solstices (January and July) and the months near the equinoxes (April and October). A good part of these differences, as well as the non-zero (O-B)/B means, are likely due to systematic biases in the ERA-I data (cf. Section 3.2). Looking at the (O-B)/B standard deviations, there are no indications of any seasonal variations. Thus, under normal circumstances, seasonal variations do not seem to have any notable impact on the quality of the data.

In Section 3.2 we verified that the statistical optimization does not introduce any appreciable bias in the bending angle below 60 km under normal circumstances. In this section we look at more unusual circumstances, such as SSW events. Figure 3.41 shows the daily mean dry temperatures at high northern latitudes (derived from Metop) for two events, one very strong SSW in early 2013, and a less strong one in early 2016. Figure 3.42 shows the statistics of the bending angle against the optimized bending angle for Metop, COSMIC, and GRACE in January 2013 (top plots) and February 2016 (bottom plots) between 40 km and 70 km. These can be compared to similar plots under normal circumstances in Fig. 3.14. In both cases, but more in 2013 than in 2016, the optimized bending angles for all three missions are slightly biased at 60 km and above. The corresponding statistics against ERA-I, for both non-optimized and optimized bending angles are shown in Figs. 3.43, 3.44, and 3.45. Again, the majority of the variations at high altitudes are believed to be mostly due to biases in the ERA-I data, but what is interesting here is that the optimized bending angle is biased positive at very high altitudes compared to the non-optimized bending angle, most for GRACE, less for COSMIC, and least for Metop. This makes good sense as we earlier verified (Section 3.1.1) that Metop data are the least noisy, followed by COSMIC, GRACE, and CHAMP, and that the altitude, above which the climatology used in the statistical optimization has influence, is lower the more noise there is. In the following subsections we look at how these biases seem

to propagate to refractivity and dry temperature, giving an idea of the impact in these higher level products.

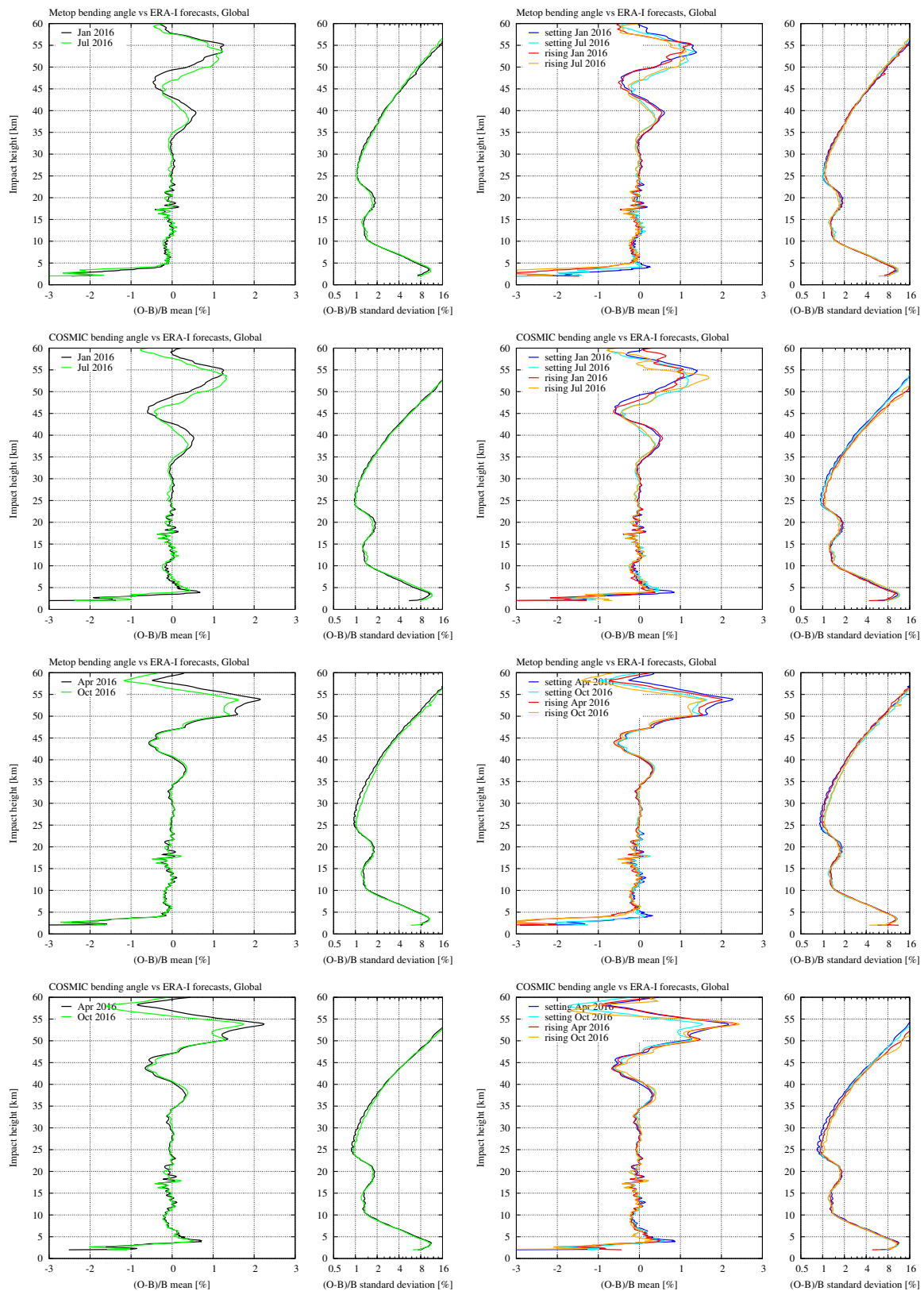


Figure 3.40: Monthly global profile statistics of bending angle for Metop and COSMIC for different seasons.

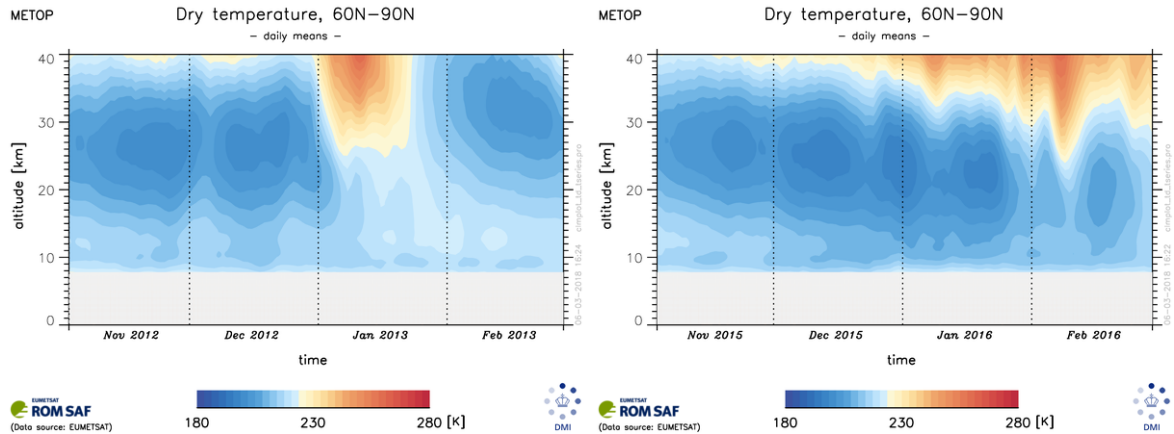


Figure 3.41: Daily mean dry temperature from Metop at northern high latitudes during the SSW events of early 2013 and 2016.

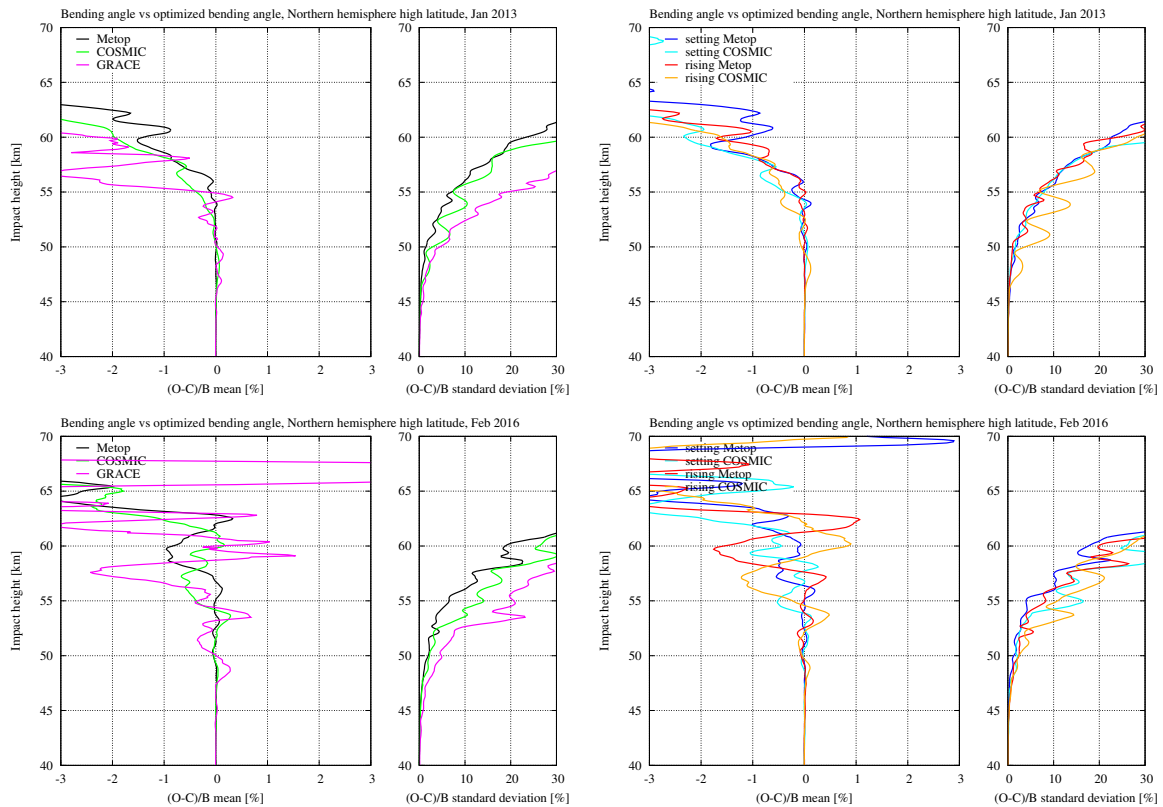


Figure 3.42: Monthly profile statistics of bending angle against optimized bending angle at northern high latitudes during the SSW events of early 2013 and 2016.

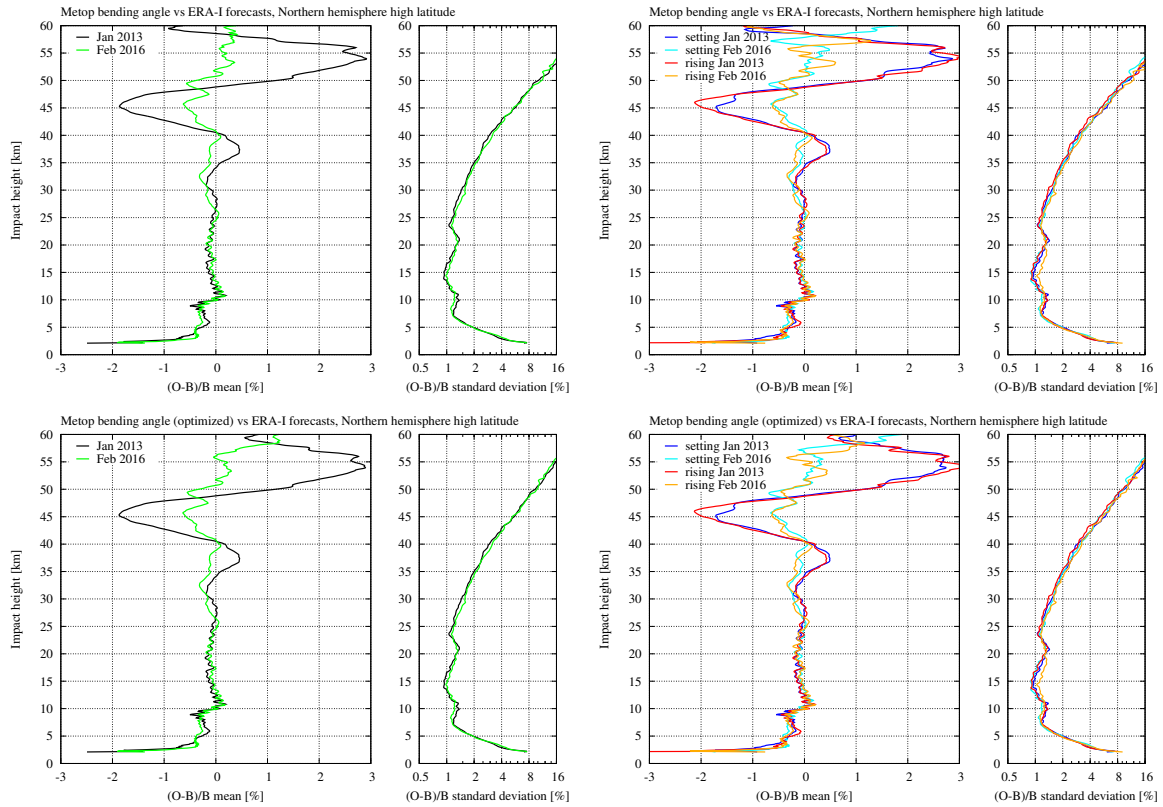


Figure 3.43: Monthly profile statistics of bending angle and optimized bending angle from Metop at northern high latitudes during the SSW events of early 2013 and 2016.

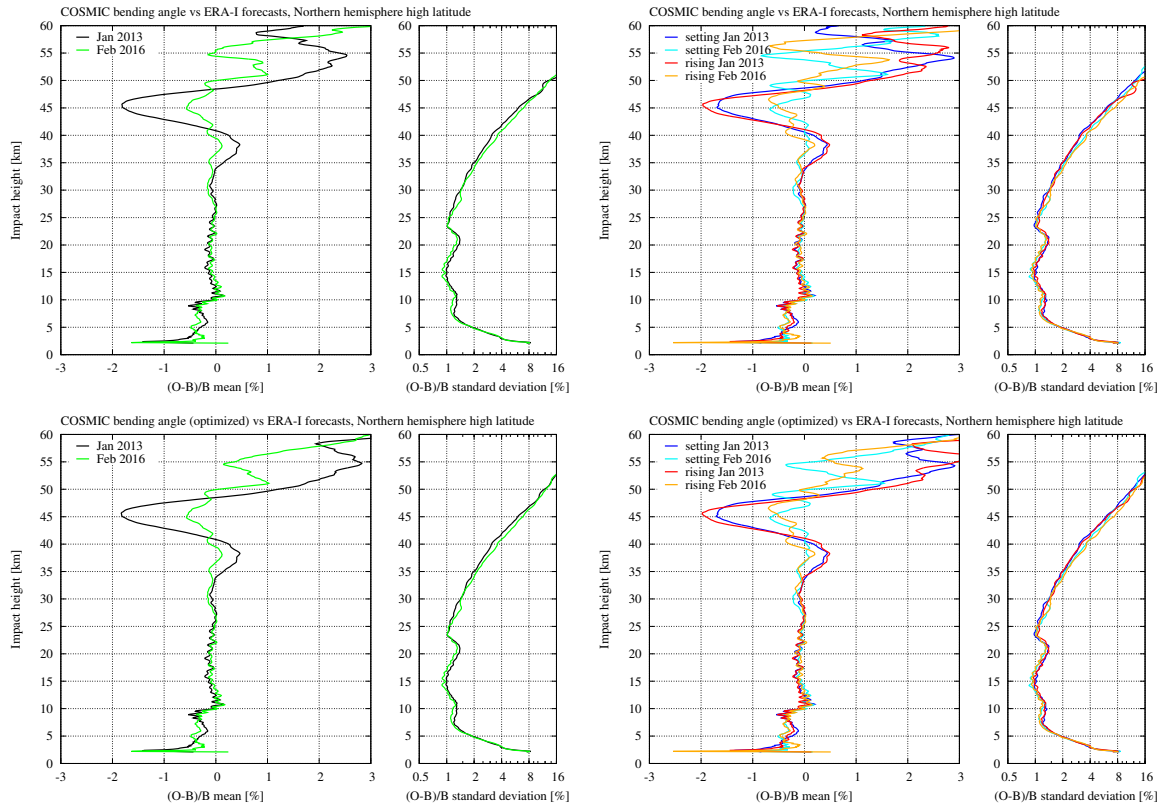


Figure 3.44: Monthly profile statistics of bending angle and optimized bending angle from COSMIC at northern high latitudes during the SSW events of early 2013 and 2016.

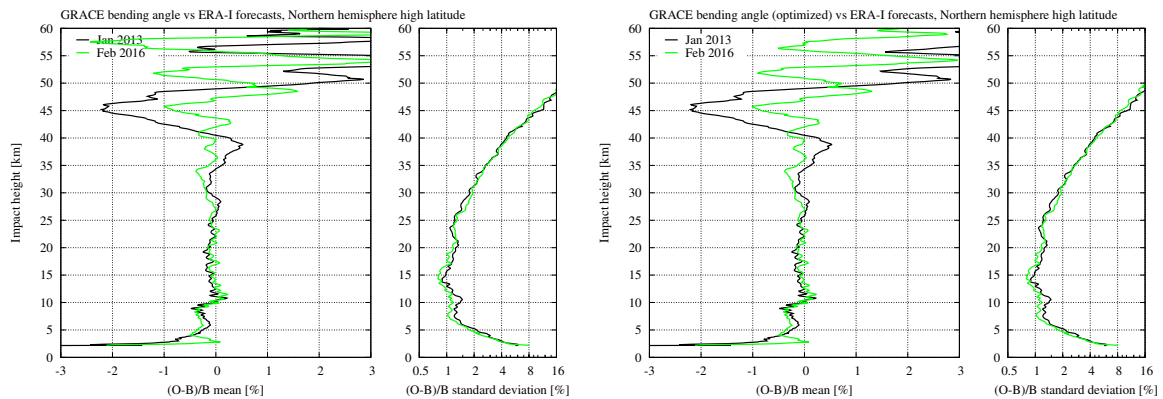


Figure 3.45: Monthly profile statistics of bending angle and optimized bending angle from GRACE at northern high latitudes during the SSW events of early 2013 and 2016.

3.5.2 Refractivity

For reference, Fig. 3.46 shows the monthly global profile statistics for refractivity for the four selected months in 2016 under normal circumstances, corresponding to the statistics for bending angle from Metop and COSMIC in Fig. 3.40. Note that the SSW event in 2016 started already in January (see Fig. 3.41), which is one of the months that we consider normal here. However, there does not seem to be much impact from this relatively weaker part of

the SSW in January 2016 on the global mean against ERA-I at high altitudes for that month; the (O-B)/B mean for January is fairly similar to the (O-B)/B mean for July, for both Metop and COSMIC.

The situation is different when we look at the months of the SSW events in January 2013 and February 2016 (noting also that we are here looking only at northern hemisphere high latitudes) in Figs. 3.47, 3.48, and 3.49, corresponding to the plots in Figs. 3.43, 3.44, and 3.45. We can not know how much of the bias is due to the ERA-I data and how much is due to the impact of the statistical optimization, but we can see that the biases at high altitudes are larger for COSMIC and GRACE than for Metop. However, there are differences between missions at high altitudes in the non-optimized bending angle as well. In fact, it is difficult to say how much of the differences in refractivity between missions is a result of the statistical optimization and how much is a result of the already different (O-B)/B means in the non-optimized bending angle. Taking everything into consideration (biases in the ERA-I data, differences between non-optimized and optimized bending angle, differences between missions and their different noise levels, as well as the corresponding plots for dry temperature in the following subsection), it does not seem that the statistical optimization in the cases of these SSW events introduces systematic biases of more than a few percent in refractivity at high altitudes (50–60 km). Likely the introduced biases are largest for GRACE and CHAMP, smaller for COSMIC, and smallest for Metop.

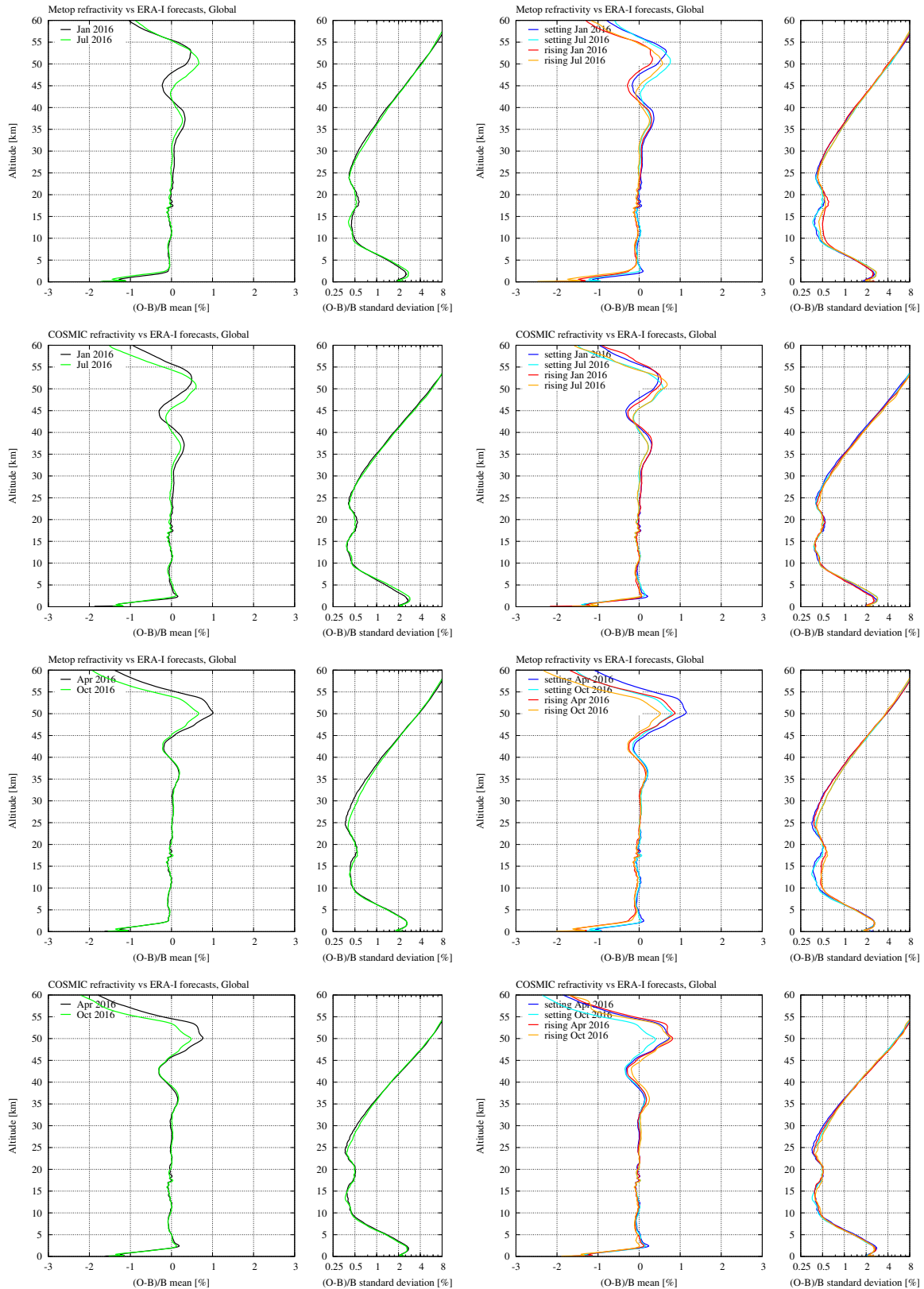


Figure 3.46: Monthly global profile statistics of refractivity from Metop and COSMIC for different seasons.

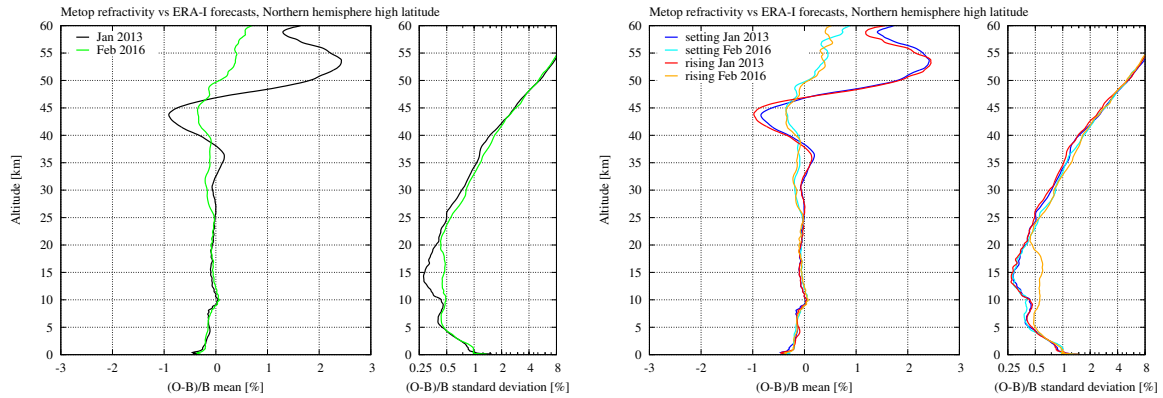


Figure 3.47: Monthly profile statistics of refractivity from Metop at northern high latitudes during the SSW events of early 2013 and 2016.

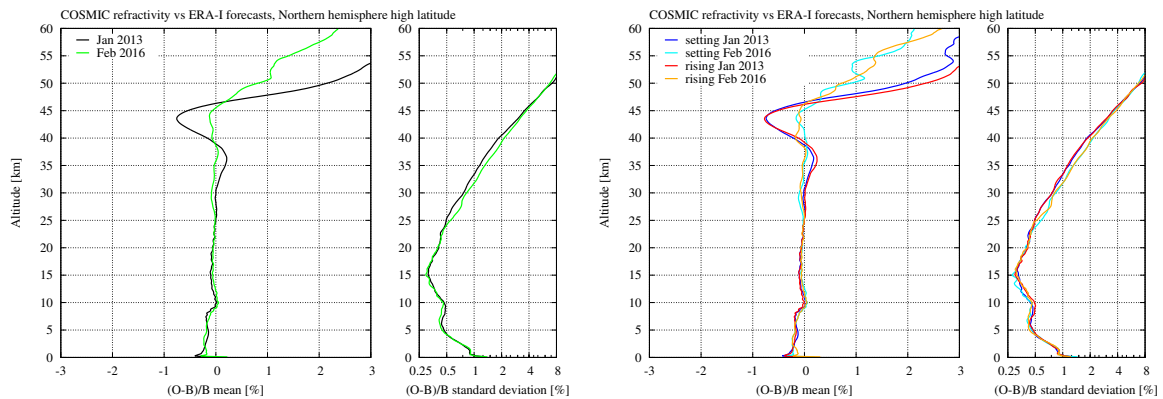


Figure 3.48: Monthly profile statistics of refractivity from COSMIC at northern high latitudes during the SSW events of early 2013 and 2016.

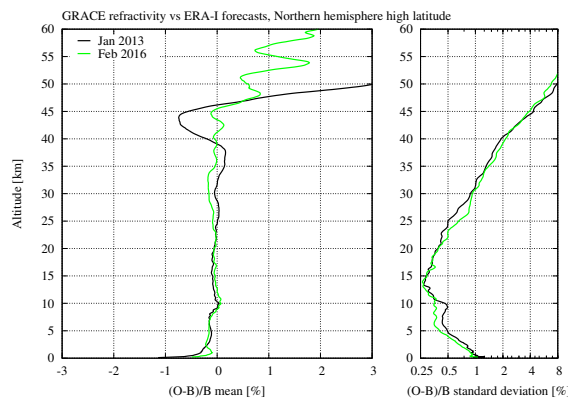


Figure 3.49: Monthly profile statistics of refractivity from GRACE at northern high latitudes during the SSW events of early 2013 and 2016.

3.5.3 Dry temperature

Figures 3.50–3.53 show the plots for dry temperature corresponding to the ones for refractivity in the previous subsection. We note here how the biases for the months of the SSW

events seem to propagate to lower altitudes in dry temperature (down to below 30 km for GRACE in Fig. 3.53), and that they are overestimations (i.e., positive) as are the refractivity biases (given that the O-B biases for COSMIC and GRACE are larger than for Metop). As discussed in Section 3.2, the fact that the refractivity and dry temperature biases are not mirrors of each other at these altitudes is related to the biases in dry pressure. These are shown for reference in Figs. 3.54–3.56. Still, the introduced dry temperature biases below 40 km are much smaller than the anomalous temperatures of the SSW events in Fig. 3.41. Thus, the dry temperature product can be used for estimation of SSW events, but one should have in mind that there may be positive biases up to a few Kelvin at 40 km, and increasingly larger biases above. Dry temperature estimates from Metop are likely more trustworthy in this respect than estimates from the other missions. However, it should be noted here that a general look at the Metop data at high altitudes in Section 3.8 reveals mean differences between rising and setting occultations of a similar size as the mean differences between the missions seen in Figs. 3.51–3.53.

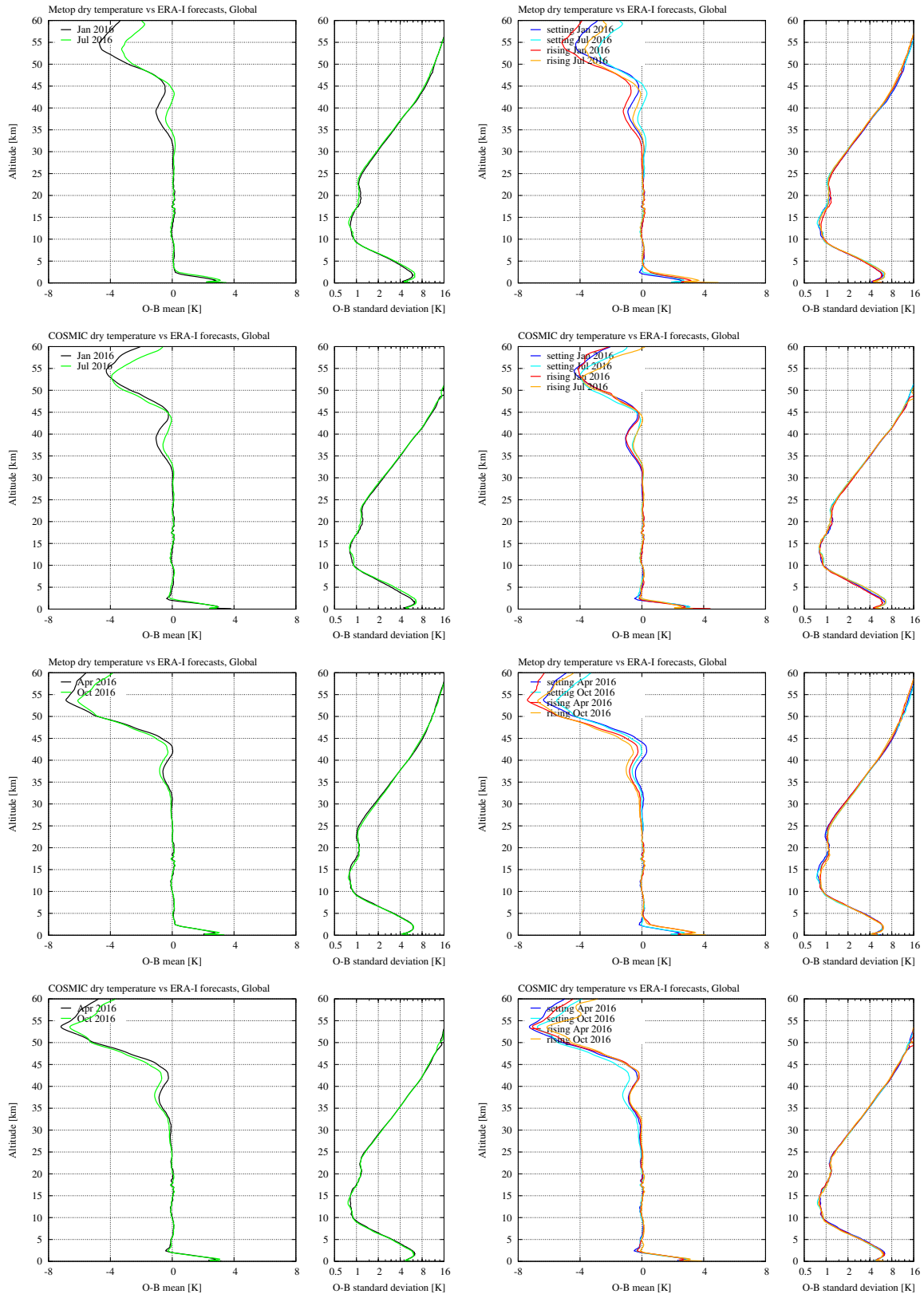


Figure 3.50: Monthly global profile statistics of dry temperature for Metop and COSMIC for different seasons.

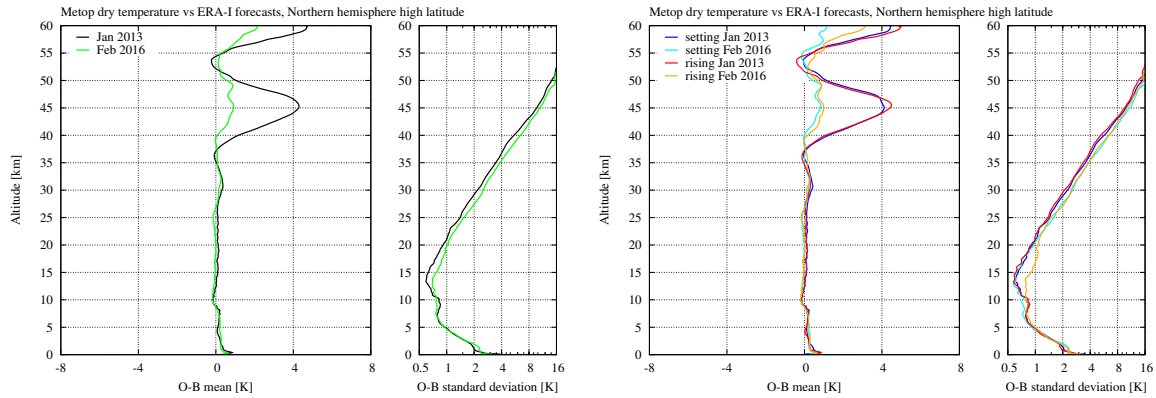


Figure 3.51: Monthly profile statistics of dry temperature from Metop at northern high latitudes during the SSW events of early 2013 and 2016.

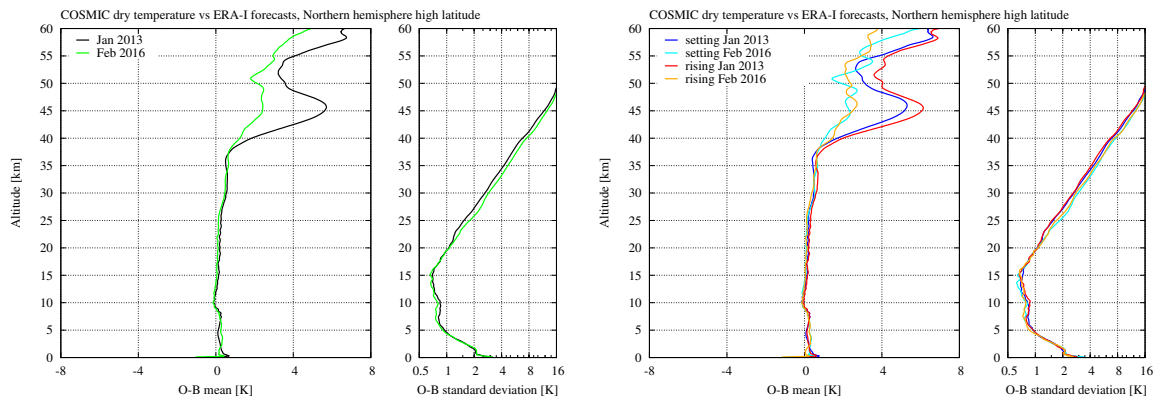


Figure 3.52: Monthly profile statistics of dry temperature from COSMIC at northern high latitudes during the SSW events of early 2013 and 2016.

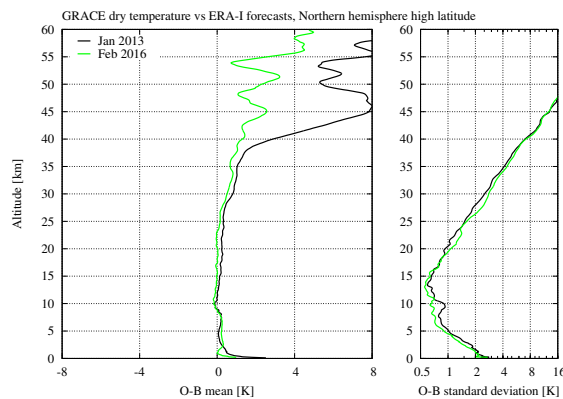


Figure 3.53: Monthly profile statistics of dry temperature from GRACE at northern high latitudes during the SSW events of early 2013 and 2016.

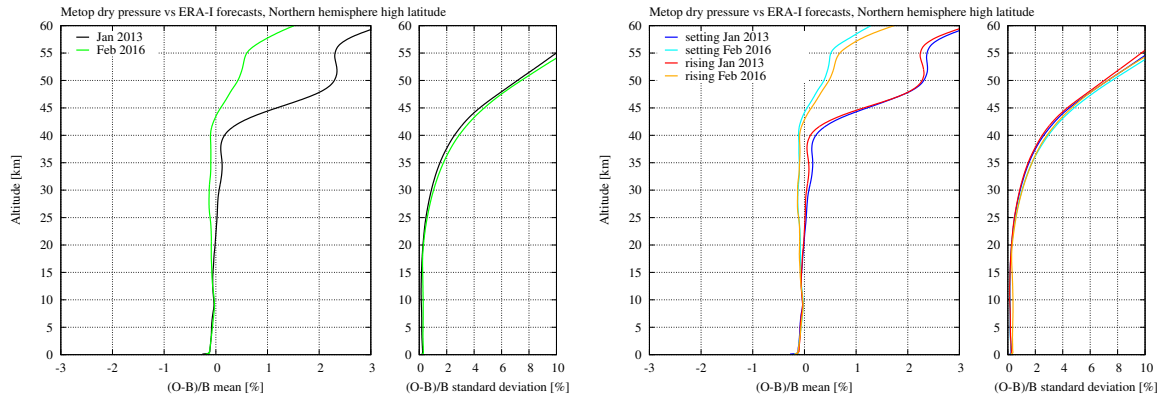


Figure 3.54: Monthly profile statistics of dry pressure from Metop at northern high latitudes during the SSW events of early 2013 and 2016.

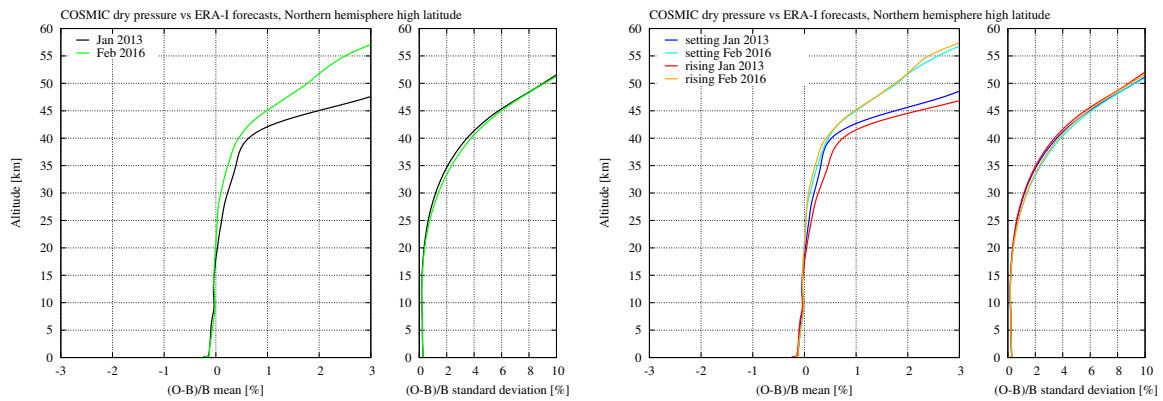


Figure 3.55: Monthly profile statistics of dry pressure from COSMIC at northern high latitudes during the SSW events of early 2013 and 2016.

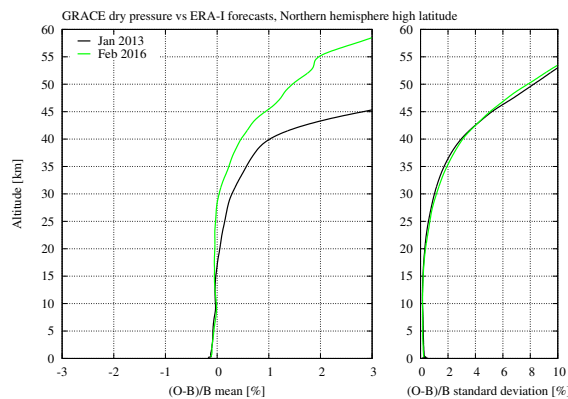


Figure 3.56: Monthly profile statistics of dry pressure from GRACE at northern high latitudes during the SSW events of early 2013 and 2016.

3.6 Comparison against products from the EUMETSAT Secretariat

This section is dedicated to the statistical comparison between the Metop bending angles from the ROM SAF CDR v1.0 and the Metop bending angles that are part of the reprocessed data record (v1.4) from the EUMETSAT Secretariat. We use the thinned data from the EUMETSAT Secretariat and show global statistics as well as statistics separated into latitude bands (cf. Section 3.1) for the October 2016 baseline month. Although we only take into account common nominal occultations, it was necessary to remove a few additional outliers in the data from the EUMETSAT Secretariat to avoid spurious spikes in the statistics.

The points to be made from this section are that the Metop bending angles from the ROM SAF CDR v1.0, for both setting and rising occultations, are very similar in the mean to those of the reprocessed data record from the EUMETSAT Secretariat above 10 km. At the highest altitudes, a very small difference is likely due to a higher order ionospheric correction in the data from the EUMETSAT Secretariat, not accounted for in the ROM SAF CDR v1.0. Between 10 km and 25 km there is a small bias difference in rising occultations since 2013. Section 3.8 contains a more detailed analysis of this difference. Below 10 km, the two data sets show very different biases, mostly due to known problems in the data from the EUMETSAT Secretariat. The standard deviations to ERA-I forecasts are generally smaller for the ROM SAF CDR v1.0, most likely also due to known problems in the data from the EUMETSAT Secretariat.

3.6.1 Bending angle

Figure 3.57 shows the monthly global profile statistics of bending angle from Metop. The top plots are a direct comparison of the ROM SAF CDR v1.0 (RE1A) to the EUMETSAT data, whereas the bottom plots show the statistics of each data set (RE1A and EUME) against ERA-I. Figures 3.58, 3.59, and 3.60 show the same for low, mid, and high latitudes.

The (O-C)/B means between the two data sets (top plots; C in the numerator here being the EUMETSAT data; B in the denominator is the ERA-I data) are very close to zero except at impact heights below 10 km, where we see a split between setting and rising occultations, and large biases. At the highest altitudes, a very small difference, largest at low latitudes, is likely due to a higher order ionospheric correction in the EUMETSAT bending angle, not accounted for in the ROM SAF CDR v1.0. The statistics against ERA-I (bottom plots; B in the numerator here being the ERA-I data) indicate that the biases below 10 km are mostly in the EUMETSAT data, but also partly in the RE1A data below 5 km as discussed in Section 3.1.1. Interestingly, the (O-B)/B mean of the EUMETSAT bending angle between 5 km and 10 km for rising occultations at high latitudes is consistent with the (O-B)/B means for both setting and rising occultations in the RE1A data. Investigations of the cause for the larger biases in the EUMETSAT data are ongoing at the EUMETSAT Secretariat.

Although difficult to see in these plots, there is a smaller, almost constant bias (percentage wise) between the two data sets in the 10–25 km range in the direct comparisons (less than 0.1%, and most noticeable at high latitudes). The bias is in rising occultations, and is related to the changed tracking strategy in 2013 discussed in Section 3.3. Differences between rising and setting occultations in the (O-B)/B means against ERA-I forecasts (difficult to see in the plots here where curves are almost on top of each other; it is more evident in the 1D monthly profile plots at <http://www.romsaf.org/re1/index.php>), as well as the absence of a

visible mean difference between setting and rising occultations in the EUMETSAT near real-time data (see <http://www.romsaf.org/monitoring/index.php>), indicate that it is more a bias in the ROM SAF CDR v1.0 than in the EUMETSAT reprocessed data. A more detailed analysis of this difference between the two data sets is given in Section 3.8.

The (O-B)/B standard deviations against ERA-I are generally smaller for the RE1A data than for the EUMETSAT data (with minor exceptions around 20 km at low and mid latitudes). Below ~15 km this is seen to be mainly a difference in setting occultations, where the standard deviations for the EUMETSAT data are considerably larger than the standard deviations for both setting and rising occultations in the RE1A data, which in turn are only slightly smaller than the standard deviations for rising occultations in the EUMETSAT data. At higher altitudes (above ~23 km), the main reason for the larger standard deviations in the EUMETSAT data is likely due to erroneous oscillations, possibly being a result of inconsistent smoothing of the L1 and L2 signals in the processing at the EUMETSAT Secretariat. Added to this comes possibly larger noise in the EUMETSAT Secretariat retrievals because wave optics processing is used at all altitudes (in the ROM SAF retrievals, geometrical optics processing is used above 25 km [RD.5]). Investigations of the erroneous oscillations in the EUMETSAT data are ongoing at the EUMETSAT Secretariat. A minor reason for the different standard deviations against ERA-I could be related to different smoothing strategies, but because of the other factors mentioned above, it is difficult to assess the real impact of different smoothings.

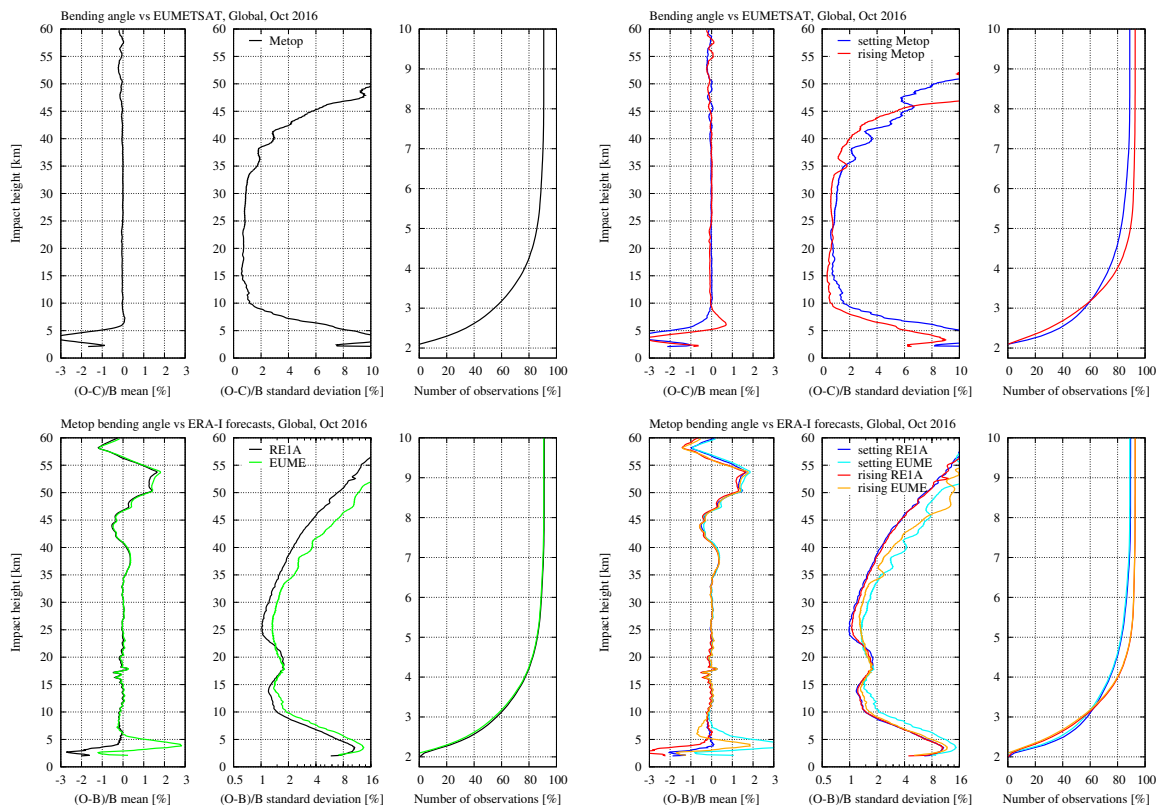


Figure 3.57: Monthly global profile statistics of bending angle from Metop (from the RE1A processing) against the bending angle processed at the EUMETSAT Secretariat.

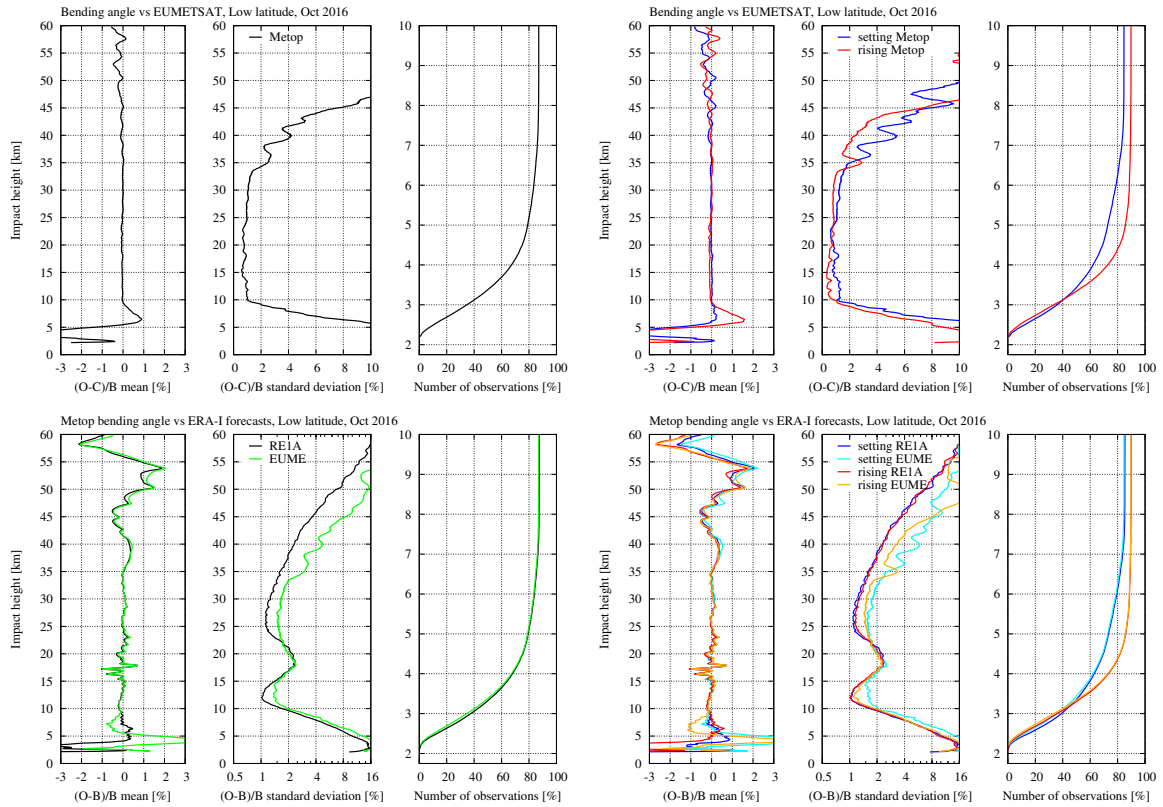


Figure 3.58: Monthly low latitude profile statistics of bending angle from Metop (from the REIA processing) against the bending angle processed at the EUMETSAT Secretariat.

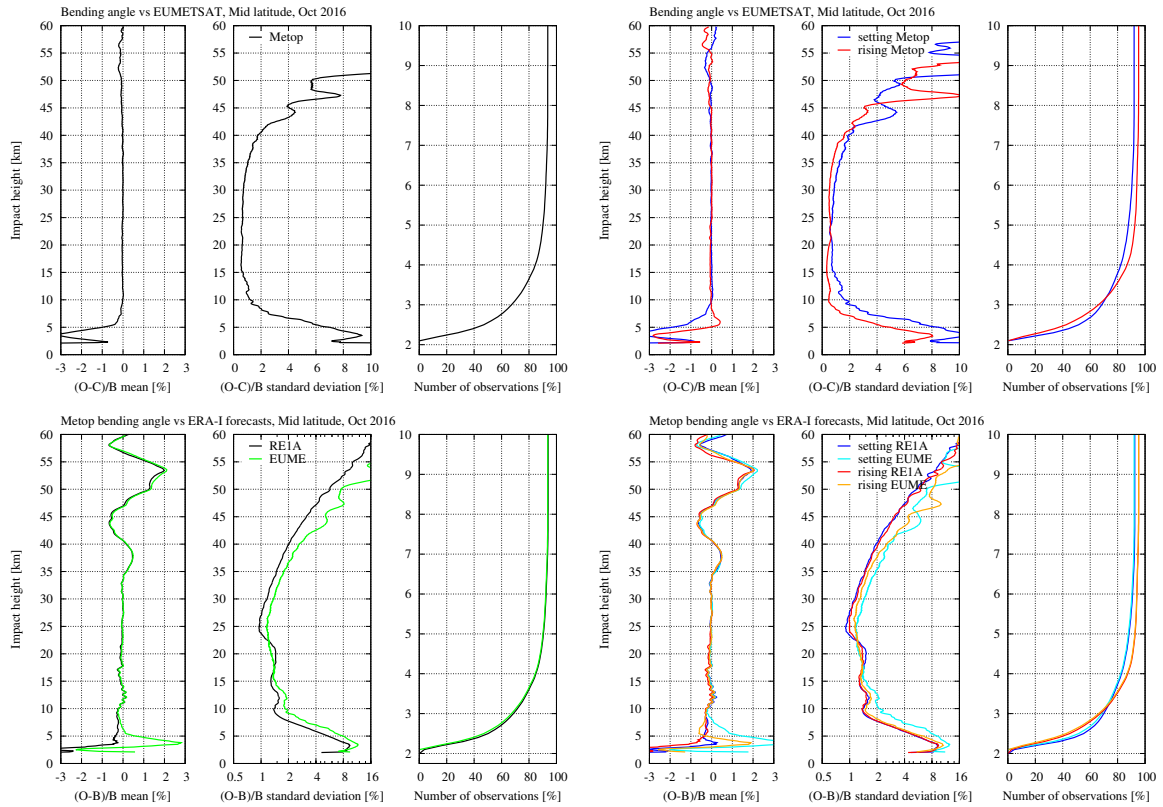


Figure 3.59: Monthly mid latitude profile statistics of bending angle from Metop (from the REIA processing) against the bending angle processed at the EUMETSAT Secretariat.

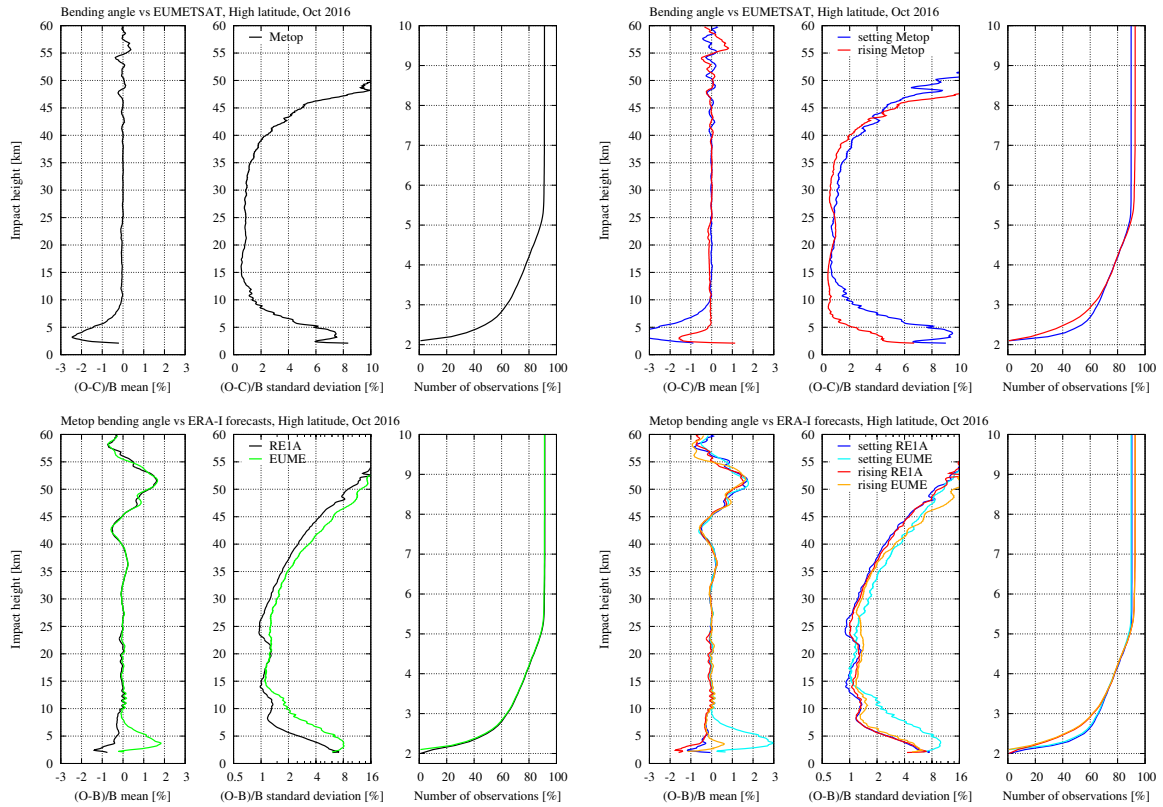


Figure 3.60: Monthly high latitude profile statistics of bending angle from Metop (from the REIA processing) against the bending angle processed at the EUMETSAT Secretariat.

3.7 Comparison against products from UCAR/CDAAC

In this section we look at the statistical comparisons between the ROM SAF CDR v1.0 for all missions and the corresponding products from UCAR/CDAAC. Again we show global statistics as well as statistics separated into latitude bands. We use both baseline months (October 2007, October 2016) to also include CHAMP in 2007, and to include differences due to different processing versions in the UCAR data over time. It should be noted that we here compare to the latest UCAR reprocessing for CHAMP, and not the version that was used as input to the ROM SAF reprocessing (cf. Table 2.2). The version numbers and the processing mode (R for reprocessed; P for post-processed) for the processed UCAR data that we compare to here are summarized in Table 3.1.

Table 3.1: Version numbers of UCAR data compared to in this section.

Mission	Metop	COSMIC	GRACE	CHAMP
Oct 2007	2016.0120(R)	2013.3520(R)	2010.2640(P)	2016.2430(R)
Oct 2016	2016.0120(P)	2014.2860(P)	2014.2760(P)	

The points to be made from this section are that the ROM SAF CDR v1.0 data, for all missions and for all of bending angle, refractivity, and dry temperature, are quite similar to the corresponding data processed at UCAR/CDAAC. Main exceptions are:

- More noise in the ROM SAF CDR v1.0 data for CHAMP at high altitudes
- Small bias differences for all missions below 8 km impact height (6 km altitude), primarily at low latitudes
- Discrepancies around 20–25 km in the (O-B)/B standard deviations against ERA-I, presumably due to different handling of the transition between geometrical optics (GO) and wave optics (WO) processing.
- Discrepancies in the standard deviations and vertical correlations against ERA-I for refractivity (and to a smaller extent for bending angle and dry temperature as well) in the 10–20 km range, most likely due to different L2-extrapolation strategies
- Bias and standard deviation differences at high altitudes for refractivity and dry temperature, being a result of different choices made in the statistical optimization approach
- Generally, slightly smaller standard deviations in bending angle for the ROM SAF CDR v1.0 data, which indicate more smoothing in the ROM SAF reprocessing.

3.7.1 Bending angle

Figures 3.61 and 3.62 show the monthly global profile statistics of bending angle from all missions for October 2007 and October 2016, respectively. The top plots are direct comparisons of the ROM SAF CDR v1.0 (RE1A/RE1B) to the UCAR data for all missions, whereas the other plots show the statistics for each mission and data set (RE1A/RE1B and UCAR) against ERA-I. Figures 3.63–3.68 show the same for low, mid, and high latitudes. The bottom right plots (three panels) for October 2016 show vertical correlations of bending angle

to supplement the corresponding results in refractivity discussed in the next subsection. They will not be discussed further here.

The (O-C)/B means between the two data sets (top plots; C in the numerator here being the UCAR data; B in the denominator is the ERA-I data) are very close to zero from about 8 km impact height and up to where the more random differences in the data sets start to dominate. Bias differences, being largest at low latitudes, appear below 8 km for all missions. This is reflected in the statistics against ERA-I. However, for CHAMP (October 2007), the (O-B)/B means against ERA-I are very similar below 8 km (basically showing no bias difference), whereas in the direct comparisons (top plots) there is a notable bias difference for CHAMP (almost 1% near 5 km impact height in the low latitude statistics). For GRACE (October 2007) it seems to be the opposite: there is very little bias difference near 5 km in the direct comparisons, but a notable difference between the (O-B)/B means against ERA-I. This seems inconsistent at first glance, but we should keep in mind the differences in the penetration statistics and how comparisons are carried out. For both missions the penetration statistics show that there are more nominal observations in the RE1B data than in the UCAR data in the lowest few kilometers. In the direct comparisons, we can naturally only include observations that are in both data sets, therefore effectively leaving out some of the lowest RE1B observations. This apparently shifts the bias around 5 km to the positive side for both GRACE and CHAMP. In the October 2016 plots there is a similar shift for GRACE, and the statistics look somewhat like CHAMP in the October 2007 plots (note that the UCAR versions for the October 2007 and October 2016 GRACE data are different). During the re-processing activity at the ROM SAF, an early trial processing of the GRACE and CHAMP data had much larger negative biases below 5 km impact height, and modifications in the re-processing software were made in an attempt to detect tracking errors for these two missions, and cut off the lowest parts of the profiles to reduce these biases. However, the results here indicate that there might still be a smaller number of occultations for which the lowest part is biased negative due to tracking errors, and that these are dealt with better (cut off) in the UCAR processing than in the ROM SAF processing.

For Metop, a good part of the (O-B)/B bias disagreement below 8 km impact height (primarily at low latitudes) is seen to be due to the UCAR rising (October 2007) and setting (October 2016) occultations being biased negative compared to the other curves, down to ~4 km (second row of plots from the top in Figs. 3.61 and 3.62). This seems to correlate with the penetration statistics, where there are fewer nominal observations in the lowest few kilometers for UCAR rising (October 2007) and setting (October 2016) occultations.

For COSMIC, the (O-B)/B bias disagreement is similar to that of Metop down to ~5 km impact height, but increases further downward and peaks around 4 km (third row of plots from the top in Figs. 3.61 and 3.62). This is apparently due to an increase in the bias in the RE1B data, which is not understood. We note that the penetration in the UCAR processing was better for the October 2016 data than for the October 2007 data due to different UCAR versions (the RE1B and the UCAR number of observations being the same all the way down to low impact heights in 2016, indicating that the penetration in the UCAR data may be even better; cf. the introductory remarks in Chapter 3), but seemingly that has no significant impact on the (O-B)/B means against ERA-I forecasts.

The (O-B)/B standard deviations are fairly similar between the two data sets, except that there seems to be more noise in the RE1B data for CHAMP at high altitudes (e.g., in the lowermost

right plot of Fig. 3.61, and that there seems to be less noise in the direct comparisons for COSMIC and GRACE in October 2016 than in October 2007 (e.g., the (O-C)/B standard deviation at 40 km is about 2% in the uppermost left plot of Fig. 3.61, whereas it is about 1.5% in the uppermost left plot of Fig. 3.62). These issues are not understood. Discrepancies around 20–25 km in the (O-B)/B standard deviations against ERA-I are presumably due to different handling of the transition between geometrical optics (GO) and wave optics (WO). In the ROM SAF reprocessing there is a gradual transition between GO above 25 km and WO below 20 km; in between it is a transitional weighted average of the GO and WO processings. Seemingly the transition is more abrupt in the UCAR data near 20 km, with the exception being GRACE for October 2007, which is an older processing. Generally, standard deviations against ERA-I are slightly larger for the UCAR data, which could perhaps be explained by more smoothing in the ROM SAF reprocessing.

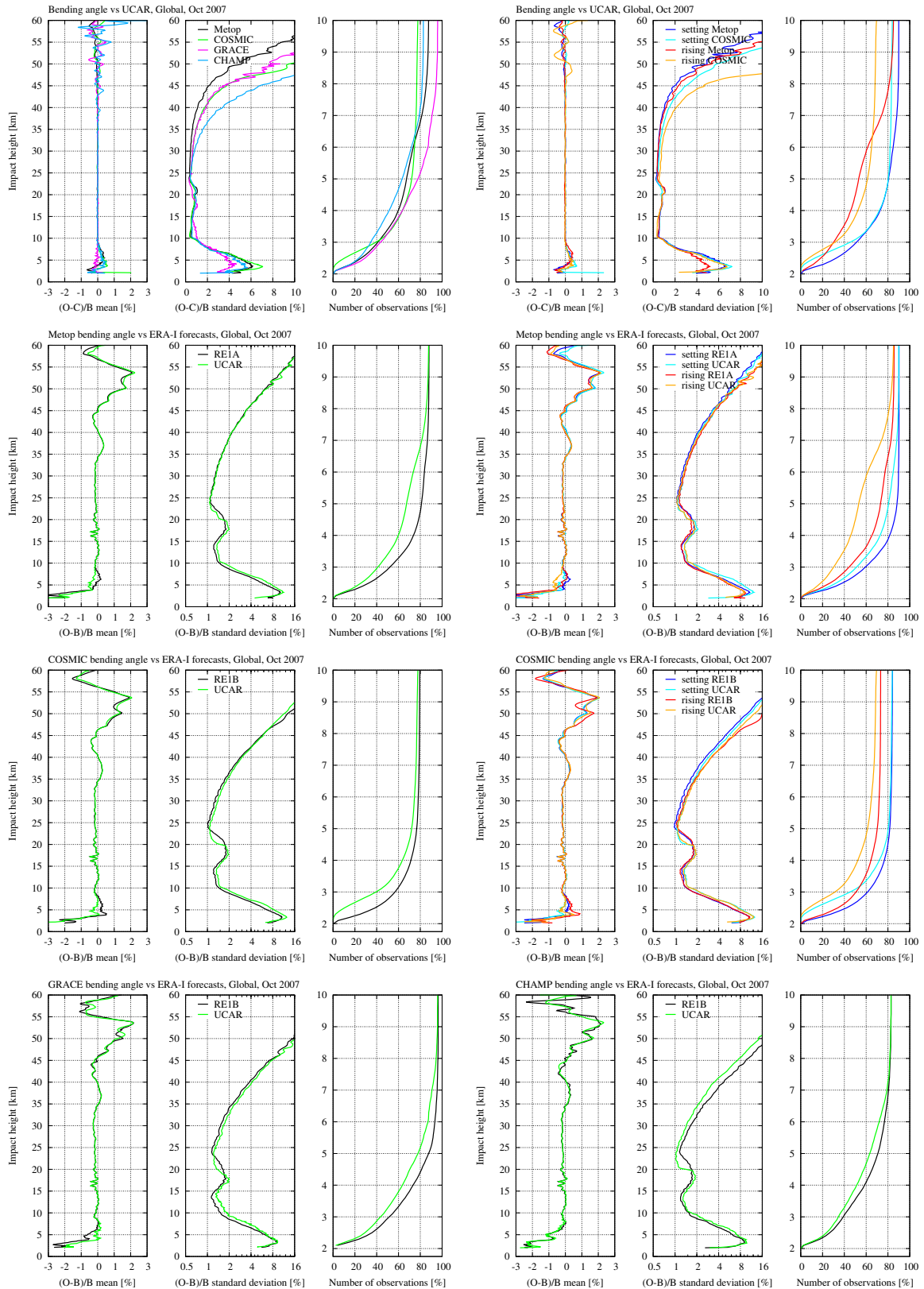


Figure 3.61: Monthly global profile statistics of bending angle from the different missions against the corresponding bending angle processed at UCAR (October 2007).

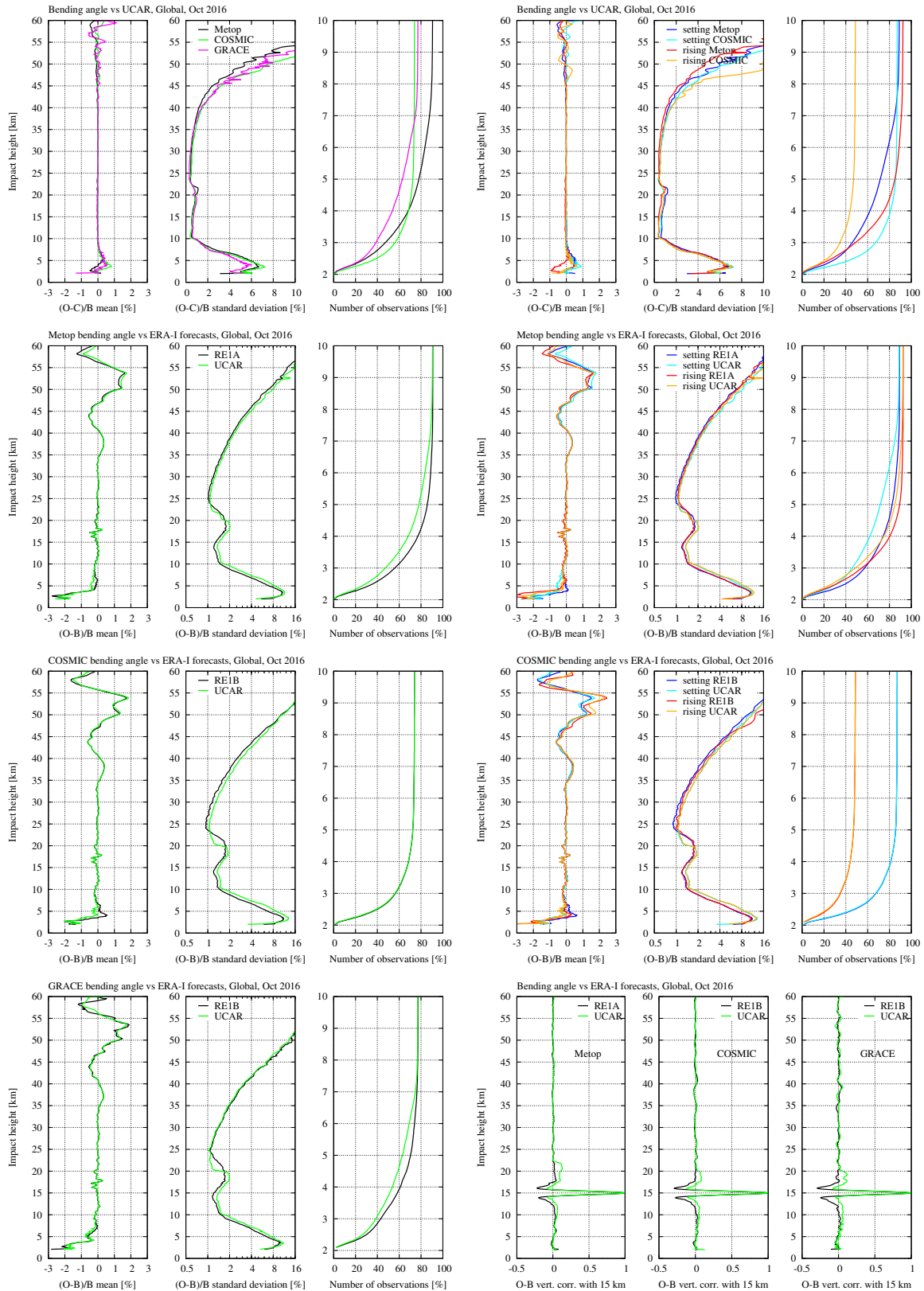


Figure 3.62: Monthly global profile statistics of bending angle from the different missions against the corresponding bending angle processed at UCAR (October 2016).

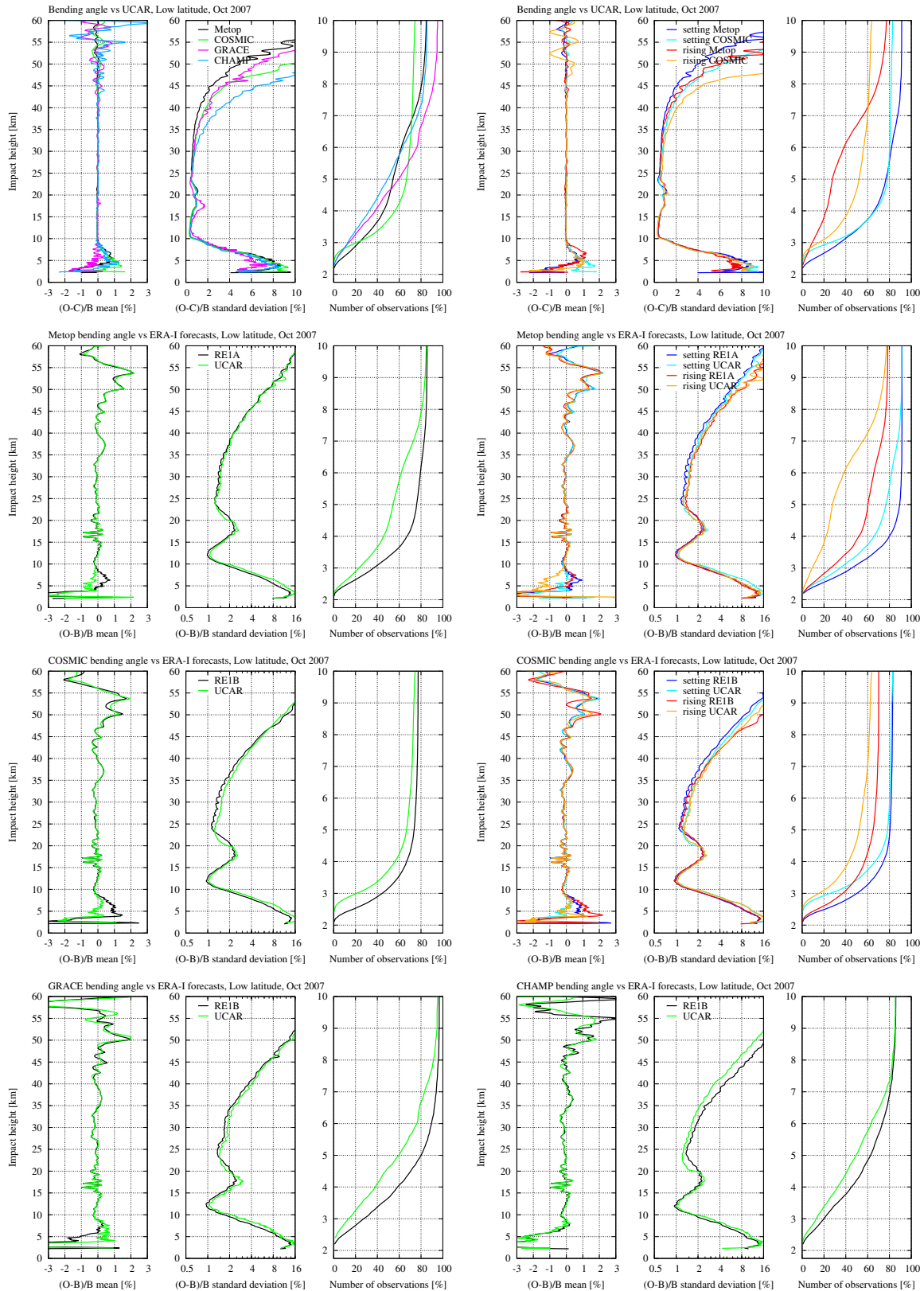


Figure 3.63: Monthly low latitude profile statistics of bending angle from the different missions against the corresponding bending angle processed at UCAR (October 2007).

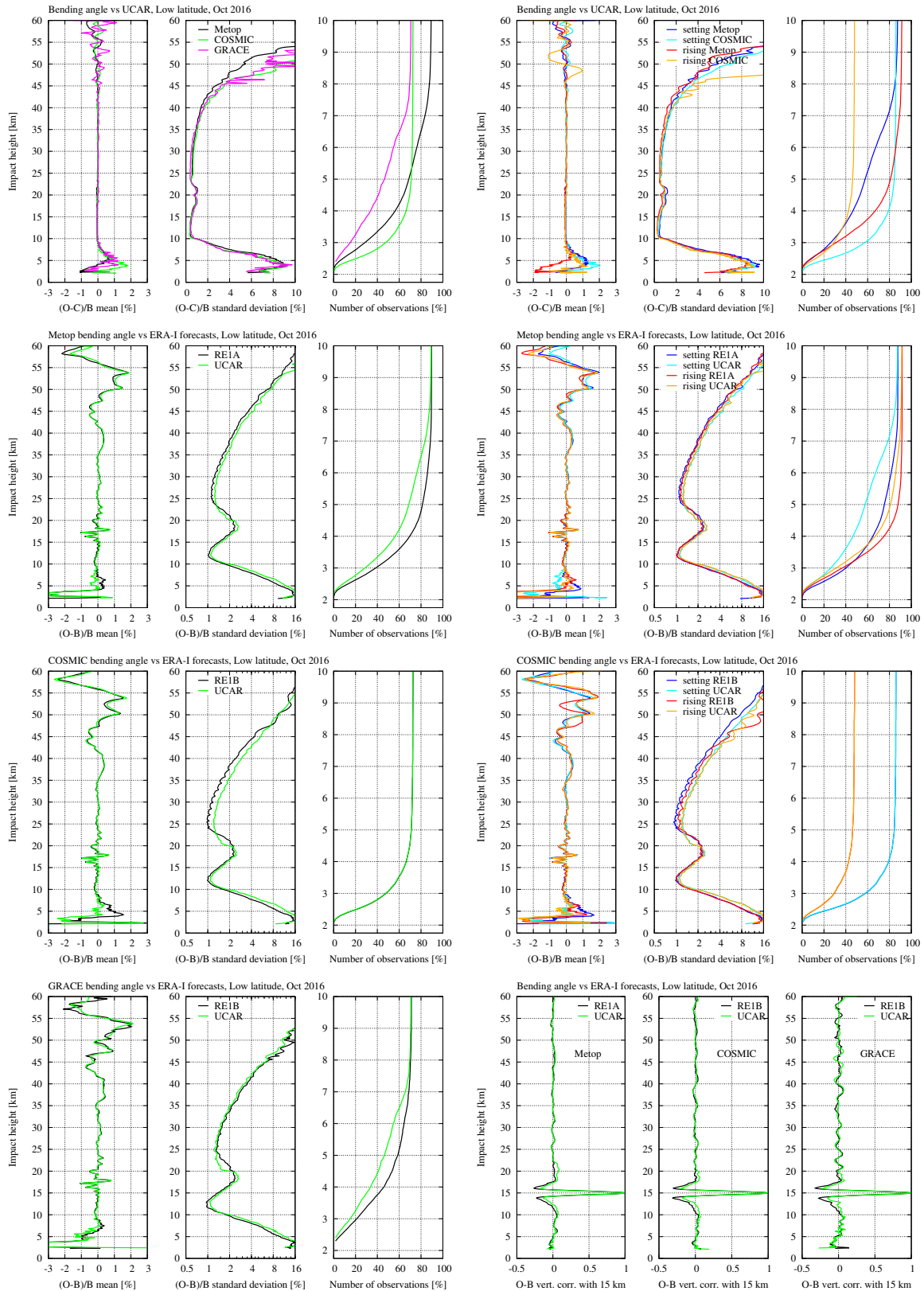


Figure 3.64: Monthly low latitude profile statistics of bending angle from the different missions against the corresponding bending angle processed at UCAR (October 2016).

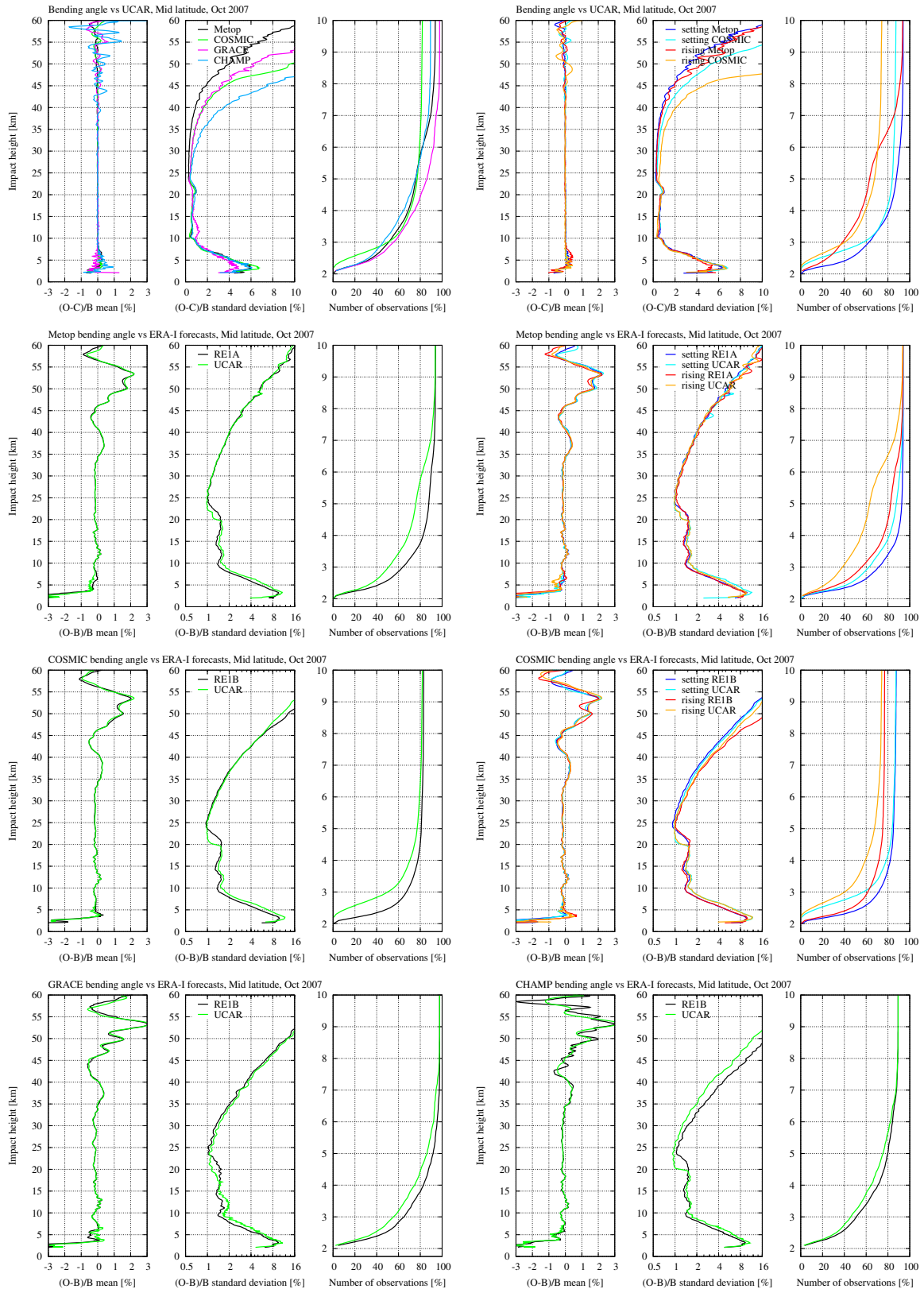


Figure 3.65: Monthly mid latitude profile statistics of bending angle from the different missions against the corresponding bending angle processed at UCAR (October 2007).

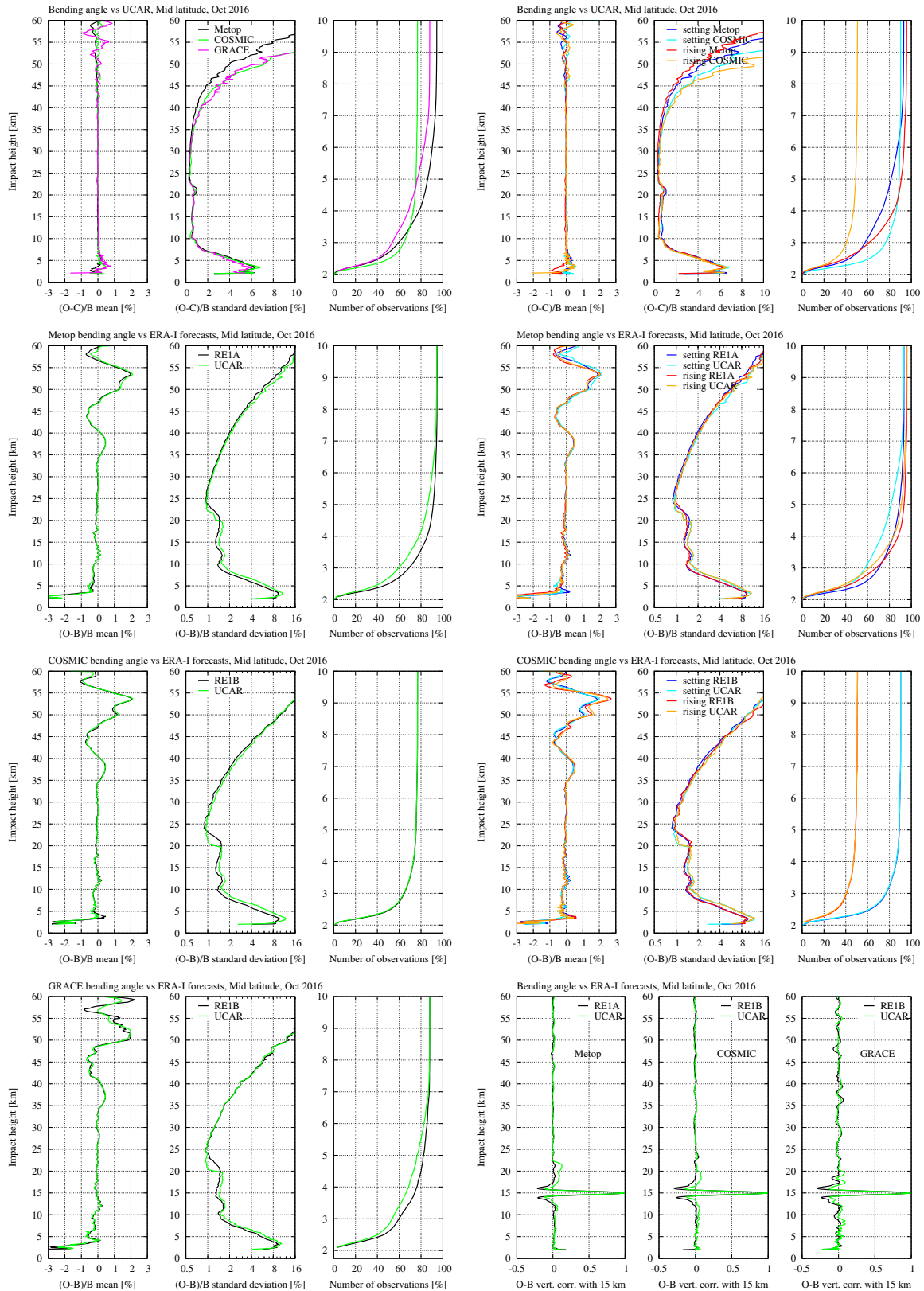


Figure 3.66: Monthly mid latitude profile statistics of bending angle from the different missions against the corresponding bending angle processed at UCAR (October 2016).

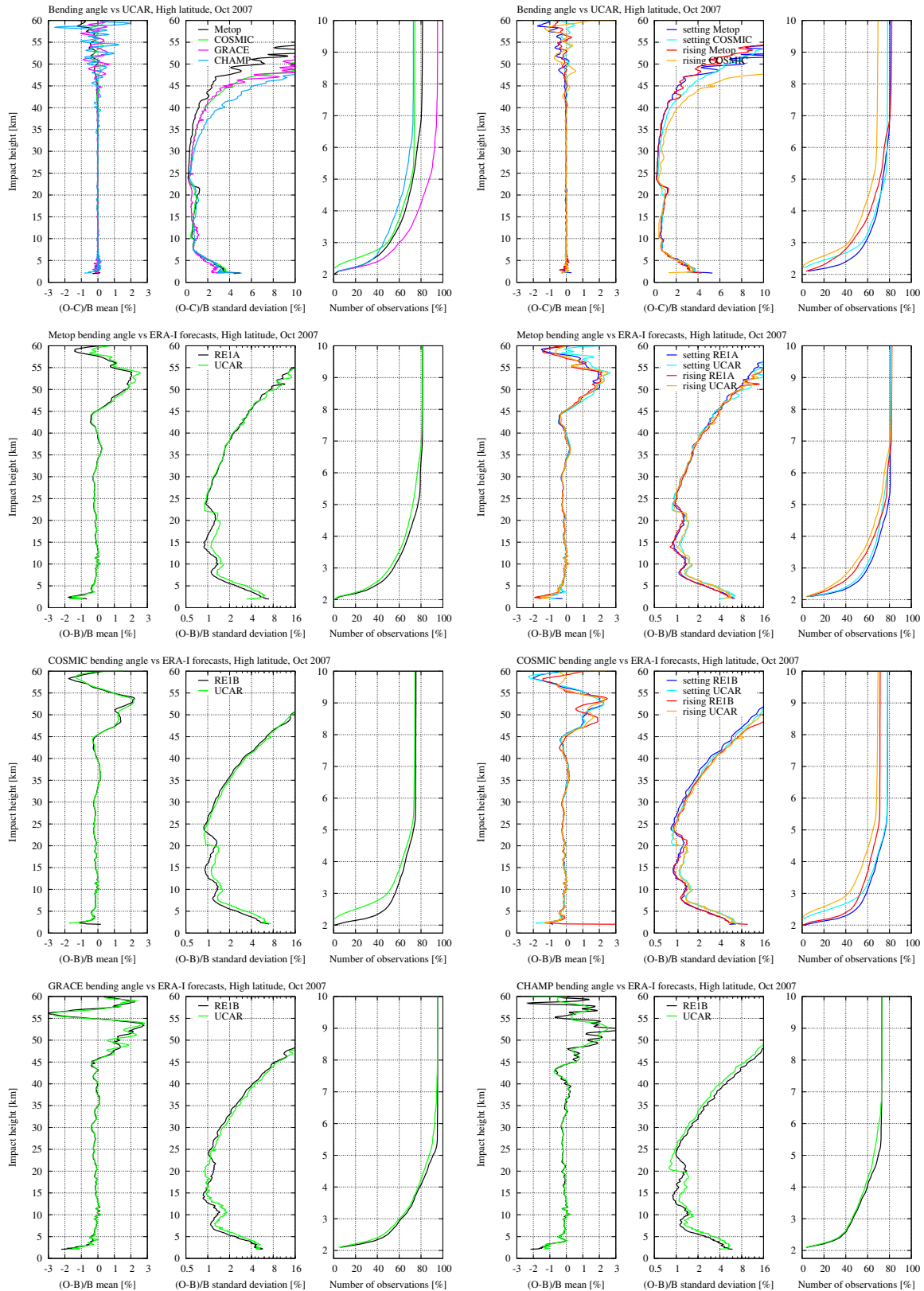


Figure 3.67: Monthly high latitude profile statistics of bending angle from the different missions against the corresponding bending angle processed at UCAR (October 2007).

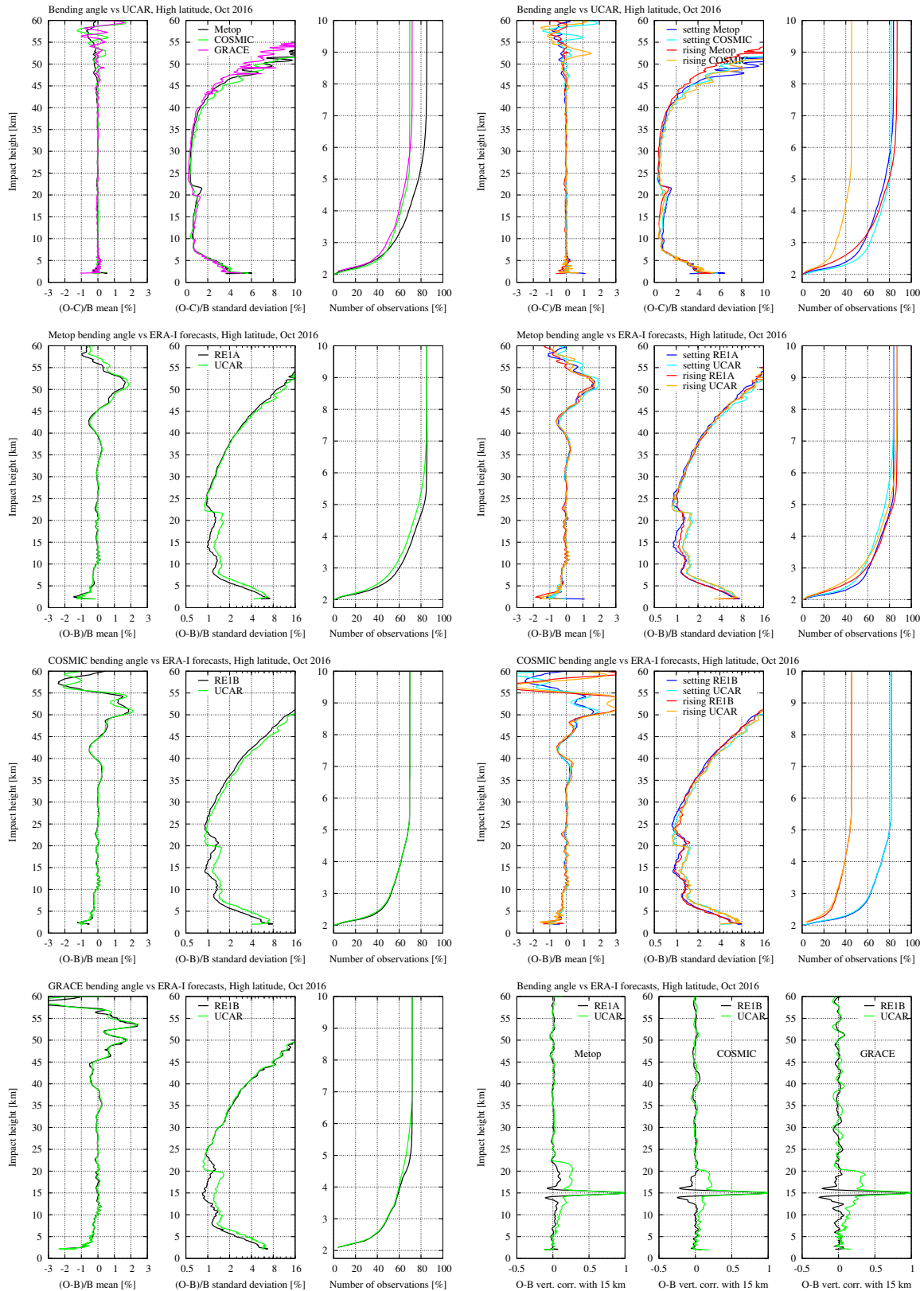


Figure 3.68: Monthly high latitude profile statistics of bending angle from the different missions against the corresponding bending angle processed at UCAR (October 2016).

3.7.2 Refractivity

Figures 3.69–3.76 show the plots for refractivity, corresponding to Figs. 3.61–3.68. Similar comments about biases (here below ~ 6 km altitude) and standard deviations can be made, but in addition, we notice the larger (O-B)/B standard deviations and associated broader correlations between 10 km and 20 km in the statistics against ERA-I for all UCAR missions, except for GRACE (October 2007). The corresponding vertical correlations in bending angle for October 2016 can be seen in the bottom right plots of Figs. 3.62, 3.64, 3.66, and 3.68. The broader correlations are likely a consequence of the changed UCAR processing in later years, where the L2 signal is extrapolated from a common fixed altitude for both setting and rising occultations, based on the philosophy to process all data similarly for climate applications [RD.8]. This is also likely the reason for the much larger vertical correlations in the direct comparisons (except for the earlier GRACE processing for October 2007), being amplified because of the otherwise very large similarity (low noise) between the data sets in this region.

At high altitudes (above 30 km), the (O-C)/B means in the direct comparisons are substantially different from zero (also reflected in the (O-B)/B means against ERA-I), and different for the October 2007 and October 2016 plots. Generally, these differences are a result of structural uncertainty, where different choices have been made in the statistical optimization approach. The structural uncertainty is also reflected in the standard deviations against ERA-I, where the ROM SAF data has larger standard deviations that continue to grow nearly exponentially above 50 km, with only a minor change in the scale height, as opposed to the standard deviations in the UCAR data. At high latitudes, especially for October 2016 above 45 km, the (O-C)/B means in the direct comparisons, are particularly large. For the UCAR data, the (O-B)/B means against ERA-I are biased positive, whereas they are biased negative for the ROM SAF data, following more consistently the means at mid and low latitudes. This, together with the analyses of the influence of the ROM SAF statistical optimization in previous sections, suggests that the high altitude mean in the refractivity at high latitudes are closer to the truth for the ROM SAF data. As verified in Section 3.2, the optimized bending angle is very similar in the mean to the non-optimized bending angle up to at least 60 km in the ROM SAF CDR v1.0, indicating minimum influence from the climatology on the mean at high altitudes, but as seen here, at the expense of more noise (larger standard deviations) in the refractivity.

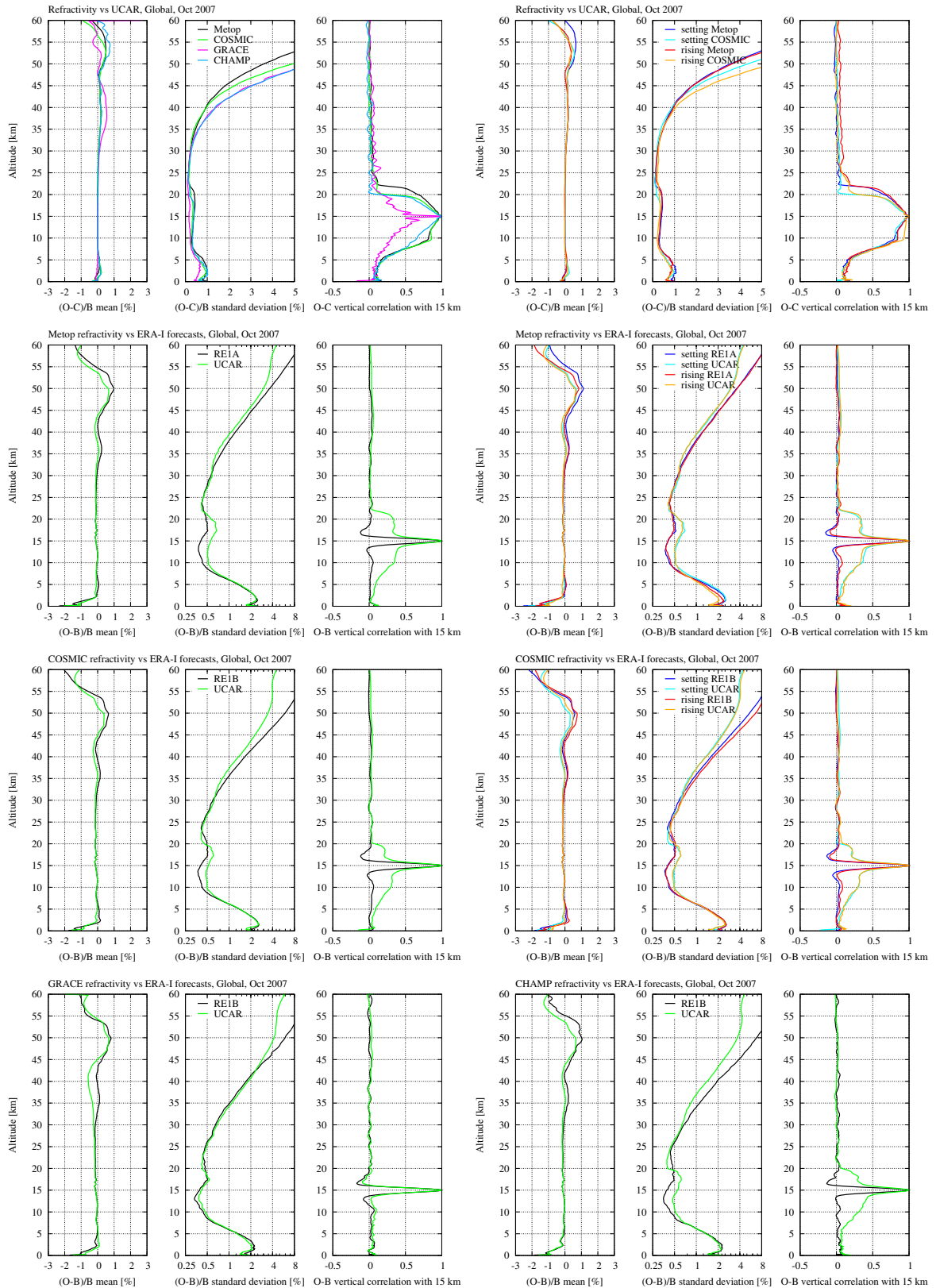


Figure 3.69: Monthly global profile statistics of refractivity from the different missions against the corresponding refractivity processed at UCAR (October 2007).

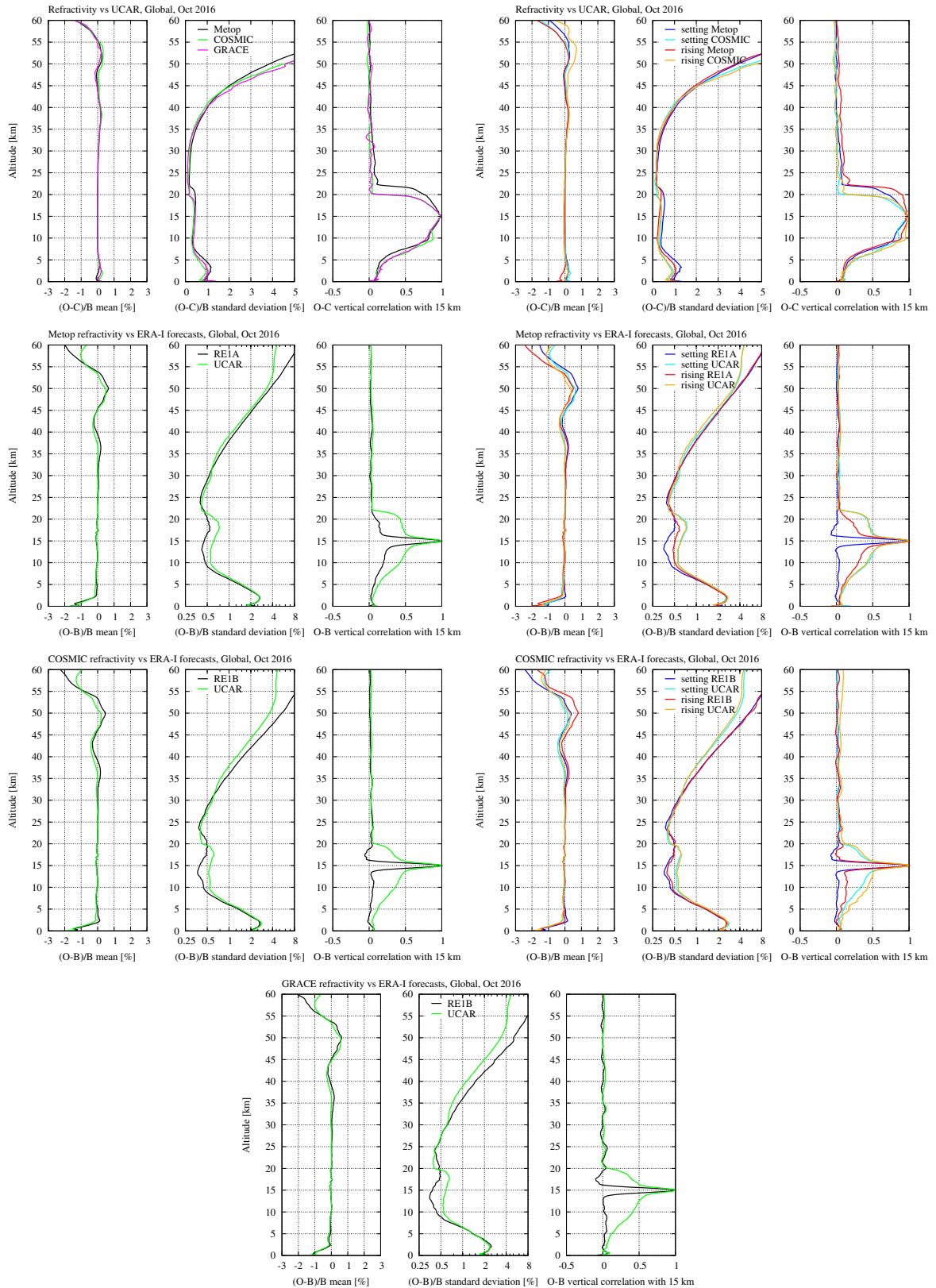


Figure 3.70: Monthly global profile statistics of refractivity from the different missions against the corresponding refractivity processed at UCAR (October 2016).

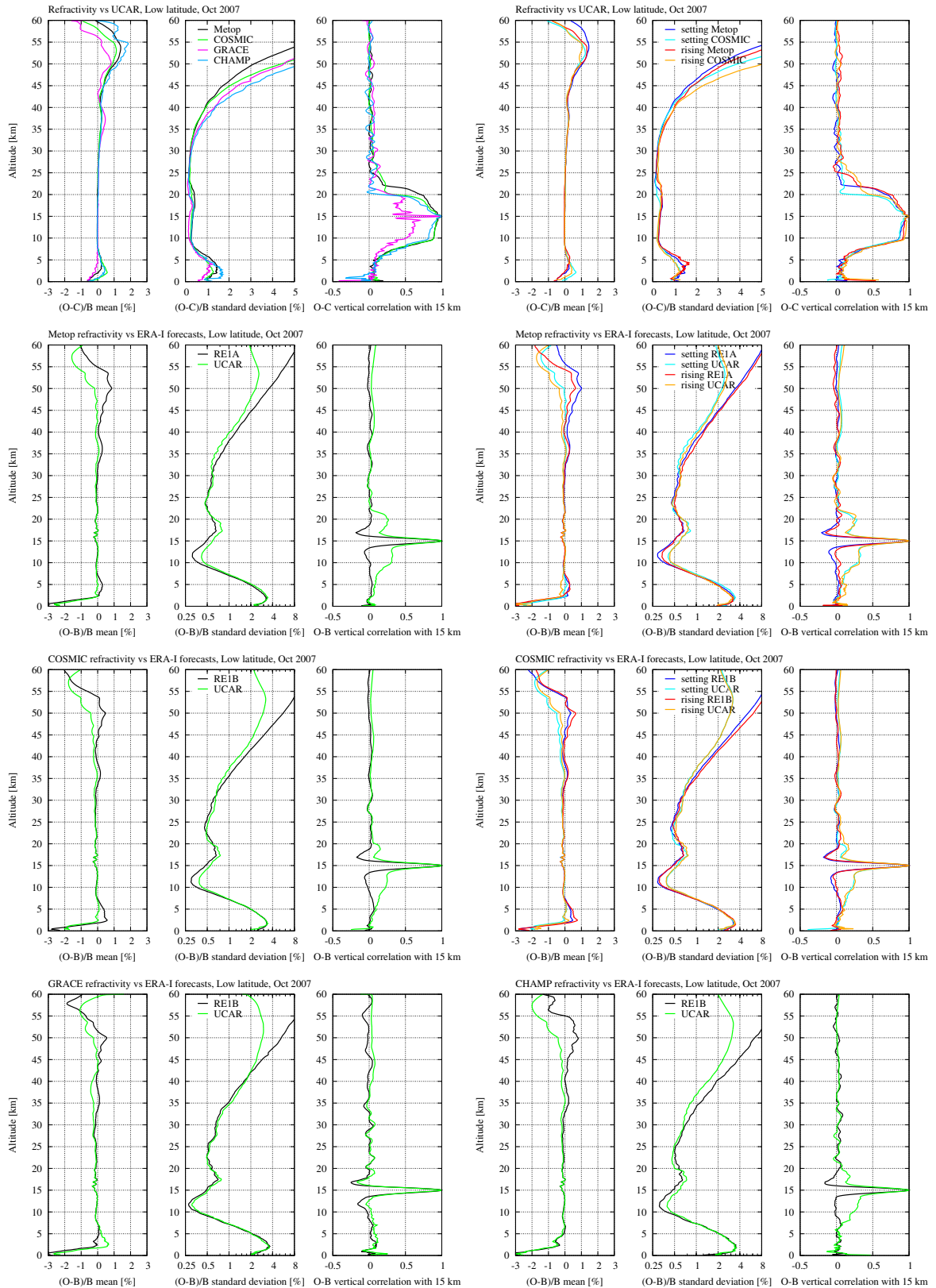


Figure 3.71: Monthly low latitude profile statistics of refractivity from the different missions against the corresponding refractivity processed at UCAR (October 2007).

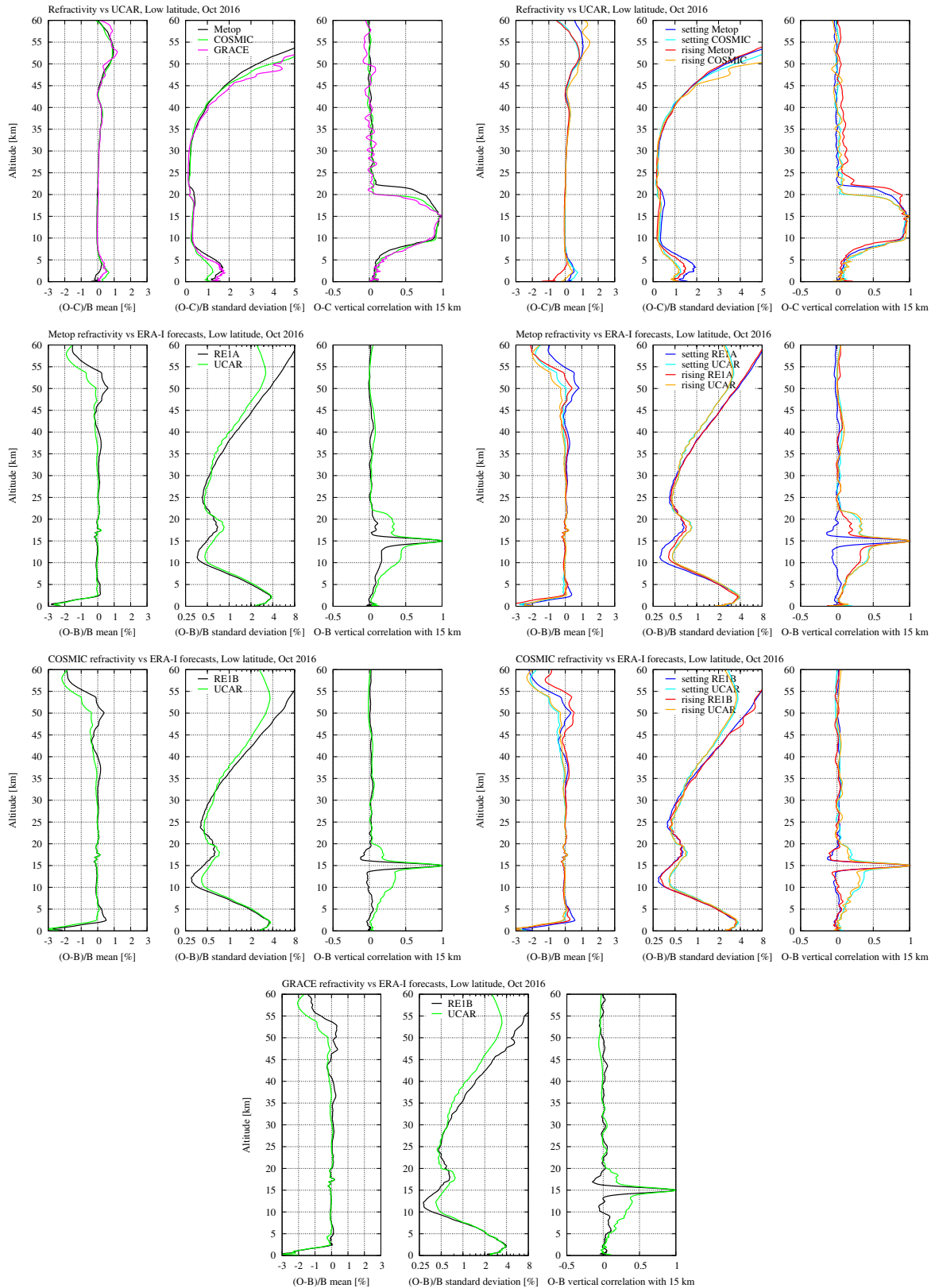


Figure 3.72: Monthly low latitude profile statistics of refractivity from the different missions against the corresponding refractivity processed at UCAR (October 2016).

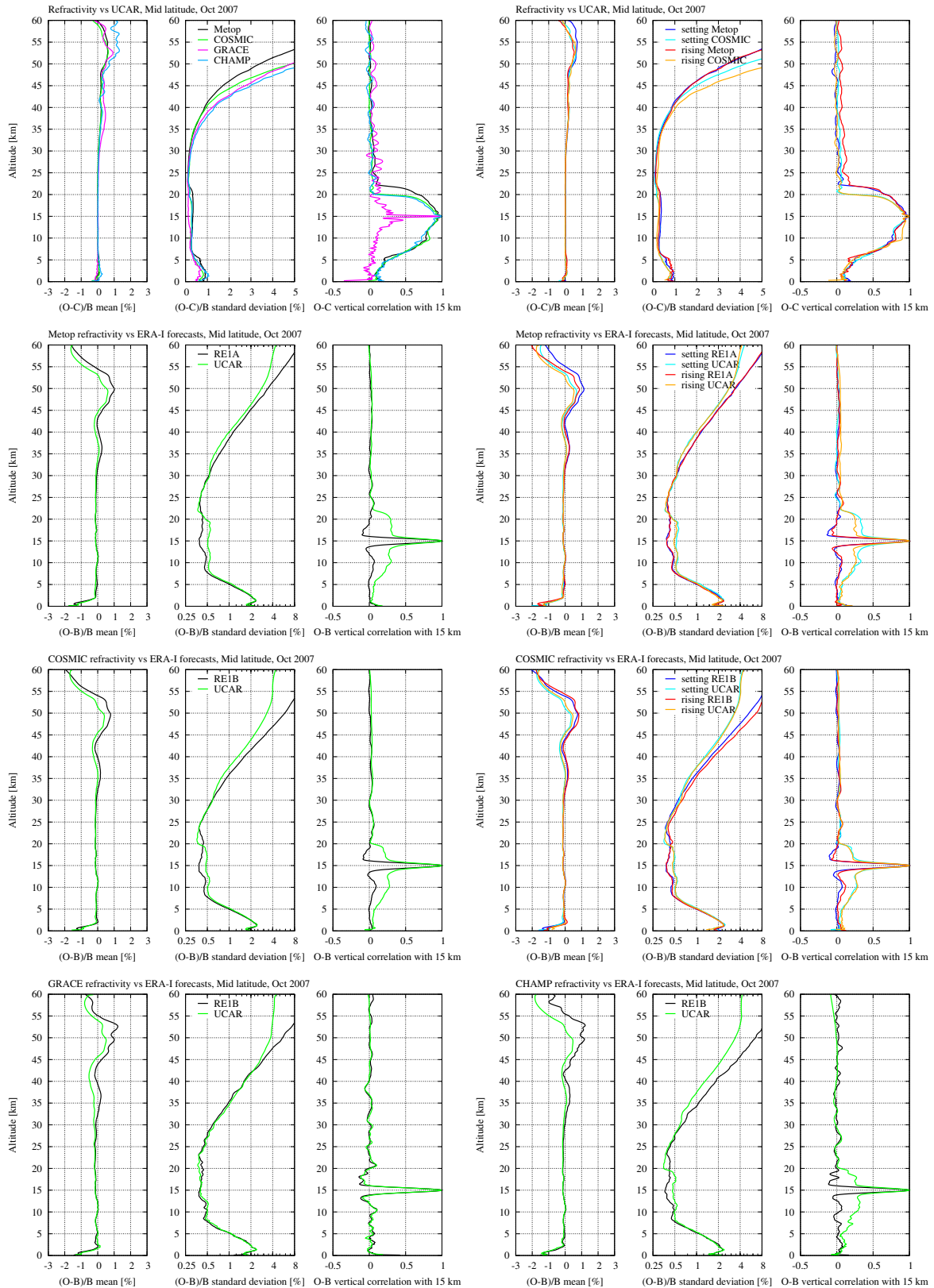


Figure 3.73: Monthly mid latitude profile statistics of refractivity from the different missions against the corresponding refractivity processed at UCAR (October 2007).

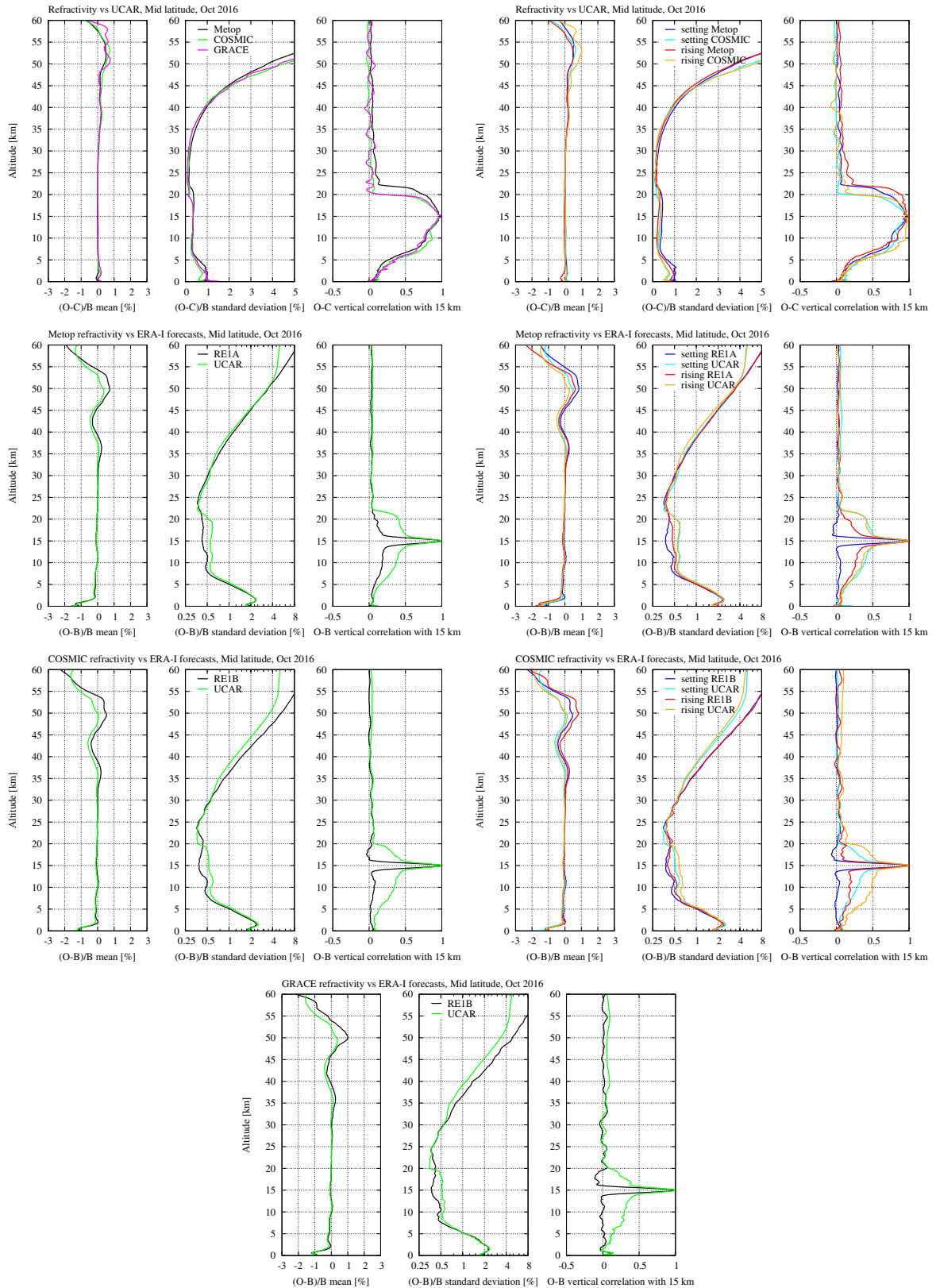


Figure 3.74: Monthly mid latitude profile statistics of refractivity from the different missions against the corresponding refractivity processed at UCAR (October 2016).

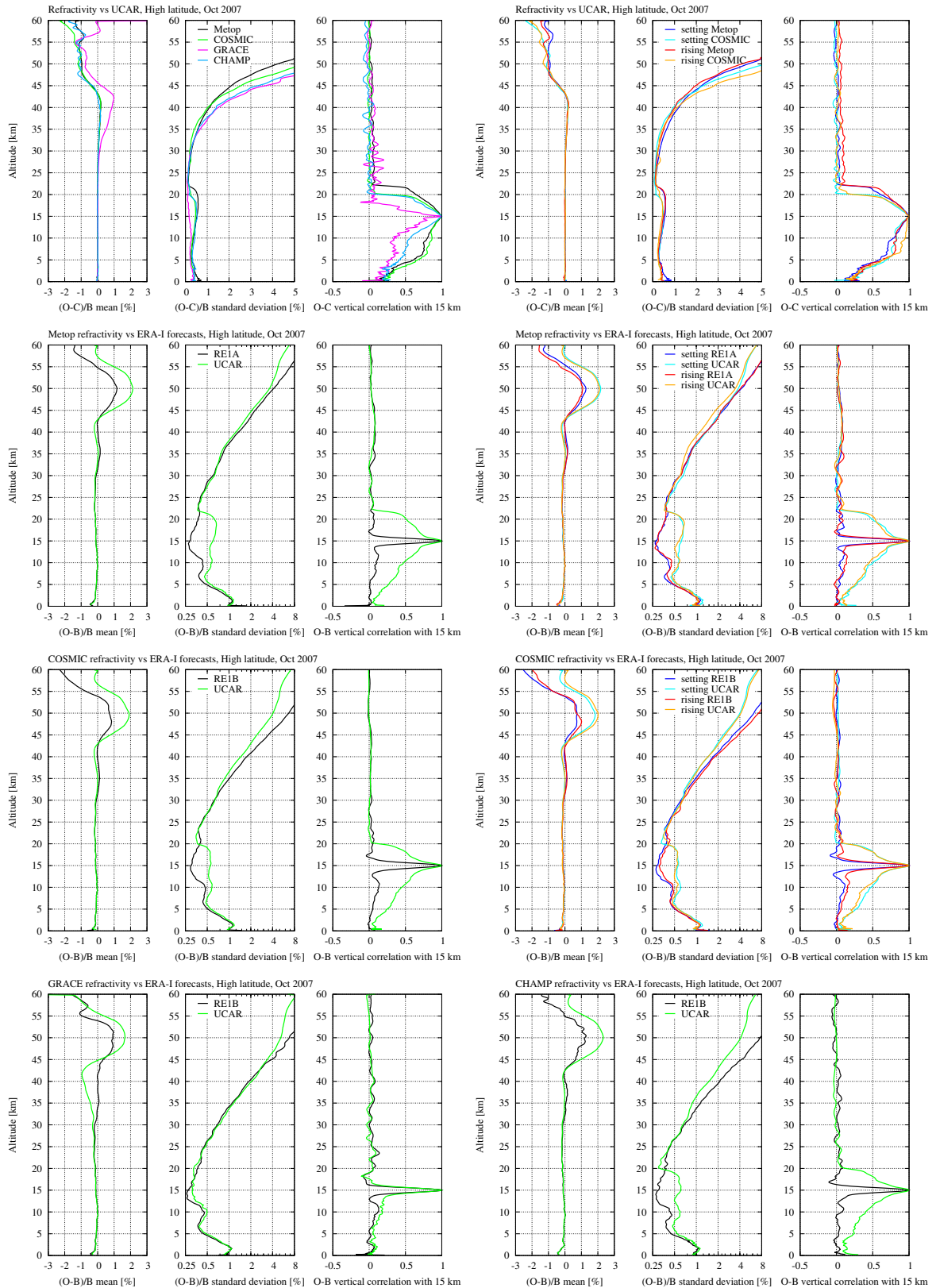


Figure 3.75: Monthly high latitude profile statistics of refractivity from the different missions against the corresponding refractivity processed at UCAR (October 2007).

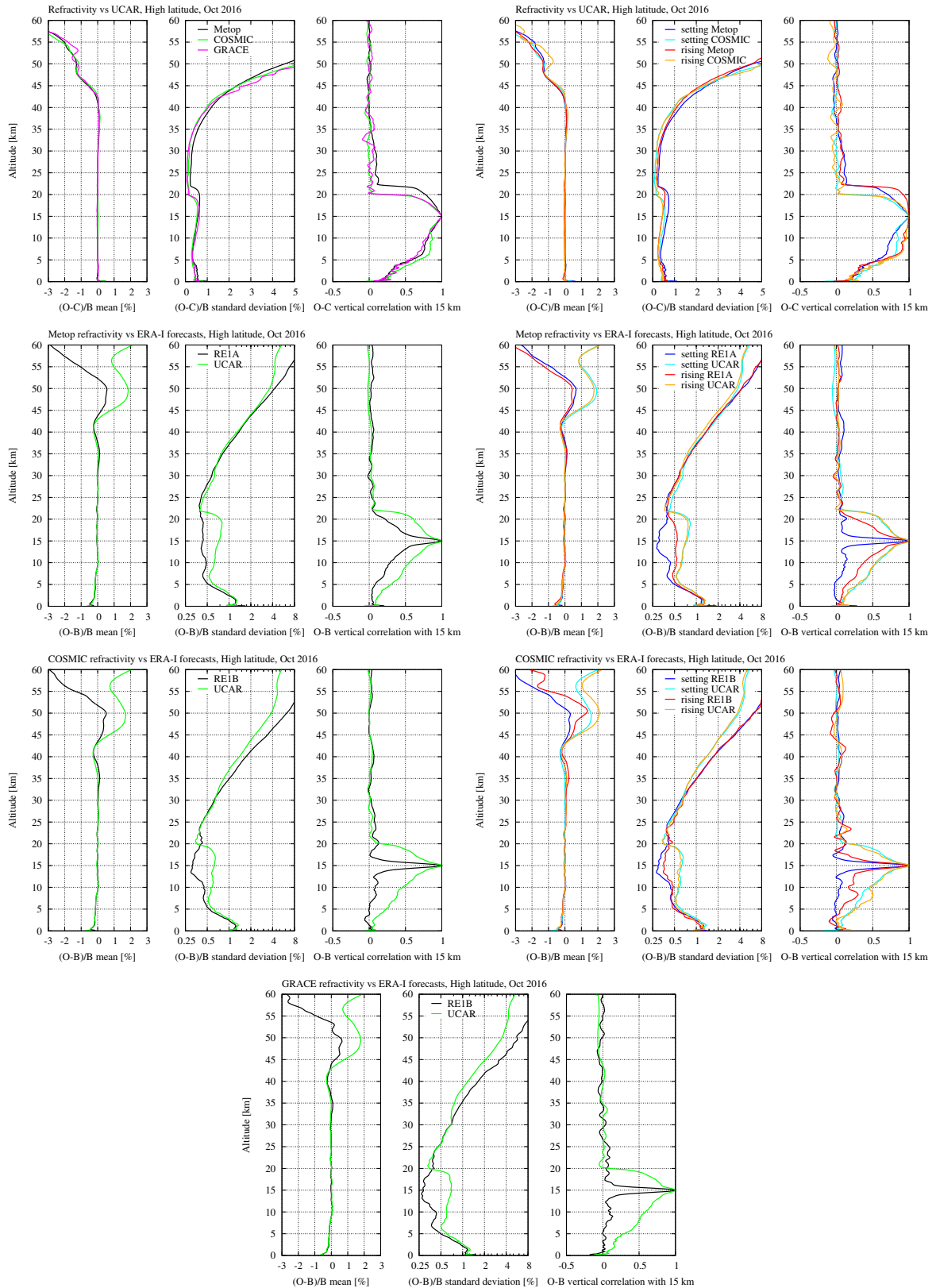


Figure 3.76: Monthly high latitude profile statistics of refractivity from the different missions against the corresponding refractivity processed at UCAR (October 2016).

3.7.3 Dry temperature

Figures 3.77–3.84 show plots for dry temperature corresponding to the ones for bending angle and refractivity. Some of the same features can be seen and similar comments can be made. One thing to be noted is how the large structural uncertainty in refractivity above 45 km at high latitudes (cf. the difference between the two datasets in the means in the left panels of Figs. 3.75 and 3.76) propagates to lower altitudes in dry temperature (down to 25–30 km). Thus, at mid and low latitudes, a good part of the structural uncertainty above 45 km in dry temperature likely originates from large differences in the refractivity above 60 km (UCAR data are not available above 60 km).

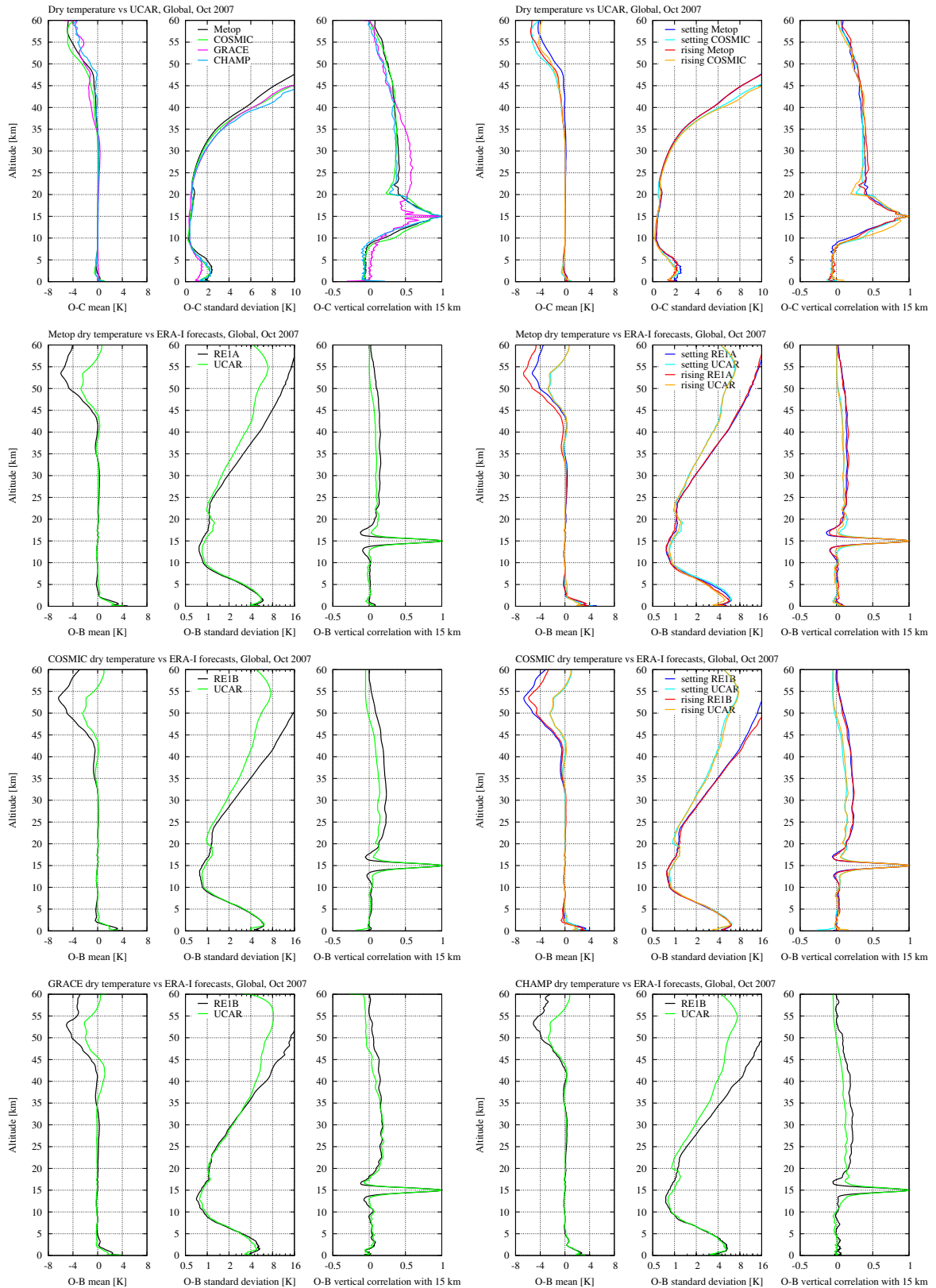


Figure 3.77: Monthly global profile statistics of dry temperature from the different missions against the corresponding dry temperature processed at UCAR (October 2007).

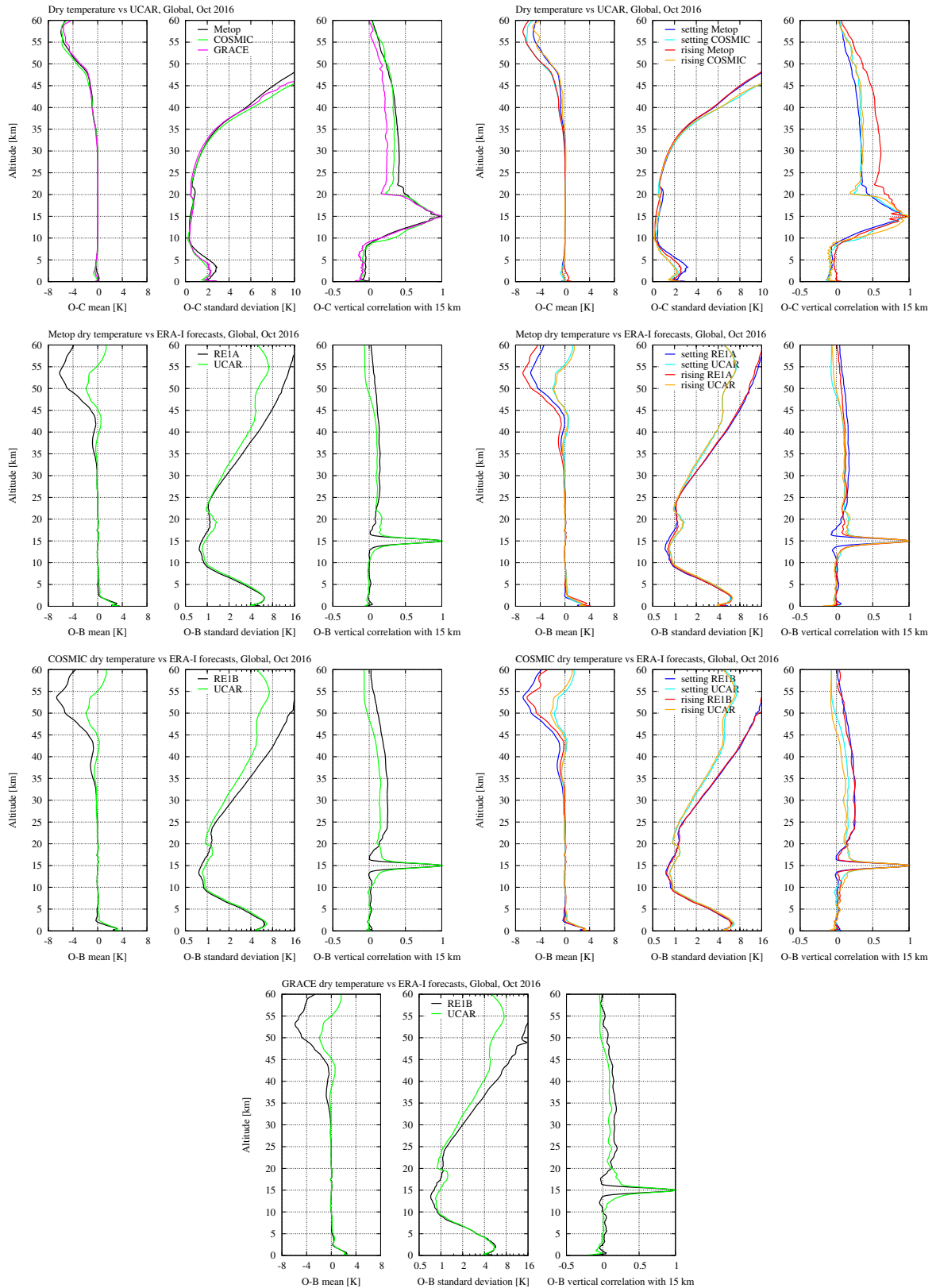


Figure 3.78: Monthly global profile statistics of dry temperature from the different missions against the corresponding dry temperature processed at UCAR (October 2016).

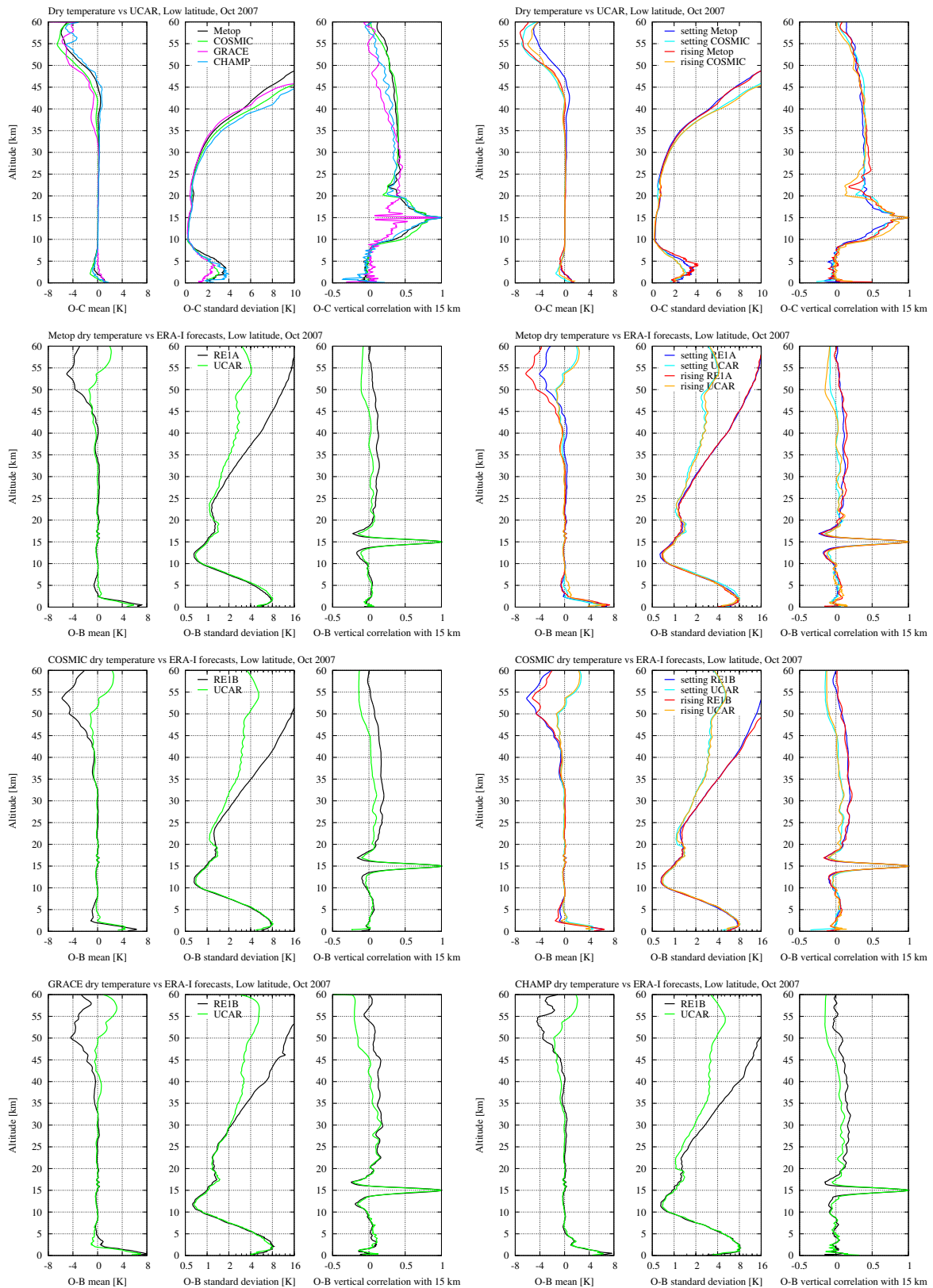


Figure 3.79: Monthly low latitude profile statistics of dry temperature from the different missions against the corresponding dry temperature processed at UCAR (October 2007).

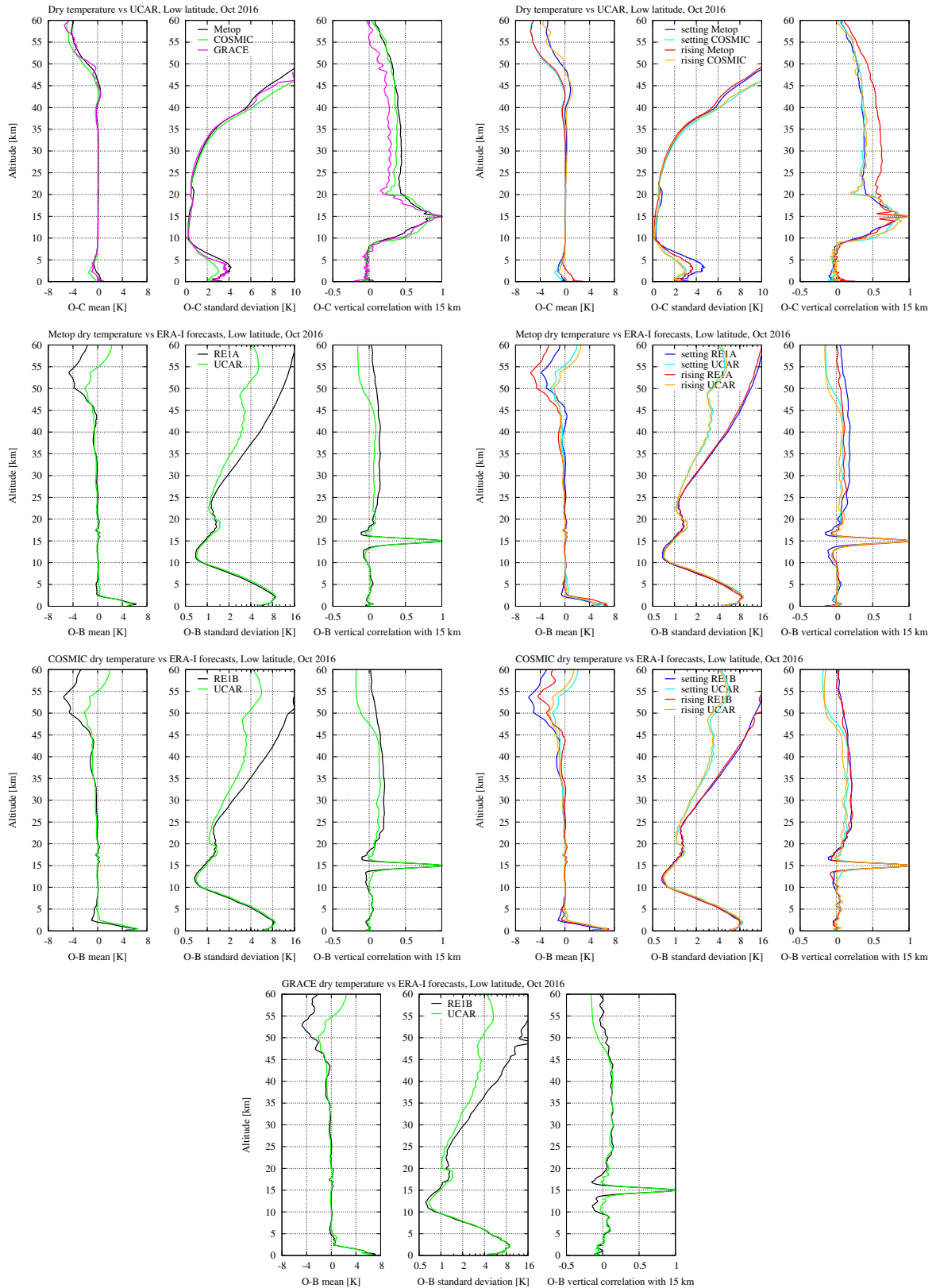


Figure 3.80: Monthly low latitude profile statistics of dry temperature from the different missions against the corresponding dry temperature processed at UCAR (October 2016).

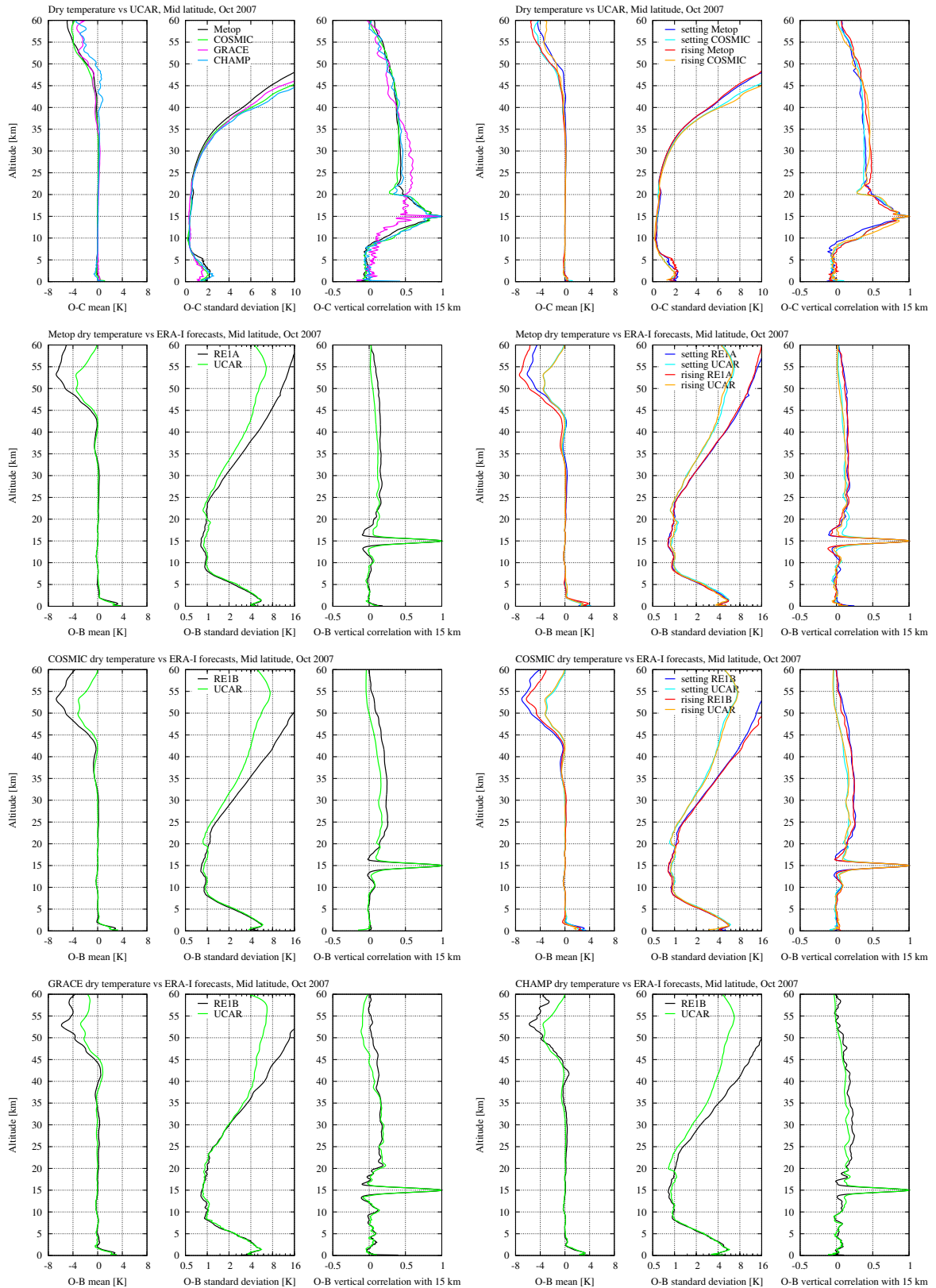


Figure 3.81: Monthly mid latitude profile statistics of dry temperature from the different missions against the corresponding dry temperature processed at UCAR (October 2007).

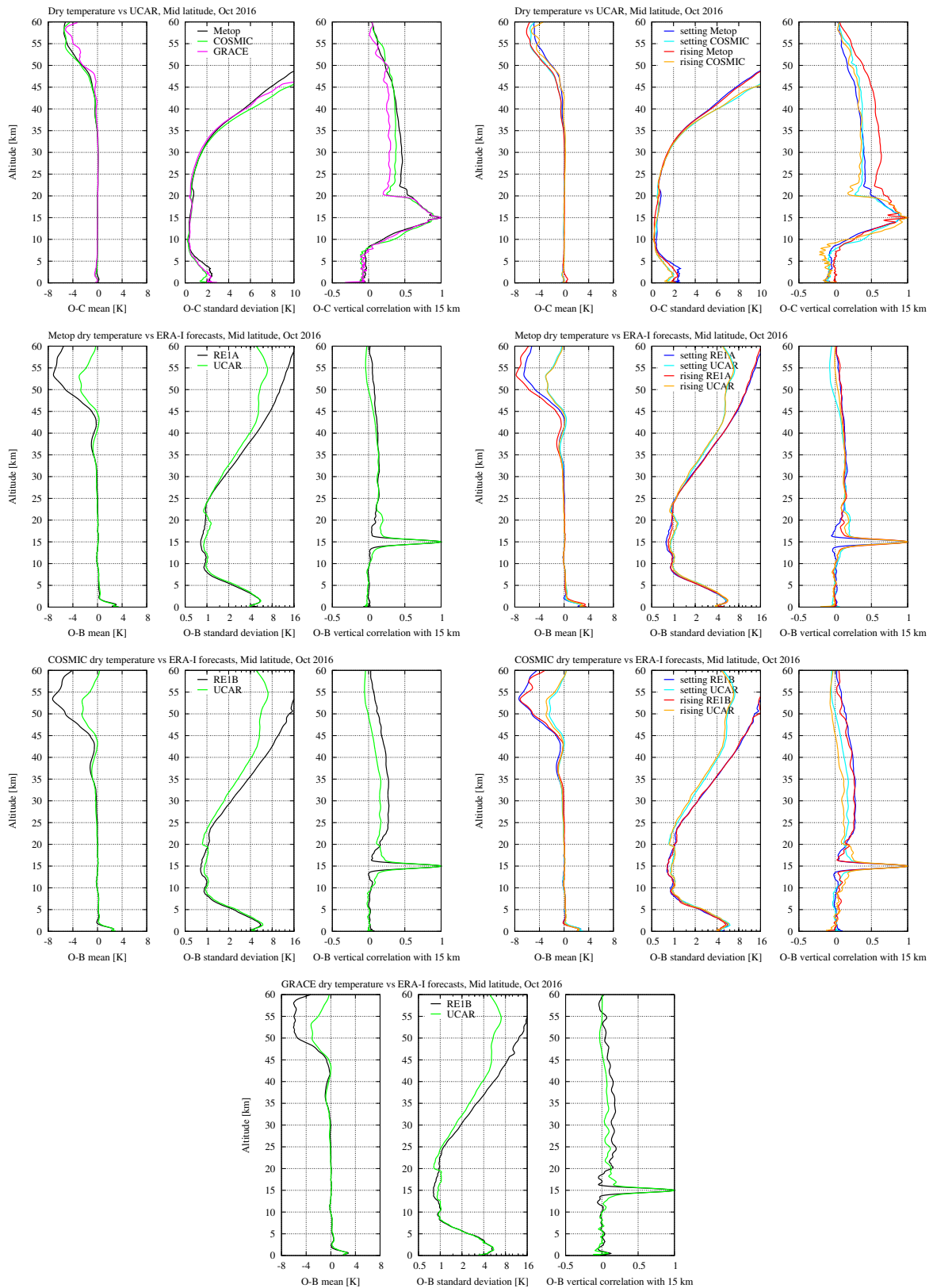


Figure 3.82: Monthly mid latitude profile statistics of dry temperature from the different missions against the corresponding dry temperature processed at UCAR (October 2016).

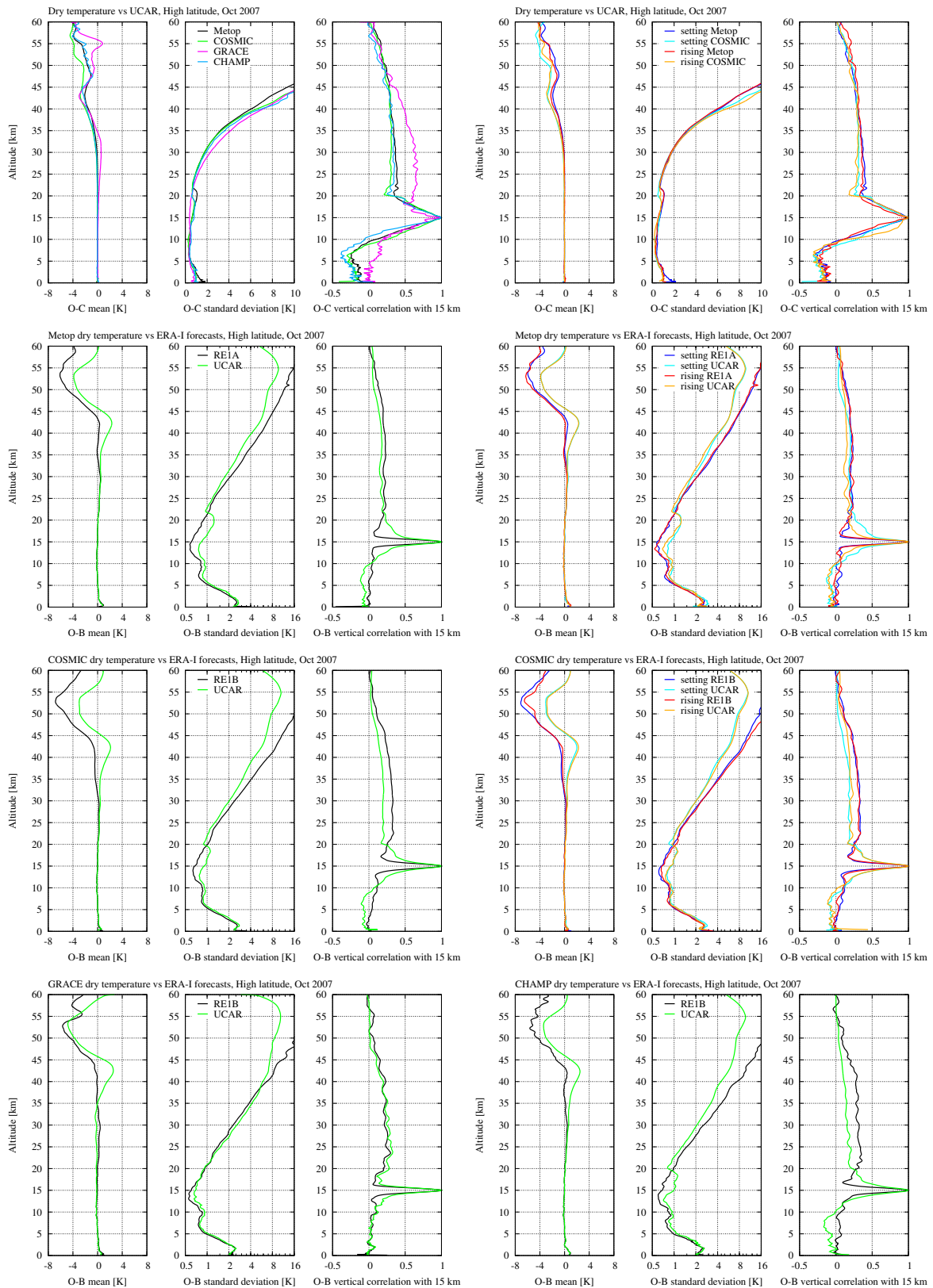


Figure 3.83: Monthly high latitude profile statistics of dry temperature from the different missions against the corresponding dry temperature processed at UCAR (October 2007).

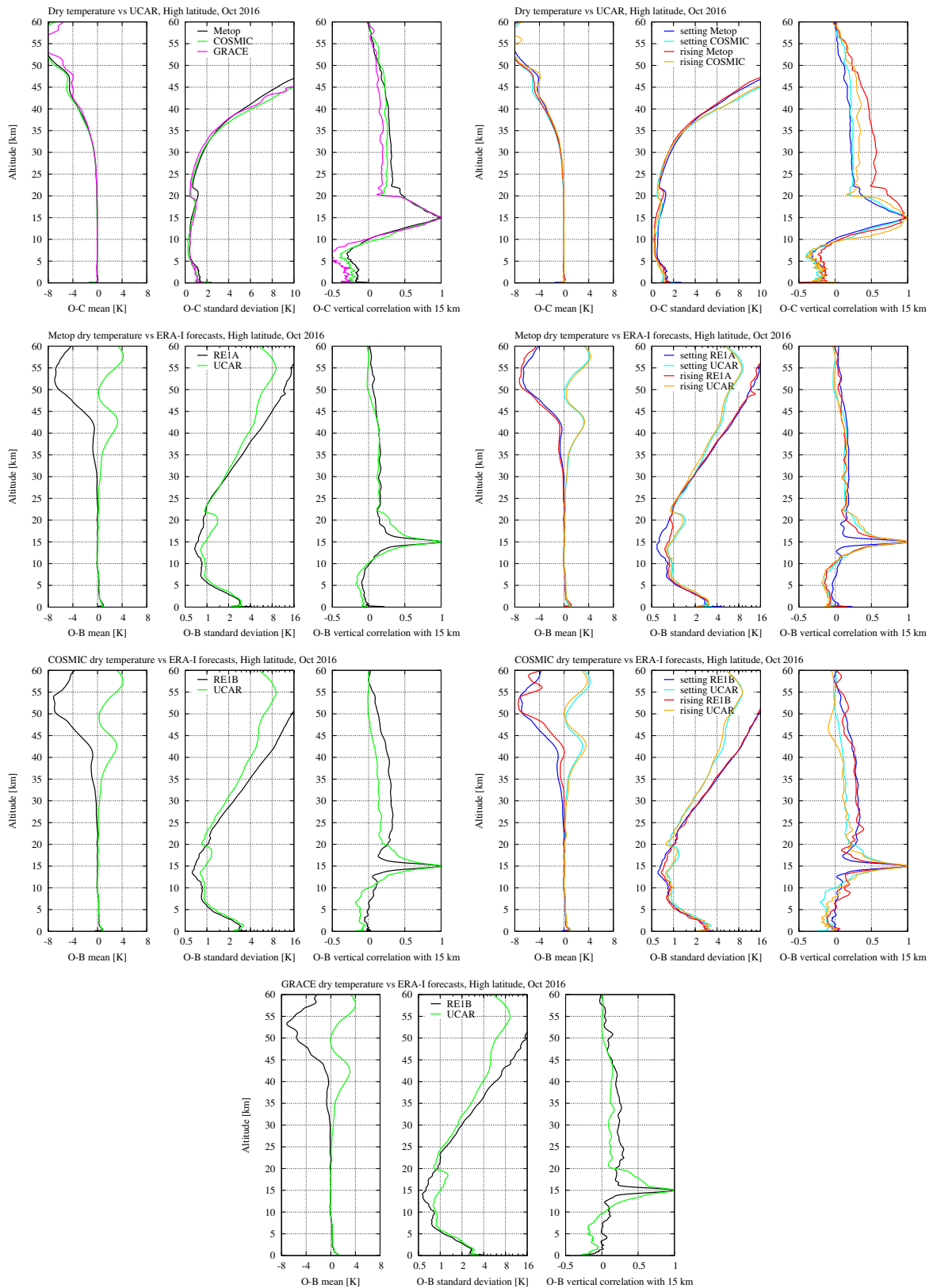


Figure 3.84: Monthly high latitude profile statistics of dry temperature from the different missions against the corresponding dry temperature processed at UCAR (October 2016).

3.8 Comparison across local time and hemispheres

In this section we look at comparisons to see if there are quality issues in the ROM SAF CDR v1.0 that depend on local time and hemispheres. We do that because earlier validations of Metop near real-time data (tests) revealed large tropospheric and stratospheric biases that could not be seen in the global statistics, but only when separating the statistics into different local times and hemispheres in combination. At least for the Metop satellites, due to their morning/evening (9:30/21:30) sun-synchronous orbits, we are in this way able to detect possible orbit-related dependencies, as well as systematic dependencies on local time and hemispheres in general. We use data from the two baseline months (October 2007, October 2016), but also in some cases data from other months in 2016 (January, April, and July) to look for possible seasonal dependencies in combination with the local time and hemispheric dependencies. We define the following local time intervals:

Morning: 7:00 to 12:00

Evening: 19:00 to 24:00

Early morning: 7:00 to 9:30

Early evening: 19:00 to 21:30

Late morning: 9:30 to 12:00

Late evening: 21:30 to 24:00

The points to be made from this section are that the data quality of the ROM SAF CDR v1.0 is fairly independent of local time and hemispheres. Main exceptions are:

- Small systematic biases for Metop at high altitudes (of order $\sim 0.1 \mu\text{rad}$ in absolute value of bending angle, depending on local time and hemispheres, and different for setting and rising occultations), presumably caused by errors in the Metop precise orbit determination
- A small constant bias in refractivity and bending angle of $\sim 0.1\%$ for CHAMP (compared to Metop and COSMIC) around 20–30 km in the southern hemisphere morning
- Larger biases than usual for CHAMP near 5 km impact height (3 km altitude) in the northern hemisphere morning and the southern hemisphere evening; in bending angle up to 2%, but smaller ($\sim 0.5\%$) in refractivity and dry temperature
- A small constant bias in bending angle and refractivity of $\sim 0.1\%$ in the 10–25 km range in rising Metop occultations since 2013 that was already mentioned in previous sections; the bias seems to be more prominent in the morning than in the evening, and is related to the L2-extrapolation

3.8.1 Bending angle

In certain local time intervals and for the two hemispheres, Figs. 3.85 and 3.86 show the monthly profile statistics of bending angle against ERA-I from all missions for October 2007 and October 2016, respectively. The two top rows of plots are for the northern hemi-

sphere (morning and evening), and the two bottom rows of plots are for the southern hemisphere (morning and evening). Statistics for CHAMP are included in the October 2007 plots, whereas statistics for GRACE are only included in the October 2016 plots. As it turns out, GRACE was far from a morning/evening orbit in October 2007, and there are not enough occultations in the local time intervals used here to make useful GRACE statistics for October 2007.

Although there are differences, most strikingly smaller standard deviations at high altitudes for Metop in the southern hemisphere morning (third row of plots from the top in Figs. 3.85 and 3.86), a small negative constant bias of $\sim 0.1\%$ for CHAMP (compared to Metop and COSMIC) around 20–30 km in the southern hemisphere morning (leftmost plot in the third row of Fig. 3.85), and somewhat larger negative biases than usual for CHAMP near 5 km in the northern hemisphere morning and the southern hemisphere evening (leftmost top and bottom plots in Fig. 3.85), there does not seem to be very large systematic issues. We should keep in mind the limited number of occultations included in the statistics in each of these plots (about 5–20% of the numbers in global statistics, depending on mission and particular plot; actual numbers for CHAMP being about 600 occultations per plot, and about 65% of that around 5 km impact height). However, the above mentioned findings are not understood, and could warrant further investigation in the future.

To include possible seasonal dependencies, the statistics against ERA-I for January and July 2016 for Metop are compared in Fig. 3.87. It is interesting to note here how the curves for January 2016 and July 2016 basically interchange between the two hemispheres, i.e., showing consistent biases and standard deviations against ERA-I for summer and winter conditions. As discussed in Section 3.2, the non-zero $(O-B)/B$ means at high altitudes are believed to be primarily due to biases in the ERA-I data. Given the differences in the global statistics between ERA-I forecasts and ECMWF operational forecasts, shown in that section, it cannot be excluded that biases in the ERA-I data could also be the main reason for the non-zero $(O-B)/B$ means between 5 km and 10 km impact height. However, part of the differences between summer and winter seen here in this vertical range could perhaps be due to errors of representativeness related to horizontal gradients (which are not taken into account in the RO retrievals).

Focusing on the $(O-B)/B$ means at high altitudes in Fig. 3.87, we see a split between setting and rising occultations above ~ 40 –50 km, and we note how the curves for setting and rising occultations basically interchange between the morning and evening local times in each hemisphere. The same picture appears when we look at the corresponding plots using the reprocessed data from the EUMETSAT Secretariat. This is shown in Fig. 3.88, and the direct comparison between the ROM SAF CDR v1.0 bending angle for Metop (RE1A) and the reprocessed data from the EUMETSAT Secretariat is shown in Fig. 3.89. However, using the reprocessed Metop bending angle that is based on input data from UCAR/CDAAC (RE1B; cf. the introductory remarks in Chapter 3), the systematic split between setting and rising occultations is not as clear, although some split is still present. This is shown in Fig. 3.90. A direct comparison in Fig. 3.91 between the RE1A and RE1B bending angles reveals a clear systematic difference in the means at high altitudes, increasing nearly exponentially (percentage wise) with altitude, and reaching 1–2% near 60 km. Given the smaller split between rising and setting occultations in the statistics against ERA-I for the RE1B data, we conclude that the biases are mostly in the RE1A data, but cannot exclude minor biases also

in the RE1B data. Relative to the RE1B data, the biases in the RE1A data are negative in the northern hemisphere, and primarily in rising occultations in the morning, and in setting occultations in the evening. They are positive in the southern hemisphere, and primarily in setting occultations in the morning, and in rising occultations in the evening. Biases are a little larger in the northern hemisphere than in the southern hemisphere. The minor bias and standard deviation differences between January 2016 and July 2016 in Fig. 3.91, both at high and low altitudes, are not understood in all details, and could warrant further investigation in the future.

Continuing the focus on the systematic bias differences at high altitudes, the plots in Fig. 3.92 verifies that the same biases are present in October 2007 and October 2016, and Fig. 3.93 shows basically the same picture when comparing the RE1A data to the Metop data processed at UCAR/CDAAC. Figure 3.94 verifies that similar biases do not seem to be present in the ROM SAF CDR v1.0 COSMIC data when comparing to the COSMIC data processed at UCAR/CDAAC. That the problem seems to be mostly in the RE1A data and the data from the EUMETSAT Secretariat is also corroborated by the results in Fig. 3.95. This shows comparisons against ECMWF operational forecasts between 40 km and 70 km for October 2016 (EUMETSAT and UCAR data are not available above 60 km). We do see some split between setting and rising occultations in the RE1B and UCAR data (right plots), especially in the southern hemisphere morning, but generally, the split is more evident in the RE1A data and the data from the EUMETSAT Secretariat (left plots). We also see that the bias between setting and rising occultations is on the order of $0.1 \mu\text{rad}$ and fairly independent of the altitude. The left plots in Fig. 3.96, being the direct comparison of RE1A and RE1B bending angles between 40 km and 70 km, show this more clearly, and also show that the bias is basically the same for Metop-A and Metop-B. Finally, the right plots in Fig. 3.96 show that there is no indication of such systematic biases between the RE1B and UCAR COSMIC bending angles for FM1 and FM6 (but a lot more noise), which were the only two COSMIC satellites operating in October 2016.

The bias differences at high altitudes over hemispheres and local times, as well as the split between setting and rising occultations, could be explained if there is a small bias in the orbit determination in the reprocessed data from the EUMETSAT Secretariat. Such a bias would have to be slowly varying over the Metop orbit with a period of one orbit revolution. Given a typical descend/ascend rate of 2 km/s (as a GPS satellite sets or rises as seen from a Metop satellite), a constant bias in bending angle of $0.1 \mu\text{rad}$ translates into a 0.2 mm/s bias in the Metop orbit velocity. Discussions between the ROM SAF and the EUMETSAT Secretariat about the issue are ongoing, and further analyses are being made. There is agreement that a periodic orbit error is possible, but it has not yet been confirmed.

Going back to the direct comparisons between the RE1A bending angles and the bending angles processed at the EUMETSAT Secretariat in Fig. 3.89, we note the small constant bias (percentage wise) in the 10–25 km range in rising Metop occultations since 2013 that was already mentioned in previous sections. The bias seems to be more prominent in the morning than in the evening. Similar biases are seen in the direct comparisons to the UCAR processed Metop data in Fig. 3.93, but here also for October 2007 in the northern hemisphere morning, and also generally for setting occultations, and sometimes with opposite signs. For the direct comparisons of COSMIC against the UCAR processed COSMIC data in Fig. 3.94 we also see varying biases depending on hemispheres and local times in this altitude range.

The detailed reasons for all these bias differences are not understood, but the explanation is likely to be found in the different handling of the L2-extrapolation. As noted in Section 3.7.2, UCAR has in later years changed the strategy for the L2-extrapolation, and extrapolates both setting and rising occultations from a common fixed altitude (20–22 km); in the ROM SAF reprocessing, the L2 bending angle is only extrapolated below where it is no longer available (if the L1 signal is), or if deemed useless and cut short during the processing. In the following we investigate closer the bias differences between 10 km and 25 km in rising Metop occultations when comparing directly the bending angles from the ROM SAF CDR v1.0 with the bending angles processed at the EUMETSAT Secretariat.

Figure 3.97 is similar to Fig. 3.89, except that it shows the results for October 2007 and October 2016 instead of for January 2016 and July 2016 (and it shows number of observations below 10 km in the right panels of each plot instead of standard deviations). We see that the bias differences for rising Metop occultations are appreciable for October 2016 and basically absent for October 2007, although there is a hint of a smaller bias difference for October 2007 below ~15 km impact height in the northern hemisphere morning, where the bias differences generally seem to be the largest. Separating the statistics further into low and combined mid and high latitudes, as well as early and late morning, Fig. 3.98 shows the bias differences for northern hemisphere morning (October 2016) in the left plots, and the corresponding mean L1 and L2 bending angle differences in the right plots. For the northern hemisphere low latitude early morning (top plots), we see the L1–L2 bending angle means for rising occultations being virtually identical for RE1A and the EUMETSAT data down to ~25 km. Below that, the extrapolation for the RE1A data is basically straight-down (constant L1–L2 extrapolation), whereas it is following more the trend at higher altitudes for the EUMETSAT data (extrapolation approach by [RD.2]). For setting occultations, where the L2 signal usually is available down to lower impact heights (mostly down to about 10 km it seems here), we see that the measured L1–L2 mean bending angle in the 10–20 km range is in fact more straight-down, for both the RE1A data and the EUMETSAT data. Below 10 km, the L1–L2 means also for setting occultations are different, which seems consistent with the different L2-extrapolation methods. We note that the size of the L1–L2 means can be different for setting and rising occultations, and also that the number of rising occultations is much larger than the number of setting occultations in the low latitude early morning area. This is due to the geometry and how the detailed locations of the occultations depend on the orbits of the GPS constellation. Fig. 3.99 shows the global distribution of Metop occultations for October 2016, and Fig. 3.100 shows the same for October 2007 (only Metop-A at that time).

Thus, in the northern hemisphere low latitude early morning, based on the observed L1–L2 means for setting occultations between 10 km and 25 km, it is possible that a more straight-down extrapolation for rising occultations below 25 km, as in the RE1A data, is more correct than the one in the EUMETSAT data. The bias differences for rising occultations in this area may therefore be more due to a bias in the EUMETSAT data, than in the RE1A data. For the other areas in Fig. 3.98, the situation is somewhat the opposite. Using the same arguments, looking at how the L1–L2 means for setting occultations behave below 25 km, it seems that the approach by [RD.2] on average gives a better L2-extrapolation below 25 km for rising occultations than the constant L1–L2 extrapolation in the ROM SAF reprocessing. The bias differences for rising occultations in these areas may therefore be more due to a bias in the RE1A data, than in the EUMETSAT data. The reason for different L1–L2 means (and the vertical distribution thereof) in different areas and local times should probably be found in

the detailed global average distribution of the ionospheric electron density and its horizontal gradients. We have not investigated such details in connection with the performance of the L2-extrapolation, but Fig. 3.101 shows the corresponding results for October 2007, which was at a time much closer to the past solar minimum, and Fig. 3.102 shows the results for the northern hemisphere evening in October 2016. In the former of these two figures, the L2-extrapolation from ~25 km and down was not necessary (before the instrument software upgrades to Metop), but is generally done from around 10–15 km in the ROM SAF processing, depending on the availability of a useful L2 signal. It is actually not clear from this picture (Fig. 3.98 and Fig. 3.101 together) which method performs better in the different areas, and it is not understood why the vertical slopes of the rising and setting L1–L2 means between 15 km and 25 km seem to be inconsistent in some of the areas. In the latter figure, there are virtually no bias differences between 10 km and 25 km, since the two L2-extrapolation methods give similar results on average, consistent with the observed L1–L2 means for setting occultations (a more or less straight-down L1–L2 extrapolation below ~25 km).

As a final remark, we note the hint of a very small, but systematic negative bias at high altitudes (increasing with height) in the direct comparisons to the EUMETSAT bending angles in the left plots of Fig. 3.98, where the ionospheric influence is the largest (indicated by the L1–L2 means in the right plots). This is likely a result of the higher order ionospheric correction in the data from the EUMETSAT Secretariat, not taken into account in the ROM SAF CDR1 v1.0 (cf. Section 3.6).

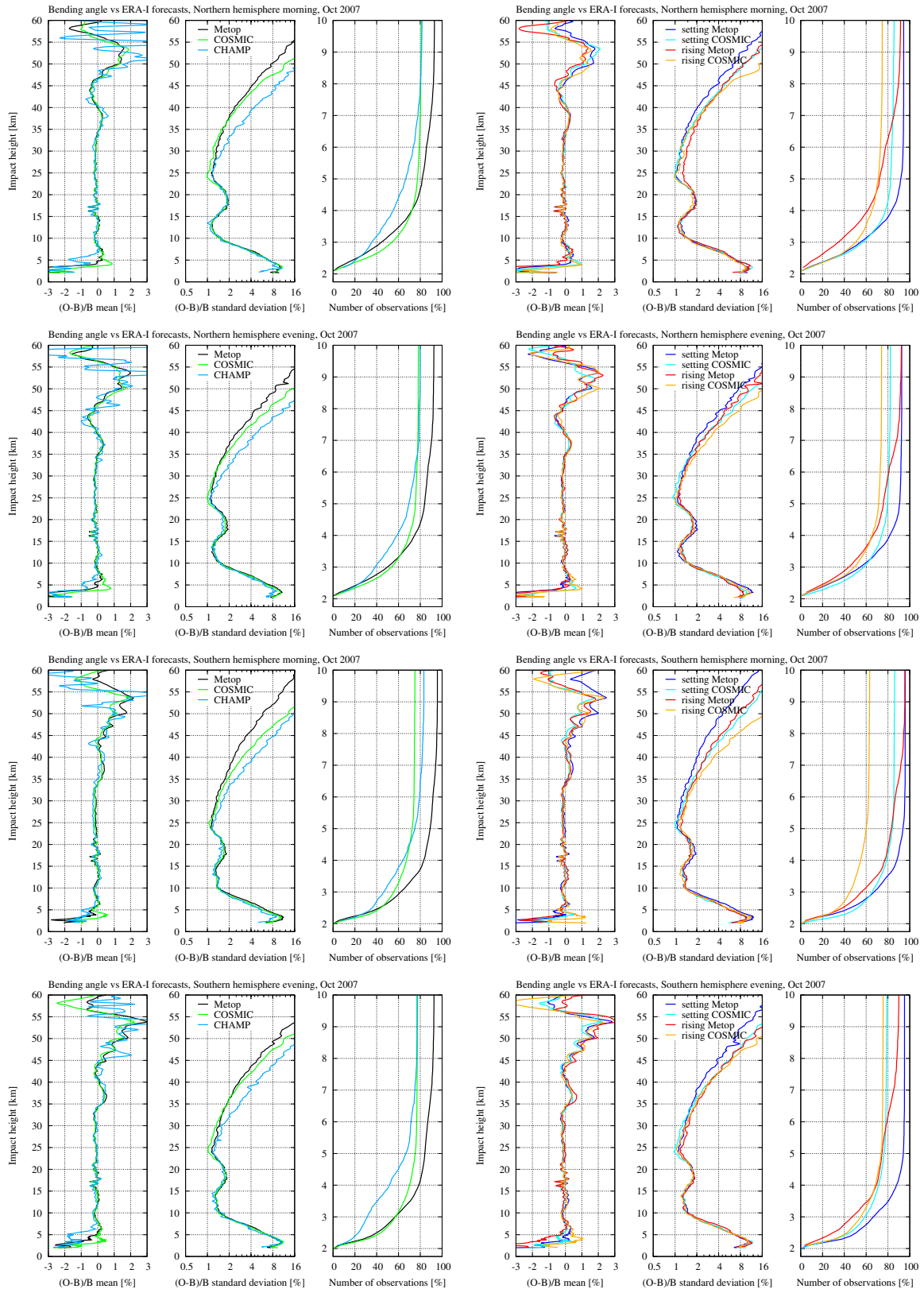


Figure 3.85: Monthly global profile statistics of bending angle for different missions at local morning and evening in the northern and southern hemispheres (October 2007).

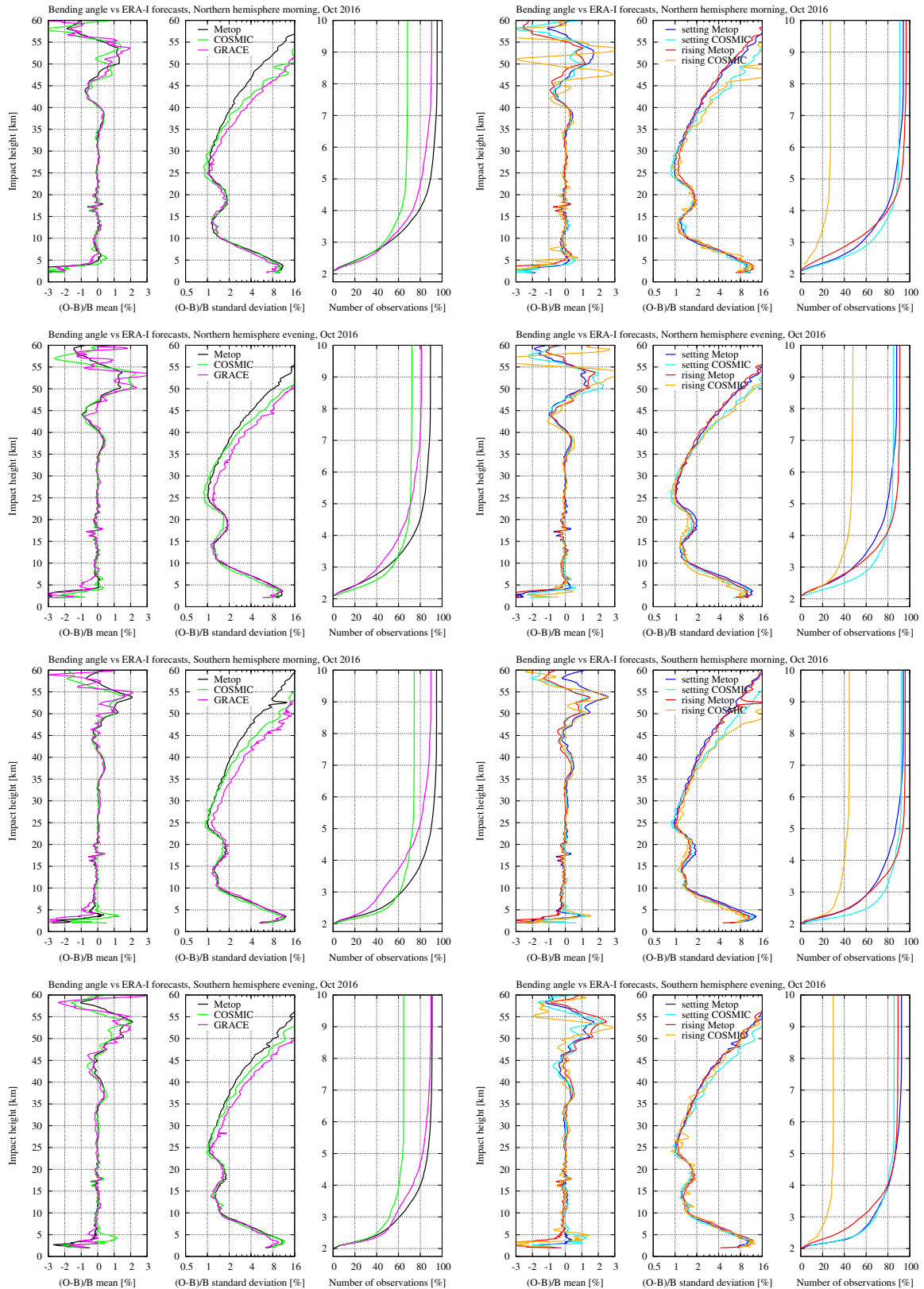


Figure 3.86: Monthly global profile statistics of bending angle for different missions at local morning and evening in the northern and southern hemispheres (October 2016).

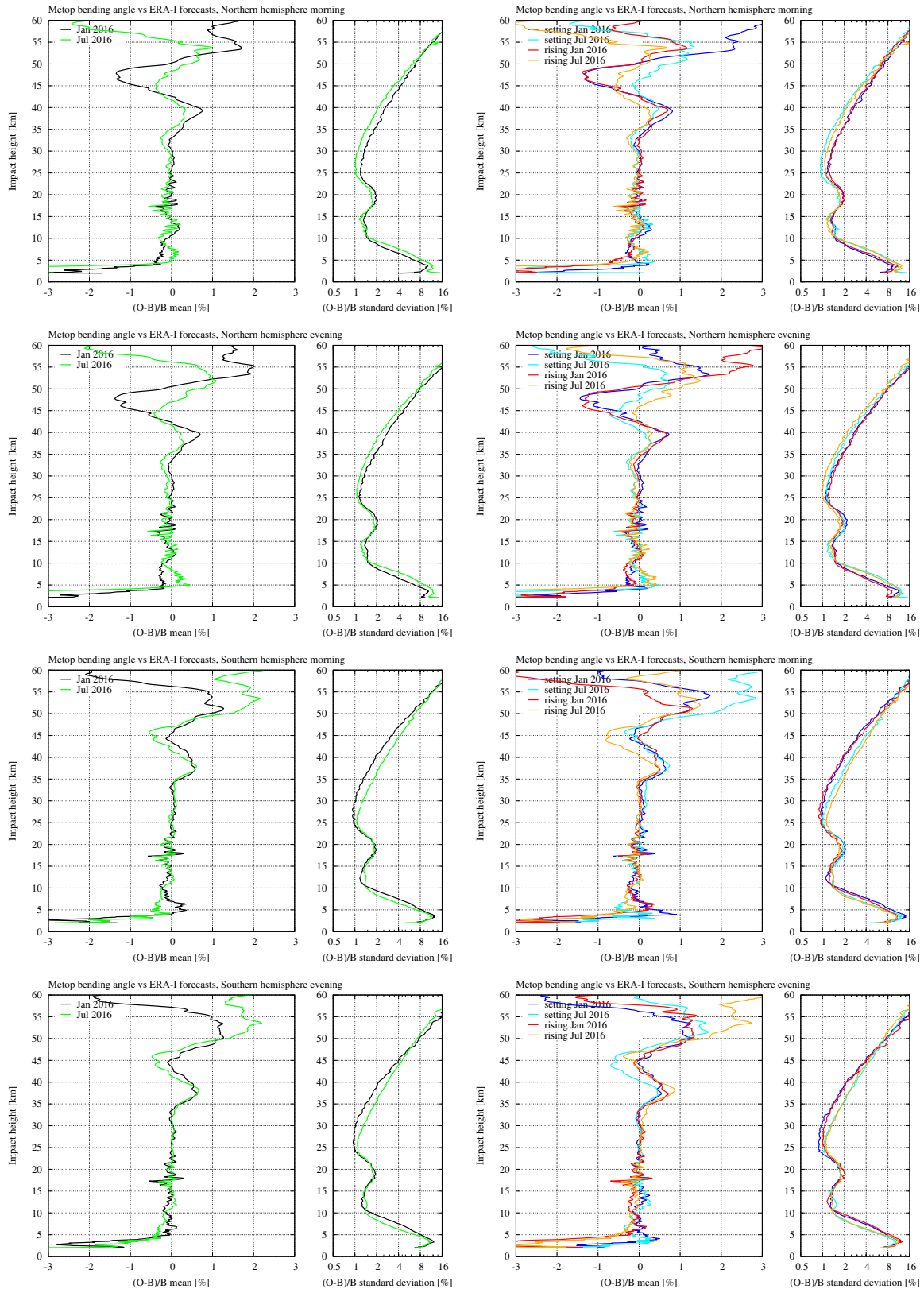


Figure 3.87: Monthly profile statistics of bending angle from Metop at opposite seasons, hemispheres, morning and evening.

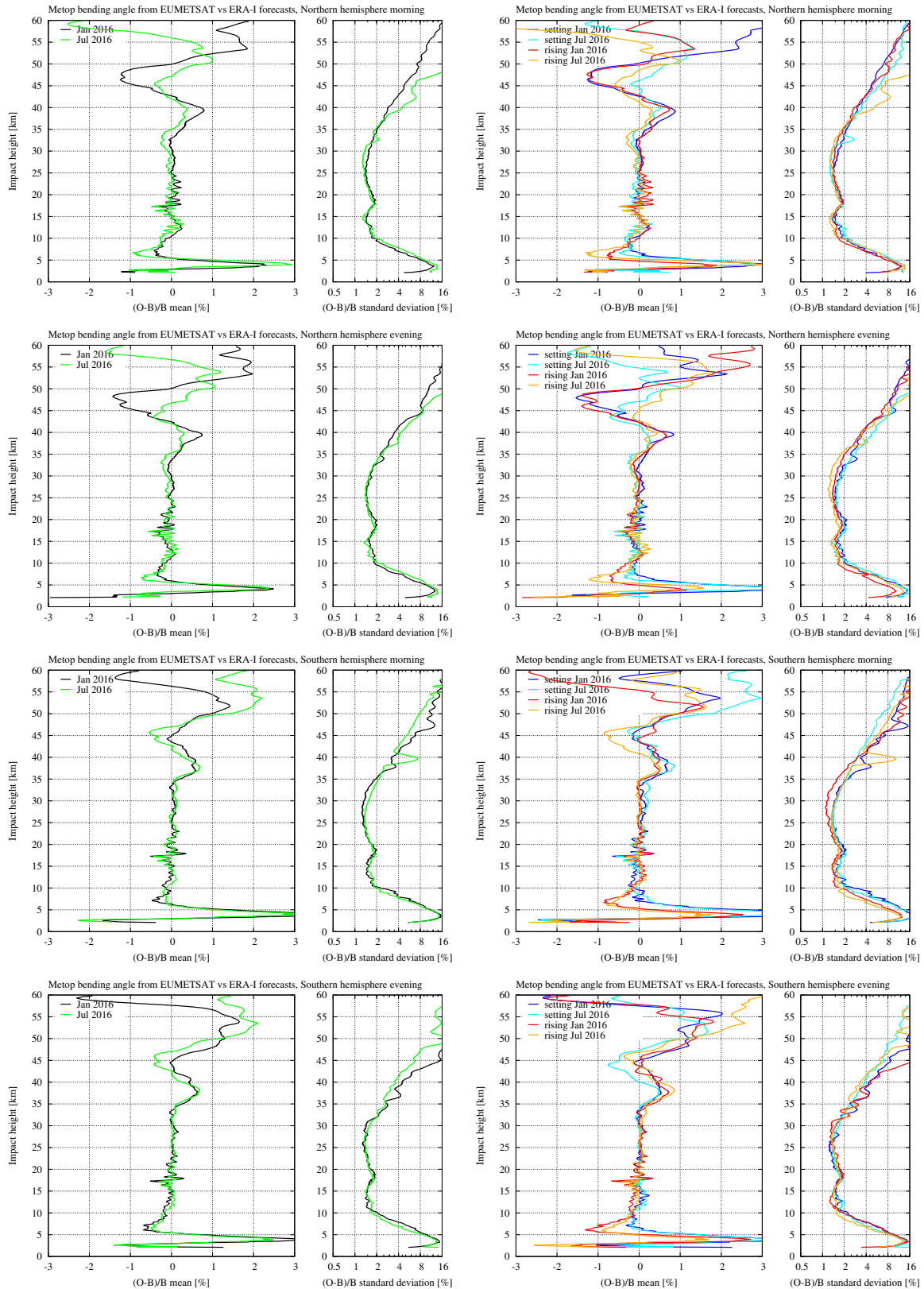


Figure 3.88: Monthly profile statistics of bending angle from Metop (processed at the EUMETSAT Secretariat) at opposite seasons, hemispheres, morning and evening.

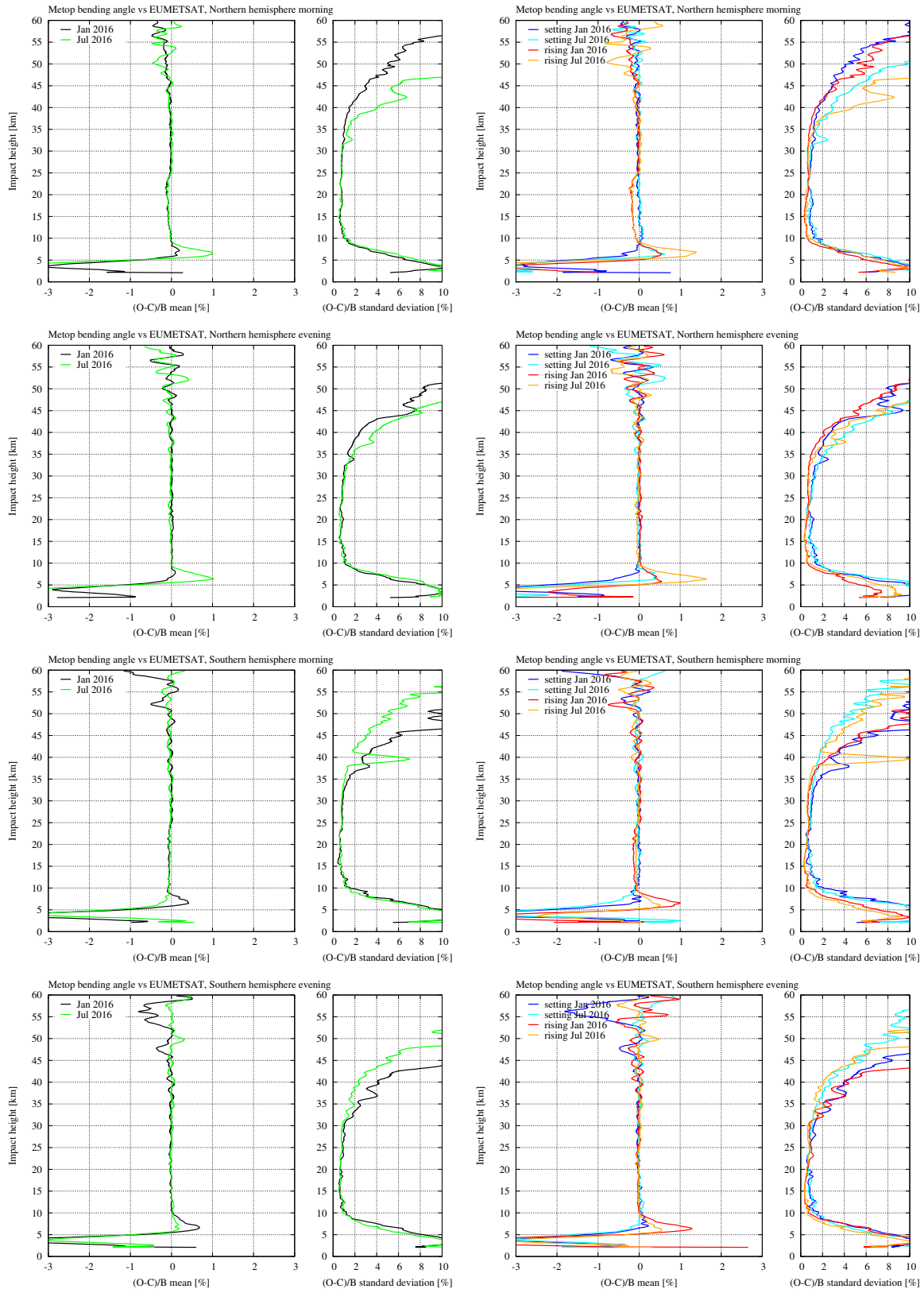


Figure 3.89: Monthly profile statistics of bending angle from Metop (from the REIA processing) against the bending angle processed at the EUMETSAT Secretariat, at opposite seasons, hemispheres, morning and evening.

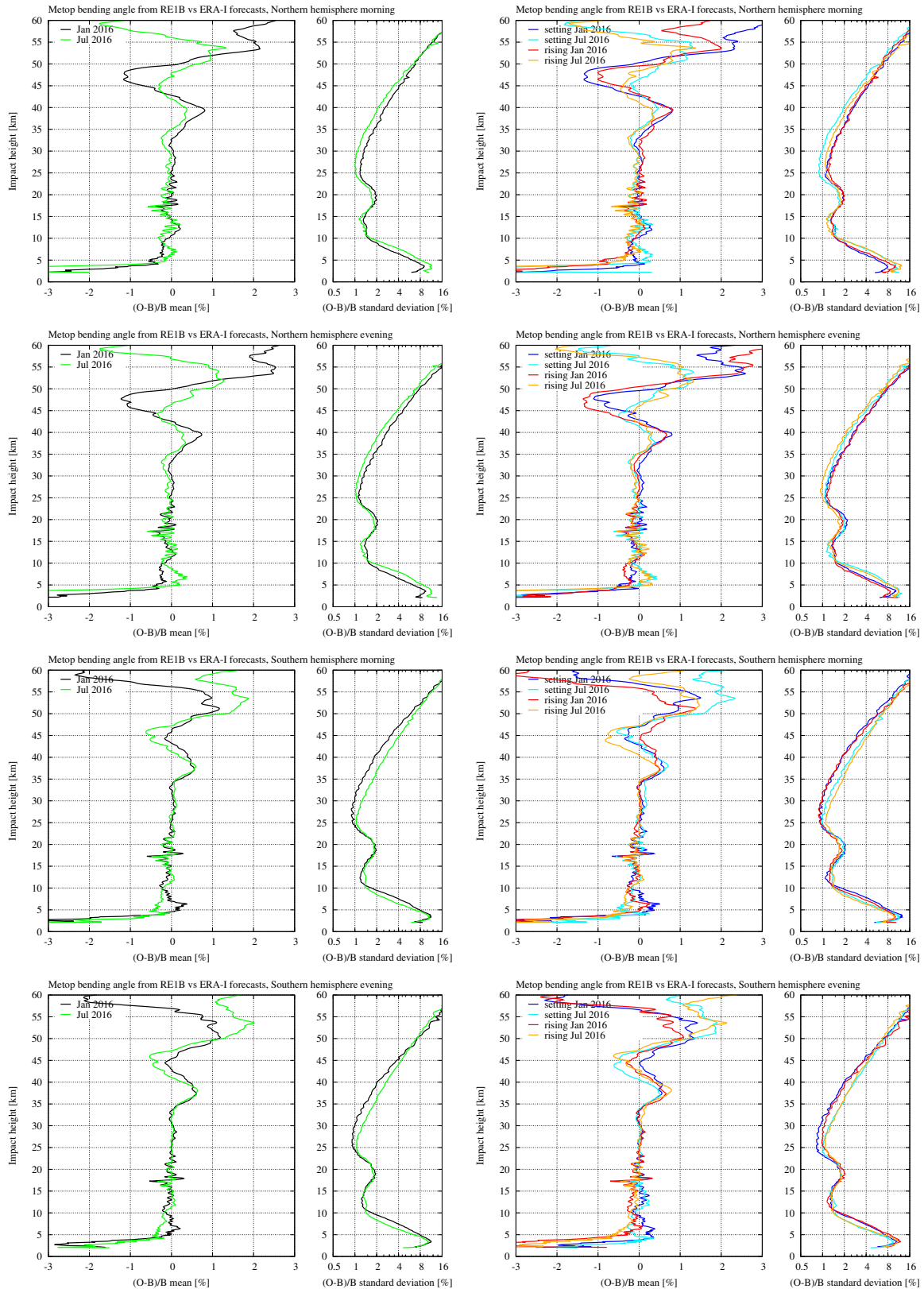


Figure 3.90: Monthly profile statistics of bending angle from Metop (from the RE1B processing), at opposite seasons, hemispheres, morning and evening.

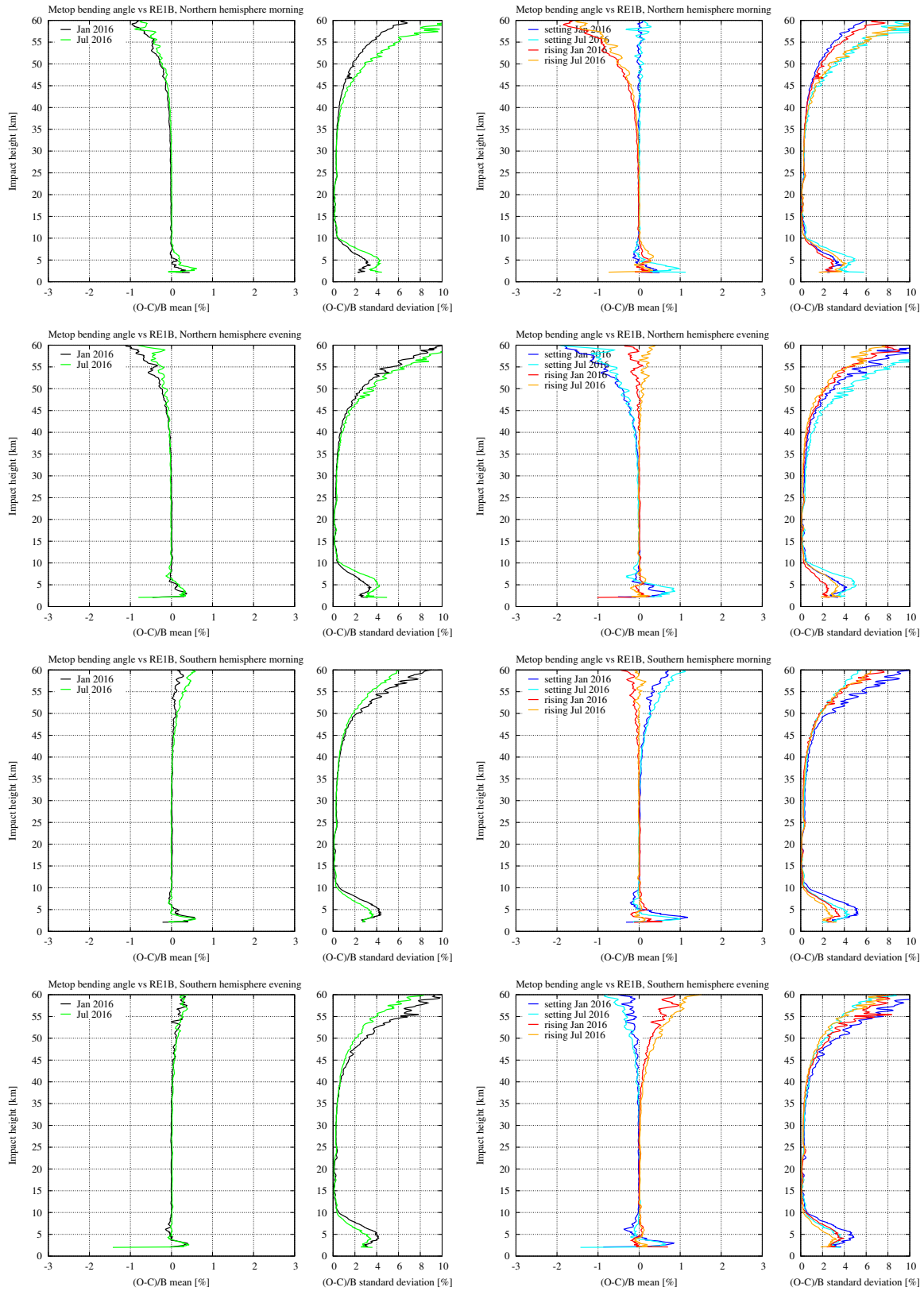


Figure 3.91: Monthly profile statistics of bending angle from Metop against the bending angle from the REIB processing, at opposite seasons, hemispheres, morning and evening.

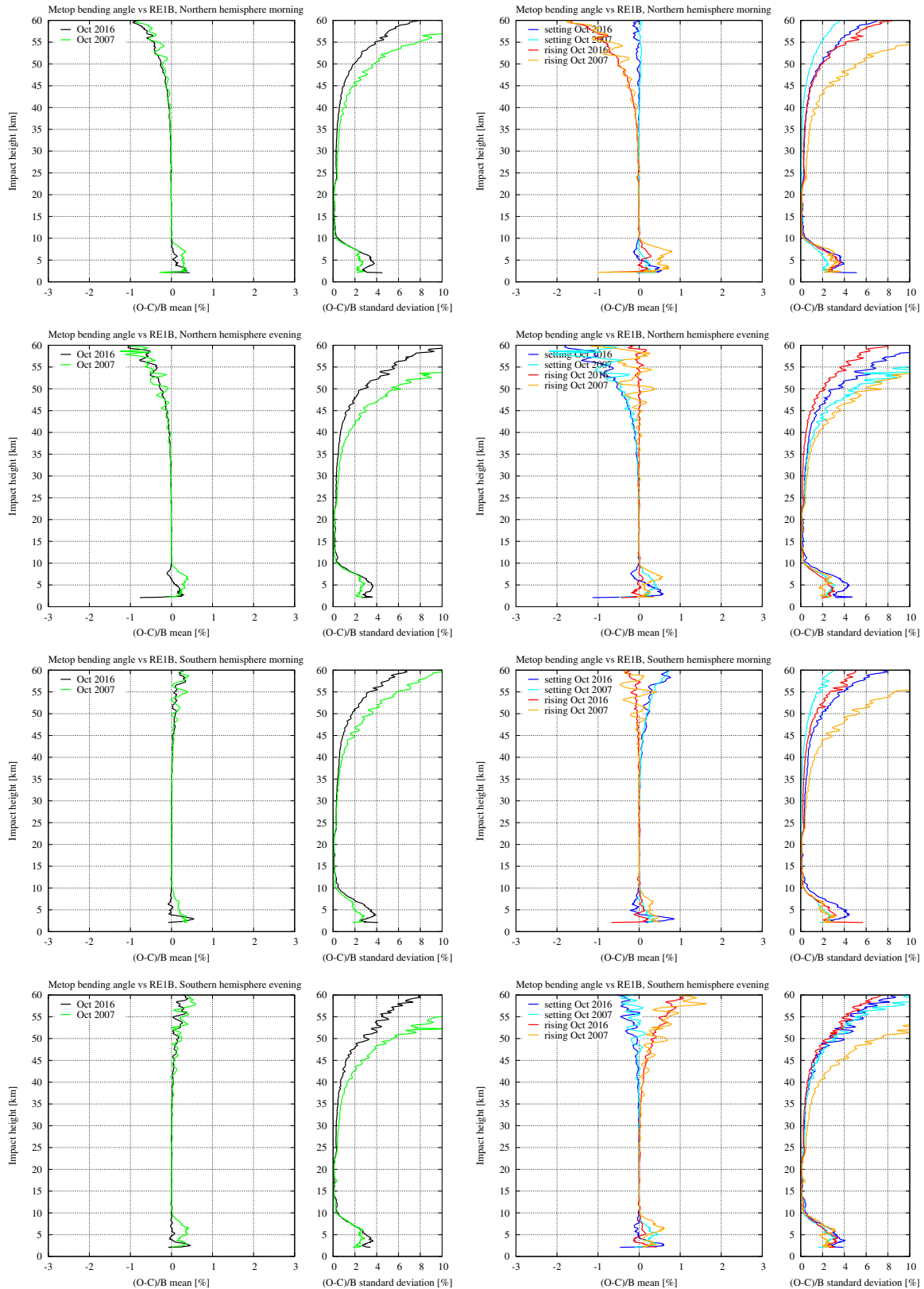


Figure 3.92: Monthly profile statistics of bending angle from Metop against the bending angle from the REIB processing, at opposite hemispheres, morning and evening.

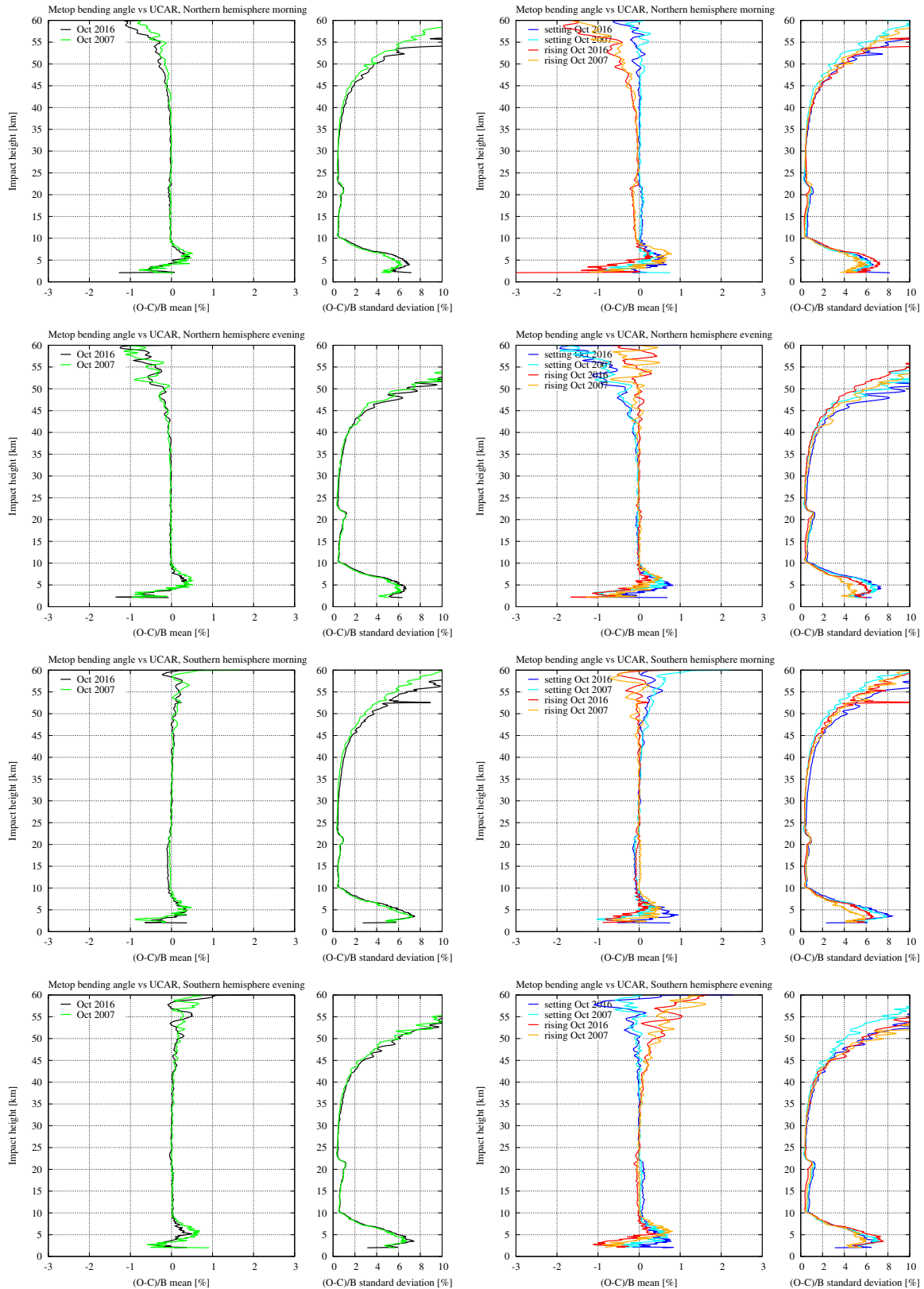


Figure 3.93: Monthly profile statistics of bending angle from Metop against the bending angle processed at UCAR, at opposite hemispheres, morning and evening.

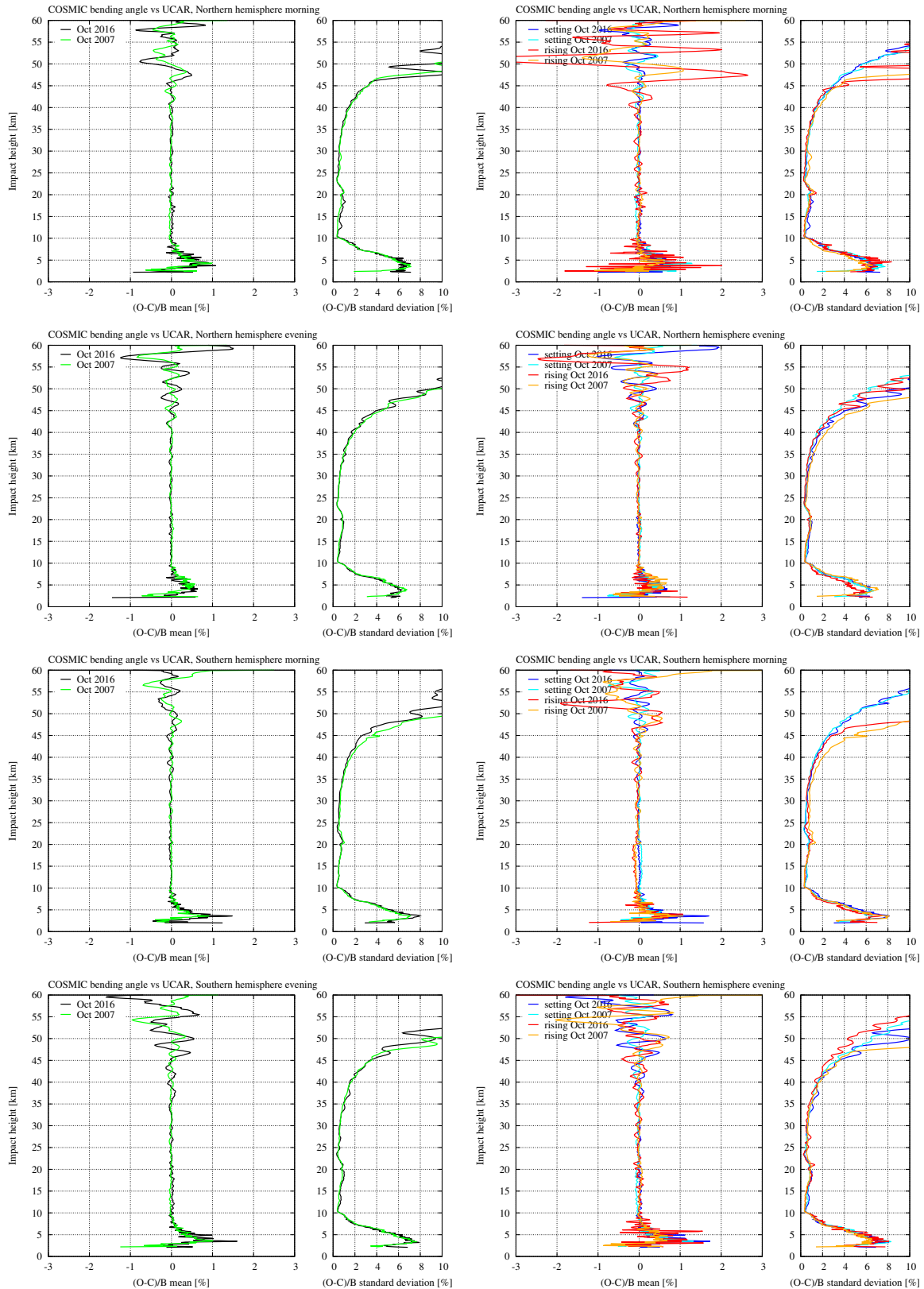


Figure 3.94: Monthly profile statistics of bending angle from COSMIC against the bending angle processed at UCAR, at opposite hemispheres, morning and evening.

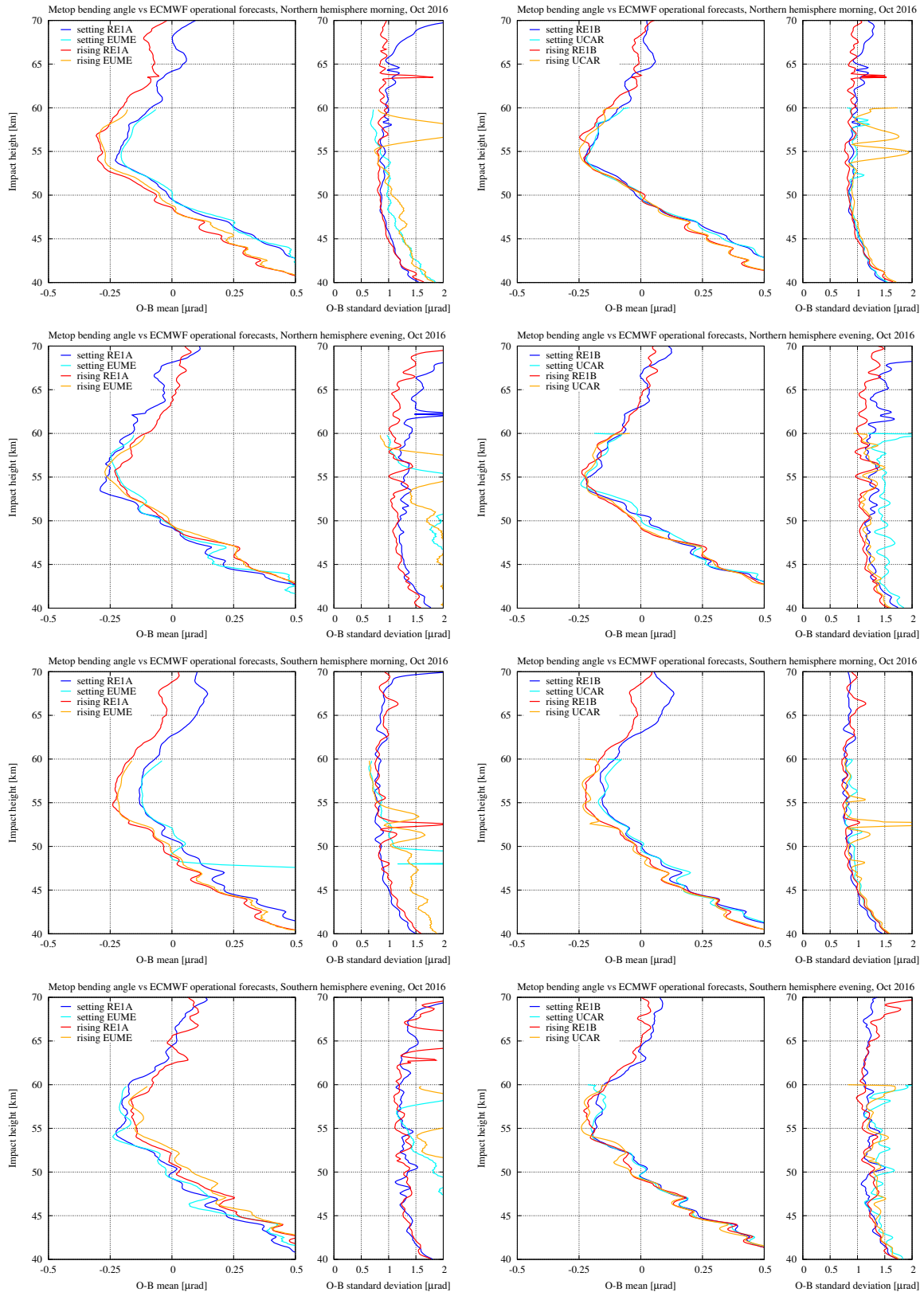


Figure 3.95: Monthly profile statistics of bending angle at high altitudes from Metop, processed in four different ways, at opposite hemispheres, morning and evening.

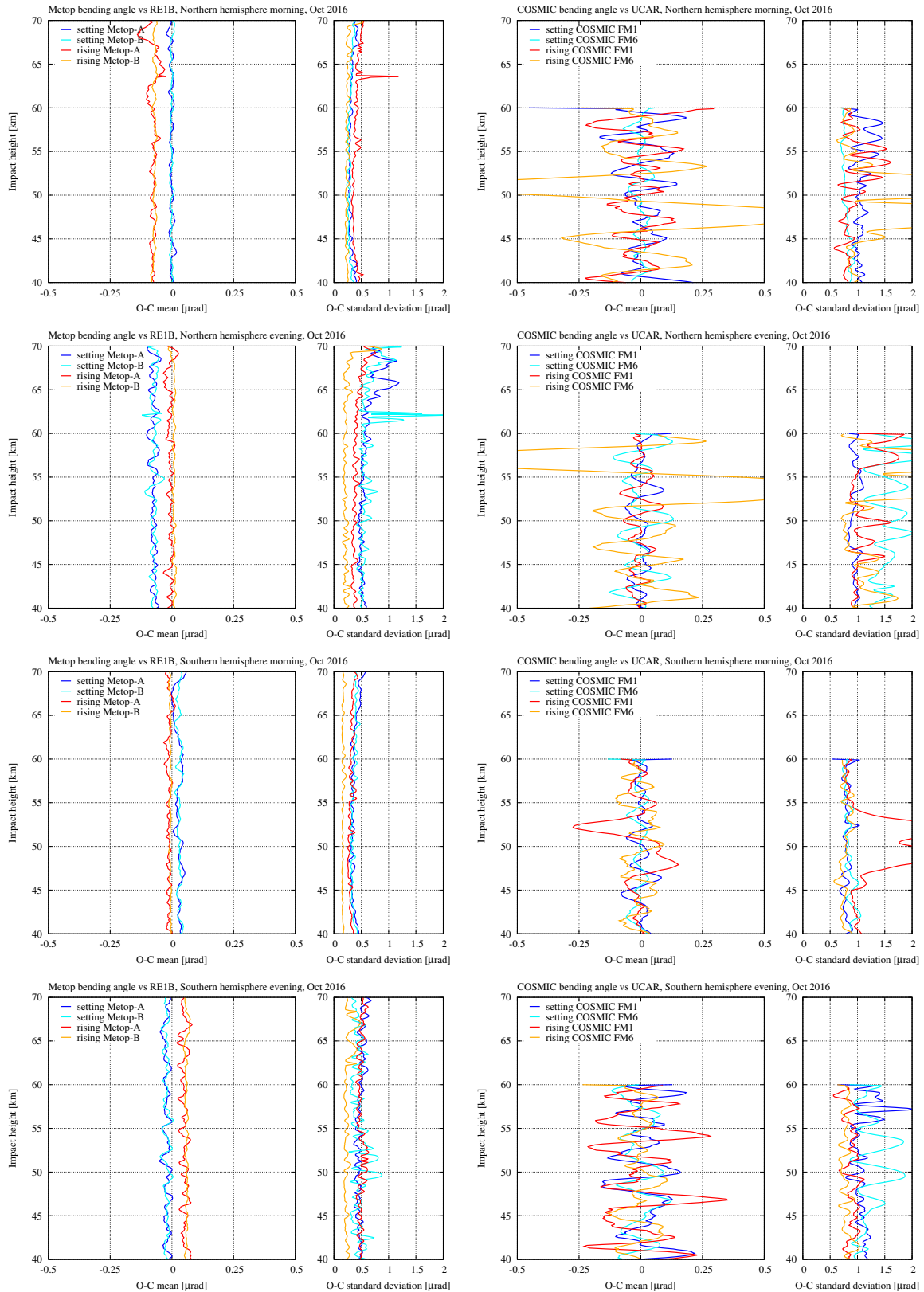


Figure 3.96: Monthly profile statistics of bending angle at high altitudes from individual Metop and COSMIC satellites against the bending angle from the RE1B processing and the bending angle processed at UCAR, at opposite hemispheres, morning and evening.

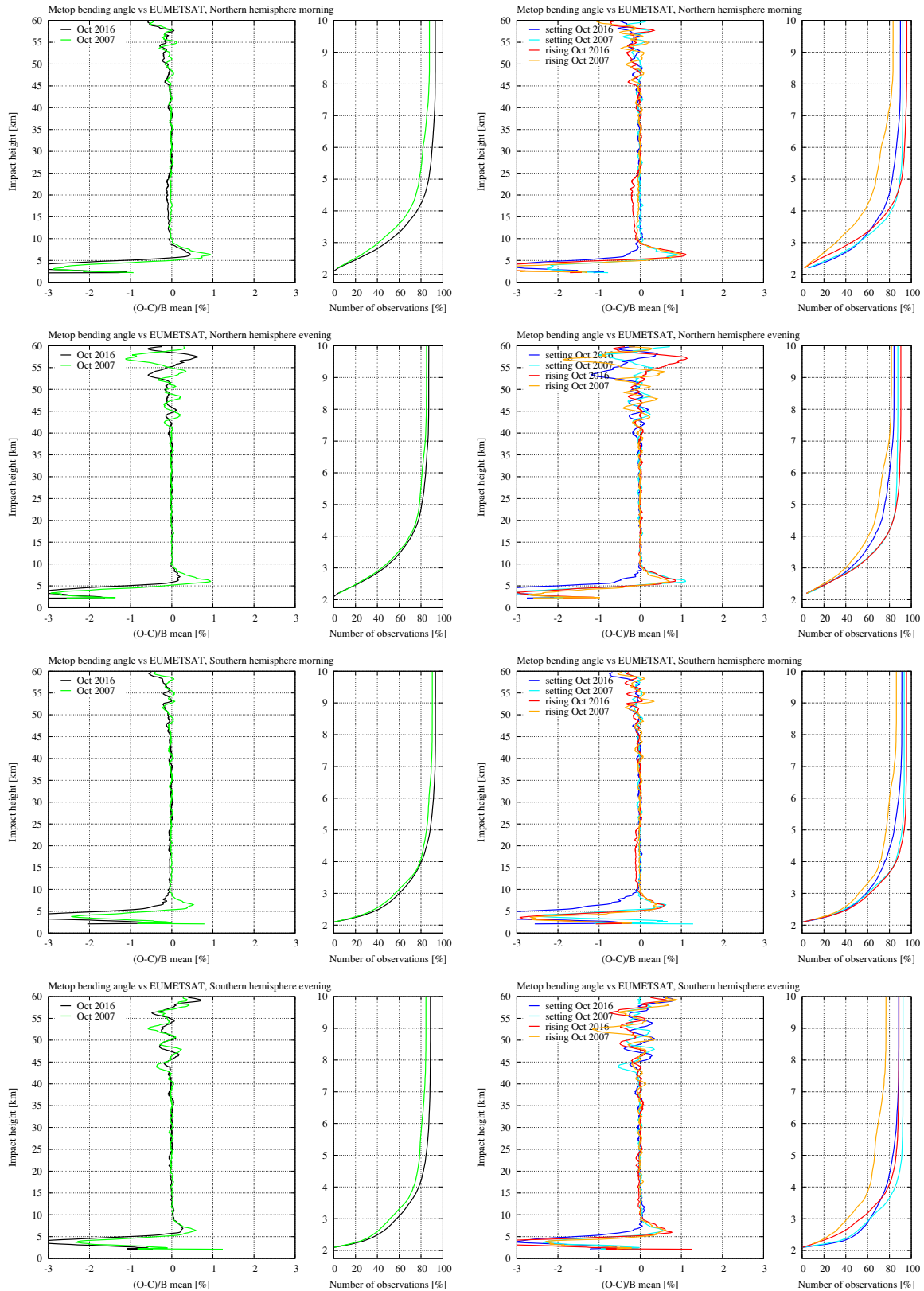


Figure 3.97: Monthly profile statistics of bending angle from Metop against the bending angle processed at the EUMETSAT Secretariat, at opposite seasons, hemispheres, morning and evening.

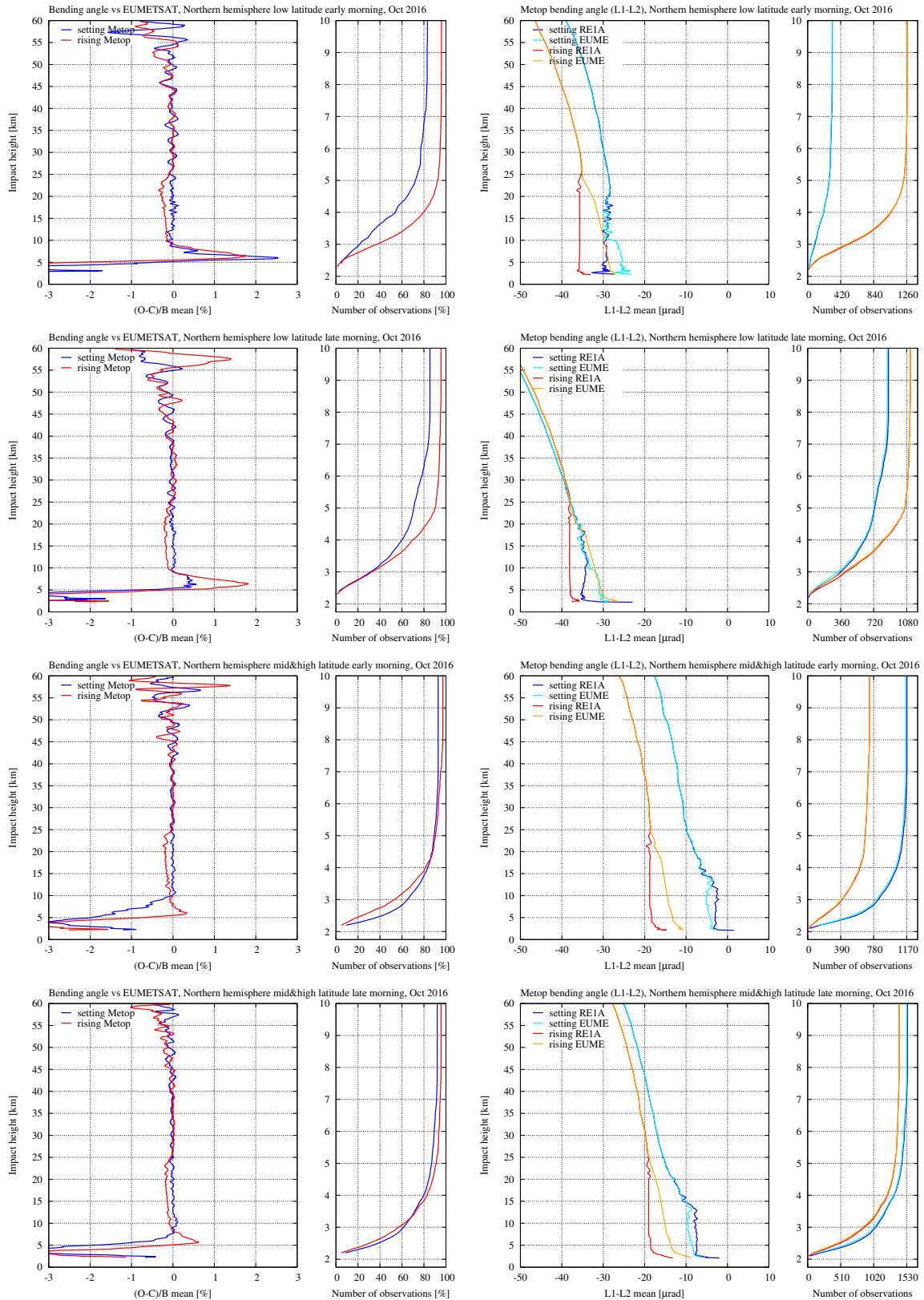


Figure 3.98: Monthly profile statistics of bending angle from Metop (from the REIA processing) against the bending angle processed at the EUMETSAT Secretariat, northern hemisphere morning (October 2016).

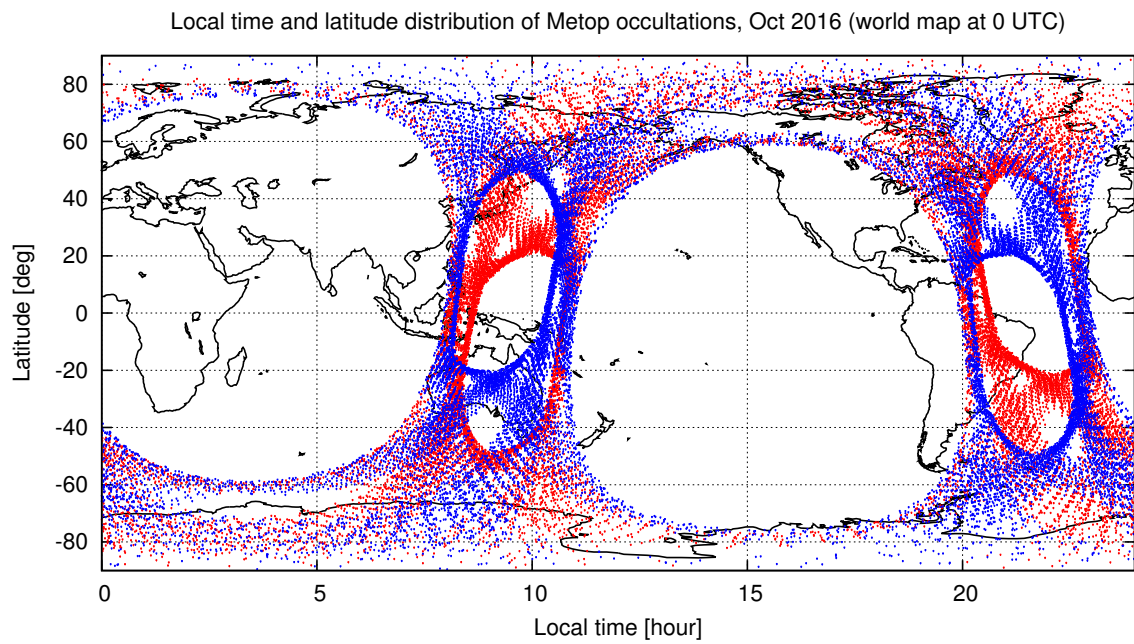


Figure 3.99: Global distribution of setting (blue) and rising (red) occultations in local time and latitude for October 2016.

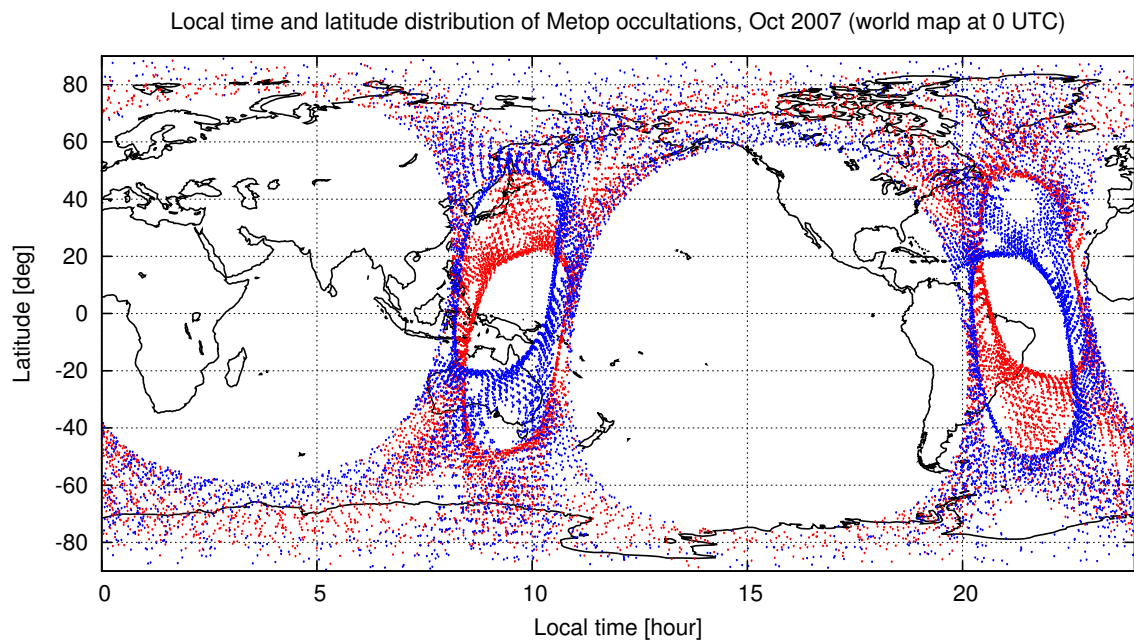


Figure 3.100: Global distribution of setting (blue) and rising (red) occultations in local time and latitude for October 2007.

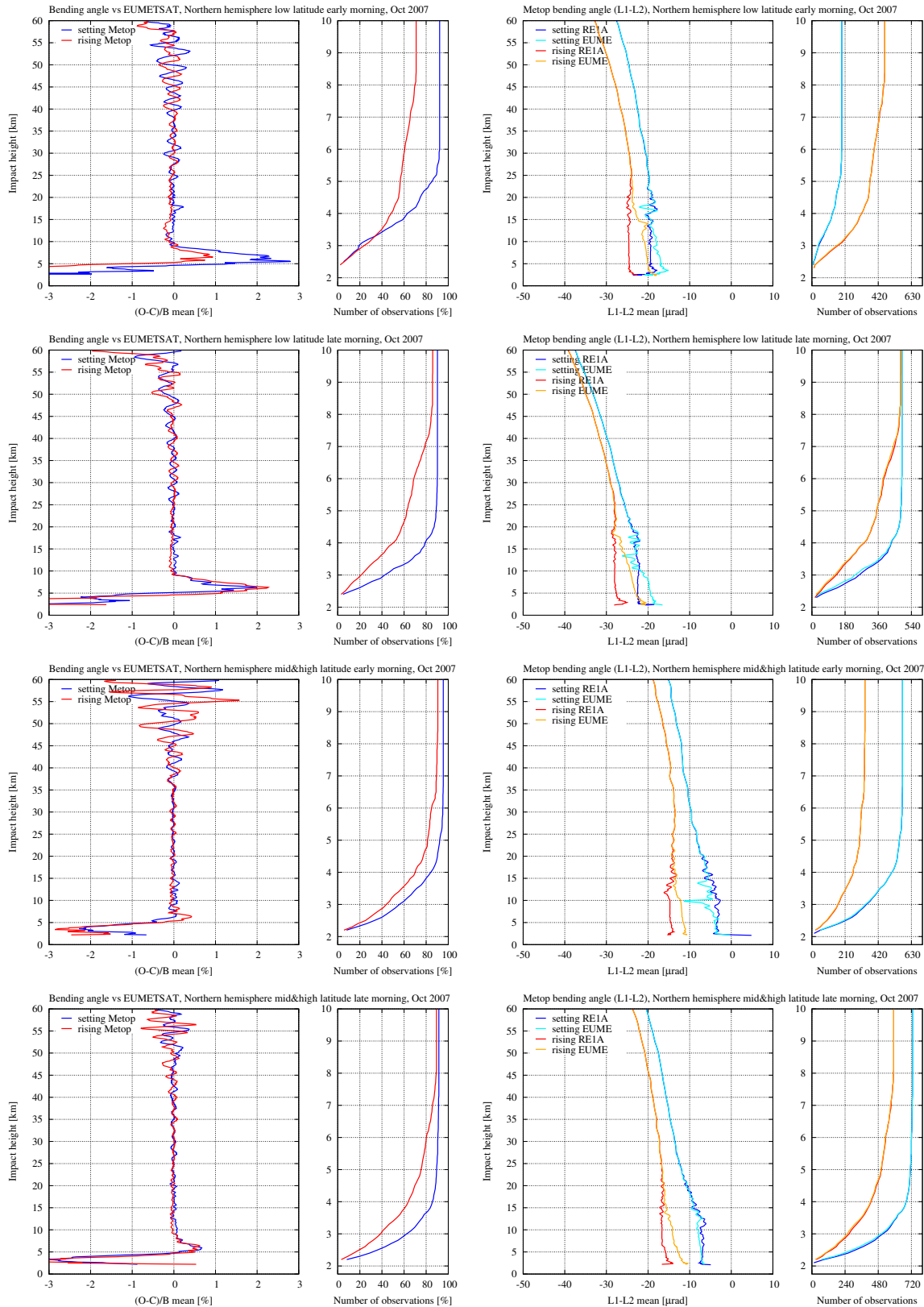


Figure 3.101: Monthly profile statistics of bending angle from Metop (from the REIA processing) against the bending angle processed at the EUMETSAT Secretariat, northern hemisphere morning (October 2007).

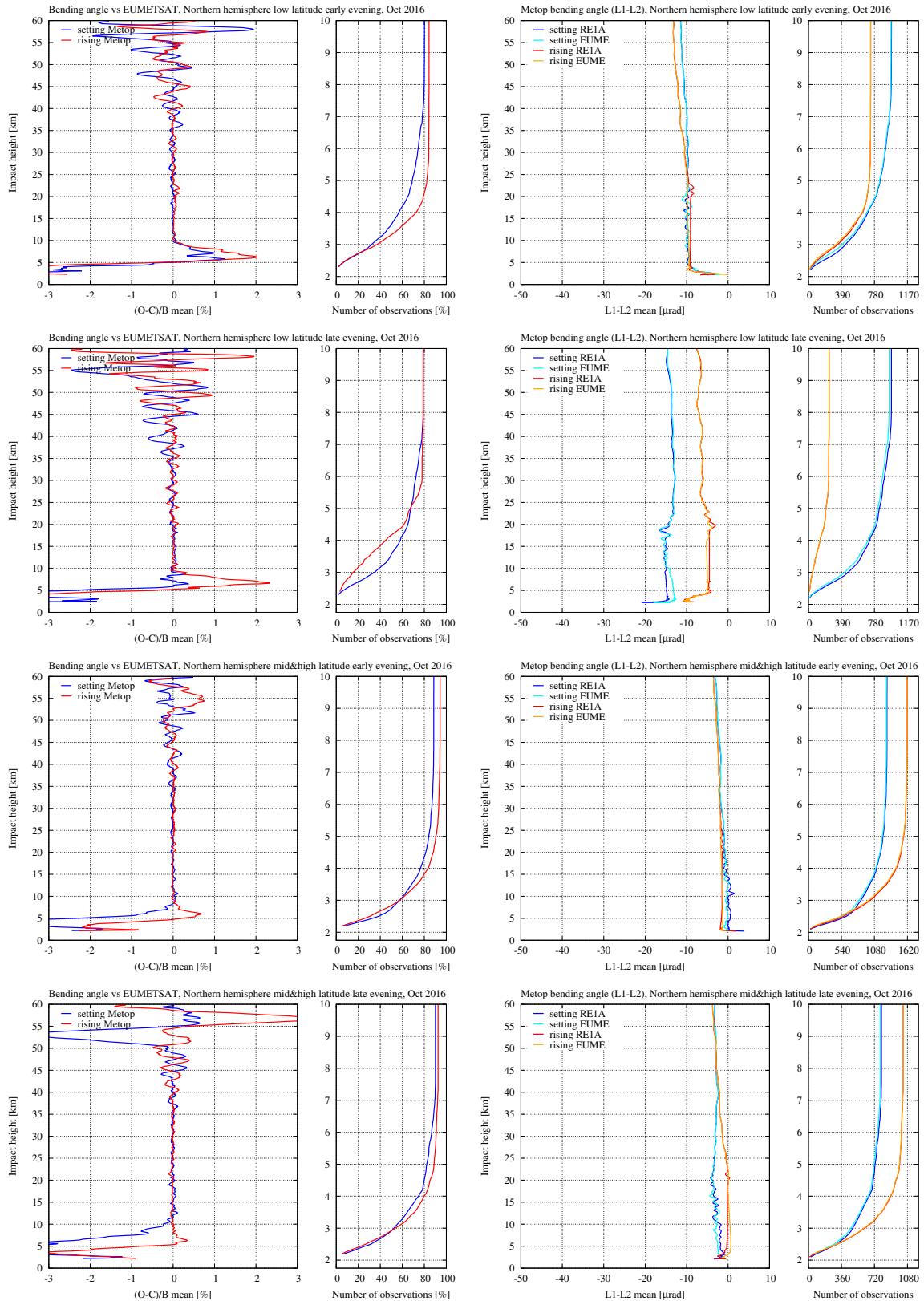


Figure 3.102: Monthly profile statistics of bending angle from Metop (from the RE1A processing) against the bending angle processed at the EUMETSAT Secretariat, northern hemisphere evening (oct 2016).

3.8.2 Refractivity

Figures 3.103–3.108 show the results for refractivity, corresponding to some of the figures for bending angle in the previous subsection. We shall not go into lengthy discussions of these results (they are similar to the results in bending angle), except noting how the bias differences between the RE1A and the RE1B data for setting and rising occultations at high altitudes in Fig. 3.106 reflect the ones in Fig. 3.92, and show how constant bending angle errors propagate to refractivity in the ROM SAF reprocessing. Percentage wise, the error is generally a little larger in refractivity, and consequently can be said to propagate to lower altitudes (5–10 km lower). The bias differences in refractivity between the ROM SAF CDR v1.0 and the UCAR data at high altitudes in Figs. 3.107 and 3.108, for Metop and COSMIC, respectively, are clearly affected by the different statistical optimization approaches (cf. Section 3.7.2).

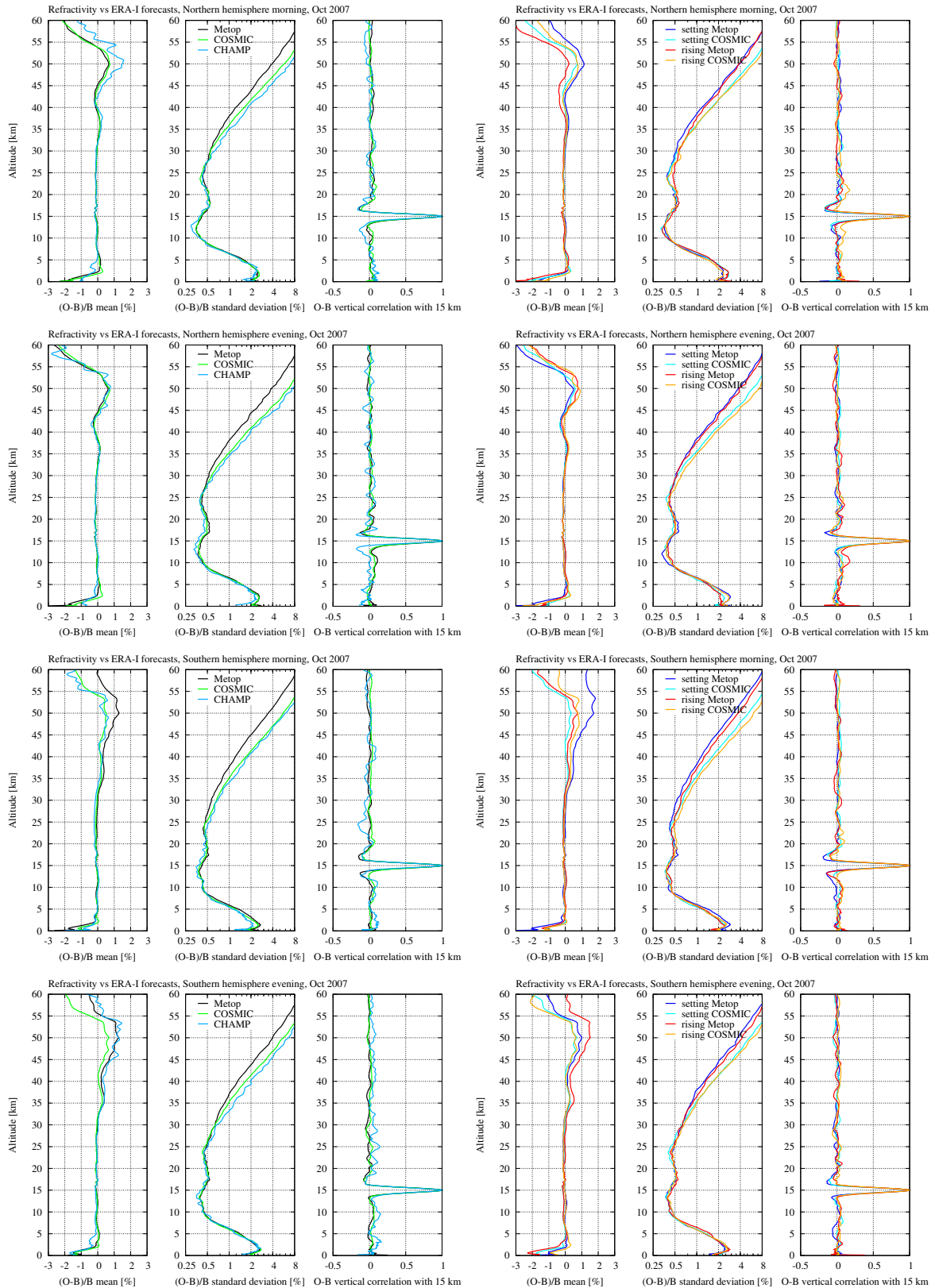


Figure 3.103: Monthly global profile statistics of refractivity for different missions at local morning and evening in the northern and southern hemispheres (October 2007).

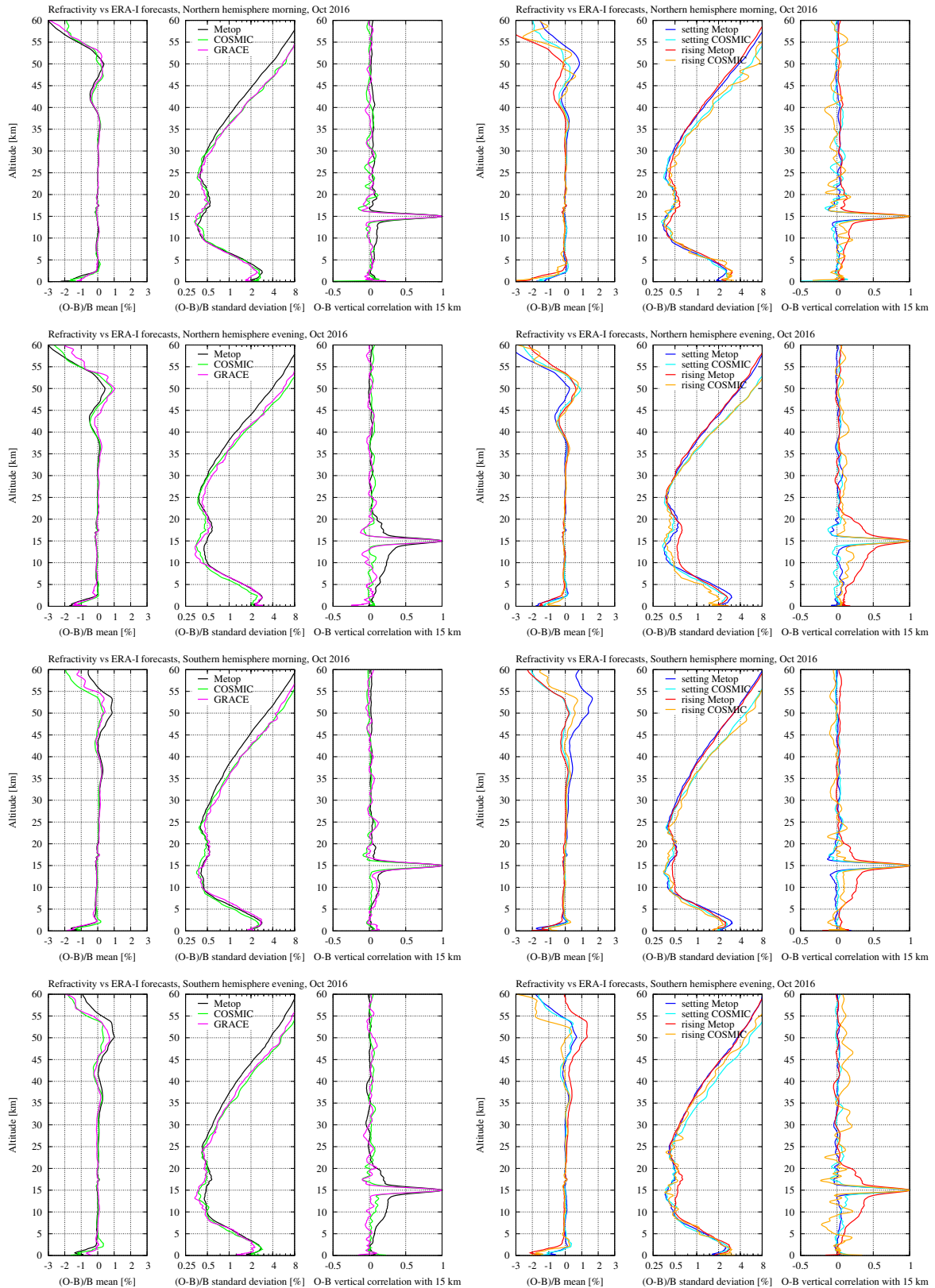


Figure 3.104: Monthly global profile statistics of refractivity for different missions at local morning and evening in the northern and southern hemispheres (October 2016).

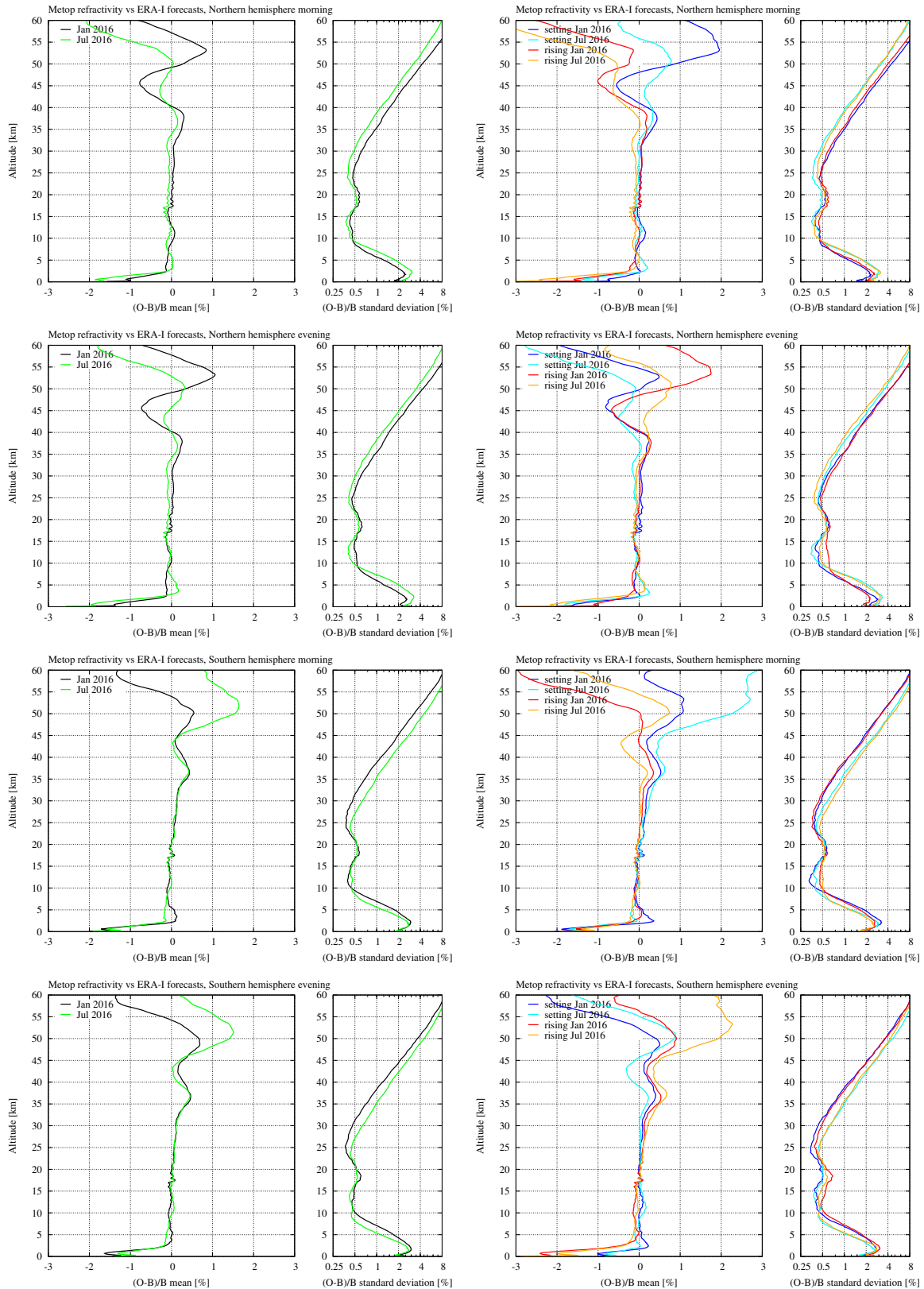


Figure 3.105: Monthly profile statistics of refractivity from Metop at opposite seasons, hemispheres, morning and evening.

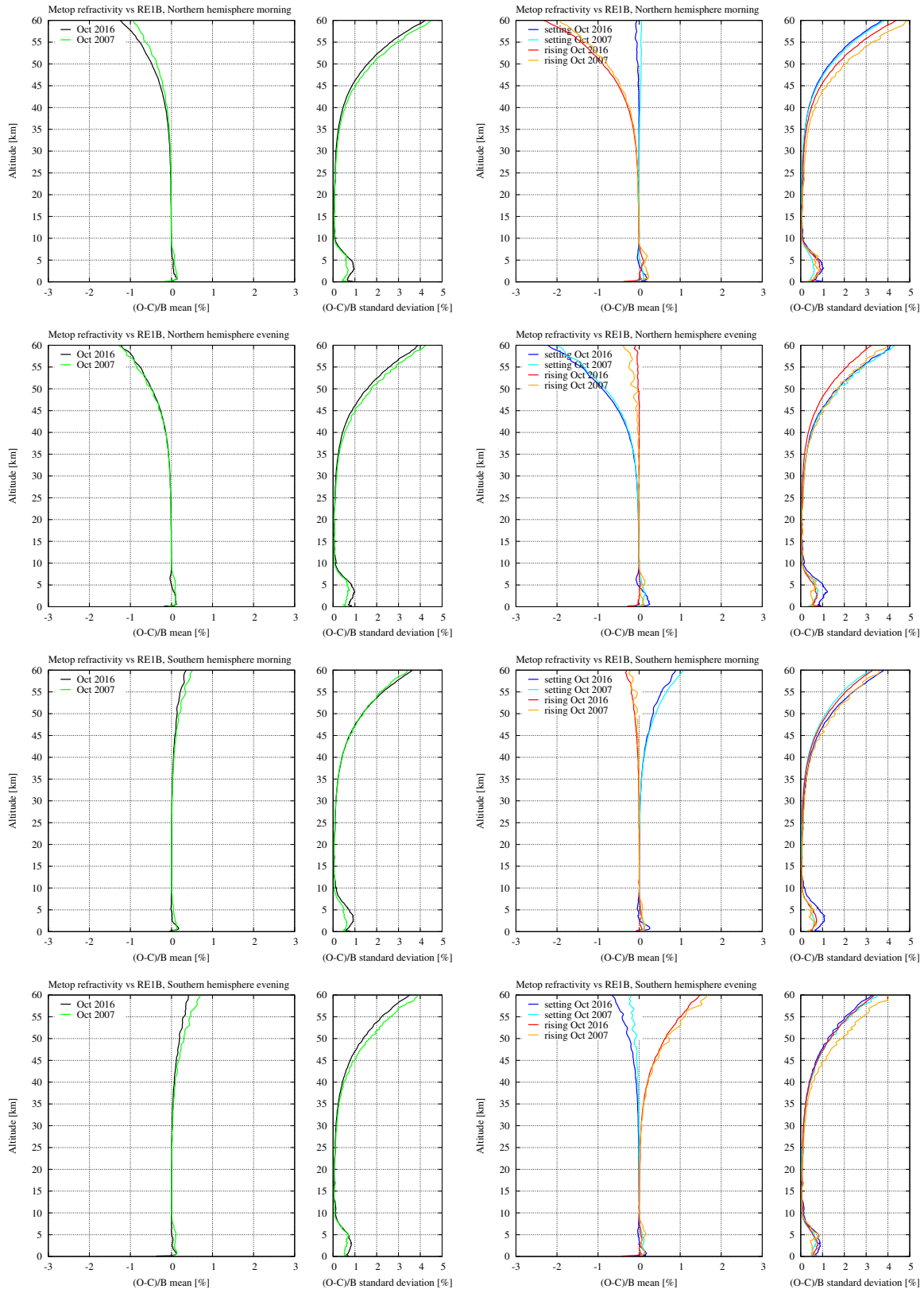


Figure 3.106: Monthly profile statistics of refractivity from Metop against the refractivity from the REIB processing, at opposite seasons, hemispheres, morning and evening.

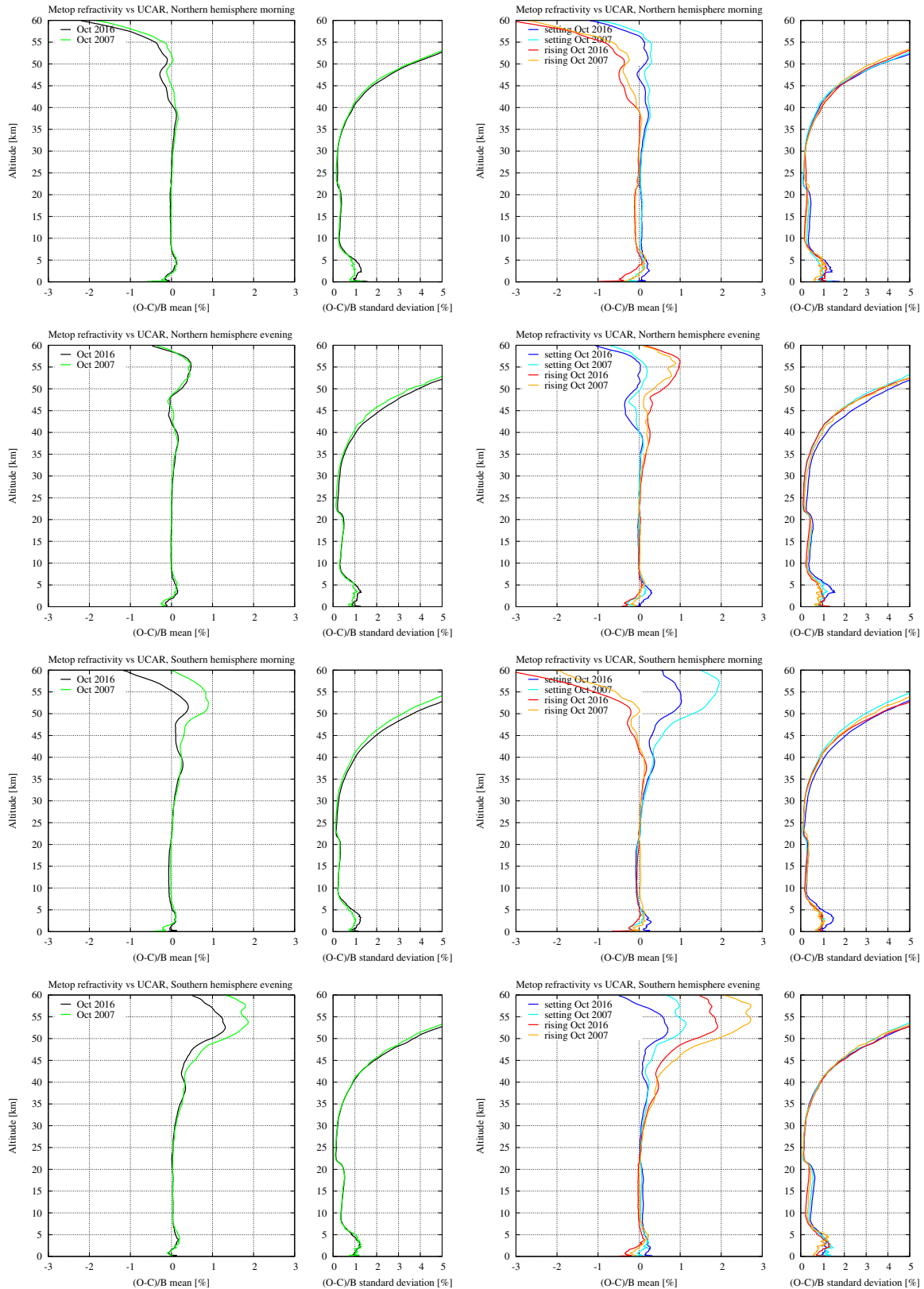


Figure 3.107: Monthly profile statistics of refractivity from Metop against the refractivity processed at UCAR, at opposite seasons, hemispheres, morning and evening.

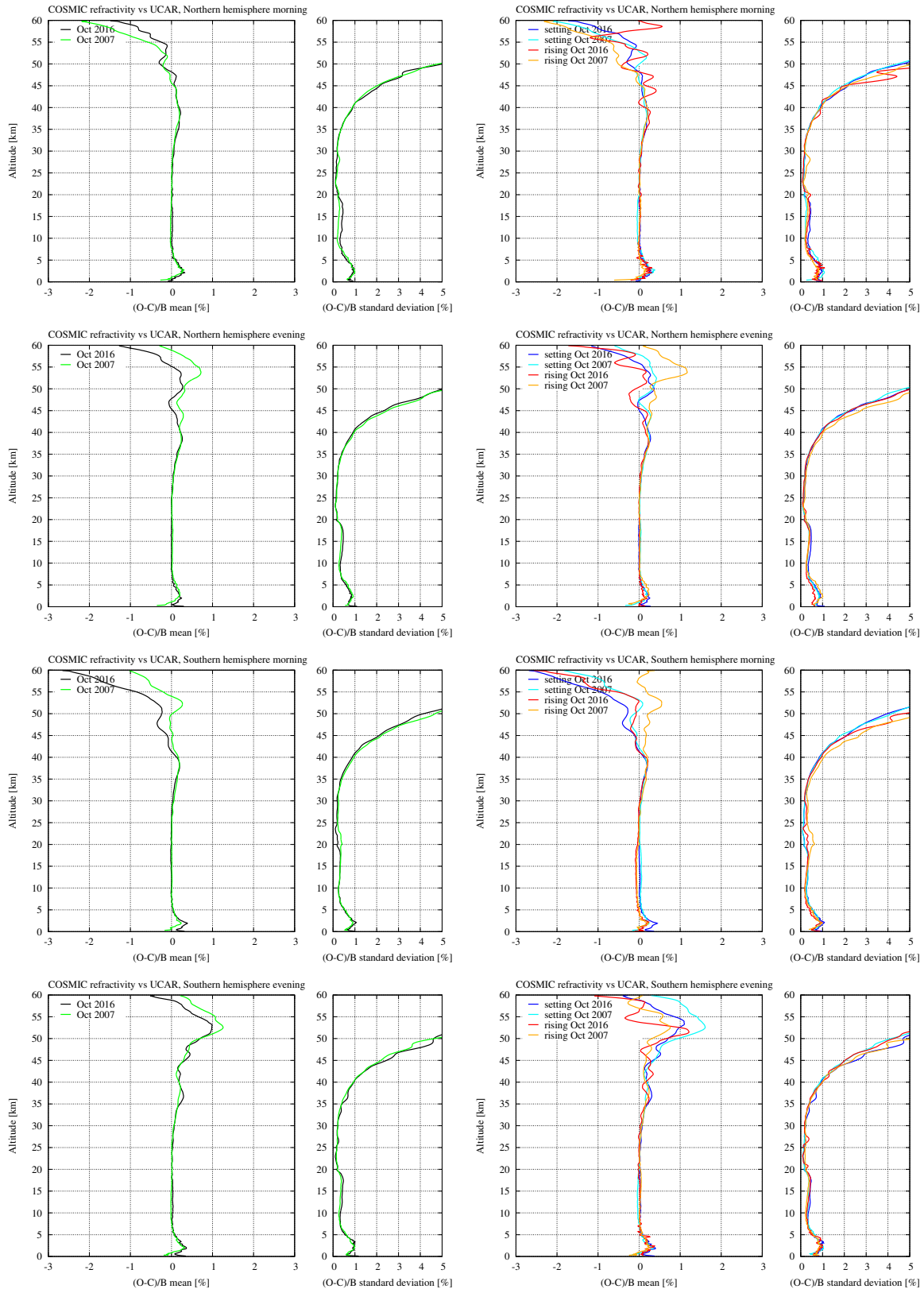


Figure 3.108: Monthly profile statistics of refractivity from COSMIC against the refractivity processed at UCAR, at opposite seasons, hemispheres, morning and evening.

3.8.3 Dry temperature

Figures 3.109–3.114 show the plots for dry temperature, corresponding to the ones for refractivity in the previous subsection. As there, we limit ourselves to note that the bias differences in Fig. 3.112 nicely illustrate how constant bending angle errors at high altitudes propagate to dry temperature in the ROM SAF reprocessing, and that the use of different statistical optimization approaches at the ROM SAF and at UCAR, affects these results as illustrated in Fig. 3.113.

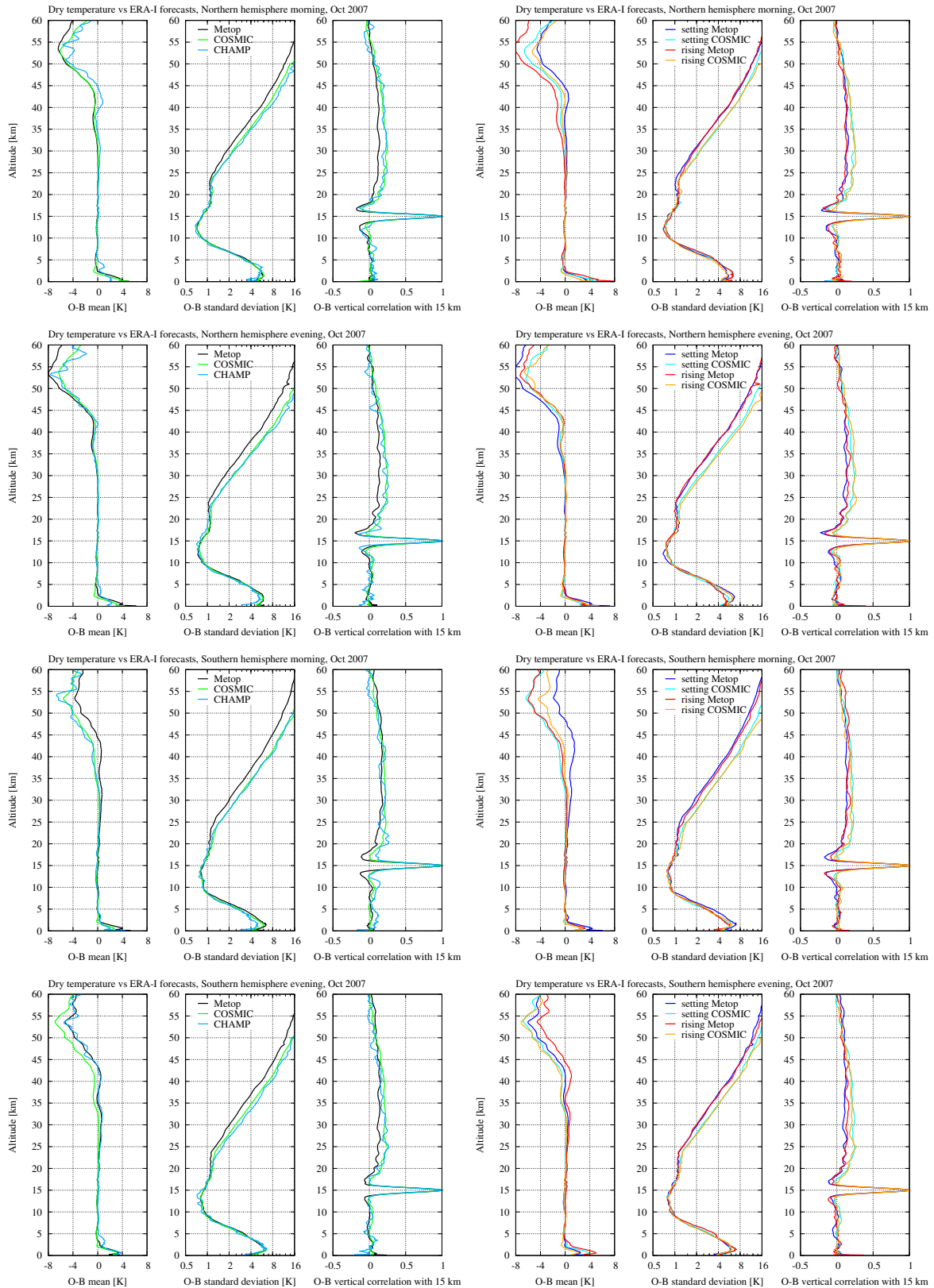


Figure 3.109: Monthly global profile statistics of dry temperature for different missions at local morning and evening in the northern and southern hemispheres (October 2007).

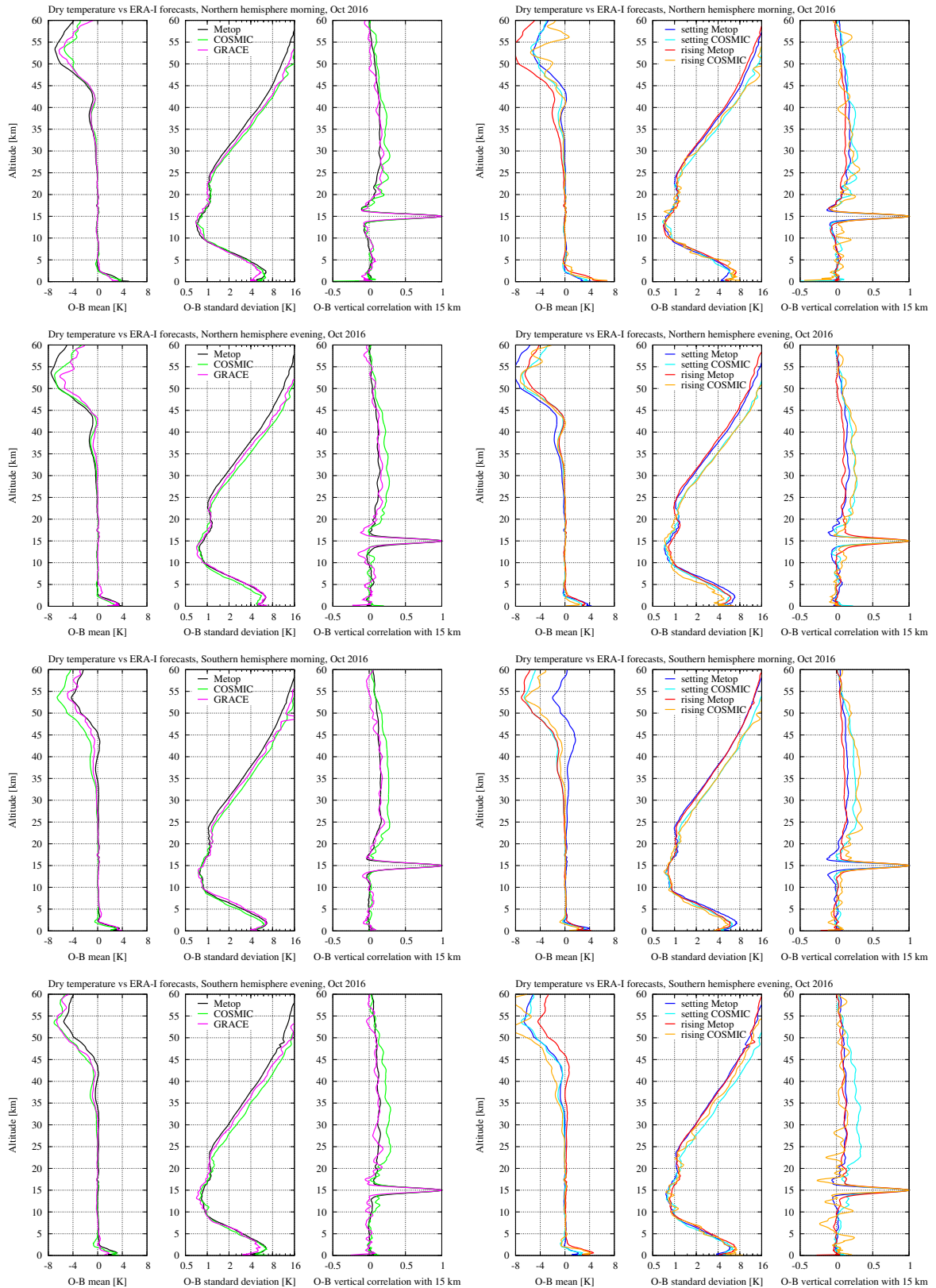


Figure 3.110: Monthly global profile statistics of dry temperature for different missions at local morning and evening in the northern and southern hemispheres (October 2016).

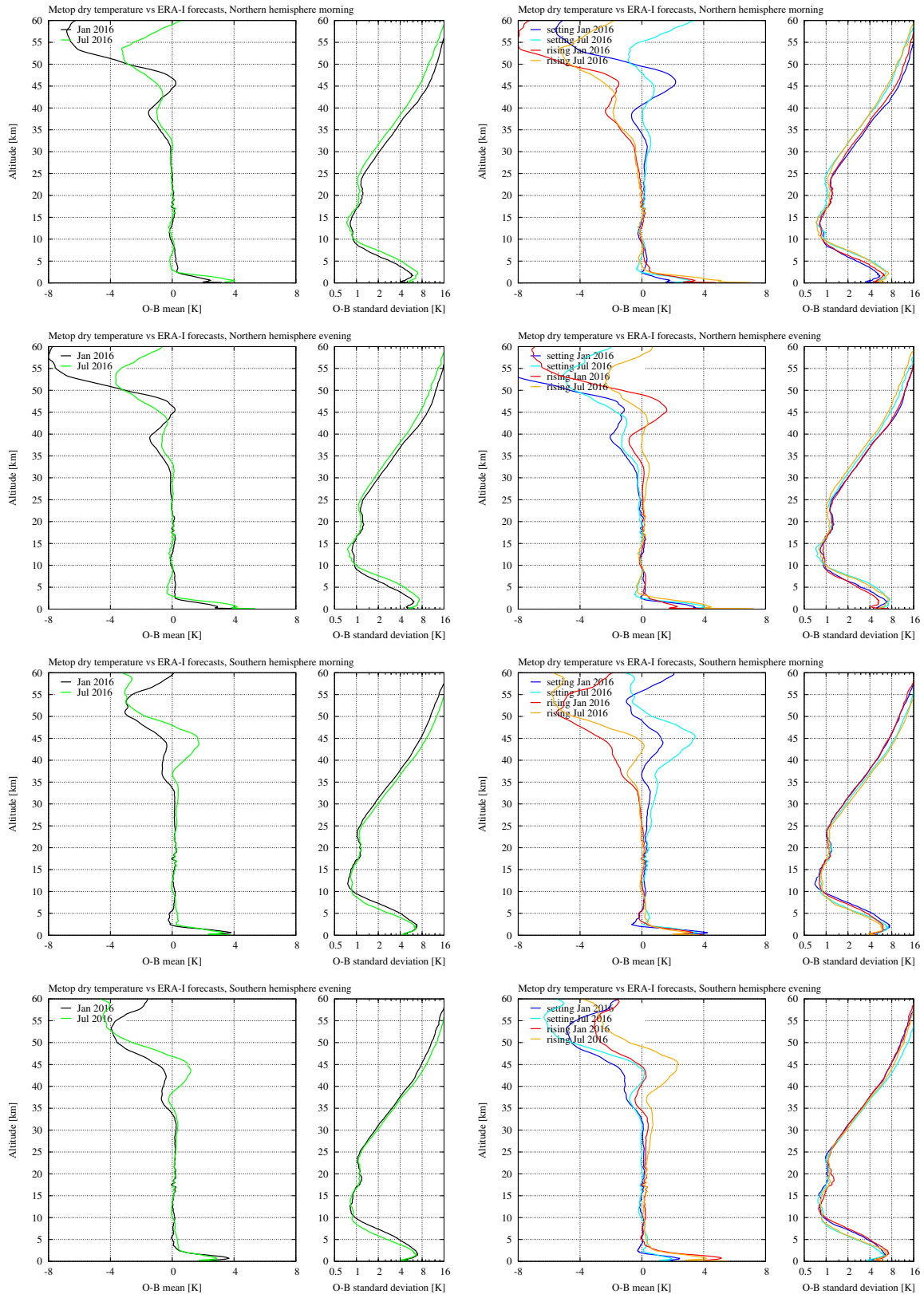


Figure 3.111: Monthly profile statistics of dry temperature from Metop at opposite seasons, hemispheres, morning and evening.

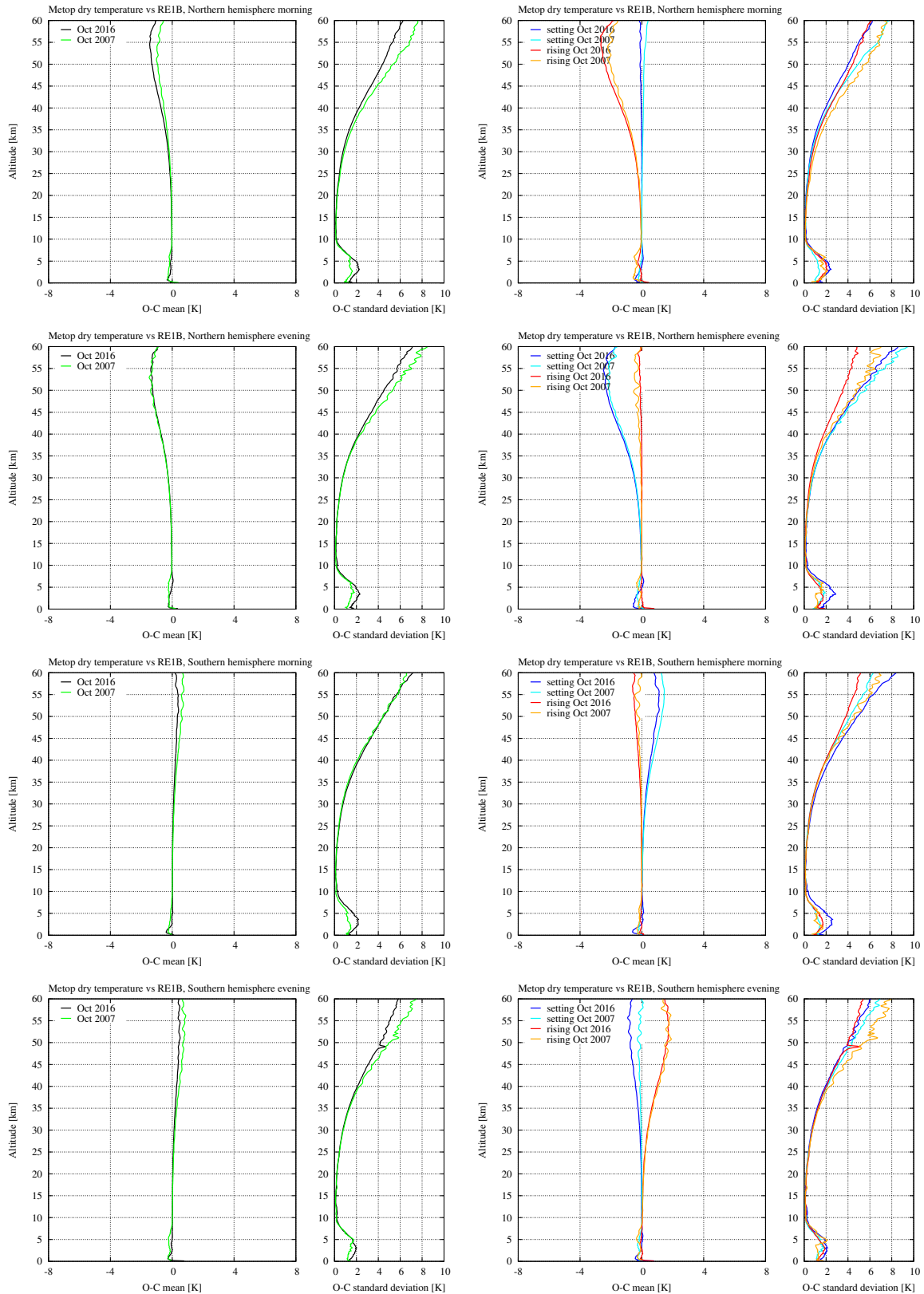


Figure 3.112: Monthly profile statistics of dry temperature from Metop against the dry temperature from the REIB processing, at opposite seasons, hemispheres, morning and evening.

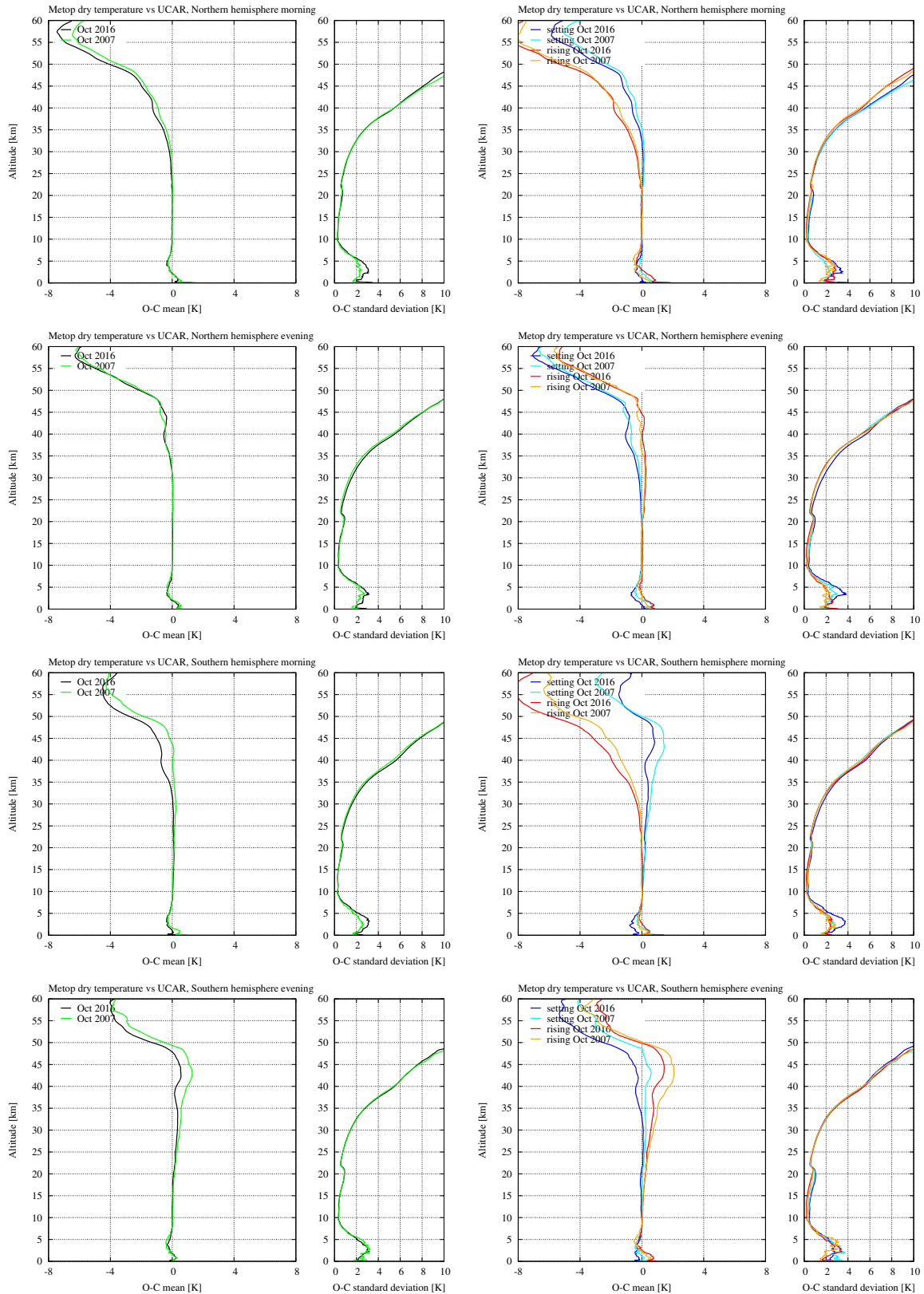


Figure 3.113: Monthly profile statistics of dry temperature from Metop against the dry temperature processed at UCAR, at opposite seasons, hemispheres, morning and evening.

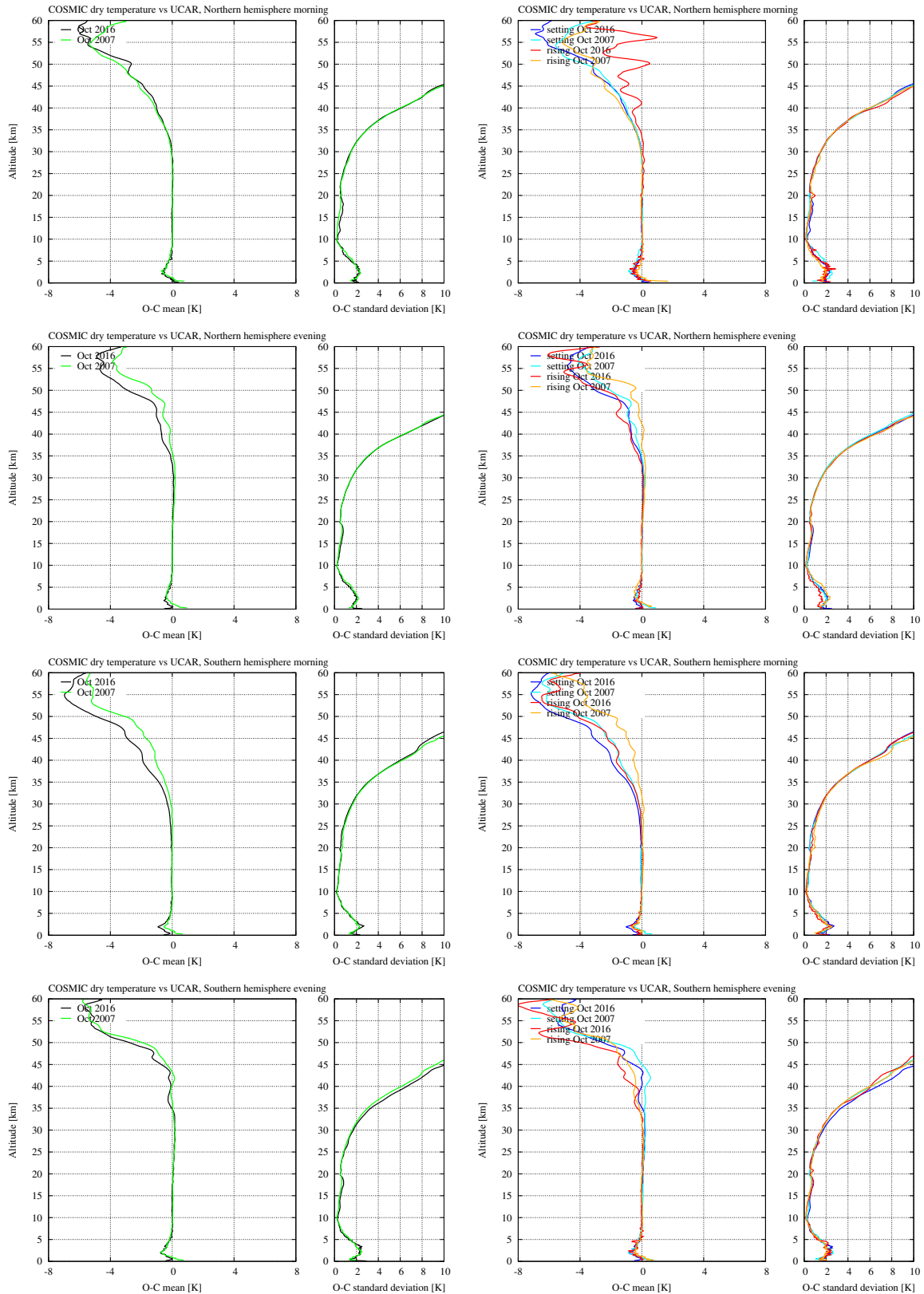


Figure 3.114: Monthly profile statistics of dry temperature from COSMIC against the dry temperature processed at UCAR, at opposite seasons, hemispheres, morning and evening.

4 Compliance with Product Requirements

The product requirements are given in tables in [AD.3], and compliance with the product requirements is visualized in the plots at <http://www.romsaf.org/re1/sesp.php>. The products are mostly within the requirements, except at low altitudes at low latitudes. However, the current product requirements only concern the standard deviation against ERA-Interim forecasts (not possible biases), and the numbers are not sufficient to assess whether the products are of state-of-the-art quality. New product requirements for future use, based on the Service Specifications given in Section 5, will be defined at a later time.

5 Service Specifications

In this chapter we give the Service Specifications for each of the twelve products in Table 1.1. The Service Specifications are determined from the so-called 'vertical mean time series' plots that can be found at http://www.romsaf.org/re1/vertical_mean_time_series.php. Using the drop-down menus at that site, it is possible to inspect a large number of plots for different missions and their individual satellites, for different products compared to both ERA-I forecasts and ECMWF operational forecasts, for different latitude bands and hemispheres, and for both setting and rising occultations separately, or combined. The Service Specifications given in the tables in the sections below are based on only the global plots comparing the ROM SAF CDR v1.0 against ERA-I forecasts, for setting and rising occultations combined. Each plot consists of a number of panels showing the time series of the biases and standard deviations calculated as averages of the monthly statistics over certain vertical intervals. The biases are calculated as the absolute value of the monthly (O-B)/B means (or O-B for dry temperature) and the biases and standard deviations are then averaged over the vertical intervals. The numbers in the tables are determined by visual inspection of these panels, ignoring a few occasional outliers (where Service Specifications are then violated) or periods where it is known that the ERA-I system does not perform as well as in other periods. In particular, the biases in the 8–30 km range for Metop, COSMIC, and GRACE are based only on the period after 2009, excluding the month of December in 2013.

It should be emphasized that the Service Specifications are highly reliant upon the comparisons to ERA-Interim forecasts, and that these in turn are not perfect; they are only approximate representations of the true state of the atmosphere.

5.1 Metop

The Service Specifications for Metop are based on the plots at the following links:

http://www.romsaf.org/re1/images/2016-12/vertical_mean_bangle_impact_atm_bgf_relative_RE1_E_MET_nominal.png

http://www.romsaf.org/re1/images/2016-12/vertical_mean_refrac_alt_refrac_atm_bgf_relative_RE1_E_MET_nominal.png

http://www.romsaf.org/re1/images/2016-12/vertical_mean_dry_temp_alt_refrac_atm_bgf_RE1_E_MET_nominal.png

5.1.1 Bending angle

Table 5.1: Service Specifications for the Metop bending angle of the ROM SAF CDR v1.0.

GRM-29-L1-B-R1	Reprocessed bending angle	RBAMET	SESP_v2.8
Type	Reprocessed Data Set		
Applications and Users	Climate and atmosphere researchers		
Characteristics and Methods	Hi-res wave optics retrieval and ionospheric correction		
Operational Satellite Input Data	Reprocessed level 1A Metop from EUMETSAT Secretariat		
Other Operational Input Data	ECMWF ERA Interim fields		
Dissemination			
Format	Means	Timeliness	
netCDF BUFR	Web	n/a	
Service Specification			
Bias	Standard deviation		
0 – 8 km: 1.5% 8 – 30 km: 0.1% 30 – 40 km: 0.3% 40 – 50 km: 0.6% 50 – 60 km: 1.5%	0 – 8 km: 7.5% 8 – 30 km: 1.5% 30 – 40 km: 2.2% 40 – 50 km: 6.5% 50 – 60 km: 25%		
Notes	The bias in the 8 - 30 km interval is based on ERA Interim only after 2009, excluding Dec 2013.		
Verification/Validation Methods	First calculation of profiles of mean and standard deviation of (Product – ERA Interim forecasts). Bias is then calculated as the absolute value of the mean. Bias and standard deviation are then averaged linearly over vertical intervals.		
Coverage, Resolution			
Spatial Coverage	Spatial Resolution	Vertical Resolution	Temporal resolution
Global	RO resolution	Hi-res wave optics sampling; interpolated to 247 fixed levels	RO resolution

Ref: SAF/ROM/DMI/REP/ATM/001 Version: 1.2 Date: 20 December 2018	Validation Report: Reprocessed profile products	
--	--	--

5.1.2 Refractivity and dry temperature

Table 5.2: Service Specifications for the Metop refractivity and dry temperature of the ROM SAF CDR v1.0.

GRM-29-L2-R-R1 GRM-29-L2-D-R1	Reprocessed refractivity profile Reprocessed dry temperature profile	RRPMET RDPMET	SESP_v2.8
Type	Reprocessed Data Set		
Applications and Users	Climate and atmosphere researchers		
Characteristics and Methods	Statistical optimization, Abel transform, and hydrostatic integration		
Operational Satellite Input Data	Reprocessed level 1A Metop from EUMETSAT Secretariat		
Other Operational Input Data	ECMWF ERA Interim fields		
Dissemination			
Format	Means	Timeliness	
netCDF BUFR	Web	n/a	
Service Specification			
Bias	Standard deviation		
Refractivity profile			
0 – 8 km: 0.5% 8 – 30 km: 0.06% 30 – 40 km: 0.3% 40 – 50 km: 0.5% 50 – 60 km: 1.5%	0 – 8 km: 1.8% 8 – 30 km: 0.55% 30 – 40 km: 1.0% 40 – 50 km: 3.0% 50 – 60 km: 8.0%		
Dry temperature profile			
0 – 8 km: 1.0K 8 – 30 km: 0.1K 30 – 40 km: 0.75K 40 – 50 km: 2.8K 50 – 60 km: 6.0K	0 – 8 km: 4.2K 8 – 30 km: 1.2K 30 – 40 km: 4.0K 40 – 50 km: 10K 50 – 60 km: 18K		
Notes	The bias in the 8 - 30 km interval is based on ERA Interim only after 2009, excluding Dec 2013.		
Verification/Validation Methods	First calculation of profiles of mean and standard deviation of (Product – ERA Interim forecasts). Bias is then calculated as the absolute value of the mean. Bias and standard deviation are then averaged linearly over vertical intervals.		
Coverage, Resolution			
Spatial Coverage	Spatial Resolution	Vertical Resolution	Temporal resolution
global	RO resolution	Hi-res wave optics sampling; interpolated to 247 fixed levels	RO resolution

5.2 COSMIC

The Service Specifications for COSMIC are based on the plots at the following links:

http://www.romsaf.org/re1/images/2016-12/vertical_mean_bangle_impact_atm_bgf_relative_RE1_U_C00_nominal.png

http://www.romsaf.org/re1/images/2016-12/vertical_mean_refrac_alt_refrac_atm_bgf_relative_RE1_U_C00_nominal.png

http://www.romsaf.org/re1/images/2016-12/vertical_mean_dry_temp_alt_refrac_atm_bgf_RE1_U_C00_nominal.png

5.2.1 Bending angle

Table 5.3: Service Specifications for the COSMIC bending angle of the ROM SAF CDR v1.0.

GRM-30-L1-B-R1	Reprocessed bending angle		RBACO1	SESP_v2.8
Type	Reprocessed Data Set			
Applications and Users	Climate and atmosphere researchers			
Characteristics and Methods	Hi-res wave optics retrieval and ionospheric correction			
Operational Satellite Input Data	Reprocessed level 1A COSMIC from UCAR CDAAC			
Other Operational Input Data	ECMWF ERA Interim fields			
Dissemination				
Format	Means	Timeliness		
netCDF BUFR	Web	n/a		
Service Specification				
Bias		Standard deviation		
0 – 8 km: 1.0%		0 – 8 km: 7.5%		
8 – 30 km: 0.1%		8 – 30 km: 1.5%		
30 – 40 km: 0.3%		30 – 40 km: 2.2%		
40 – 50 km: 0.6%		40 – 50 km: 7.5%		
50 – 60 km: 1.5%		50 – 60 km: 30%		
Notes	The bias in the 8 - 30 km interval is based on ERA Interim only after 2009, excluding Dec 2013.			
Verification/Validation Methods	First calculation of profiles of mean and standard deviation of (Product – ERA Interim forecasts). Bias is then calculated as the absolute value of the mean. Bias and standard deviation are then averaged linearly over vertical intervals.			
Coverage, Resolution				
Spatial Coverage	Spatial Resolution	Vertical Resolution	Temporal resolution	
Global	RO resolution	Hi-res wave optics sampling; interpolated to 247 fixed levels	RO resolution	

5.2.2 Refractivity and dry temperature

Table 5.4: Service Specifications for the COSMIC refractivity and dry temperature of the ROM SAF CDR v1.0.

GRM-30-L2-R-R1 GRM-30-L2-D-R1	Reprocessed refractivity profile Reprocessed dry temperature profile	RRPCO1 RDPCO1	SESP_v2.8
Type		Reprocessed Data Set	
Applications and Users		Climate and atmosphere researchers	
Characteristics and Methods		Statistical optimization, Abel transform, and hydrostatic integration	
Operational Satellite Input Data		Reprocessed level 1A COSMIC from UCAR CDAAC	
Other Operational Input Data		ECMWF ERA Interim fields	
Dissemination			
Format	Means	Timeliness	
netCDF BUFR	Web	n/a	
Service Specification			
Bias		Standard deviation	
Refractivity Profile			
0 – 8 km: 0.5% 8 – 30 km: 0.06% 30 – 40 km: 0.25% 40 – 50 km: 0.4% 50 – 60 km: 1.5%		0 – 8 km: 1.8% 8 – 30 km: 0.5% 30 – 40 km: 1.2% 40 – 50 km: 4.0% 50 – 60 km: 10.0%	
Dry temperature Profile			
0 – 8 km: 1.0K 8 – 30 km: 0.1K 30 – 40 km: 1.0K 40 – 50 km: 3.0K 50 – 60 km: 6.0K		0 – 8 km: 4.2K 8 – 30 km: 1.3K 30 – 40 km: 4.5K 40 – 50 km: 12K 50 – 60 km: 22K	
Notes	The bias in the 8 - 30 km interval is based on ERA Interim only after 2009, excluding Dec 2013.		
Verification/Validation Methods	First calculation of profiles of mean and standard deviation of (Product – ERA Interim forecasts). Bias is then calculated as the absolute value of the mean. Bias and standard deviation are then averaged linearly over vertical intervals.		
Coverage, Resolution			
Spatial Coverage	Spatial Resolution	Vertical Resolution	Temporal resolution
global	RO resolution	Hi-res wave optics sampling; interpolated to 247 fixed levels	RO resolution

5.3 CHAMP

The Service Specifications for CHAMP are based on the plots at the following links:

http://www.romsaf.org/re1/images/2016-12/vertical_mean_bangle_impact_atm_bgf_relative_RE1_U_CHMP_nominal.png

http://www.romsaf.org/re1/images/2016-12/vertical_mean_refrac_alt_refrac_atm_bgf_relative_RE1_U_CHMP_nominal.png

http://www.romsaf.org/re1/images/2016-12/vertical_mean_dry_temp_alt_refrac_atm_bgf_RE1_U_CHMP_nominal.png

5.3.1 Bending angle

Table 5.5: Service Specifications for the CHAMP bending angle of the ROM SAF CDR v1.0.

GRM-32-L1-B-R1	Reprocessed bending angle	RBACHA	SESP_v2.8
Type	Reprocessed Data Set		
Applications and Users	Climate and atmosphere researchers		
Characteristics and Methods	Hi-res wave optics retrieval and ionospheric correction		
Operational Satellite Input Data	Reprocessed level 1A CHAMP from UCAR CDAAC		
Other Operational Input Data	ECMWF ERA Interim fields		
Dissemination			
Format	Means	Timeliness	
netCDF BUFR	Web	n/a	
Service Specification			
Bias		Standard deviation	
0 – 8 km: 2.0%		0 – 8 km: 7.0%	
8 – 30 km: 0.2%		8 – 30 km: 1.7%	
30 – 40 km: 0.5%		30 – 40 km: 3.5%	
40 – 50 km: 1.0%		40 – 50 km: 14%	
50 – 60 km: 2.5%		50 – 60 km: 50%	
Notes	The values are based on ERA Interim before 2009.		
Verification/Validation Methods	First calculation of profiles of mean and standard deviation of (Product – ERA Interim forecasts). Bias is then calculated as the absolute value of the mean. Bias and standard deviation are then averaged linearly over vertical intervals.		
Coverage, Resolution			
Spatial Coverage	Spatial Resolution	Vertical Resolution	Temporal resolution
Global	RO resolution	Hi-res wave optics sampling; interpolated to 247 fixed levels	RO resolution

5.3.2 Refractivity and dry temperature

Table 5.6: Service Specifications for the CHAMP refractivity and dry temperature of the ROM SAF CDR v1.0.

GRM-32-L2-R-R1 GRM-32-L2-D-R1	Reprocessed refractivity profile Reprocessed dry temperature profile	RRPCHA RDPCHA	SESP_v2.8
Type		Reprocessed Data Set	
Applications and Users		Climate and atmosphere researchers	
Characteristics and Methods		Statistical optimization, Abel transform, and hydrostatic integration	
Operational Satellite Input Data		Reprocessed level 1A CHAMP from UCAR CDAAC	
Other Operational Input Data		ECMWF ERA Interim fields	
Dissemination			
Format		Means	Timeliness
netCDF BUFR		Web	n/a
Service Specification			
Bias		Standard deviation	
Refractivity Profile			
0 – 8 km: 0.6% 8 – 30 km: 0.14% 30 – 40 km: 0.5% 40 – 50 km: 1.0% 50 – 60 km: 1.5%		0 – 8 km: 1.8% 8 – 30 km: 0.55% 30 – 40 km: 1.5% 40 – 50 km: 5.0% 50 – 60 km: 12.0%	
Dry temperature Profile			
0 – 8 km: 1.2K 8 – 30 km: 0.3K 30 – 40 km: 0.6K 40 – 50 km: 3.5K 50 – 60 km: 7.0K		0 – 8 km: 4.2K 8 – 30 km: 1.3K 30 – 40 km: 5.0K 40 – 50 km: 14K 50 – 60 km: 25K	
Notes		The values are based on ERA Interim before 2009.	
Verification/Validation Methods		First calculation of profiles of mean and standard deviation of (Product – ERA Interim forecasts). Bias is then calculated as the absolute value of the mean. Bias and standard deviation are then averaged linearly over vertical intervals.	
Coverage, Resolution			
Spatial Coverage	Spatial Resolution	Vertical Resolution	Temporal resolution
global	RO resolution	Hi-res wave optics sampling; interpolated to 247 fixed levels	RO resolution

5.4 GRACE

The Service Specifications for GRACE are based on the plots at the following links:

http://www.romsaf.org/re1/images/2016-12/vertical_mean_bangle_impact_atm_bgf_relative_RE1_U_GRA_nominal.png

http://www.romsaf.org/re1/images/2016-12/vertical_mean_refrac_alt_refrac_atm_bgf_relative_RE1_U_GRA_nominal.png

http://www.romsaf.org/re1/images/2016-12/vertical_mean_dry_temp_alt_refrac_atm_bgf_RE1_U_GRA_nominal.png

5.4.1 Bending angle

Table 5.7: Service Specifications for the GRACE bending angle of the ROM SAF CDR v1.0.

GRM-33-L1-B-R1	Reprocessed bending angle	RBAGRA	SESP_v2.8
Type	Reprocessed Data Set		
Applications and Users	Climate and atmosphere researchers		
Characteristics and Methods	Hi-res wave optics retrieval and ionospheric correction		
Operational Satellite Input Data	Reprocessed level 1A GRACE from UCAR CDAAC		
Other Operational Input Data	ECMWF ERA Interim fields		
Dissemination			
Format	Means	Timeliness	
netCDF BUFR	Web	n/a	
Service Specification			
Bais	Standard deviation		
0 – 8 km: 1.8% 8 – 30 km: 0.1% 30 – 40 km: 0.3% 40 – 50 km: 0.6% 50 – 60 km: 1.5%	0 – 8 km: 7.0% 8 – 30 km: 1.6% 30 – 40 km: 3.0% 40 – 50 km: 12% 50 – 60 km: 40%		
Notes	The bias in the 8 - 30 km interval is based on ERA Interim only after 2009, excluding Dec 2013.		
Verification/Validation Methods	First calculation of profiles of mean and standard deviation of (Product – ERA Interim forecasts). Bias is then calculated as the absolute value of the mean. Bias and standard deviation are then averaged linearly over vertical intervals.		
Coverage, Resolution			
Spatial Coverage	Spatial Resolution	Vertical Resolution	Temporal resolution
Global	RO resolution	Hi-res wave optics sampling; interpolated to 247 fixed levels	RO resolution

5.4.2 Refractivity and dry temperature

Table 5.8: Service Specifications for the GRACE refractivity and dry temperature of the ROM SAF CDR v1.0.

GRM-33-L2-R-R1 GRM-33-L2-D-R1	Reprocessed refractivity profile Reprocessed dry temperature profile	RRPGRA RDPGRA	SESP_v2.8
Type		Reprocessed Data Set	
Applications and Users		Climate and atmosphere researchers	
Characteristics and Methods		Statistical optimization, Abel transform, and hydrostatic integration	
Operational Satellite Input Data		Reprocessed level 1A GRACE from UCAR CDAAC	
Other Operational Input Data		ECMWF ERA Interim fields	
Dissemination			
Format		Means	Timeliness
netCDF BUFR		Web	n/a
Service Specification			
Bias		Standard deviation	
Refractivity Profile			
0 – 8 km: 0.5% 8 – 30 km: 0.06% 30 – 40 km: 0.2% 40 – 50 km: 0.4% 50 – 60 km: 1.5%		0 – 8 km: 1.8% 8 – 30 km: 0.5% 30 – 40 km: 1.3% 40 – 50 km: 4.5% 50 – 60 km: 11.0%	
Dry temperature Profile			
0 – 8 km: 1.0K 8 – 30 km: 0.12K 30 – 40 km: 1.0K 40 – 50 km: 3.0K 50 – 60 km: 6.0K		0 – 8 km: 4.2K 8 – 30 km: 1.25K 30 – 40 km: 4.5K 40 – 50 km: 13K 50 – 60 km: 25K	
Notes		The bias in the 8 - 30 km interval is based on ERA Interim only after 2009, excluding Dec 2013.	
Verification/Validation Methods		First calculation of profiles of mean and standard deviation of (Product – ERA Interim forecasts). Bias is then calculated as the absolute value of the mean. Bias and standard deviation are then averaged linearly over vertical intervals.	
Coverage, Resolution			
Spatial Coverage	Spatial Resolution	Vertical Resolution	Temporal resolution
global	RO resolution	Hi-res wave optics sampling; interpolated to 247 fixed levels	RO resolution

6 Conclusions

The overall conclusion is that the Level 1B and 2A products of the ROM SAF CDR v1.0 are of a very high quality, and mostly within the product requirements, except at low altitudes at low latitudes. However, the current product requirements only concern the standard deviation against ERA-Interim forecasts (not possible biases), and the numbers are not sufficient to assess whether the products are of state-of-the-art quality. New product requirements for future use, based on the determined Service Specifications in this report, will be defined at a later time.

Although the ROM SAF CDR v1.0 consists of RO data from four different satellite missions¹, with different instruments and onboard software that has been upgraded several times over the years, the quality of the processed data is fairly similar among the different missions, at least above 8 km impact height (6 km altitude). The quality is also fairly consistent over time, and the data compares well to both ERA-I forecasts and ECMWF operational forecasts between 5 km and 35 km, and generally much better (and to higher altitudes) when compared to reprocessed or post-processed data from the EUMETSAT Secretariat and UCAR/CDAAC.

We conclude that the quality of the ROM SAF CDR v1.0 generally matches the quality of the corresponding products from these two RO data providers, which are considered to deliver state-of-the-art products of good quality to users around the world.

6.1 Limitations

During the course of the validation activity, a few minor issues appeared. They are listed below as limitations together with the well known issue that RO data are biased at the lowest altitudes, especially at low latitudes. These biases are considered more or less fundamentally linked to the instrument tracking, and are different for different missions, but they are also different for different RO data providers, and different for setting and rising occultations. At the end of the list we also note two more technical issues, related to the difference between GPS time and UTC, and to the content in a few fields in the BUFR files of the ROM SAF CDR v1.0.

Limitations of the ROM SAF CDR v1.0 are:

- Biases in all products below 8 km impact height (6 km altitude), largest at low latitudes; near the surface at low latitudes, these biases are about 3% in all products when compared to ERA-Interim forecasts
- Large biases for CHAMP near 5 km impact height (3 km altitude) in the northern hemisphere morning and the southern hemisphere evening; these biases are up to 2% in bending angle and about 0.5% in refractivity and dry temperature
- Small systematic biases for Metop at high altitudes of order 0.1 μ rad in bending angle, depending on local time and hemispheres, and different for setting and rising occultations; percentage wise, these biases increase with altitude and are up to about 0.5% at

¹ Future CDR's will include more satellite missions.

50 km and 45 km in bending angle and refractivity, respectively, and up to 1 K at 35 km in dry temperature

- A small negative constant bias of $\sim 0.1\%$ in bending angle and refractivity for CHAMP between 20 km and 30 km in the southern hemisphere morning local time
- Small negative constant biases in rising Metop occultations between 10 km and 20 km after the instrument software upgrades in 2013; these biases are up to $\sim 0.1\%$ in bending angle and refractivity, and largest in the morning local time
- Larger standard deviations and vertical correlations between 10 km and 20 km for rising Metop occultations after the instrument software upgrades in 2013, mostly so for refractivity, and largest at high latitudes
- Generally low quality for COSMIC before the instrument software upgrades in mid 2006
- The timing in the products for COSMIC, CHAMP, and GRACE are according to GPS time, whereas the timing for Metop is in UTC; this distinction is not clear from the data files
- The one sample satellite positions and velocities in the BUFR files are given in True-of-Date ECI coordinates; they were supposed to be given in an ECF-aligned inertial system as described in documents that can be found at <http://irowg.org/workshops/irowg-4/bufr-discussions-at-and-following-irowg-4/>.

In various sections throughout Chapter 3, we noted when results were not fully understood, or we used words as 'might', 'could', or 'may' in attempts to provide plausible explanations for them. Some of the issues that we noted are listed as limitations above, but others are not considered limitations as such, but rather small things that would need further investigation to be fully understood. Below we list all issues that could warrant further investigation in the future, with reference to sections and key figures in Chapter 3.

Issues that could warrant further investigation in the future:

- Different biases for Metop and COSMIC below 8 km impact height, and for both missions notable difference between setting and rising occultations (cf. Section 3.1.1, e.g., Fig. 3.1)
- Lower standard deviation for COSMIC than for the other missions around 25–30 km, especially at low latitudes (cf. Section 3.1.1, Fig. 3.2)
- Similar standard deviations in refractivity at high altitudes for COSMIC, GRACE, and CHAMP, as opposed to in bending angle, where standard deviations are more different (cf. Section 3.1.2, e.g., Fig. 3.5)
- Larger sensitivity at higher latitudes to the effects of the L2-extrapolation (cf. Sections 3.1.2, Fig. 3.8)
- Smaller sensitivity in dry temperature statistics to the effects of the L2-extrapolation (cf. Section 3.1.3, e.g., Fig. 3.9)

- Small vertical correlations in dry temperature above 20 km, more for COSMIC and CHAMP than for Metop and GRACE (cf. Section 3.1.3, e.g., Fig. 3.9)
- Larger standard deviation in bending angle below 30 km for CHAMP around 2004 (cf. Section 3.4.1, Fig. 3.28)
- Three distinct periods from June 2007 to January 2008 with increased noise in rising occultations for the COSMIC-FM5 satellite (cf. Section 3.4.1, Fig. 3.31)
- A maximum around mid 2014 in the standard deviations and vertical correlations in refractivity between ~10 km and 20 km for Metop and COSMIC rising occultations (cf. Sections 3.1.2 and 3.4.2, e.g., Figs. 3.32 and 3.36)
- Indications of a smaller number of CHAMP and GRACE occultations for which the lowest part is biased negative due to tracking errors (cf. Section 3.7.1, e.g., Fig. 3.61)
- Larger positive bias at low altitudes for COSMIC than for Metop, peaking around 4 km impact height (cf. Section 3.7.1, e.g., Fig. 3.61)
- Larger standard deviation in bending angle for CHAMP at high altitudes, when comparing to the corresponding data from UCAR/CDAAC (cf. Section 3.7.1, e.g., Fig. 3.61)
- Larger standard deviations in bending angle for COSMIC and GRACE at high altitudes in 2007 than in 2016 (cf. Section 3.7.1, e.g., Figs. 3.61 and 3.62)
- Smaller standard deviation in bending angle for Metop at high altitudes in the southern hemisphere morning local time (cf. Section 3.8.1, Figs. 3.85 and 3.86)
- A small negative bias for CHAMP between 20 km and 30 km in the southern hemisphere morning local time (cf. Section 3.8.1, Fig. 3.85)
- Larger negative biases for CHAMP near 5 km in the northern hemisphere morning and the southern hemisphere evening (cf. Section 3.8.1, Fig. 3.85)
- Small bias and standard deviation differences between January 2016 and July 2016, both at high and low altitudes (cf. Section 3.8.1, Fig. 3.91)
- Bias differences for Metop at high altitudes, depending on hemispheres and local times, as well as differences between rising and setting occultations (cf. Section 3.8.1, e.g., Fig. 3.92)
- Small rising and setting biases for both Metop and COSMIC between ~10 km and 20 km, depending on hemispheres and local times, when comparing to the corresponding data from UCAR/CDAAC (cf. Section 3.8.1, Figs. 3.93 and 3.94)
- Inconsistent vertical slopes of rising and setting L1–L2 means between 15 km and 25 km (cf. Section 3.8.1, Fig. 3.101)

Additionally, future ROM SAF reprocessing activities will include the higher order ionospheric correction that is already included in the reprocessed EUMETSAT bending angle (version 1.4). The systematic differences at high altitudes between these two datasets, e.g.,

in the left plots of Fig. 3.98, gives a hint of the size of the average impact of this correction in different regions and for different local times (up to about 0.5% at 60 km).

Finally, the netCDF files for all missions include error estimates for the bending angle products based on radio holographic filtering [RD.3]. These error estimates have not been validated here, and they have not been compared to the statistics presented throughout this report, but they are provided for the expert user as an unofficial demonstration product.

6.2 Interim Climate Data Record

The ROM SAF CDR v1.0 covers the period up to the end of 2016. A ROM SAF reprocessing #2 is planned for 2020 and will cover more missions from their launch until sometime in 2020. In the meantime, the ROM SAF will provide an Interim Climate Data Record (ICDR) for Metop. This data record will be made available shortly after the publication of the ROM SAF CDR v1.0, and cover the period from the beginning of 2017 and until the present time, with a new month of data being made available once a month with about 30 days delay.

The input Level 1A data for the ICDR will be identical to the input Level 1A data for the offline processing (see Section 6.3), and the algorithms and the quality control at the ROM SAF will be identical to the ones used for reprocessing #1. The validation of the Level 1B and Level 2A ICDR products is addressed in Annex A.

6.3 Offline products

The input Level 1A data for the offline products are provided by the EUMETSAT Secretariat, and the processing and the quality control at the ROM SAF will to begin with be similar to the one used for reprocessing #1. In particular, the offline processing will be using the GPAC system version 2.3.1, with ROPP software version 9.0 as a key integral part, including the same modifications that were made to ROPP 8.1 in the preparations for the reprocessing #1 (cf. Chapter 2). Over time the algorithms used in the offline processing may evolve, and in such cases the offline products will be subject to additional review cycles.

The verification that the quality of the current Level 1B and Level 2A offline products are on a par with the quality of the Metop data from the ROM SAF CDR v1.0 is given in Annex B. The successful verification indicates that the quality of higher level offline products will also be on par with those of the corresponding higher level products from the ROM SAF CDR v1.0.

A Annex

A.1 Interim Climate Data Record

The purpose of this Annex is to address the validation of the Level 1B and Level 2A products of the Metop ICDR formally referred to as GRM-29-I1.

A.1.1 Description of ICDR products being validated in this Annex

Table A.1: List of ICDR products covered by this report.

Product ID	Product name	Product acronym	Product type	Operational satellite input	Dissemination means	Dissemination format
GRM-29-L1-B-I1	ICDR Bending Angle	IBAMET	Interim Climate Data Record	Metop Level 1A data from EUM Secretariat	web	BUFR/netCDF
GRM-29-L2-R-I1	ICDR Refractivity Profile	IRPMET	Interim Climate Data Record	Metop Level 1A data from EUM Secretariat	web	BUFR/netCDF
GRM-29-L2-D-I1	ICDR Dry Temperature Profile	IDPMET	Interim Climate Data Record	Metop Level 1A data from EUM Secretariat	web	BUFR/netCDF

A.1.2 Validation

As described in the definitions section (Section 1.4), the CDRs have been generated in a dedicated reprocessing activity using the same algorithms throughout the length of the data records, while ICDRs are generated on a regular basis with the same algorithms as the CDRs, but using currently available input data. The main rationale for the ICDRs is that they extend the CDRs until data from a new reprocessing become available. There is a strong focus on the consistency between the ICDRs and the CDRs, and the ICDRs are expected to have very similar characteristics as the corresponding CDRs. Hence, the validation of the reprocessed data products described in this report also applies to the corresponding ICDR products.

A.1.3 Service Specifications

The Service Specifications for the Metop Level 1B and 2A ICDR products are given in Table A.2.

Table A.2: Service Specifications for the Metop ICDR products.

Accuracy targets, Level 1B and 2A	Same as for GRM-29-R1
Methods for validation	Same as for GRM-29-R1

B Annex

B.1 Offline products

The purpose of this Annex is to provide validation for the Metop offline Level 1B and Level 2A products formally referred to as GRM-08, GRM-09, GRM-46, GRM-47, GRM-101, and GRM-103.

B.1.1 Description of offline products being validated in this Annex

Table B.1: List of offline products covered by this report.

Product ID	Product name	Product acronym	Product type	Operational satellite input	Dissemination means	Dissemination format
GRM-08	Offline Bending Angle	OBAMEA	Offline product	Metop-A Level 1A data from EUM Secretariat	web	BUFR/netCDF
GRM-46	Offline Bending Angle	OBAMEB	Offline product	Metop-B Level 1A data from EUM Secretariat	web	BUFR/netCDF
GRM-09	Offline Refractivity Profile	ORPMEA	Offline product	Metop-A Level 1A data from EUM Secretariat	web	BUFR/netCDF
GRM-47	Offline Refractivity Profile	ORPMEB	Offline product	Metop-B Level 1A data from EUM Secretariat	web	BUFR/netCDF
GRM-101	Offline Dry Temperature Profile	ODPMEA	Offline product	Metop-A Level 1A data from EUM Secretariat	web	BUFR/netCDF
GRM-103	Offline Dry Temperature Profile	ODPMEB	Offline product	Metop-B Level 1A data from EUM Secretariat	web	BUFR/netCDF

B.1.2 Profile comparisons

Figure B.1 shows two plots (each with three panels) of the monthly global profile statistics of bending angle for Metop offline data for January 2017. The left plots show the total statistics, whereas the right plots show the statistics separated into setting and rising occultations. Figures B.2 and B.3 show the same for the refractivity and dry temperature offline products, respectively. These figures can be compared to the ones in the bottom plots of Figs. 3.19, 3.21, and 3.23 in Section 3.3, which are from July 2013, shortly after the instrument software upgrade to the Metop satellites. Visible differences between the 2013 and 2017 plots, at least above 5 km impact height, are assumed to be mostly due to seasonal variations in the biases of the ERA-I data, as well as the fact that July 2013 was closer to the last solar maximum than January 2017 (possibly the reason for the slightly smaller O-B vertical correlations between 10 km and 20 km in refractivity for rising occultations in 2017; cf. discussions in Section 3.4).

We conclude that the quality of the Metop offline data for both Metop-A and Metop-B are on a par with the quality of the ROM SAF CDR v1.0 for Metop since July 2013.

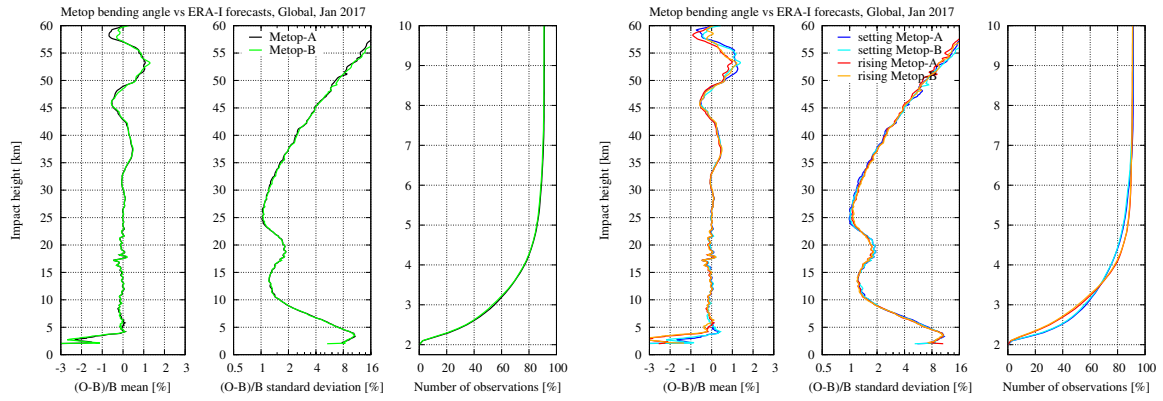


Figure B.1: Monthly global profile statistics of bending angle from Metop (offline) data for January 2017.

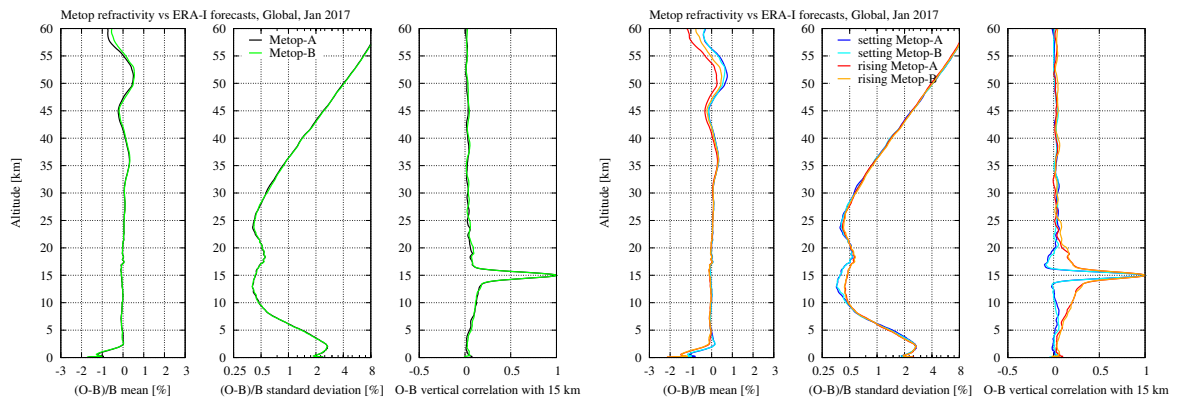


Figure B.2: Monthly global profile statistics of refractivity from Metop (offline) data for January 2017.

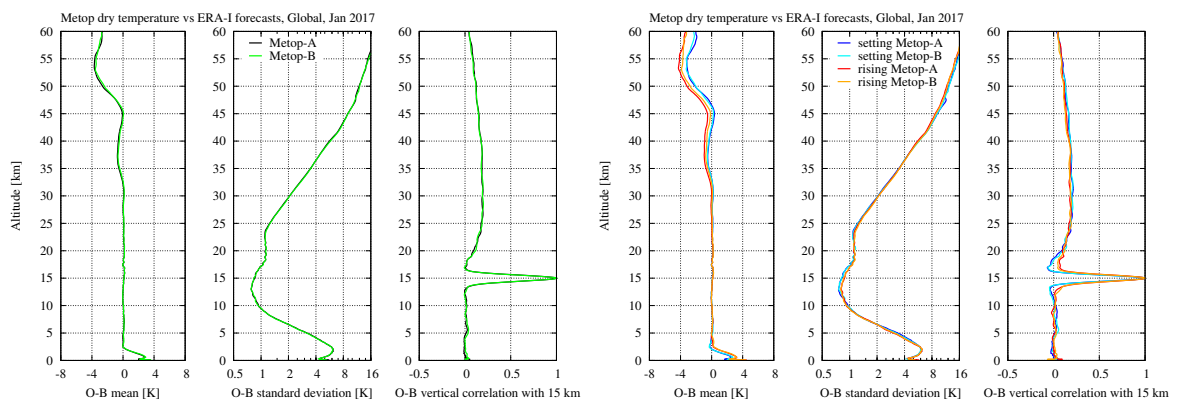


Figure B.3: Monthly global profile statistics of dry temperature from Metop (offline) data for January 2017.

B.1.3 Service Specifications

The Service Specifications for the Metop Level 1B and 2A offline products are given in Table B.2 (for bending angle) and Table B.3 (for refractivity and dry temperature). The values are identical to the values for the Service Specifications for the corresponding GRM-29-R1 products, given that the quality of the offline Metop data is very similar to that of the reprocessed Metop data, as verified in the previous subsection, and that the offline data are processed with basically the same software as that used for the reprocessing.

Table B.2: Service Specifications for the offline Metop bending angle.

GRM-08 GRM-46	Offline bending angle (Metop-A) Offline bending angle (Metop-B)	OBAMEA OBAMEB	SESP_v2.8
Type	Off-line Product		
Applications and Users	Climate and atmosphere researchers		
Characteristics and Methods	Hi-res wave optics retrieval and ionospheric correction		
Operational Satellite Input Data	Metop-A and B Level 1A from EUMETSAT Secretariat		
Other Operational Input Data	ECMWF operational and ERA-I FC, AN		
Dissemination			
Format	Means	Timeliness	
netCDF BUFR	Web	30 d	
Service Specification			
Bias		Standard deviation	
0 – 8 km: 1.5% 8 – 30 km: 0.1% 30 – 40 km: 0.3% 40 – 50 km: 0.6% 50 – 60 km: 1.5%		0 – 8 km: 7.5% 8 – 30 km: 1.5% 30 – 40 km: 2.2% 40 – 50 km: 6.5% 50 – 60 km: 25%	
Notes	The values are based on the values for GRM-29-L1-B-R1		
Verification/Validation Methods	First calculation of profiles of mean and standard deviation of (Product – ERA Interim forecasts). Bias is then calculated as the absolute value of the mean. Bias and standard deviation are then averaged linearly over vertical intervals.		
Coverage, Resolution			
Spatial Coverage	Spatial Resolution	Vertical Resolution	Temporal resolution
global	RO resolution	hi-res wave optics sampling; interpolated to 247 fixed levels	RO resolution

Table B.3: Service Specifications for the offline Metop refractivity and dry temperature.

GRM-09	Offline refractivity profile (Metop-A)	ORPMEA	SESP_v2.8
GRM-47	Offline refractivity profile (Metop-B)	ORPMEB	
GRM-101	Offline dry temperature profile (Metop-A)	ODPMEA	
GMR-103	Offline dry temperature profile (Metop-B)	ODPMEB	
Type		Off-line Product	
Applications and Users		Climate and atmosphere researchers	
Characteristics and Methods		Statistical optimization, Abel transform, and hydrostatic integration	
Operational Satellite Input Data		Metop-A and B Level 1A from EUMETSAT Secretariat	
Other Operational Input Data		ECMWF operational and ERA-I FC, AN	
Dissemination			
Format	Means	Timeliness	
netCDF BUFR	Web	30 d	
Service Specification			
Bias		Standard deviation	
Refractivity Profile			
0 – 8 km: 0.5%		0 – 8 km: 1.8%	
8 – 30 km: 0.06%		8 – 30 km: 0.55%	
30 – 40 km: 0.3%		30 – 40 km: 1.0%	
40 – 50 km: 0.5%		40 – 50 km: 3.0%	
50 – 60 km: 1.5%		50 – 60 km: 8.0%	
Dry temperature Profile			
0 – 8 km: 1.0K		0 – 8 km: 4.2K	
8 – 30 km: 0.1K		8 – 30 km: 1.2K	
30 – 40 km: 0.75K		30 – 40 km: 4.0K	
40 – 50 km: 2.8K		40 – 50 km: 10K	
50 – 60 km: 6.0K		50 – 60 km: 18K	
Notes	The values are based on the values for GRM-29-L2-R-R1 and GRM-29-L2-D-R1		
Verification/Validation Methods	First calculation of profiles of mean and standard deviation of (Product – ERA Interim forecasts). Bias is then calculated as the absolute value of the mean. Bias and standard deviation are then averaged linearly over vertical intervals.		
Coverage, Resolution			
Spatial Coverage	Spatial Resolution	Vertical Resolution	Temporal resolution
global	RO resolution	hi-res wave optics sampling; interpolated to 247 fixed levels	RO resolution